

LEVEL

(12) B.S.

# NOSC

NOSC TR 543

NOSC TR 543



Technical Report 543

ADA 087404

## EQUATORIAL SCINTILLATION OF SATELLITE SIGNALS AT uhf AND L-BAND FOR TWO DIFFERENT ELEVATION ANGLES

MR Paulson

1 May 1980

1 January 1979 — 1 May 1980

Prepared for  
Office of Naval Research

Code 465

THIS DOCUMENT IS BEST QUALITY PRACTICALLY  
THE COPY FURNISHED TO DDC CONTAINED A  
SIGNIFICANT NUMBER OF PAGES WHICH DO NOT  
REPRODUCE LEGIBLY.

Approved for public release; distribution unlimited.

DDC FILE COPY.

NAVAL OCEAN SYSTEMS CENTER  
SAN DIEGO, CALIFORNIA 92152

80 7 31 050



NAVAL OCEAN SYSTEMS CENTER, SAN DIEGO, CA 92152

AN ACTIVITY OF THE NAVAL MATERIAL COMMAND

SL GUILLE, CAPT, USN

Commander

HL BLOOD

Technical Director

ADMINISTRATIVE INFORMATION

Work was performed under NOSC 61153N, RR03208, RRO320801, 532-MP41 and was sponsored by the Office of Naval Research. The report covers work from 1 January 1979 to 1 May 1980.

Uhf and L-band satellite signal measurements used in this report were made by personnel at the NASA Tracking Station in Dandan, Guam under the direction of John Cornwell.

Some additional uhf signal measurements used were made by personnel at the Naval Communications Area Master Station (NAVCAMS) in Guam under the direction of RM-1 Smith.

Released by  
JH Richter, Head  
EM Propagation Division

Under Authority of  
JD Hightower, Head  
Environmental Sciences Department

Accession For	
NTIS G.M&I	<input checked="checked" type="checkbox"/>
DDC TAB	<input type="checkbox"/>
Unannounced	<input type="checkbox"/>
Justification	
By	
Distribution/	
Availability Codes	
Dist	Avail and/or special
A	23

## **DISCLAIMER NOTICE**

**THIS DOCUMENT IS BEST QUALITY PRACTICABLE. THE COPY FURNISHED TO DTIC CONTAINED A SIGNIFICANT NUMBER OF PAGES WHICH DO NOT REPRODUCE LEGIBLY.**

SECURITY CLASSIFICATION OF THIS PAGE (When Data Entered)

**READ INSTRUCTIONS  
BEFORE COMPLETING FORM**

DD FORM 1 JAN 73 1473

EDITION OF 1 NOV 65 IS OBSOLETE  
S/N 0102-LF-014-6601

UNCLASSIFIED

**SECURITY CLASSIFICATION OF THIS PAGE (When Data Entered)**

393 ± 59

## OBJECTIVES

1. Obtain long term scintillation data at uhf and L-band frequencies for two satellites at two different elevation angles.
2. Use these data to try to evaluate diurnal and seasonal variations and solar activity dependence of equatorial scintillation for the two frequencies and the two elevation angles.
3. Try to determine from the data the generating mechanism which produces the ionospheric irregularities.

## RESULTS

1. Averaged diurnal plots of uhf scintillation intensity showed onset times of the scintillation for the Indian Ocean satellite were usually around 2030-2100 LST from March through August and around 2000 LST for September through November. Onset times for the Pacific Ocean satellite were about one hour earlier.
2. An averaged diurnal plot using 9 nights of L-band scintillation data for the Indian Ocean satellite showed maximum scintillation intensity centered around 2330 LST.
3. Seasonal variation in uhf equatorial scintillation showed a minimum in December and January then a rapid increase through February and March, a broad maximum through the summer, and a rapid increase in late October and November.
4. Seasonal variation in the occurrence of L-band scintillation showed two maxima, one in April and the other in September, with a decrease in the occurrence in the summer months.
5. Cross correlations between daily occurrence of scintillation and daily measurements of solar flux showed little correlation for either satellite; if there is any daily dependence it is so small that other causes obscure it.

A year-to-year dependence of the occurrence of scintillation on solar activity, using a common 11-day period for 5 different years, showed good linear dependence.
6. A pronounced periodicity is evident in the occurrence of scintillation data, particularly during the first half of the year. The period is on the order of 30 days. It is proposed here that this periodicity is caused by the gravitational field of the moon increasing or decreasing (depending on the moon's location) zonal winds at F-region heights and thus increasing or decreasing the occurrence and the intensity of the scintillation.

Around full moon the occurrence and intensity are at a maximum and around new moon they are at a minimum.
7. Cumulative fade duration distributions at uhf showed the fading rates were usually slower on the lower elevation angle satellite resulting in fewer but longer fades. The total time spent below a 6-dB level for a one-hour sample ranged up to 20-22 percent on the Pacific Ocean satellite and up to 25-30 percent on the Indian Ocean satellite. At 12 dB these were 4-5 percent and 6-8 percent, respectively.
8. Very little L-band scintillation with fades greater than 6 dB occurred on the Pacific Ocean satellite about 0.3 percent of the time in September, and none greater than 12 dB. Considerably more scintillation with fades greater than 6 dB was observed on the

Indian Ocean satellite, occurring about 3 percent of the time during April and September. Scintillation with fades greater than 12 dB was quite limited, however.

### RECOMMENDATIONS

1. Investigate further the possible lunar influence on the occurrence and intensity of equatorial scintillation. Make a space receiver study of equatorial scintillation over the better part of a year to correlate the variation in occurrence and intensity of scintillation with ionospheric drift velocities and with phases of the moon. Compare ionospheric drift velocities with phases of the moon.
2. Correlate solar activity and geomagnetic activity with scintillation activity and with ionospheric drift velocities.
3. Analyze the above measurements and attempt to identify the factors affecting the occurrence and intensity of equatorial scintillation, and the degree of contribution of each.

## **CONTENTS**

**INTRODUCTION . . .1**

**OBJECTIVES . . .5**

**APPROACH . . .5**

**MEASUREMENT TECHNIQUE . . .5**

**DATA ANALYSIS AND RESULTS . . .6**

Daily occurrence of scintillation . . .6

Diurnal variation of scintillation . . .6

Seasonal variation of scintillation . . .8

Frequency dependence of scintillation . . .10

Elevation angles dependence of scintillation . . .14

Solar dependence of scintillation . . .19

Lunar dependence of scintillation . . .19

Fade duration distributions . . . 22

**SUMMARY . . .27**

**RECOMMENDATIONS . . .28**

**REFERENCES . . .29**

**APPENDIX A:** Total hours each day that uhf scintillation fading exceeded 6 dB and total hours each day that L-band scintillation fading exceeded 3 dB . . . A-1

**APPENDIX B:** Daily diurnal variation of standard deviation/mean resulting from equatorial scintillation at uhf and L-band . . . B-1

**APPENDIX C:** Cumulative fade duration distributions at uhf and L-band for signal levels 6 and 12 dB below the undisturbed signal . . . C-1

## INTRODUCTION

The highly disruptive effects of equatorial scintillation to uhf satellite communications have been recognized since operation at equatorial sites began with TACSAT-1. Many of the characteristics of equatorial scintillation were observed during field tests conducted by Naval Electronics Laboratory Center (now Naval Ocean Systems Center) workers in the early and mid 1970's. The results of these tests are summarized in references 1 and 2.

Scintillation occurs when the satellite signals pass through an ionosphere which has an irregular electron density distribution. These irregularities result in irregularities in the ionospheric refractive index. Refraction or diffraction of the radio wave by this ionosphere results in the radio wave emerging from the ionosphere with a highly irregular wave front. As this wave front propagates to the ground a standing wave pattern is set up. This pattern has regions of signal intensity stronger than the undisturbed signal and regions of weak or no signal at all. As the irregularities in the ionosphere drift and change, the pattern moves past a receiving site on the ground causing the received signal to fluctuate in intensity. Peak-to-peak intensity fluctuations of 40 dB or more are regularly observed at satellite frequencies around 250 MHz.

Figures 1 and 2 show some examples of uhf scintillation. The scintillation in the upper two charts of figure 1 is for two different satellites. This type of scintillation is usually attributed to electron density irregularities in the ionospheric F-region. This region occurs at an altitude of about 200 to 400 kilometres (ref 3).

The bottom chart of figure 1 and those shown in figure 2 are examples of scintillation that is probably caused by electron density irregularities referred to as sporadic-E. These irregularities occur in the E-region at an altitude of about 100 to 120 kilometres. Because of their limited vertical extent they affect only signals, at vhf/uhf frequencies, from satellites at low elevation angles such that the propagation distance through the irregularity region is appreciable.

The charts shown in figure 3 are examples of scintillation at L-band. Here the radio frequency is sufficiently high that a difference in scintillation intensity is observed between the two satellites, with the more intense scintillation occurring on the lower elevation angle satellite where the propagation path through the F-region of the ionosphere is longer (ref 4).

<sup>1</sup> Naval Electronics Laboratory Center TR 1875, Effects of Equatorial Scintillation Fading on SATCOM Signals, by MR Paulson and RUF Hopkins, 8 May 1973.

<sup>2</sup> Naval Ocean Systems Center TR 113, Spatial Diversity Characteristics of Equatorial Scintillation, by MR Paulson and RUF Hopkins, 2 May 1977.

<sup>3</sup> Koster, JR, Equatorial Scintillation, Planetary and Space Science, vol 20, no 12, p 1999-2014, 1972.

<sup>4</sup> Briggs, BH and Parkin, IA, On the Variation of Radio Star and Satellite Scintillations with Zenith Angle, Journal of Atmospheric and Terrestrial Physics, vol 25, p 339-365, 1963.



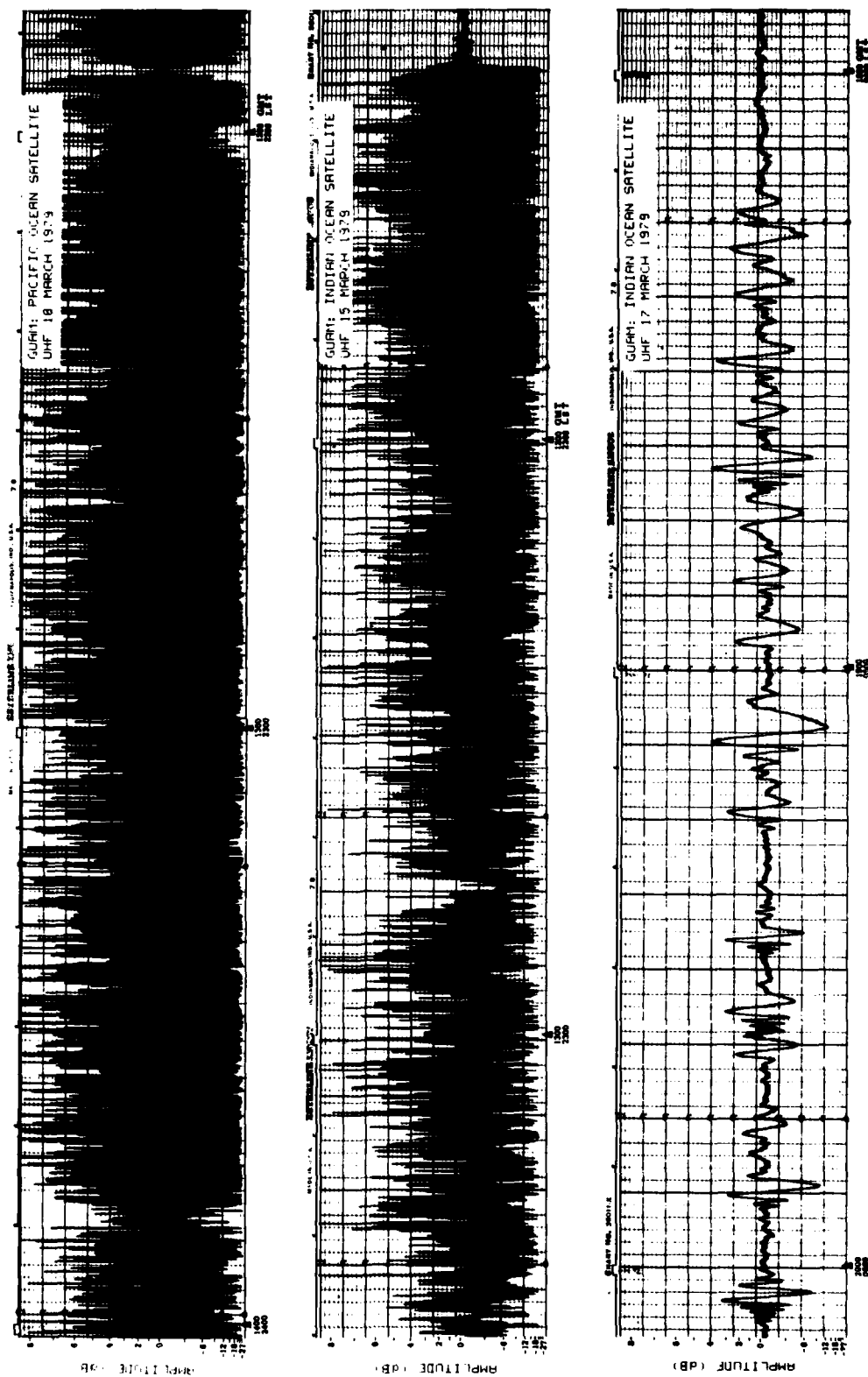


Figure 1. Examples of uhf amplitude scintillation for the Pacific and Indian Ocean satellites. Scintillation shown in bottom graph may have been caused by sporadic-E.

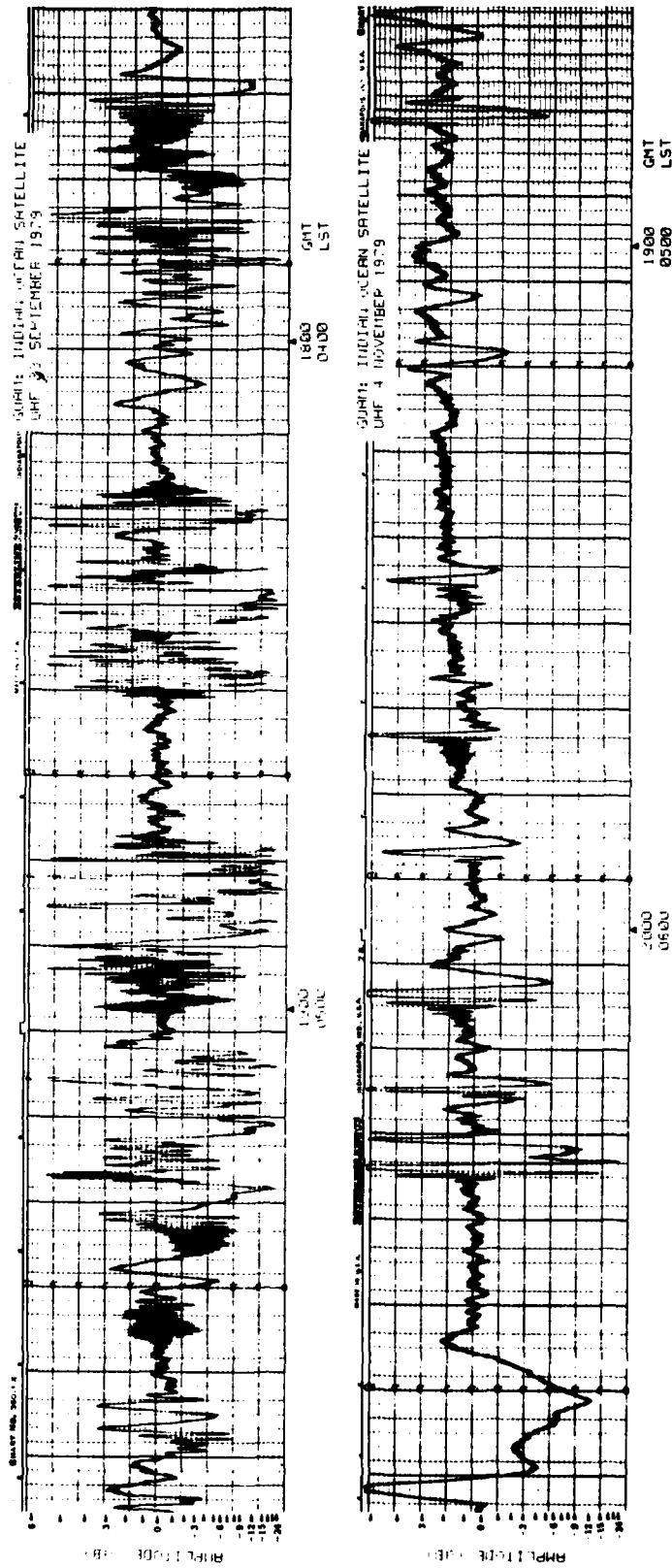


Figure 2. Examples of uhf amplitude scintillation for the Indian Ocean satellite which may have been caused by sporadic-E.

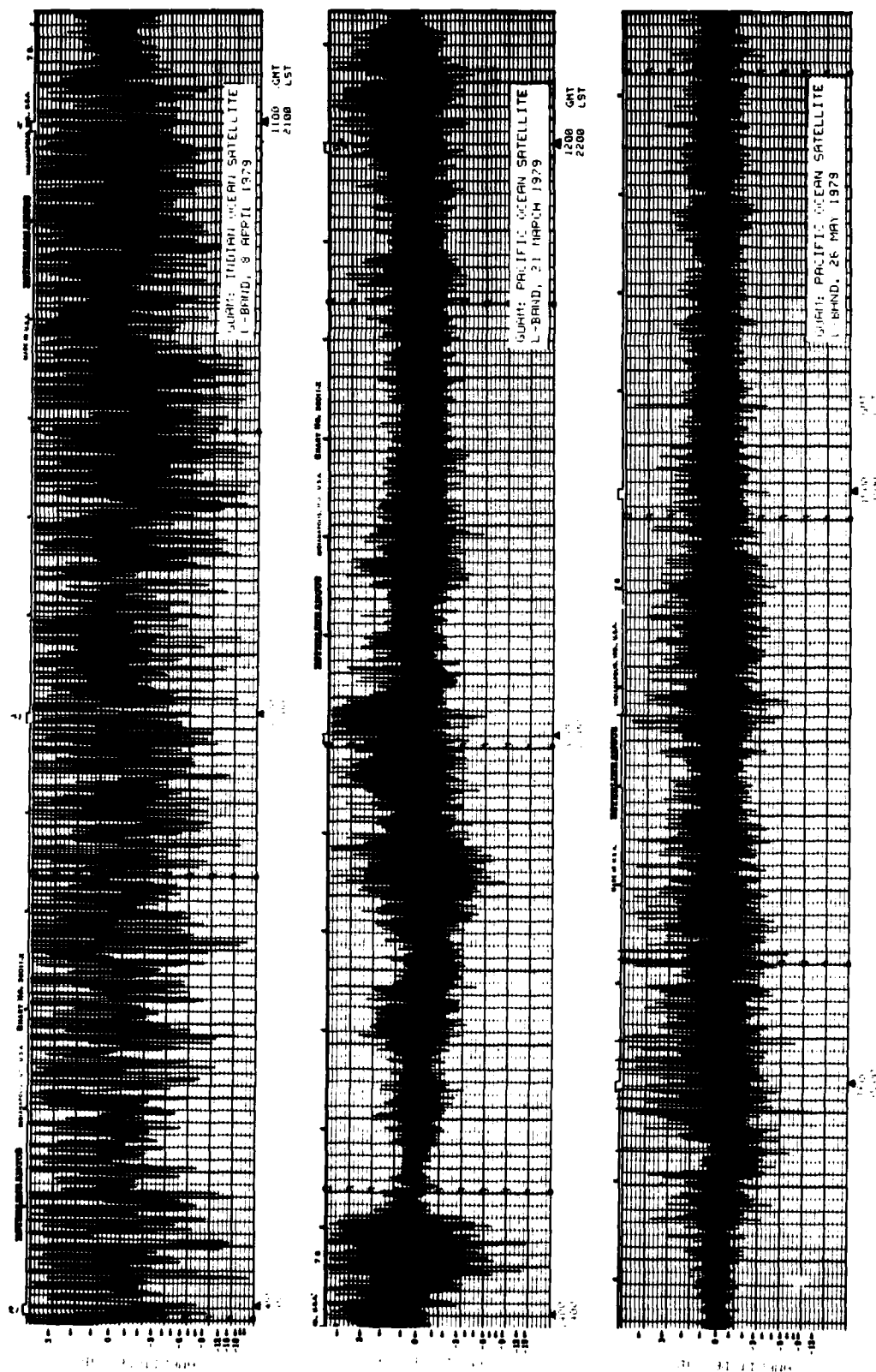


Figure 3. Examples of L-band amplitude scintillation for the Indian and Pacific Ocean satellites.

## OBJECTIVES

The objectives of this program are to obtain long term scintillation data at uhf and L-band frequencies for two satellites at two different elevation angles and to use these data to try to evaluate such things as diurnal and seasonal variations and solar activity dependence of equatorial scintillation for the two frequencies and the two elevation angles.

An additional objective is to try to determine from the data the generating mechanism which produces the ionospheric irregularities.

## APPROACH

Personnel at the Naval Communications Area Master Station (NAVCAMS) in Guam have been recording on strip charts the amplitude of uhf broadcast signals from two of the MARISAT/GAPFILLER satellites continuously since March 1978 to provide the long term data needed. Much of their data was reported in reference 5, but the signals are continuing to be recorded.

One of the satellites is positioned over the Indian Ocean, which gives it an elevation angle from Guam of about 10 degrees; the other is over the Pacific Ocean with an elevation angle of about 50 degrees.

In order to provide information on scintillation at L-band frequencies and to provide the capability for a more detailed analysis of the scintillation data, personnel at the NASA Tracking Station in Dandan, Guam recorded for us the uhf and the L-band signals from each of the two satellites on analog magnetic tape recorders in parallel with strip chart recorders. These recordings were made for the period from late February through December 1979.

This report is primarily concerned with the data recorded at the NASA Tracking Station. However, some of the data recorded at the NAVCAMS will be used as well.

## MEASUREMENT TECHNIQUE

The amplitudes of the uhf and the L-band signals were recorded from each satellite on strip chart recorders 24 hours a day. During the day the recorders were run at 3 inches per hour and at night at 12 inches per hour. Time marks were automatically put on the charts at 10-minute and at hourly intervals.

Analog magnetic tape recorders were operated in parallel with the strip chart recorders at night from 0900 to 1700 GMT (1900 to 0300 LST). An IRIG-B time code was recorded on one of the channels. Each night, before the tape recorders were started, receiver tuning was checked and the signal level set to a predetermined level.

Although scintillation occasionally started before 0900 GMT and at times continued past 1700 GMT, these occurrences were not recorded on the tape, since the recording time for one tape was 8 hours and a second tape was not run. All of the scintillation data were recorded on the strip charts, however.

---

<sup>5</sup> Naval Ocean Systems Center TR 446, Scintillation of Uhf SATCOM Signals, by MR Paulson, 15 August 1979.

## DATA ANALYSIS AND RESULTS

### DAILY OCCURRENCE OF SCINTILLATION

Starting times and ending times for uhf scintillation with fades greater than 6 dB were read from the strip charts for each of the satellites. These times were summed on a daily basis to give the total number of hours each day that scintillation fading exceeded 6 dB. No attempt was made to distinguish between F-region scintillation and sporadic-E scintillation for the low elevation angle satellite. The results are shown for the Indian Ocean satellite in the top graph of figure 4 and for the Pacific Ocean satellite in the middle graph. Results are also shown in detail in appendix A. The bottom graph shows the measured daily 2800-MHz solar flux (ref 6).

Figure 5 shows a cross correlation between the occurrence of scintillation for the Indian Ocean satellite and for the Pacific Ocean satellite. There is a maximum correlation of 0.64 at zero delay. This indicates that when scintillation was seen on one satellite for any given night it was probably observed on the other as well. Also, when the duration of the scintillation was long on one satellite, it tended to be long on the other. Probably the correlation is not higher because the ionospheric penetration points for the two satellites are on the order of 1600 kilometres apart. Also, the Indian Ocean satellite, because of its low elevation angle, has a longer propagation path through the ionosphere, and can also be affected by sporadic-E at times.

Daily total hours of scintillation with fades greater than 3 dB and with fades greater than 6 dB were also determined for the two satellites at L-band. These daily values are shown in appendix A for the 3-dB level. Since the occurrence was quite low at 6 dB these have not been plotted.

### DIURNAL VARIATION OF SCINTILLATION

The magnetic tapes were digitized for periods of scintillation as shown by the strip charts without regard for the intensity of the scintillation. In general, the digitizing was started just prior to the first start of uhf scintillation and was done continuously past the final scintillation occurrence or until the tape ran out. The L-band data were also digitized for the same periods. The digitized tapes were then processed using 15-minute sample intervals, and standard deviation divided by the mean was calculated for each sample as an indication of scintillation intensity. These were plotted as a function of time of night for each satellite and for both uhf and L-band. (See figure 6.) The rest of the data are plotted in appendix B. Unless otherwise stated, on days that are missing there was no scintillation. The upper curve, as seen in figure 6, is for the uhf and the lower one is for the L-band.

Since the magnetic tape records were linear in voltage, the standard deviation divided by the mean plotted in these graphs is not the same as the commonly used S4 index. A comparison of the two is shown in figure 7 for one night of data. A straight-line fit to the plot gives

$$S4 = 0.0026 + 1.947 (\text{Standard Deviation}/\text{Mean})$$

with a goodness-of-fit correlation of 0.9994.

<sup>6</sup> Solar-Geophysical Data, Prompt Reports, National Oceanic and Atmospheric Administration Environmental Data and Information Service, Boulder, CO.

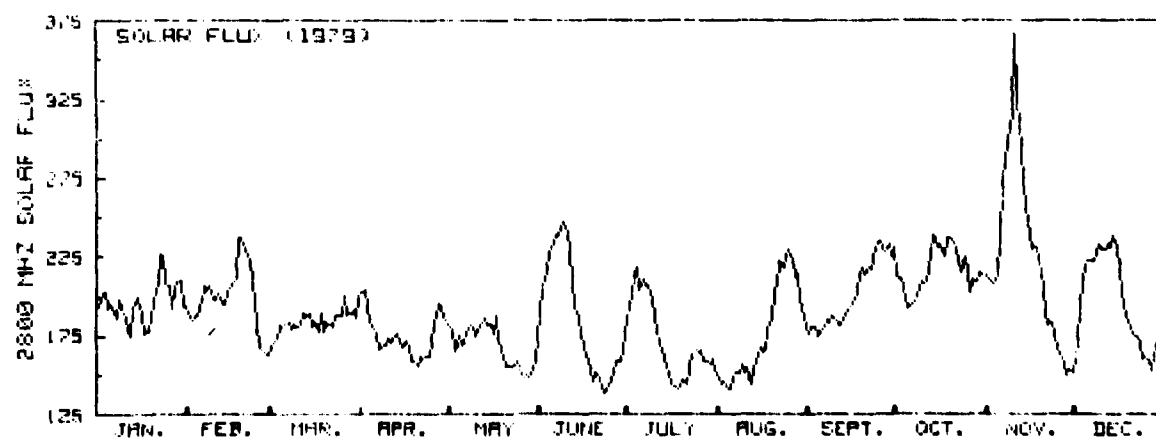
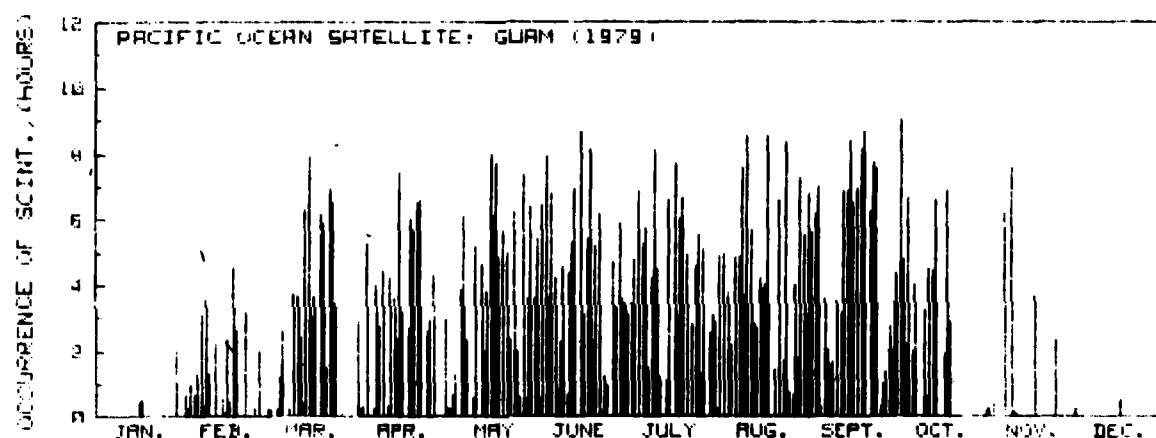
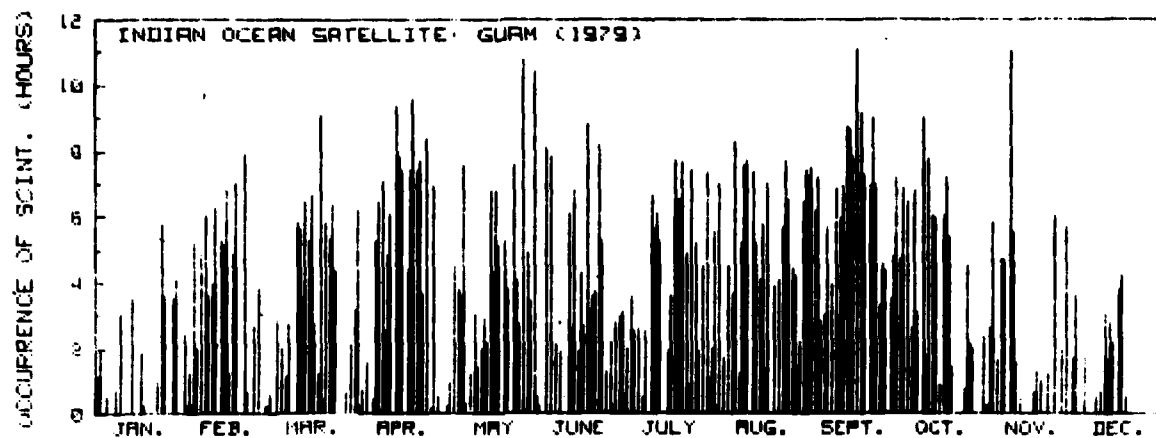


Figure 4. Total hours each day that uhf scintillation fading exceeded 6 dB. Bottom graph is the daily value of the 2800-MHz solar flux measurement.

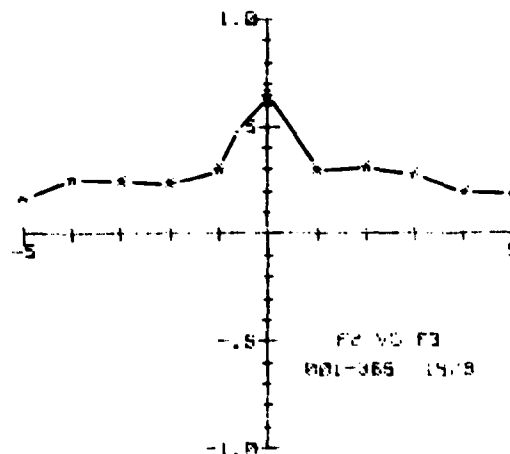


Figure 5. Cross correlation between the daily occurrence of uhf scintillation on the Indian and Pacific Ocean satellites as shown in the upper two graphs in figure 4.

In order to get an indication of the diurnal variation of uhf scintillation intensity, values of Standard Deviation/Mean were averaged for each month for each 15-minute time interval during the night. These smoothed curves of intensity versus time of night are shown in figure 8 for the months of March through November for each satellite.

Onset time of the scintillation for the Indian Ocean satellite was usually around 2030 to 2100 LST from March through August, but closer to 2000 LST during September through November. Onset of scintillation was around 1930 to 2000 LST for March through August for the Pacific Ocean satellite but about 1900 LST during September and October. These times are probably related to the local times for sunset at F-region heights for each of the propagation paths. This time is about an hour different for the two satellites, with sunset occurring on the Pacific Ocean satellite path first.

There does not appear to be a specific time when scintillation intensity reaches a maximum. A broad maximum usually occurred sometime between 2200 and 0100 LST. This is probably because the scintillation is at a saturation level much of the time. The scintillation also frequently continued past the 0300 LST end of the magnetic tape.

An average of nine days of relatively intense L-band scintillation which occurred in April is shown in figure 9. Here the scintillation intensity appears to be centered around 2330 LST. However, this could change with the addition of more data.

### SEASONAL VARIATION OF SCINTILLATION

Sixty-one days' running averages of the data shown in figure 4 were calculated and plotted in figure 10 to investigate the seasonal variation of equatorial scintillation. These curves show a minimum in the occurrence of scintillation during December and January, with the occurrence increasing rapidly in February and March to a broad maximum through the summer and decreasing again in October and November.

Some asymmetry is evident, with a higher occurrence being seen in September than in the March-April period. This is particularly noticeable on the Indian Ocean satellite

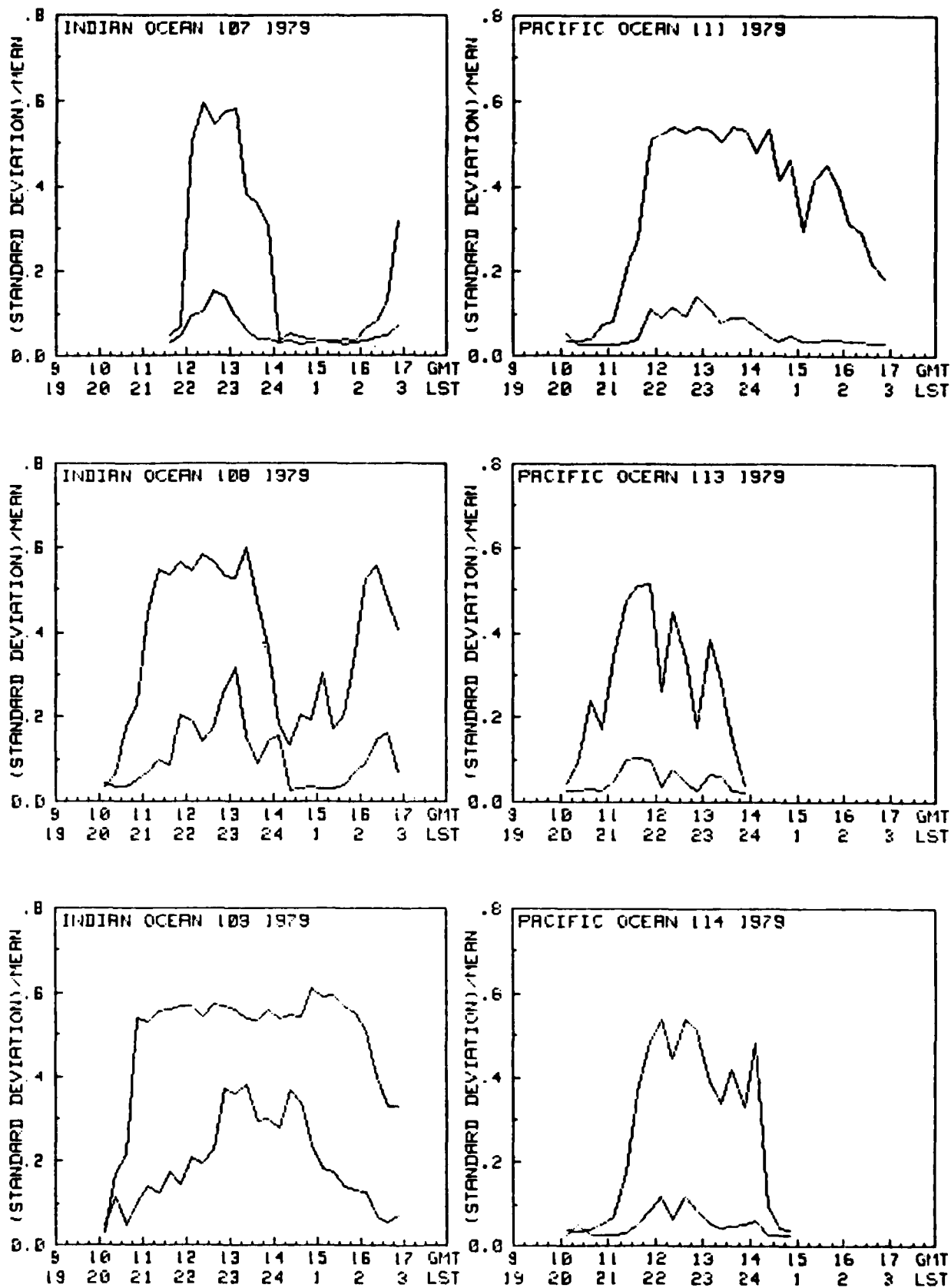


Figure 6. Examples of daily variation of Standard Deviation/Mean for the Indian and Pacific Ocean satellites for both uhf and L-band. The higher curve is the uhf.



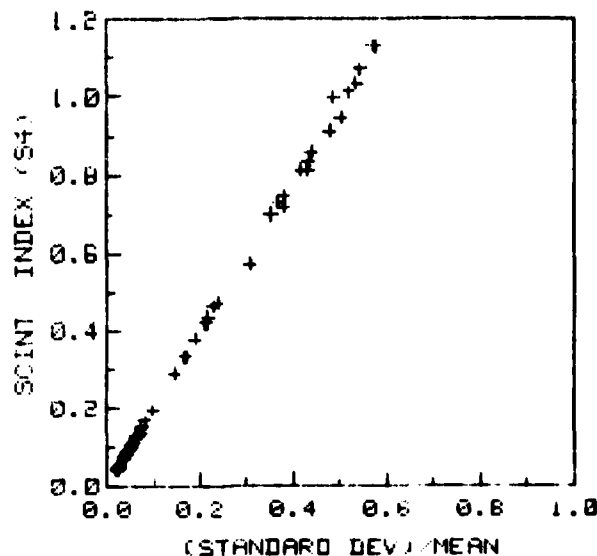


Figure 7. Comparison of Standard Deviation/ Mean to scintillation index, S4, for one night of data.

plot. This may be a result of variation in solar activity. In the bottom graph, which is a sixty-one day running average of the 2800-MHz solar flux, the smoothed solar activity decreases from late January through the middle of July, then increases rapidly through the middle of October.

Another way of showing the seasonal variation of scintillation is plotted in figure 11. Here the hours of scintillation occurrence when fading exceeded 6 dB are totaled for each month and shown as the percent of time that scintillation occurred that month. The results are quite similar to figure 10, with the occurrence being somewhat higher in September than in March or April.

When the percent occurrence of scintillation is determined on a monthly basis for L-band, a double peak in the occurrence is observed. Figure 12 shows the percent of occurrence for fades greater than 3 dB and figure 13 shows the same thing for fades greater than 6 dB. Maxima are in April and September for fades greater than 3 dB for both satellites, with a somewhat higher occurrence in September. The same holds true for fades greater than 6 dB for the Indian Ocean satellite, but in the case of the Pacific Ocean satellite the occurrence was probably too small to be statistically significant.

## FREQUENCY DEPENDENCE OF SCINTILLATION

One way to get a frequency dependence for scintillation is to compare the scintillation intensity at two or more frequencies for the same time period and the same propagation path. In theory, one can then deduce an equation for scintillation intensity in terms of radio frequency. This has been done by quite a few people (ref 7).

This approach is not very useful, however, when the frequencies are as widely spaced as they are here. Looking at figure 6 we see that the uhf scintillation appears to

<sup>7</sup> Crane, RK, Ionospheric Scintillation, Proceedings of the IEEE, vol 65, no 2, p 180-199, February 1977.

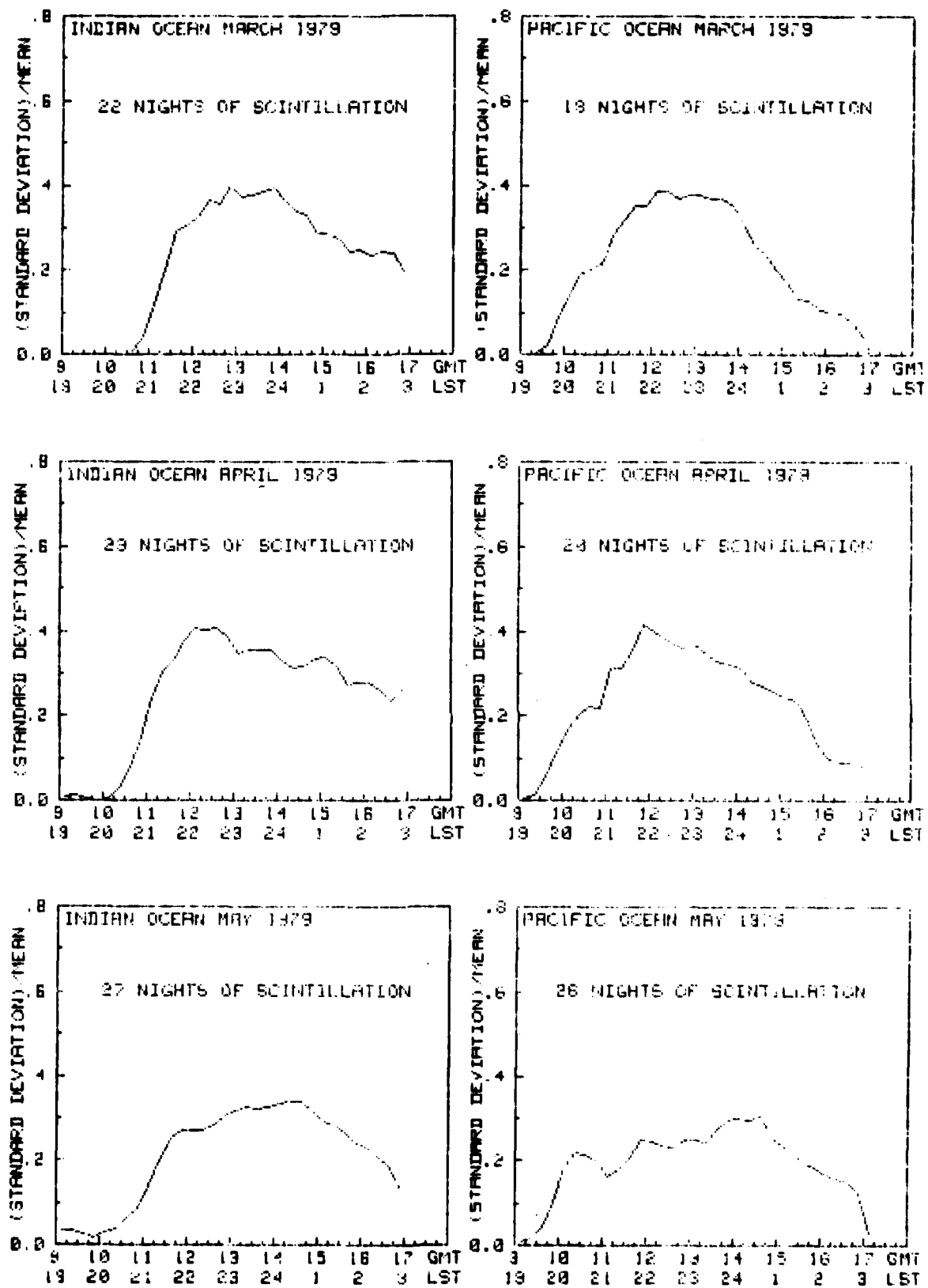


Figure 8. Monthly averages of diurnal variation of Standard Deviation/Mean for the two satellites at uhf.

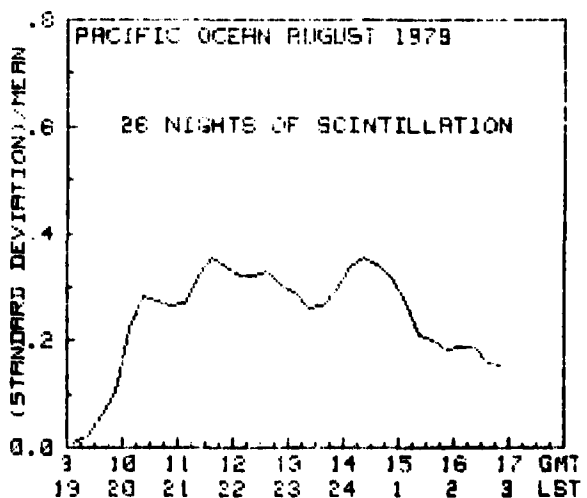
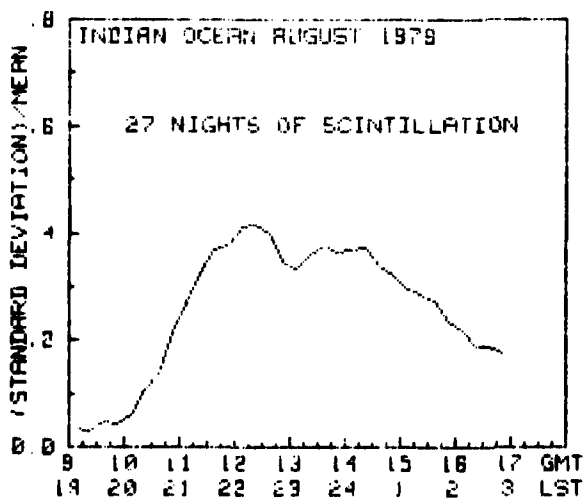
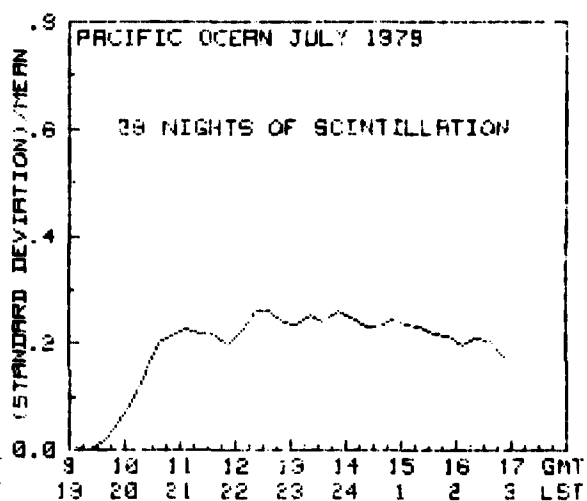
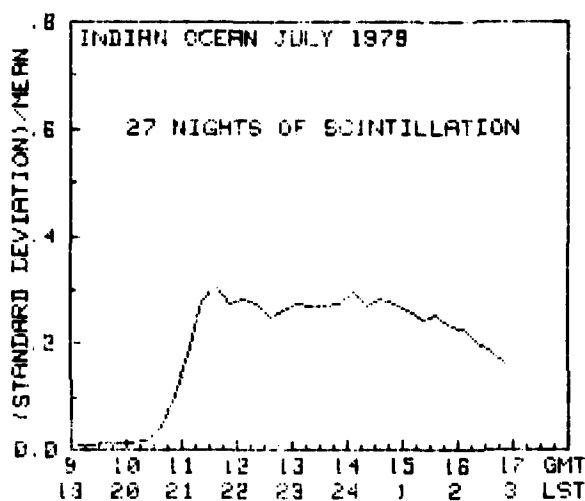
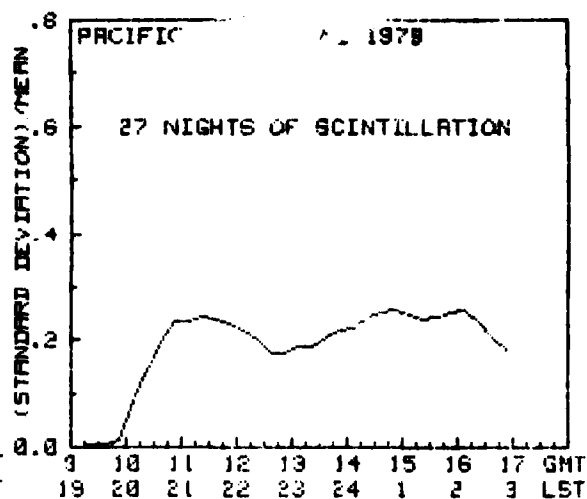
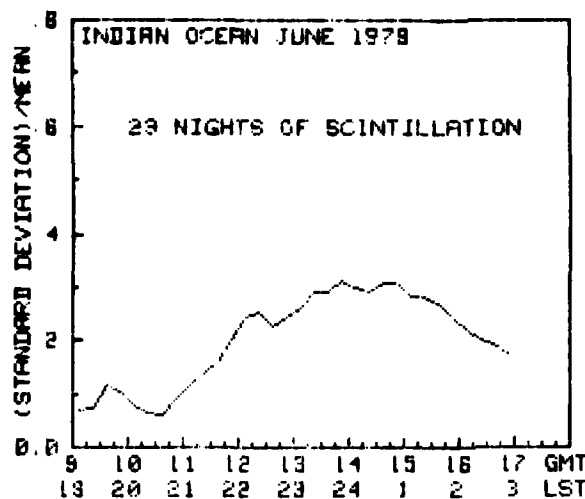


Figure 8. (continued)

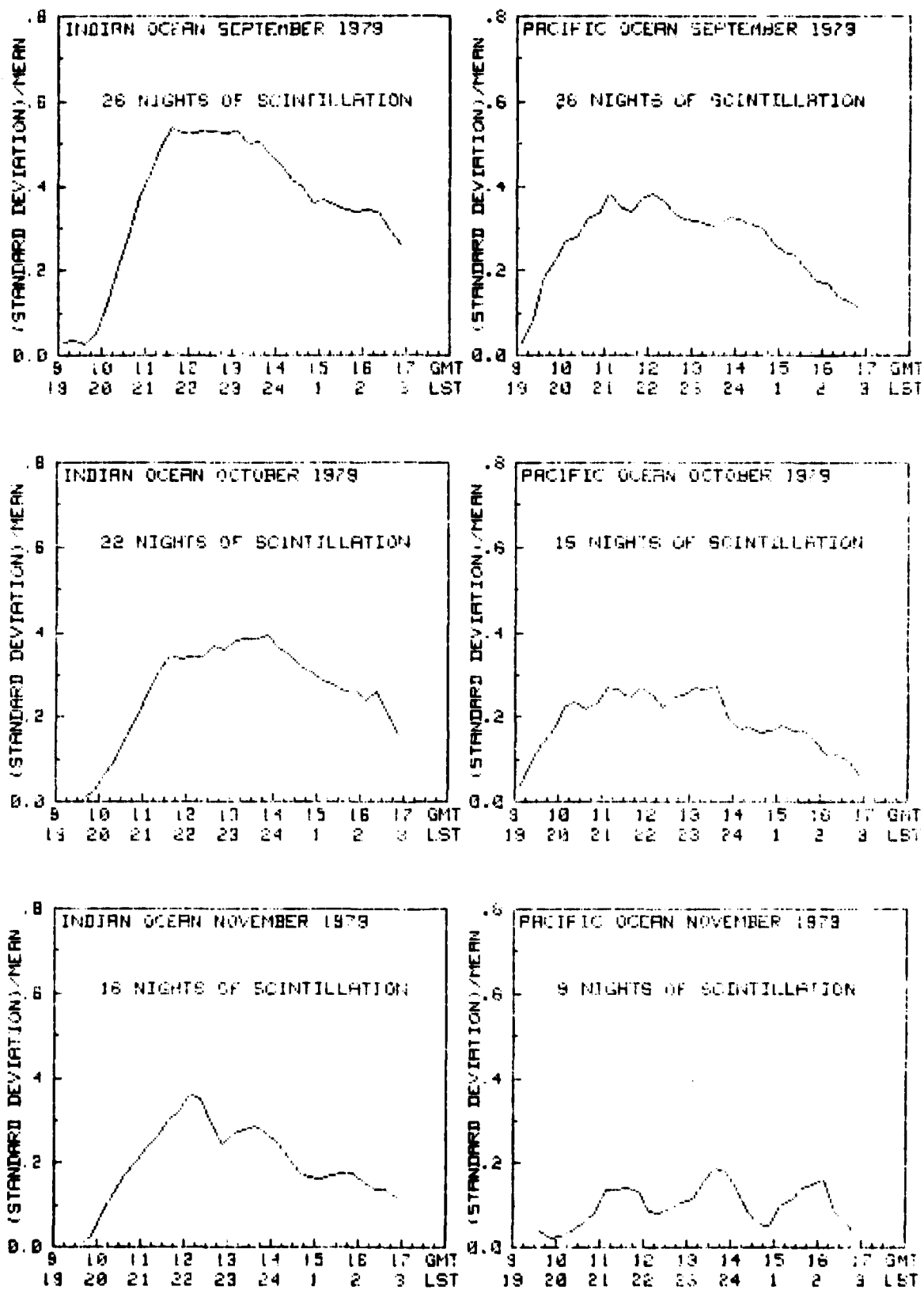


Figure 8. (continued)

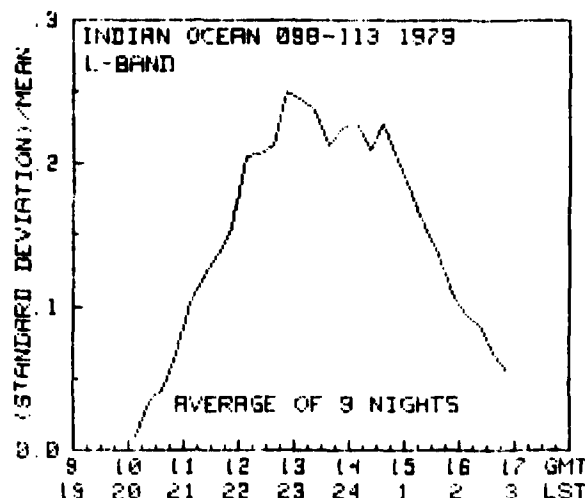


Figure 9. Average diurnal variation of Standard Deviation/Mean for the Indian Ocean satellite at L-band using 9 nights of relatively intense scintillation.

reach a limit, or saturation, much of the time while the L-band scintillation intensity is quite variable.

To get some idea of the system improvement that might be expected at L-band as compared to frequencies around 250 MHz we can compare the occurrence of scintillation with fades greater than 6 dB for the two frequencies. For the Indian Ocean satellite uhf scintillation occurred 14.8 percent of the time period from 1 March through 30 November 1979. During this same time period, L-band scintillation occurred 0.94 percent of the time. On the Pacific Ocean satellite for the period 1 March through 20 October 1979 uhf scintillation occurred 12.3 percent of the time and L-band 0.11 percent of the time.

#### ELEVATION ANGLES DEPENDENCE OF SCINTILLATION

A theory to describe how scintillation intensity varies with zenith angle has been developed by Briggs and Parkin (ref 4). This theory is not applicable to much of the scintillation which occurs in equatorial regions, however. In the case of frequencies around 250 MHz, the scintillation intensity reaches saturation much of the time at all elevation angles. To express scintillation intensity as a function of zenith angle in this case would not be very useful.

The theory would probably apply to the scintillation at L-band, but a difficulty arises in just how to apply it. The scintillation at the two elevation angles occurred at two locations in the ionosphere about 1600 kilometres apart. Also, the scintillation did not necessarily occur at the same time, and possibly not even the same night.

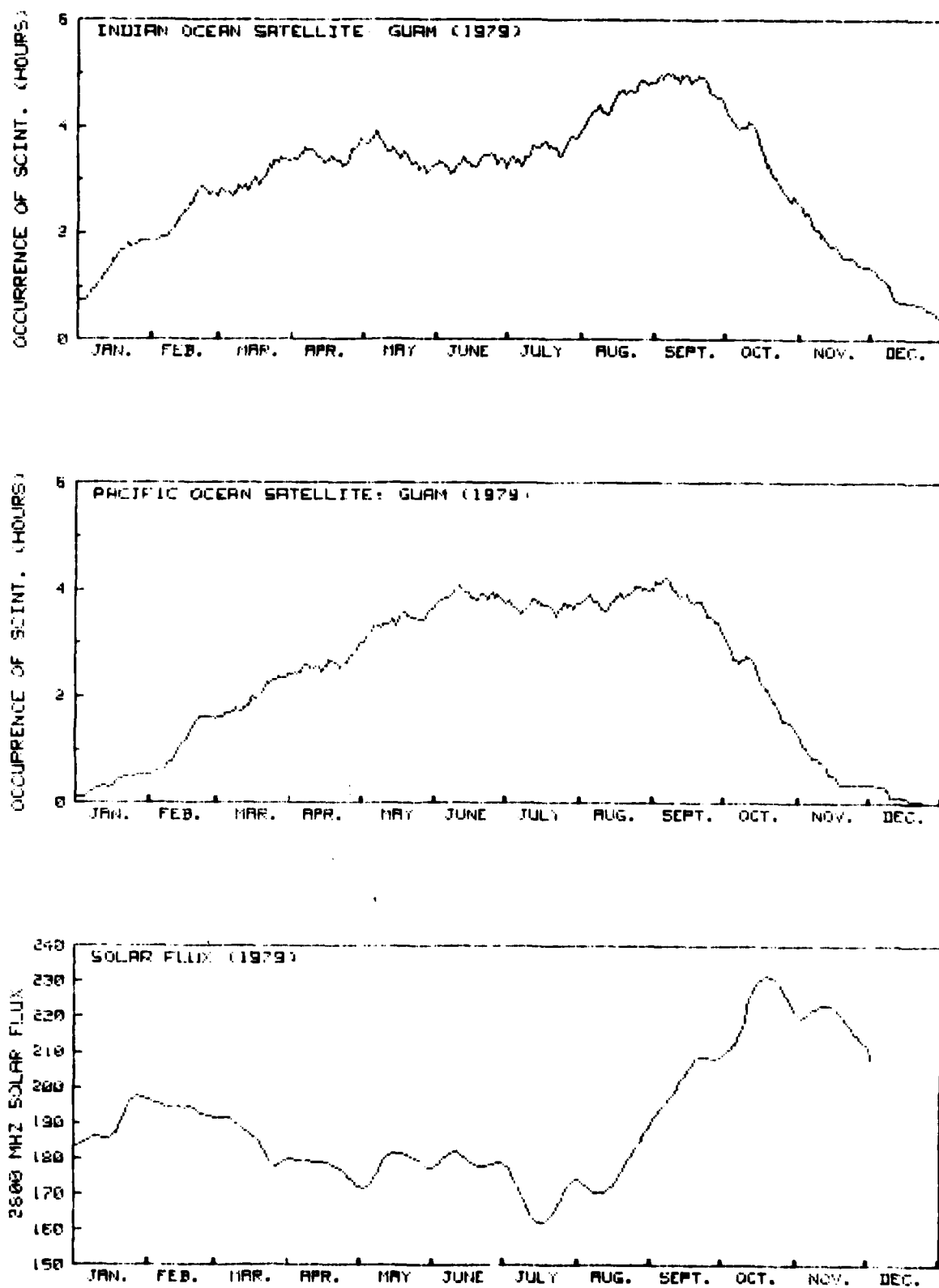


Figure 10. Sixty-one-day running averages of daily occurrences of uhf scintillation for the two satellites. Bottom graph is 61-day running average of the 2800-MHz solar flux.

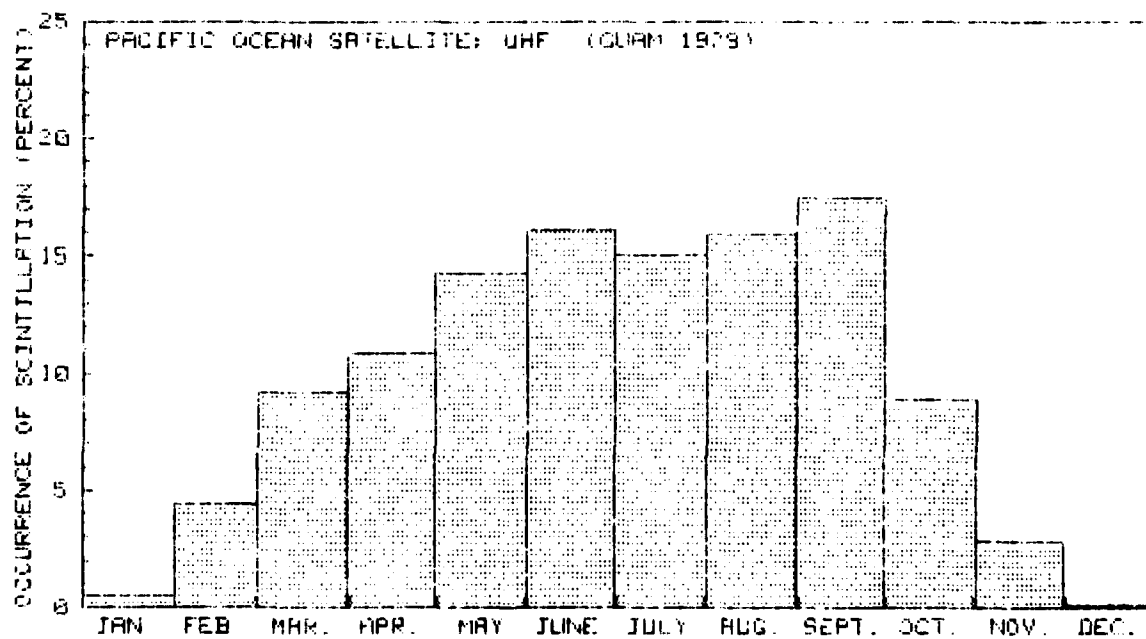
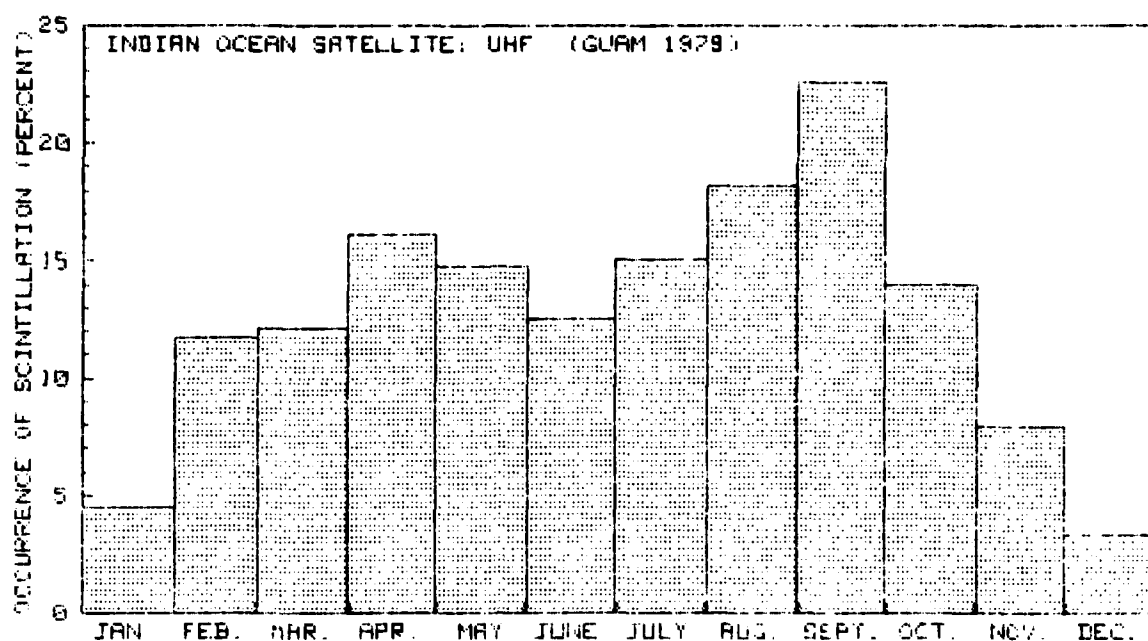


Figure 11. Monthly percent of time uhf scintillation occurred with fades greater than 6 dB for the two satellites.

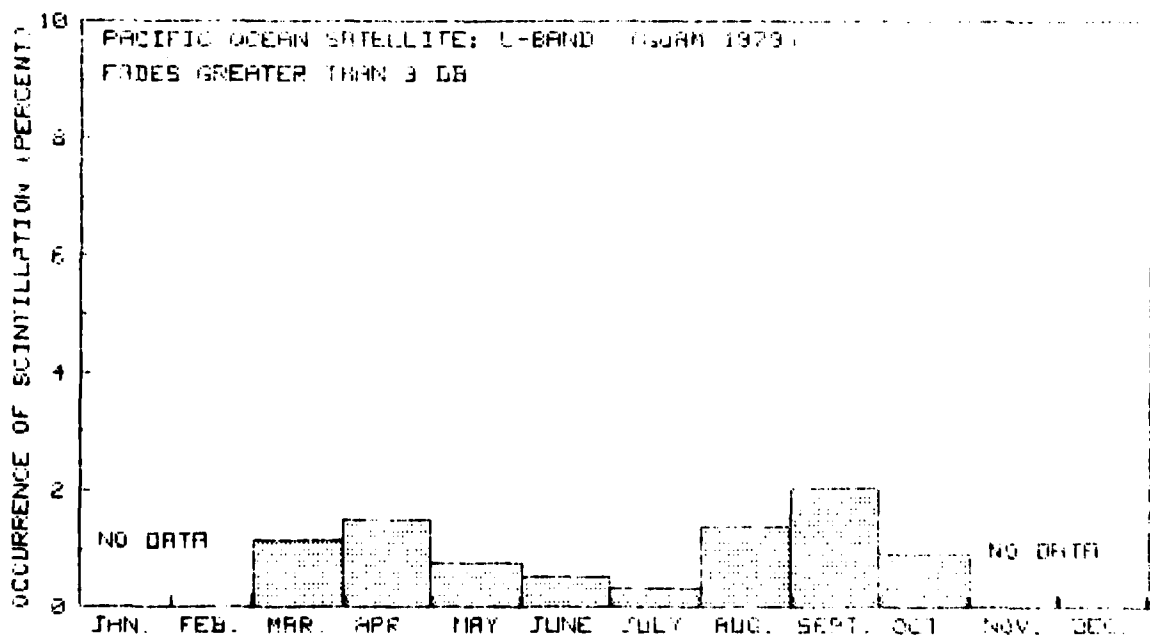
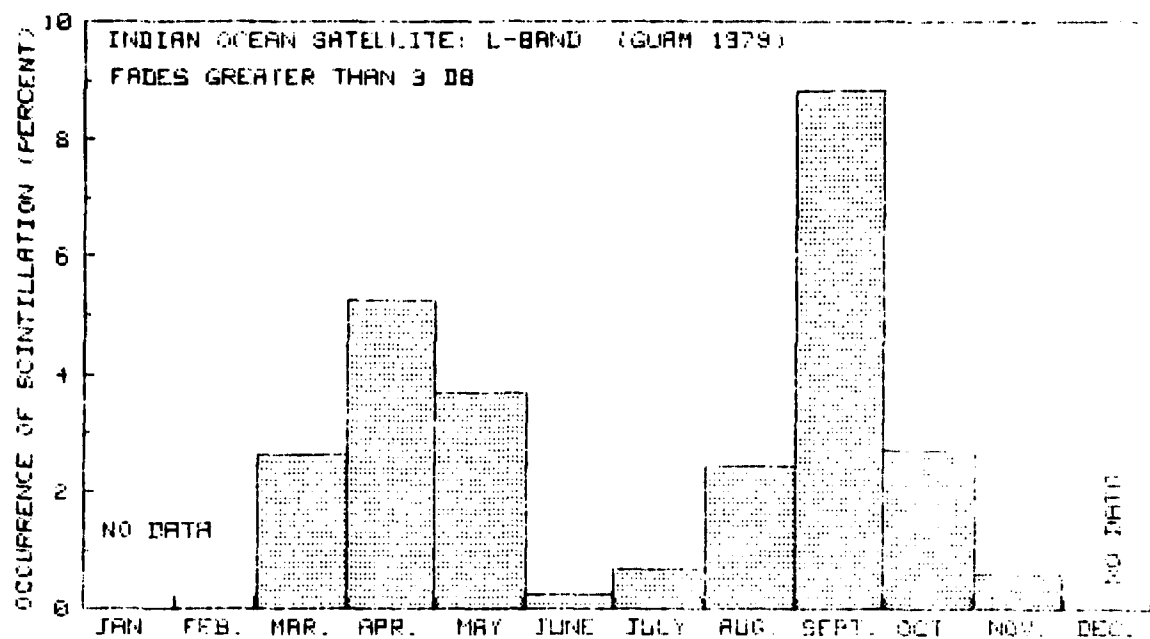


Figure 12. Monthly percent of time L-band scintillation occurred with fades greater than 3 dB for the two satellites.



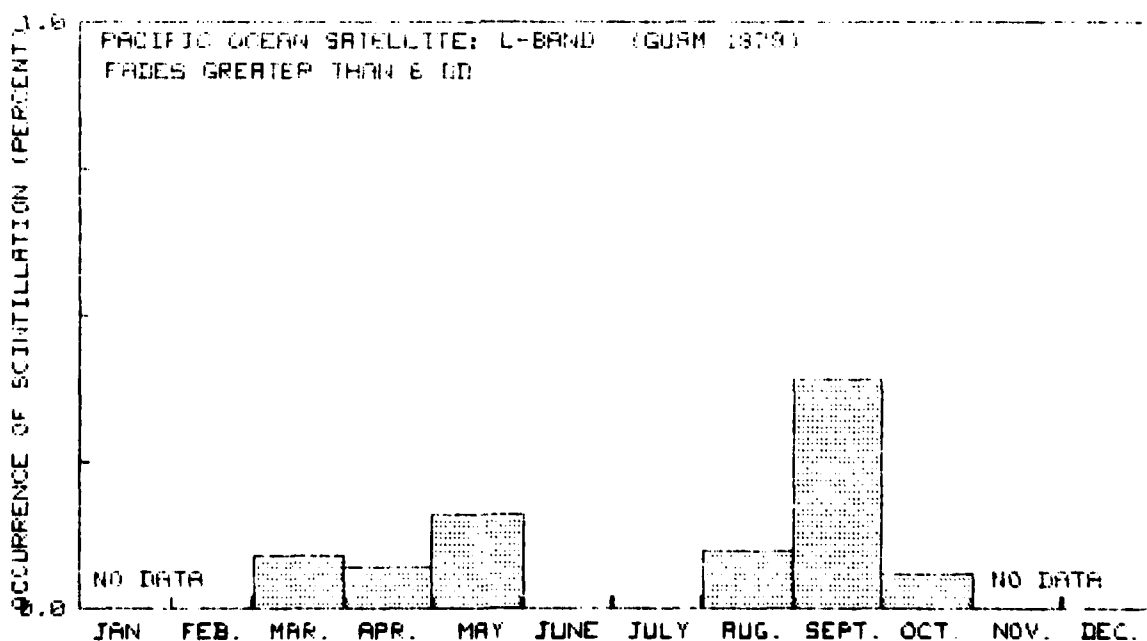
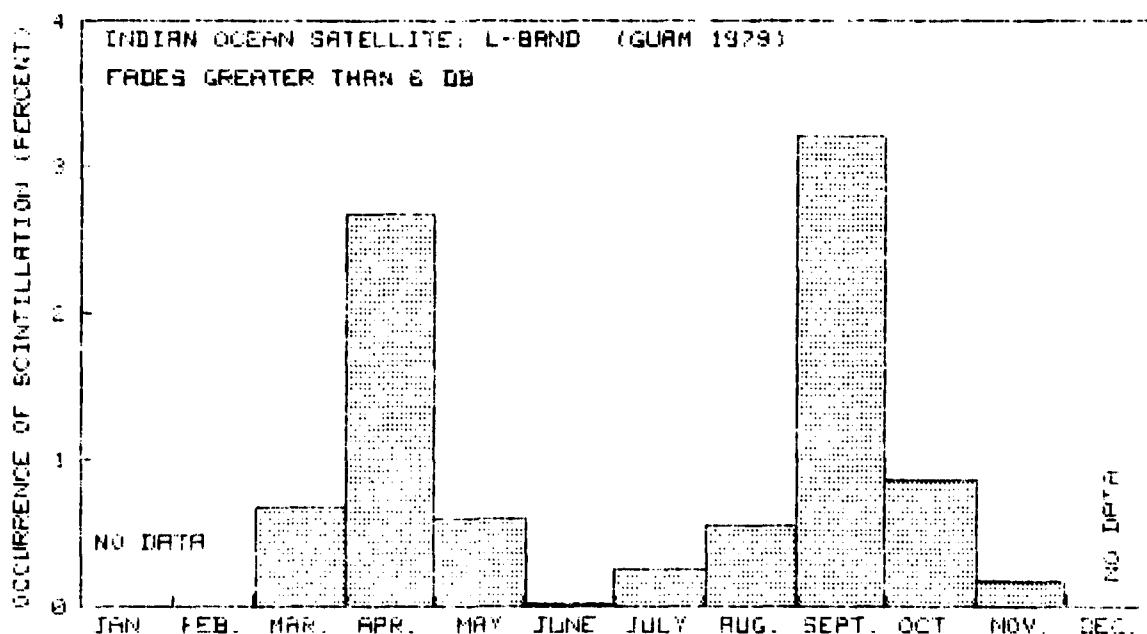


Figure 13. Monthly percent of time L-band scintillation occurred with fades greater than 6 dB for the two satellites.

To get some indication of how the elevation angle affected the scintillation, we can again use the occurrence of scintillation with fades greater than 6 dB. For the uhf during the period 1 January through 31 December 1979 the occurrence was 12.7 percent for the Indian Ocean satellite and 9.7 percent for the Pacific Ocean satellite. At L-band this becomes 1.1 percent for the Indian Ocean satellite and 0.11 percent for the Pacific Ocean satellite, for the period 1 March through 20 October 1979.

### **SOLAR DEPENDENCE OF SCINTILLATION**

The daily hours of occurrence of scintillation for each of the satellites, shown in the upper two graphs of figure 4, have been correlated with the daily solar flux values shown in the bottom graph of figure 4. The resulting correlations are shown in figure 14, where F2 is the Indian Ocean satellite and F3 is the Pacific Ocean satellite. The data have been lagged 10 days in each direction even though it was not expected that any change in scintillation activity would lead to a change in solar activity. What correlation there is, is negative, and does not appear to be significant.

A year-to-year dependence of scintillation on solar activity was reported in reference 5. A common 11-day period was used for each of 5 years and percent occurrence of scintillation was plotted against the average 2800-MHz solar flux value for the period. The results showed a good linear dependence of the occurrence of scintillation on the solar flux. The curve is reproduced in figure 15 along with the corresponding data point for 1979. This point is well off the line generated by other data points. One possible explanation for this is that, when using a 6-dB fading margin as a criterion, the occurrence of scintillation may approach a limiting value as solar activity increases.

Alternatively, there may be other factors influencing the occurrence of scintillation. It was reported in reference 5 that, when the occurrence of scintillation for different years was plotted on a monthly basis against solar activity, some months showed good linear dependence while others showed no consistent dependence at all.

Another possible explanation is that there is a time lag between a change in solar and a change in scintillation activity; and when solar activity is changing rapidly, as it did in this case, the scintillation activity has not caught up. When average values for the full month of September are used the point falls much closer to the line.

### **LUNAR DEPENDENCE OF SCINTILLATION**

Running averages were calculated for the scintillation data in figure 4 to try to identify other possible causes affecting the occurrence of scintillation. Running averages ranging from 5 to 30 days were used. Figure 16 shows a plot for each of the satellites using a running average of 11 days. A pronounced periodicity is seen in these curves, particularly for the first half of the year. A spectrum analysis of the data showed a line with a period around 30 days, suggesting that this periodicity might be connected with the phases of the moon. To investigate this, a sine wave plot is superimposed on these curves to show the moon phases, with the maximum corresponding to full moon and the minimum to a new moon.

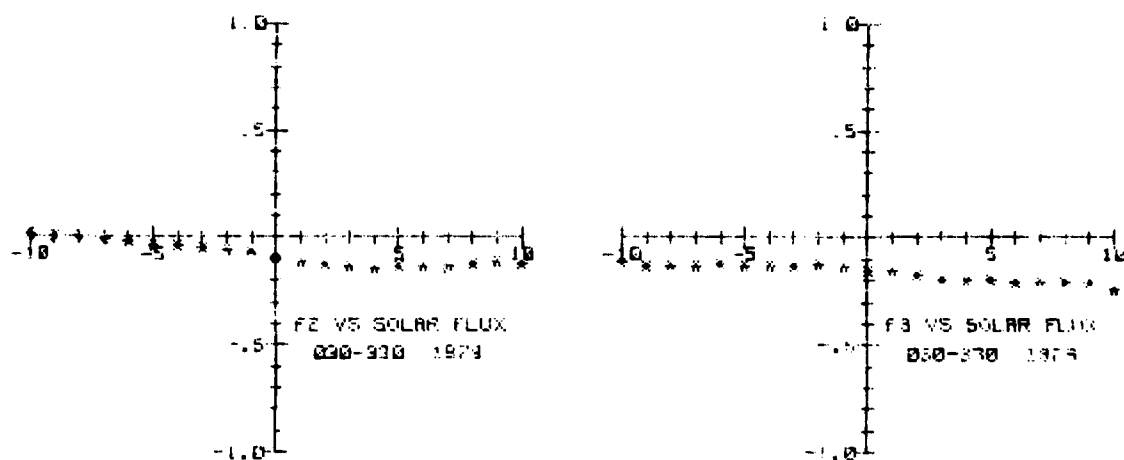


Figure 14. Cross correlation between daily occurrence of uhf scintillation with fades greater than 6 dB for each satellite and the daily 2800-MHz solar flux measurement. F2 is the Indian Ocean satellite and F3 is the Pacific Ocean satellite.

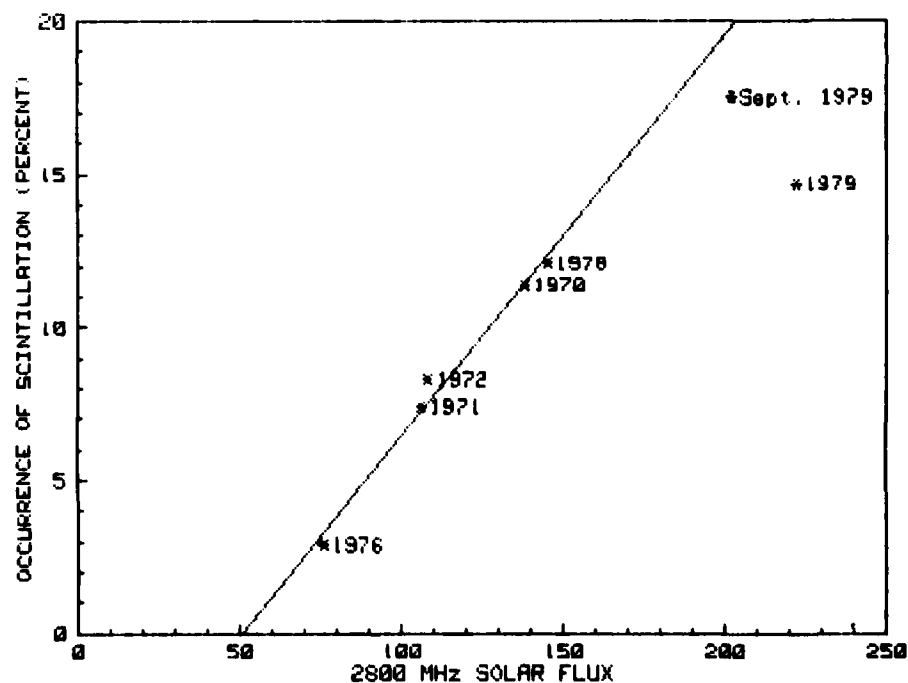


Figure 15. Occurrence of uhf scintillation during a common 11-day period compared to the average 2800-MHz solar flux for the same period. Point labeled Sept. 1979 was for the whole month of September.

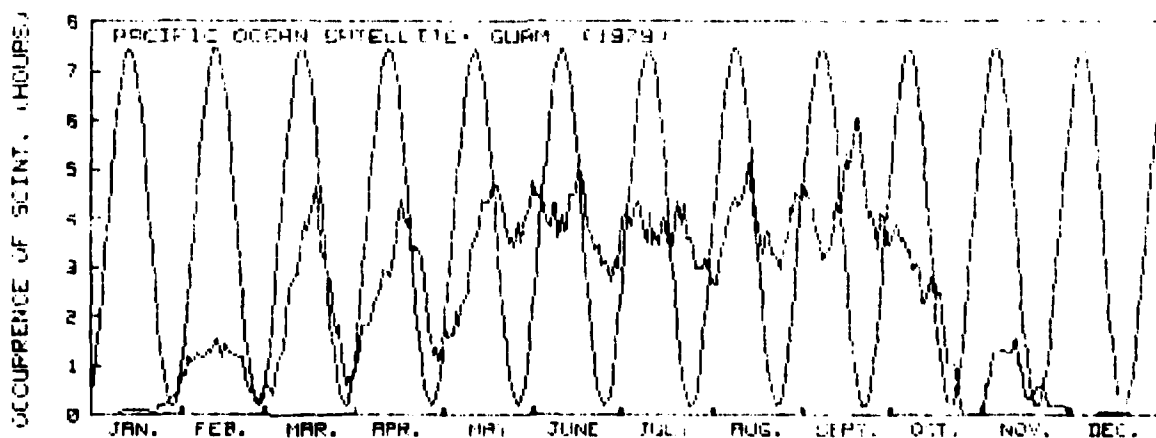
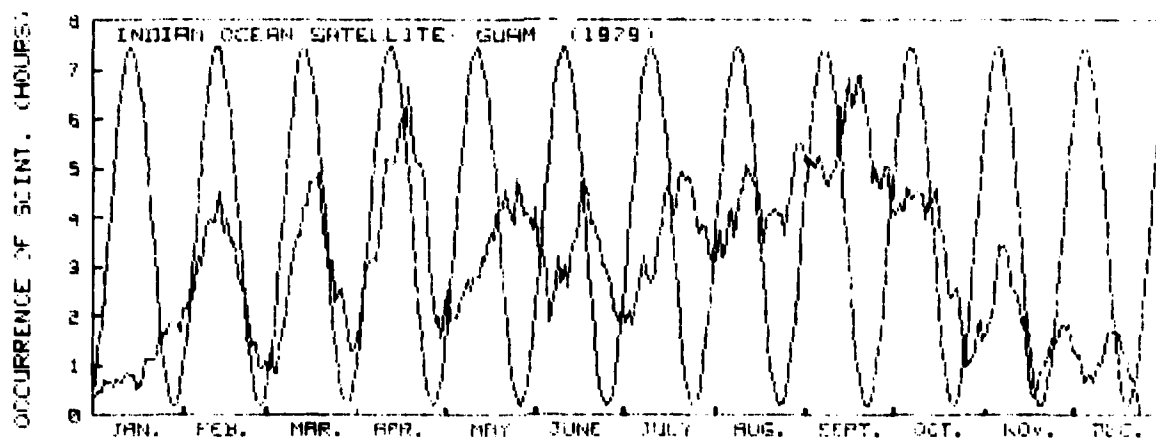


Figure 16. Eleven day running averages of the occurrences of scintillation data shown in figure 4 with the phases of the moon superimposed.

Cross correlations were calculated between phases of the moon and the scintillation curves for progressively larger segments of the scintillation data. These are shown in figure 17, where F2 is the Indian Ocean satellite and F3 is the Pacific Ocean satellite. Using data from 30 January through 30 May the correlation is 0.7 or better and the maximum occurrence of scintillation is 3 or 4 days after full moon. Using data between 30 January and 29 June the correlation is somewhat lower, between 0.5 and 0.6. When data between 30 January and 26 November are used the correlation values are between 0.4 and 0.5 and the maximum occurs about 5 days after full moon.

On the chance that using the 6-dB fading criterion for determining when scintillation occurs is not a sensitive enough indicator, the values of standard deviation/mean for 15-minute sample periods were summed for each night and used in the same way. Running 11-day averages were calculated and are shown for each satellite in figure 18 with the phases of the moon superimposed. Cross correlations between phases of the moon and these curves gave values nearly identical to those shown for the curves in figure 16.

From the preceding discussion it appears that the moon had a very strong influence on the occurrence and intensity of the scintillation. This is particularly true during the first half of the year. From July through October an additional factor appears to have become important, or the lunar influence may have become less.

In an earlier report (ref 8) this author suggested that turbulence resulting from zonal winds generated the irregularities in the ionospheric electron density which caused equatorial scintillation. If this is the case, then it can be argued that the moon's gravitational field can influence equatorial scintillation by increasing or decreasing the zonal wind, depending on the location of the moon. Around full moon, when the moon is on the night side of the earth, its gravitational attraction would tend to increase zonal winds. Around new moon, when the moon is on the day side of the earth, it would tend to reduce the zonal winds.

Misra (ref 9) has reported a lunar effect on the horizontal ionospheric drift at the equator. His study covers the years from 1964 to 1969. Figure 2 of reference 9 shows his results for the F-region. He says that the F-region showed a significant lunar tide in winter and summer for the 08-10 and 14-16 solar hour groups, and was most clear at 1100 hours for all seasons as well as for the annual plot. He appears to limit his investigation to three time groups during the day, however; no nighttime information is available.

#### FADE DURATION DISTRIBUTIONS

Cumulative fade duration distributions have been calculated for fade durations below 6 and below 12 dB down from the undisturbed signal. This has been done for each satellite at both uhf and L-band for a number of nights. The results are shown in appendix C.

<sup>8</sup> Naval Ocean Systems Center TR 290, Zonal Winds as a Generating Mechanism for the Ionospheric Irregularities that Cause Equatorial Scintillation of Satellite Signals, by MR Paulson, 26 June 1978.

<sup>9</sup> Misra, RK, Lunar Tidal Oscillations in the Horizontal Ionospheric Drift at the Equator, Planetary and Space Science, vol 21, p 1109-1114, 1973.

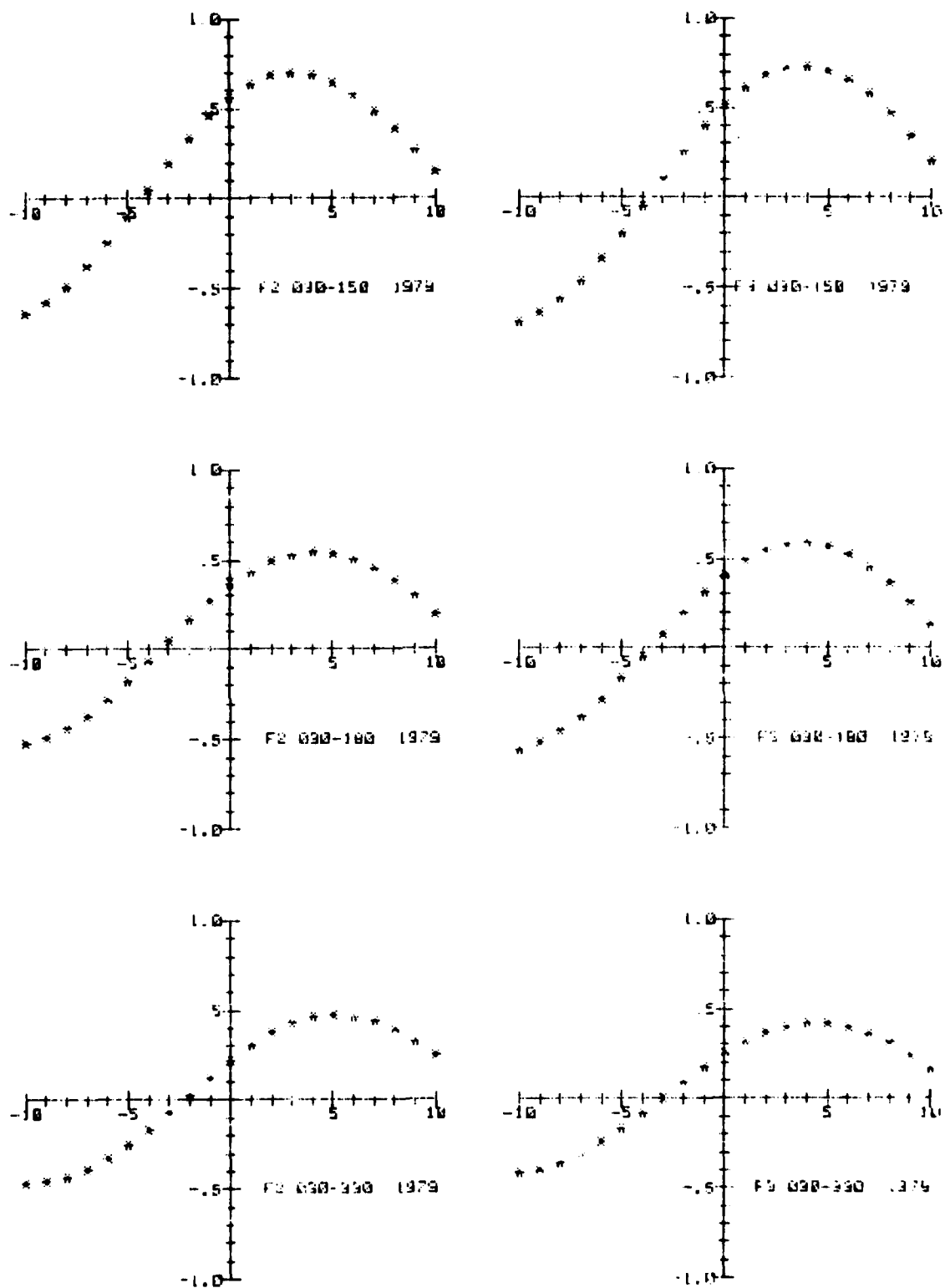


Figure 17. Cross correlation between phases of the moon and various portions of the averaged occurrence of uhf scintillation data shown in figure 16. F2 is the Indian Ocean satellite and F3 is the Pacific Ocean satellite.

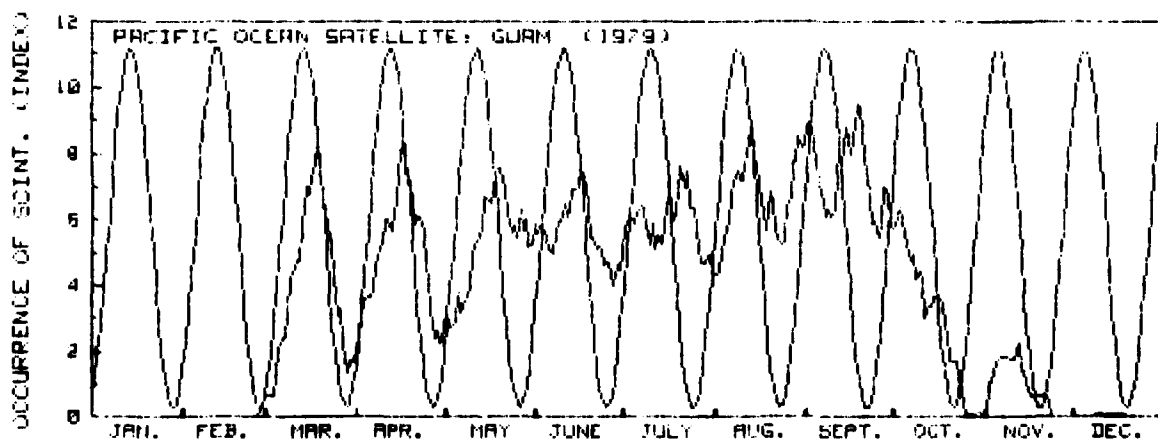
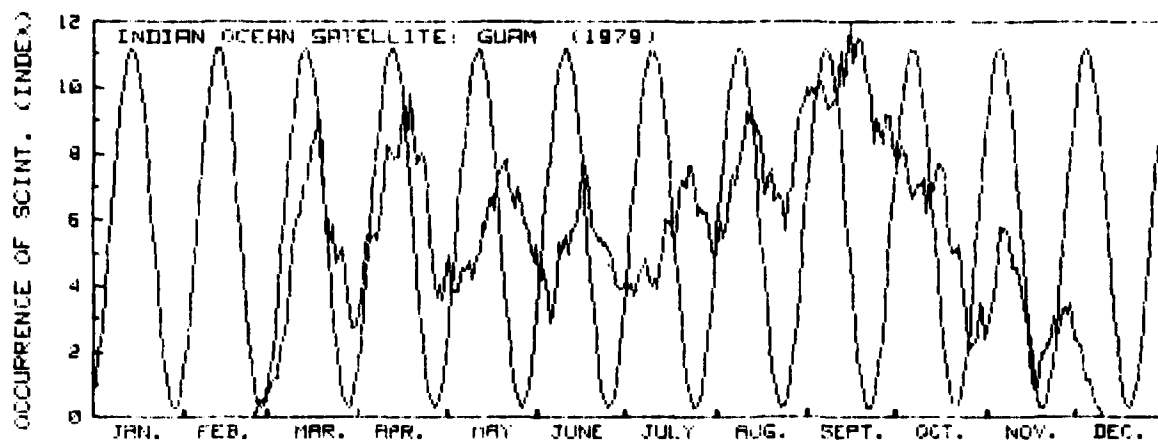


Figure 18. Eleven days running averages of the daily summed values of Standard Deviation/Mean at uhf. The phases of the moon are superimposed.

The fading rates were usually slower on the lower elevation angle satellite, resulting in fewer but longer fades. Figure 19 is an example of the plots for a common one-hour period on the night of 13 September 1979. The percent values shown on the graph are the total time the signal spent below the indicated level expressed as a percent of the one-hour sample period. These values ranged up to 20-22 percent at the 6-dB level and up to 4-5 percent at the 12-dB level on the Pacific Ocean satellite. On the Indian Ocean satellite they became as high as 25-30 percent for the 6-dB level and 6-8 percent for the 12-dB level.

When the percent values were averaged for all the uhf data in appendix C for each of the satellites, the averages were 16.0 percent for the Indian Ocean satellite and 10.5 percent for the Pacific Ocean satellite at the 6-dB level. They were 3.9 percent and 2.2 percent at the 12-dB level.

These numbers show a significant difference between the Indian Ocean satellite at about 10 degrees elevation angle and the Pacific Ocean satellite at about 50 degrees elevation angle. The differences can probably be attributed to the difference in elevation angle.

Fade duration distributions have been plotted for nearly all of the L-band scintillation data with fades greater than 6 dB. Very little L-band scintillation occurred on the Pacific Ocean satellite with fades greater than 6 dB and none with fades greater than 12 dB. Considerably more fading was observed for fades greater than 6 dB on the Indian Ocean satellite but fades greater than 12 dB were quite limited, with the total time spent below the level usually less than 1 percent for any 1-hour sample period.



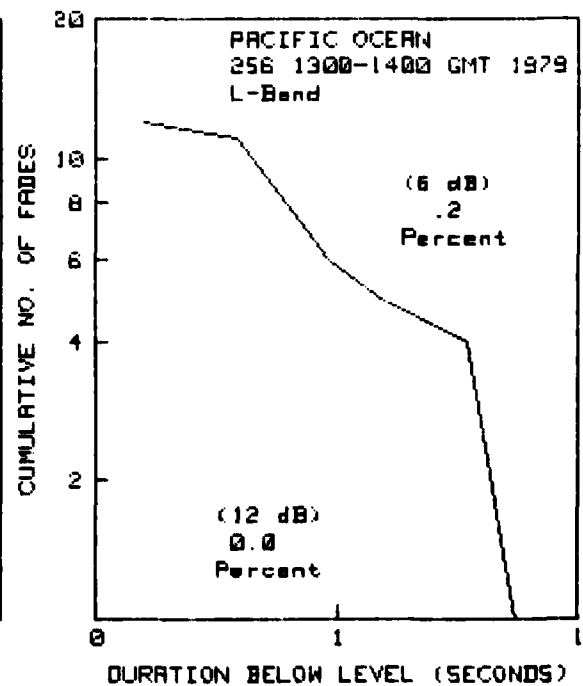
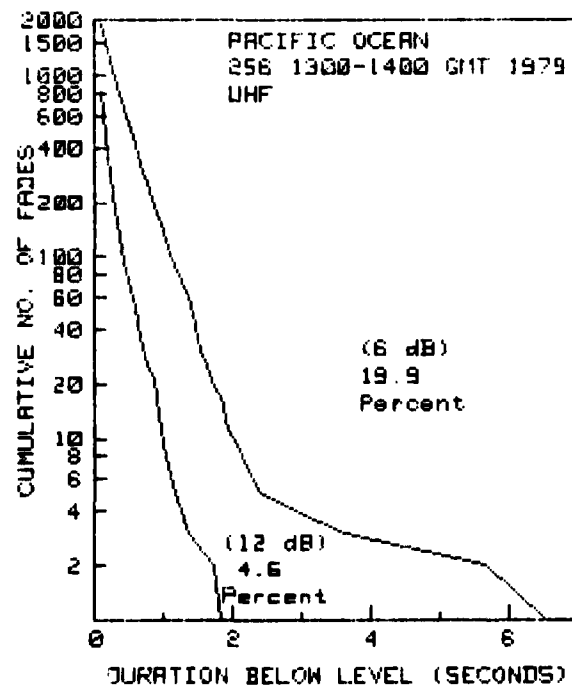
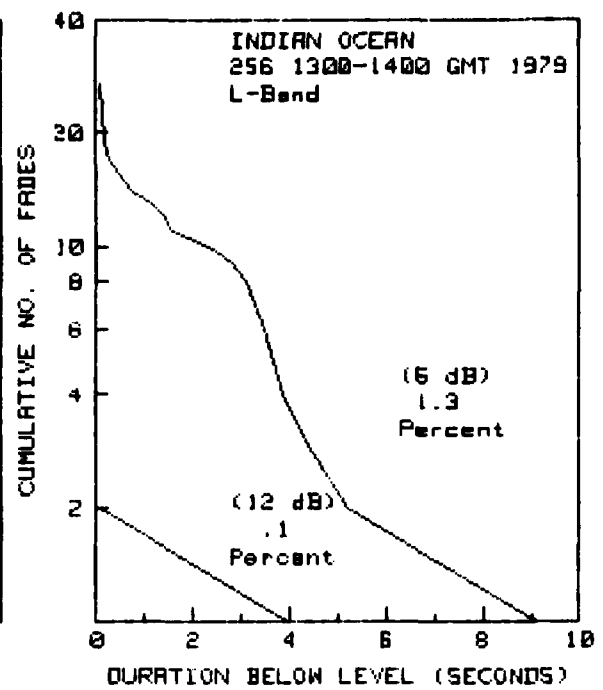
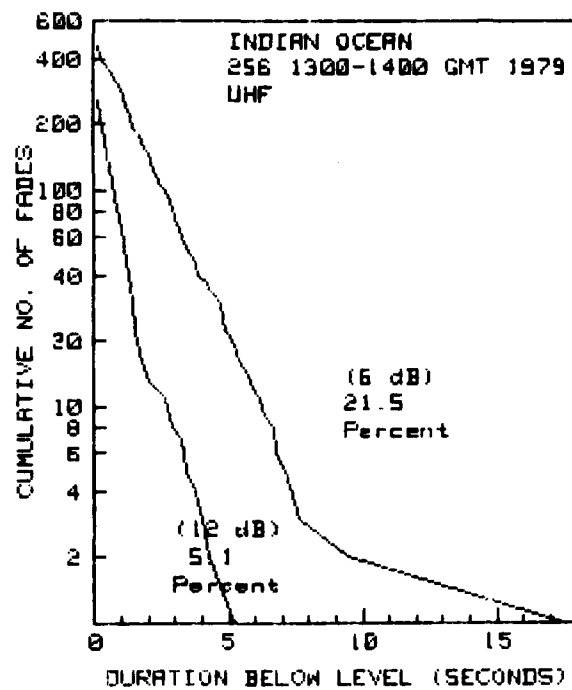


Figure 19. Examples of cumulative fade duration distribution at uhf and L-band for the two satellites.

## SUMMARY

1. Averaged diurnal plots of uhf scintillation intensity showed onset times of the scintillation for the Indian Ocean satellite were usually around 2030-2100 LST from March through August and around 2000 LST for September through November. Onset times for the Pacific Ocean satellite were about one hour earlier. These times are probably related to local sunset at the ionospheric penetration points at F-region heights for the two propagation paths.

Scintillation intensity usually increased rapidly to a high level and remained at a high level past 0100 or 0200 LST then decreased slowly, with significant scintillation sometimes occurring past 0300 or 0400 LST. No definite time of peak intensity was observed. This is probably because the scintillation was at a saturation level much of the time.

2. An averaged diurnal plot using 9 nights of L-band scintillation data for the Indian Ocean satellite showed maximum scintillation intensity centered around 2330 LST. Inclusion of additional data could modify this somewhat, however.

3. Seasonal variation in uhf equatorial scintillation showed a minimum in December and January then a rapid increase through February and March, broad maximum through the summer, and a rapid decrease in late October and November. The occurrence was somewhat higher in September than it was in the March-April period, but this was probably due to a large sustained increase in solar activity from mid-July through mid-October.

4. Seasonal variation in the occurrence of L-band scintillation showed two maxima, one in April and the other in September, with a decrease in the occurrence in the summer months.

5. Cross correlations between daily occurrence of scintillation and daily measurements of solar flux showed little correlation for either satellite; if there is any daily dependence it is so small that other causes obscure it.

A year-to-year dependence of the occurrence of scintillation on solar activity, using a common 11-day period for 5 different years, showed good linear dependence. However, when the values for the same period in 1979 are plotted, the point is well off the line generated by the other data points. It is possible that, when using a 6-dB fading criterion, the occurrence of scintillation may approach some limiting value as solar activity increases. Another possible explanation is that there is a time lag between a change in solar activity and a change in scintillation activity and, when solar activity is changing rapidly as it did in this case, the scintillation activity has not caught up. When average values for the full month of September are used, the point falls much closer to the line.

6. A pronounced periodicity is evident in the occurrences of scintillation data, particularly during the first half of the year. The period is on the order of 30 days. It is proposed here that this periodicity is caused by the gravitational field of the moon increasing or decreasing (depending on the moon's location) zonal winds at F-region heights and thus increasing or decreasing the occurrence and the intensity of the scintillation.

Around full moon the occurrence and intensity are at a maximum and around new moon they are at a minimum.

7. Cumulative fade duration distributions at uhf showed the fading rates were usually slower on the lower elevation angle satellite, resulting in fewer but longer fades.

The total time spent below a 6-dB level for a one-hour sample ranged up to 20-22 percent on the Pacific Ocean satellite and up to 25-30 percent on the Indian Ocean satellite. At 12 dB these were 4-5 percent and 6-8 percent, respectively.

When these values were averaged for all the uhf data in appendix C, the average time spent below the 6-dB level was 16.0 percent for the Indian Ocean satellite and 10.5 percent for the Pacific Ocean satellite. The corresponding numbers at 12 dB were 3.9 percent and 2.2 percent. From these results it can be deduced that scintillation is somewhat more intense at the lower elevation angle.

8. Very little L-band scintillation with fades greater than 6 dB occurred on the Pacific Ocean satellite—about 0.3 percent of the time in September, and none greater than 12 dB. Considerably more scintillation with fades greater than 6 dB was observed on the Indian Ocean satellite, occurring about 3 percent of the time during April and September. Scintillation with fades greater than 12 dB was quite limited, however.

### RECOMMENDATIONS

1. The possible lunar influence on the occurrence and intensity of equatorial scintillation needs further investigation. It is suggested that a spaced-receiver study be made of equatorial scintillation over the better part of a year to correlate the variation in occurrence and intensity of scintillation with ionospheric drift velocities, with phases of the moon, and also to compare the ionospheric drift velocities with phases of the moon.

2. Solar activity and geomagnetic activity should also be correlated with scintillation activity and with ionospheric drift velocities.

3. It appears that there are several factors affecting the occurrence and intensity of equatorial scintillation. The above measurements should be used to try to identify these factors and the degree of contribution of each. It may just be possible that zonal winds are a common factor that ties them all together.

## REFERENCES

1. Naval Electronics Laboratory Center TR 1875, Effects of Equatorial Scintillation Fading on SATCOM Signals, by MR Paulson and RUF Hopkins, 8 May 1973.
2. Naval Ocean Systems Center TR 113, Spatial Diversity Characteristics of Equatorial Scintillation, by MR Paulson and RUF Hopkins, 2 May 1977.
3. Koster, JR, Equatorial Scintillation, Planetary and Space Science, vol 20, no 12, p 1999-2014, 1972.
4. Briggs, BH and Parkin, IA, On the Variation of Radio Star and Satellite Scintillations with Zenith Angle, Journal of Atmospheric and Terrestrial Physics, vol 25, p 339-365, 1963.
5. Naval Ocean Systems Center TR 446, Scintillation of Uhf SATCOM Signals, by MR Paulson, 15 August 1979.
6. Solar-Geophysical Data, Prompt Reports, National Oceanic and Atmospheric Administration Environmental Data and Information Service, Boulder, CO.
7. Crane, RK, Ionospheric Scintillation, Proceedings of the IEEE, vol 65, no 2, p 180-199, February 1977.
8. Naval Ocean Systems Center TR 290, Zonal Winds as a Generating Mechanism for the Ionospheric Irregularities that Cause Equatorial Scintillation of Satellite Signals, by MR Paulson, 26 June 1978.
9. Misra, RA, Lunar Tidal Oscillations in the Horizontal Ionospheric Drift at the Equator, Planetary and Space Science, vol 21, p 1109-1114, 1973.

**APPENDIX A**  
**TOTAL HOURS EACH DAY THAT UHF SCINTILLATION FADING**  
**EXCEEDED 6 dB AND TOTAL HOURS EACH DAY THAT**  
**L-BAND SCINTILLATION FADING EXCEEDED 3 dB**

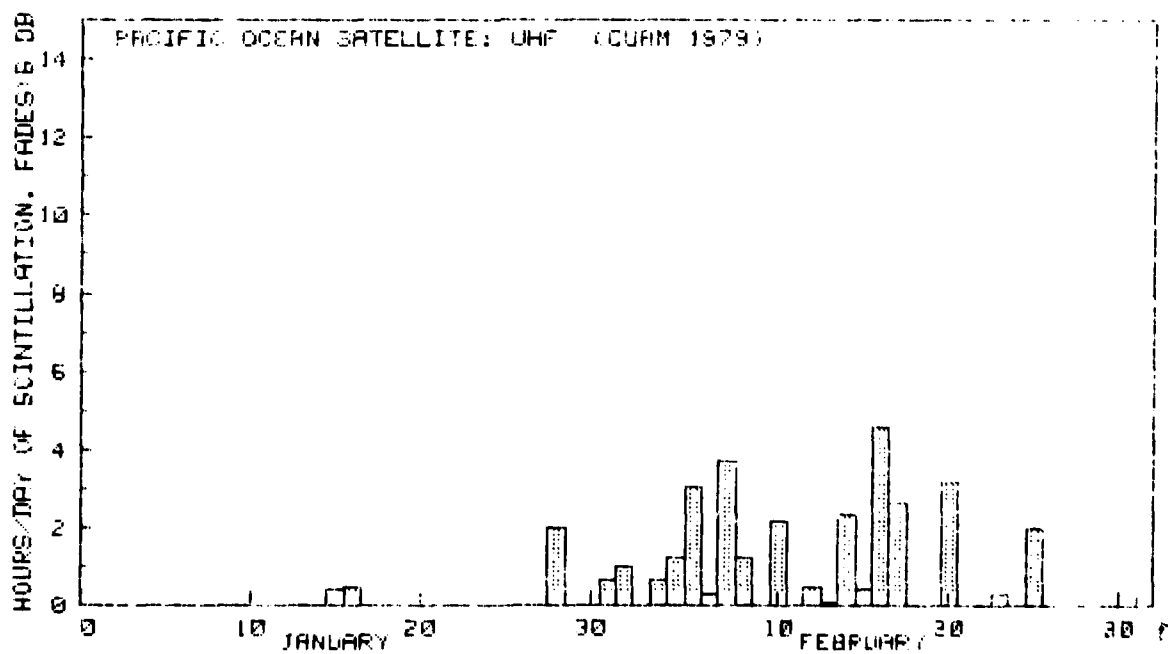
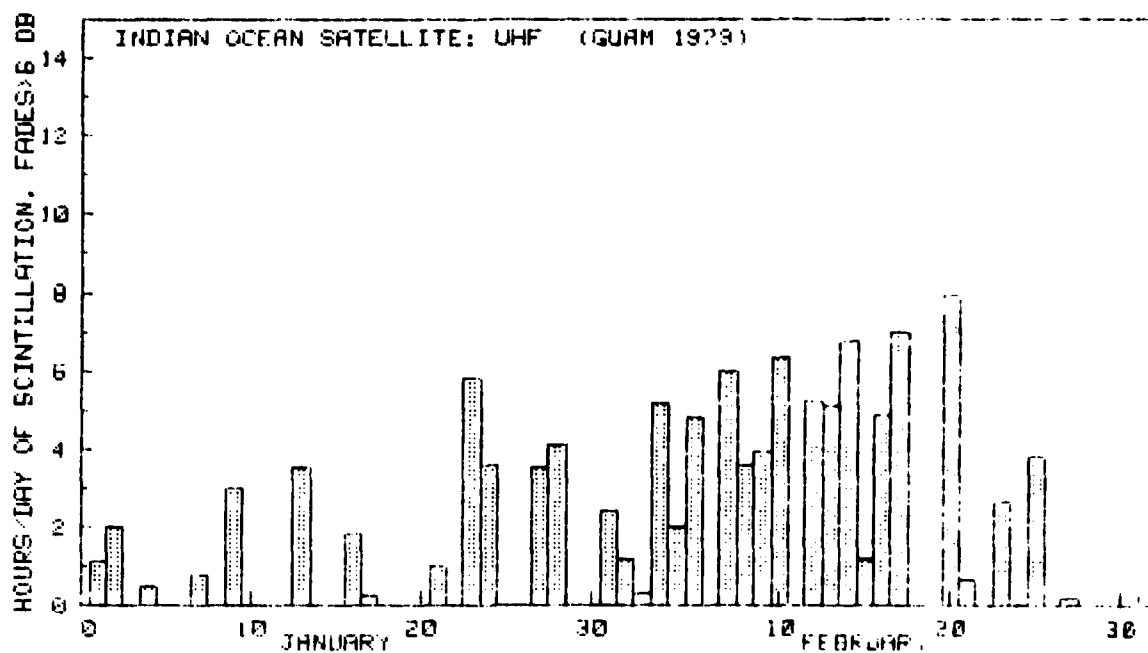
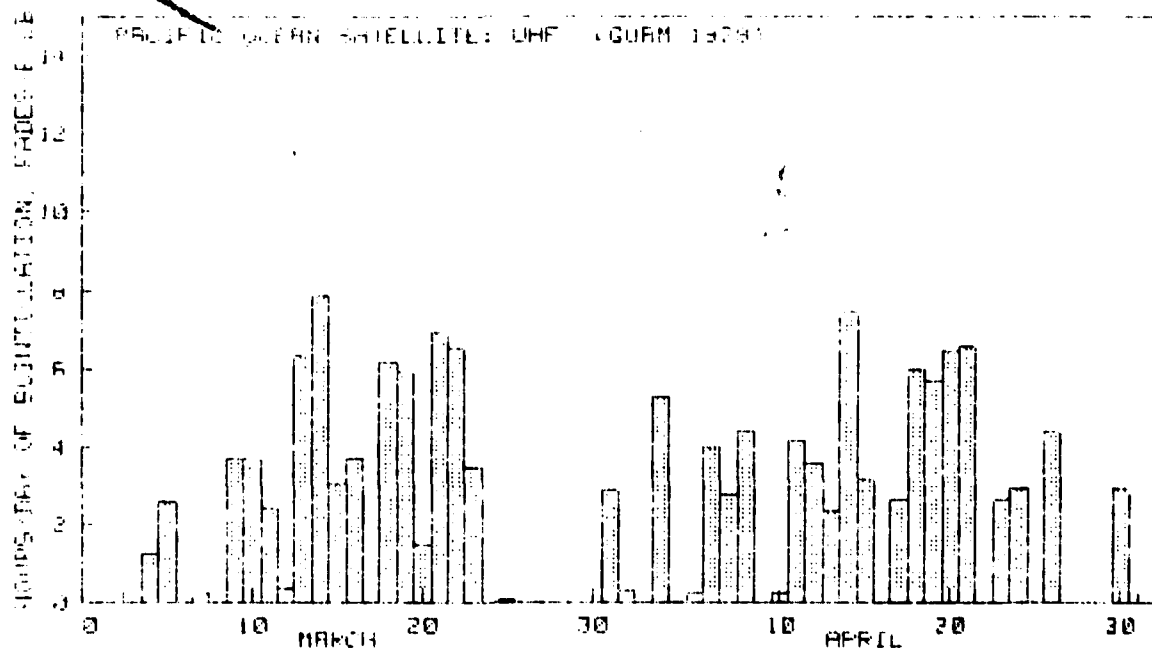
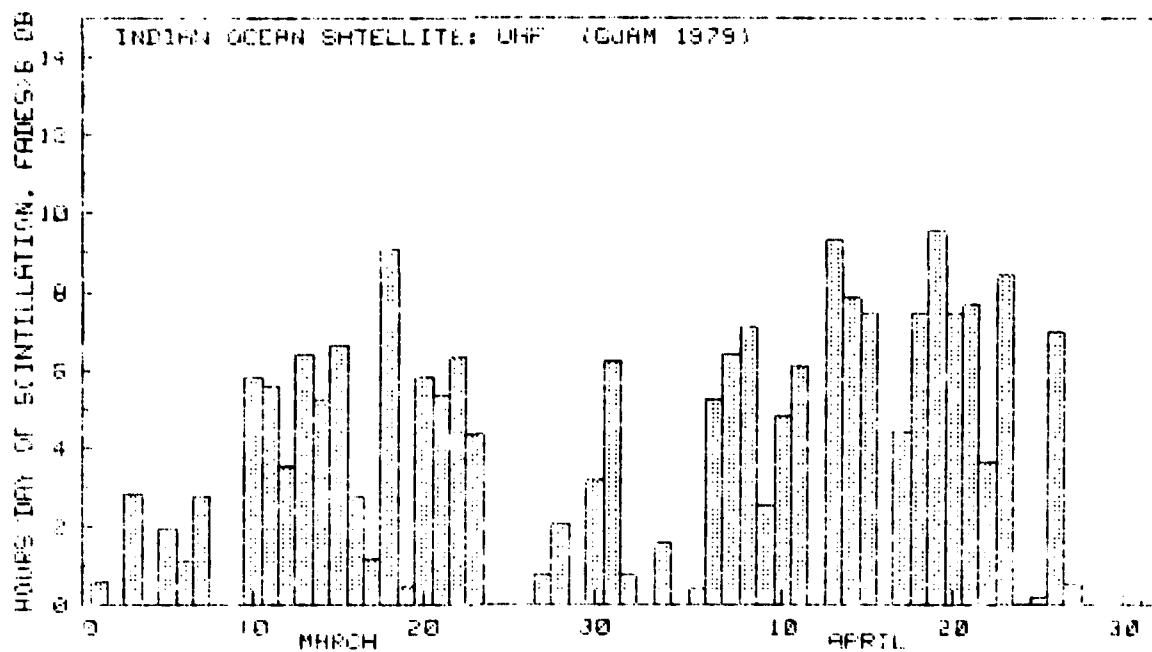
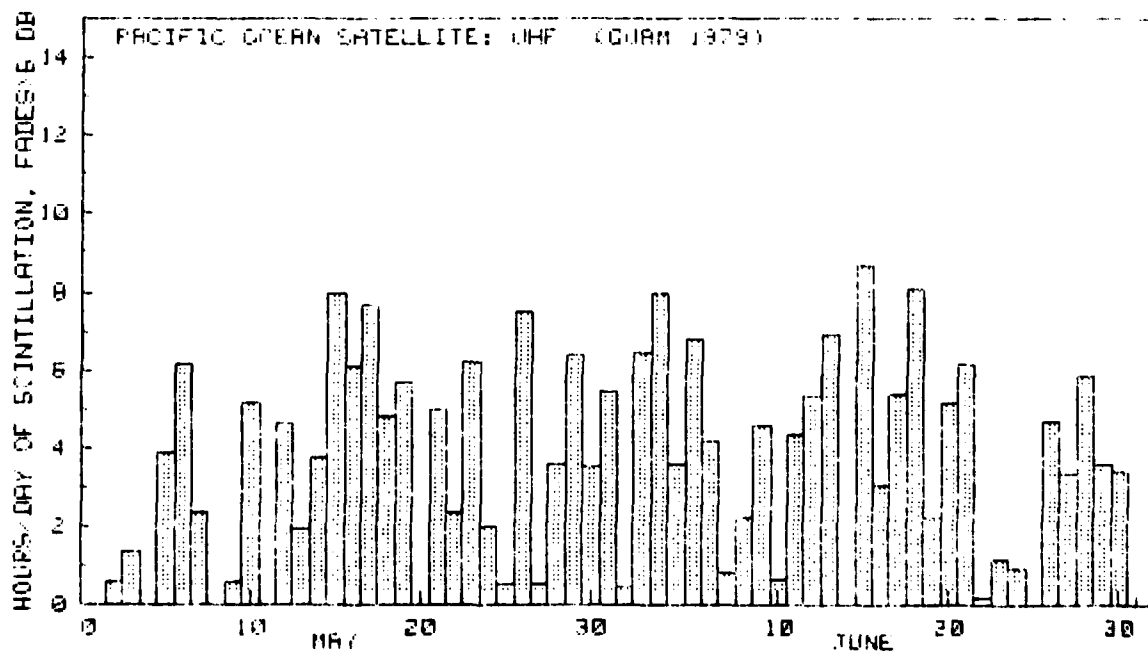
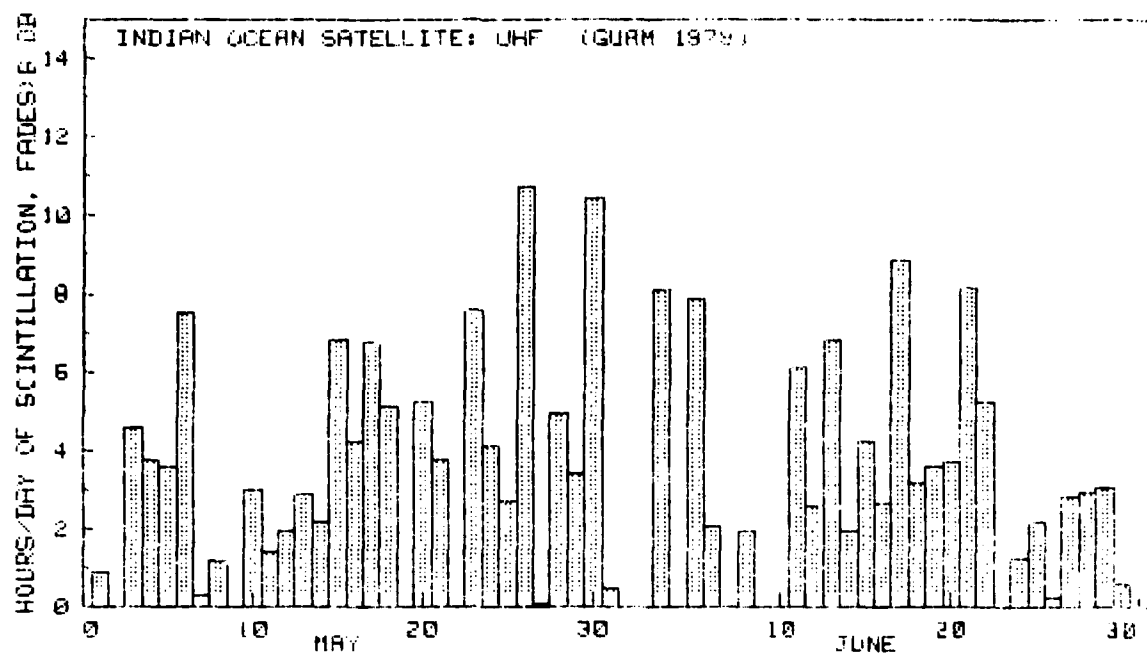


Figure A1. Total hours each day that uhf scintillation fading exceeded 6 dB.

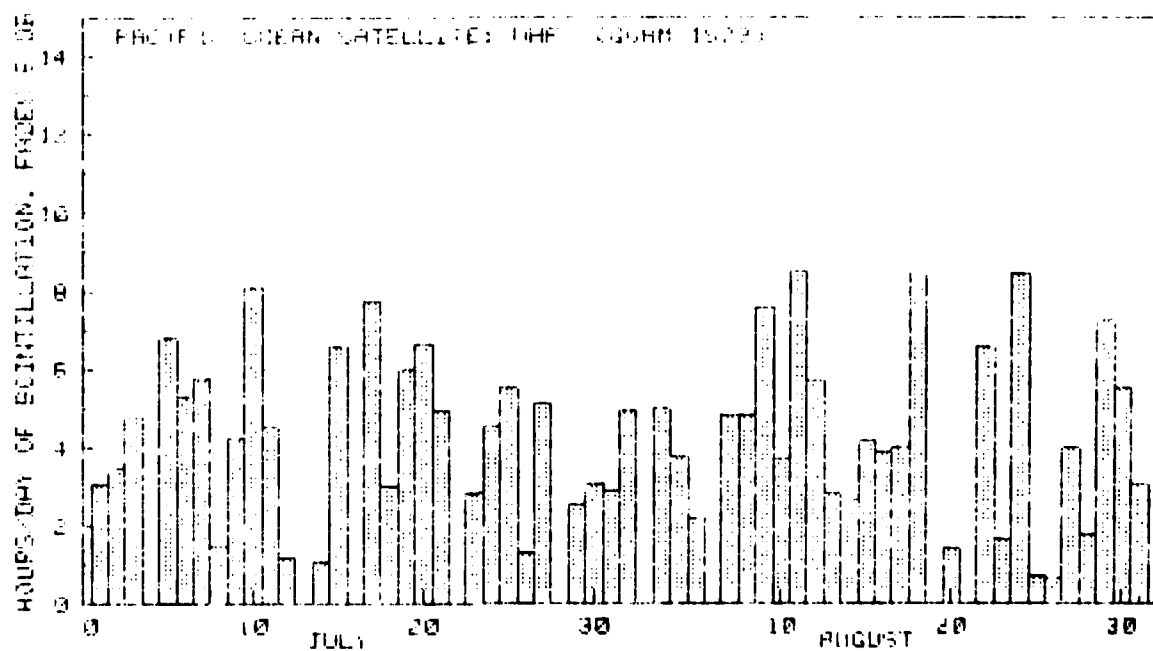
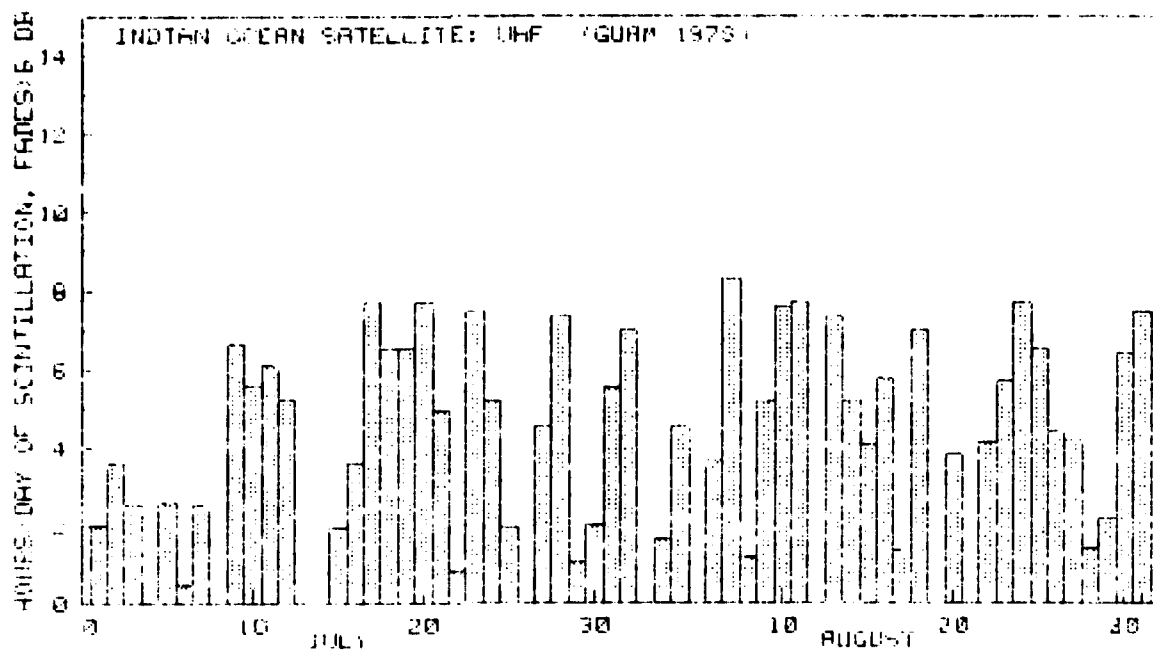


A1 (continued)

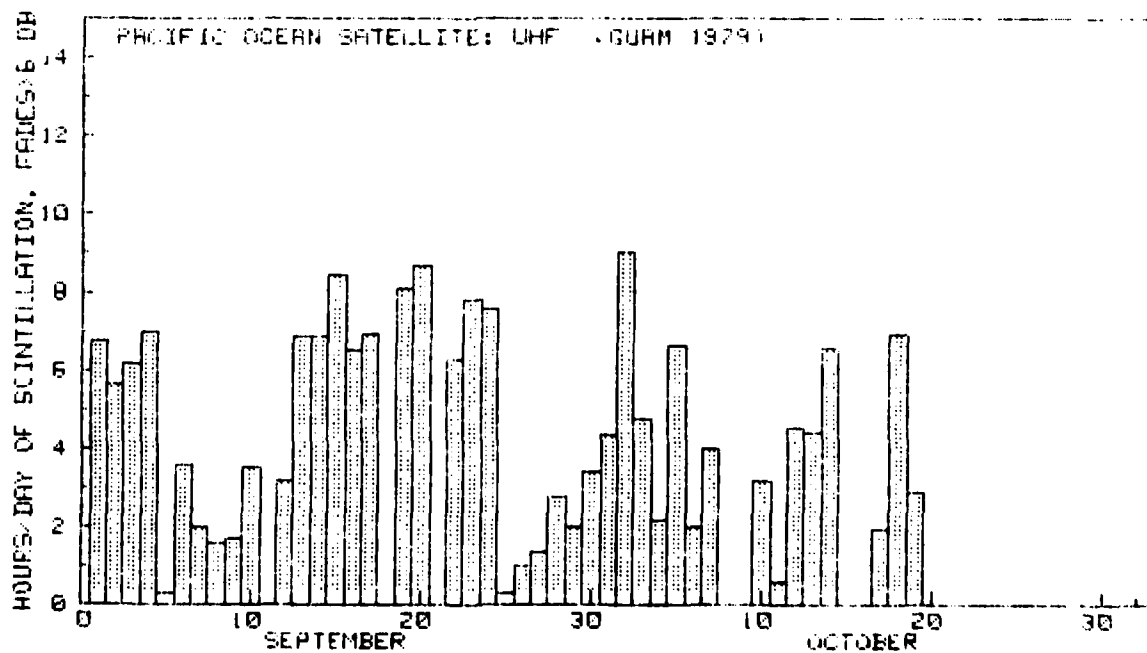
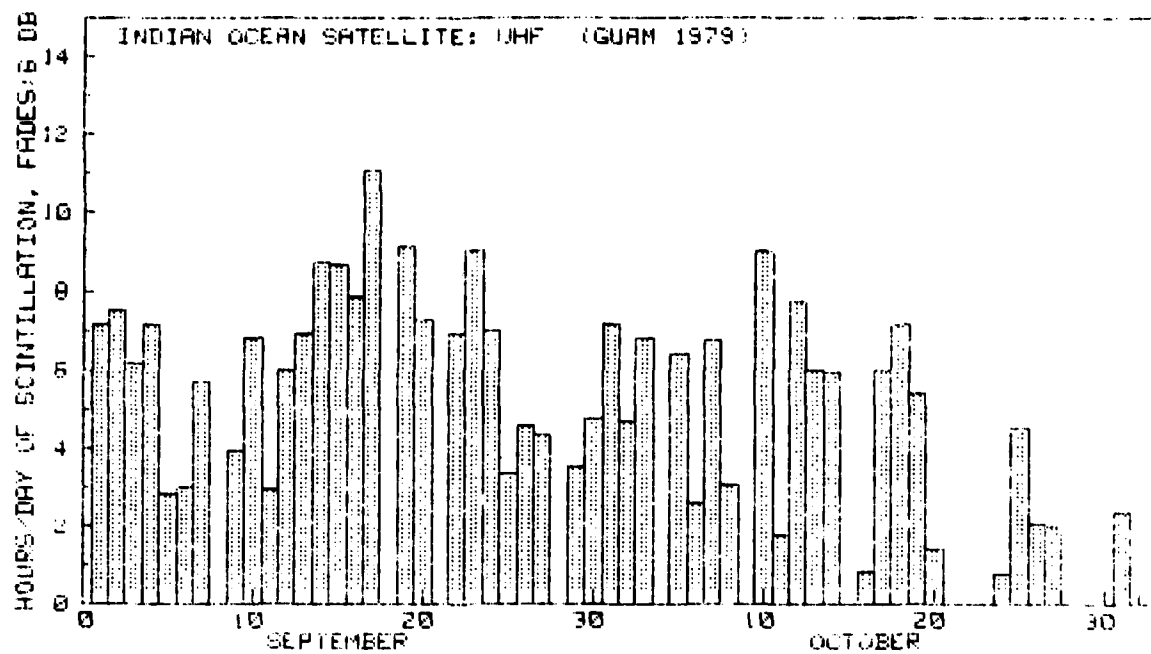


A1 (continued)

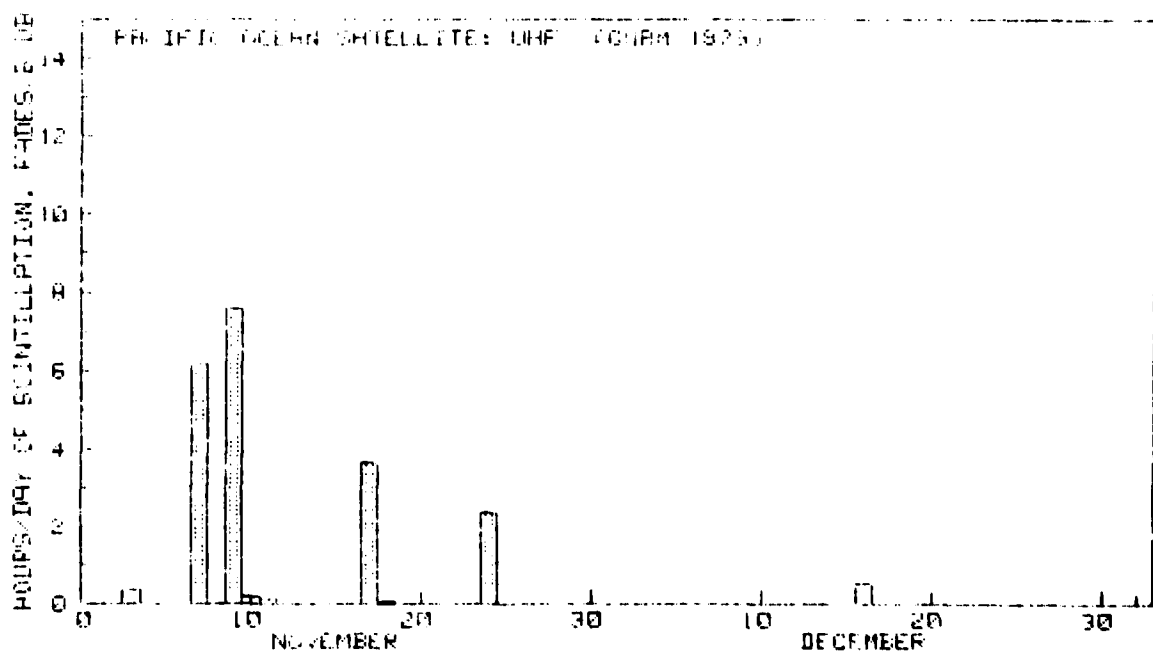
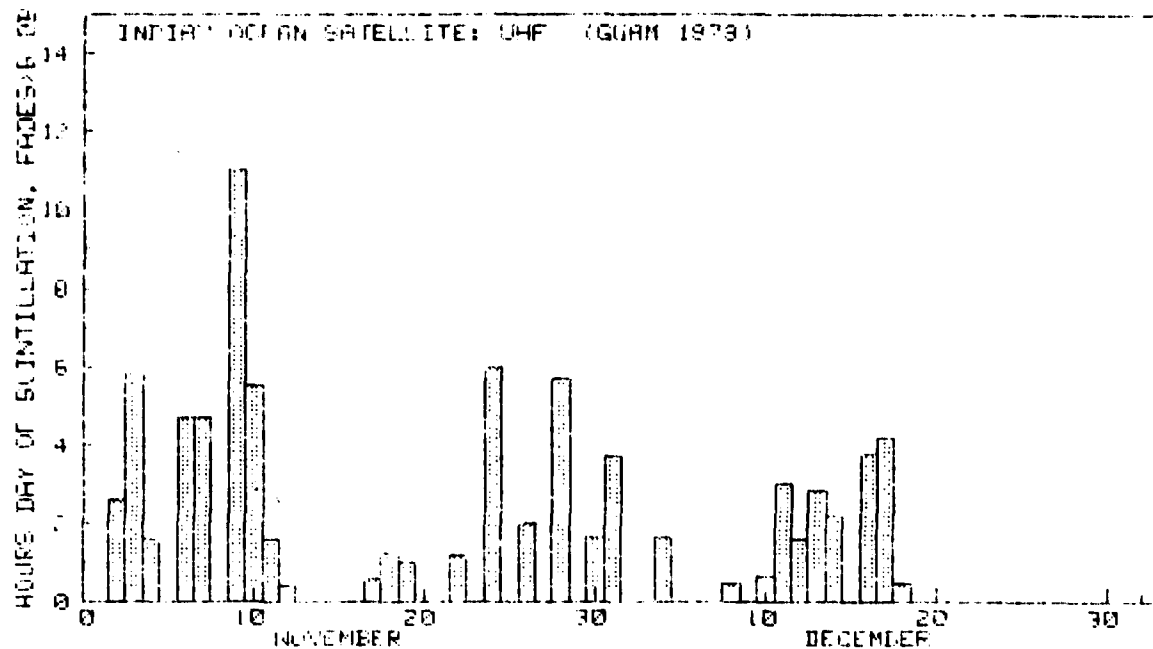




A1 (continued)



A1 (continued)



A1 (continued)

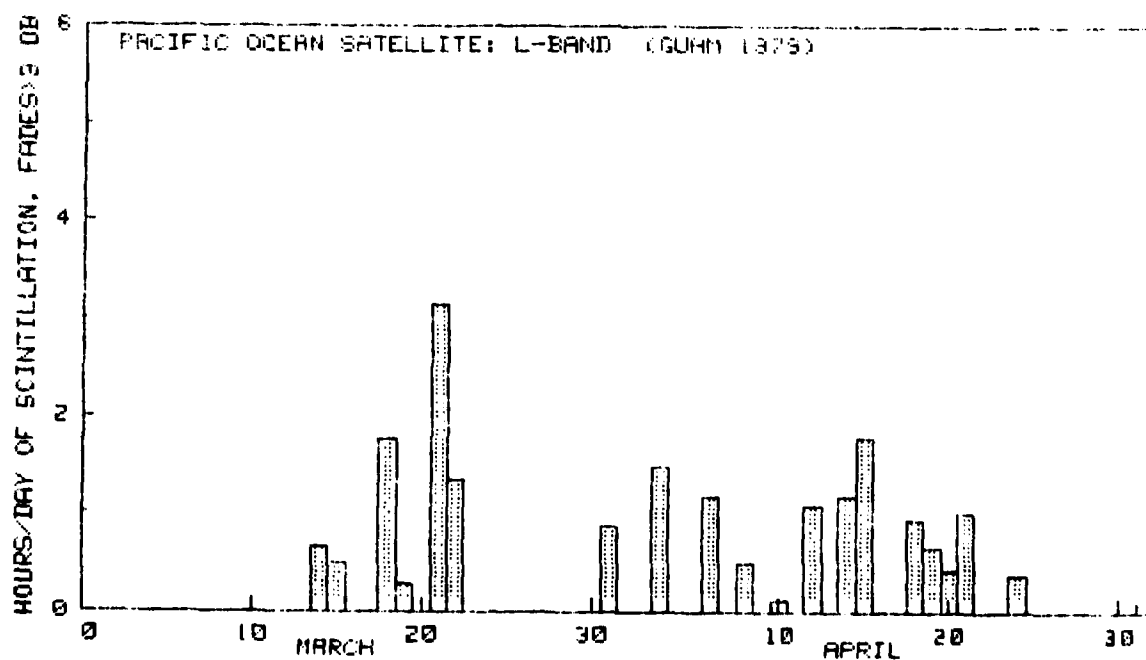
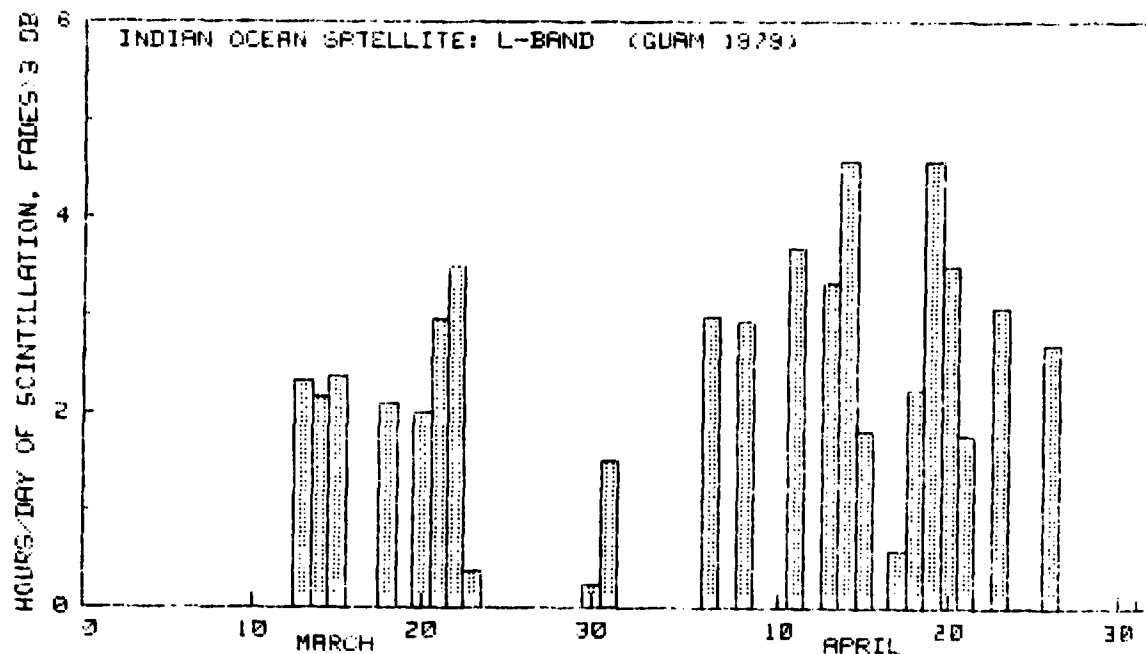
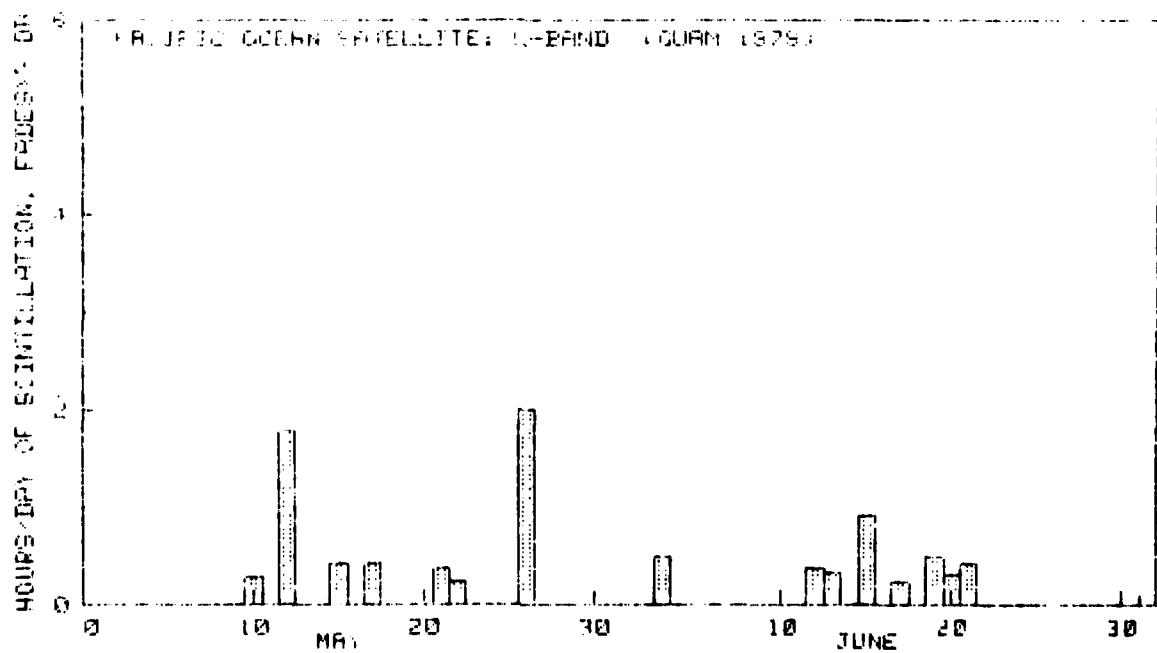
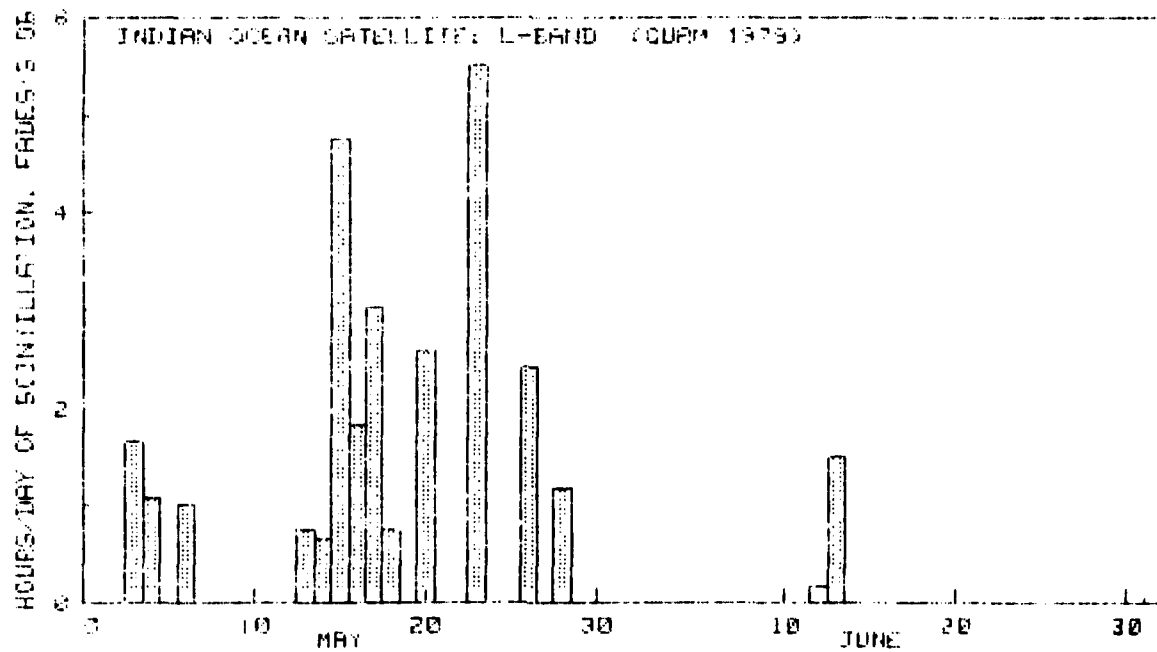
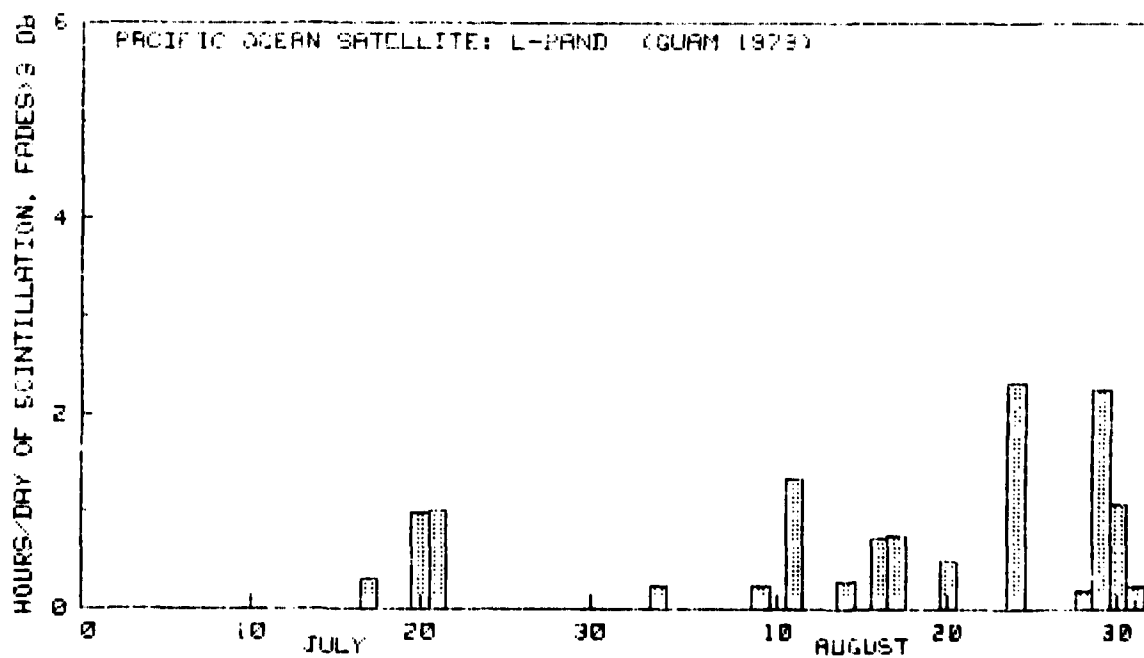
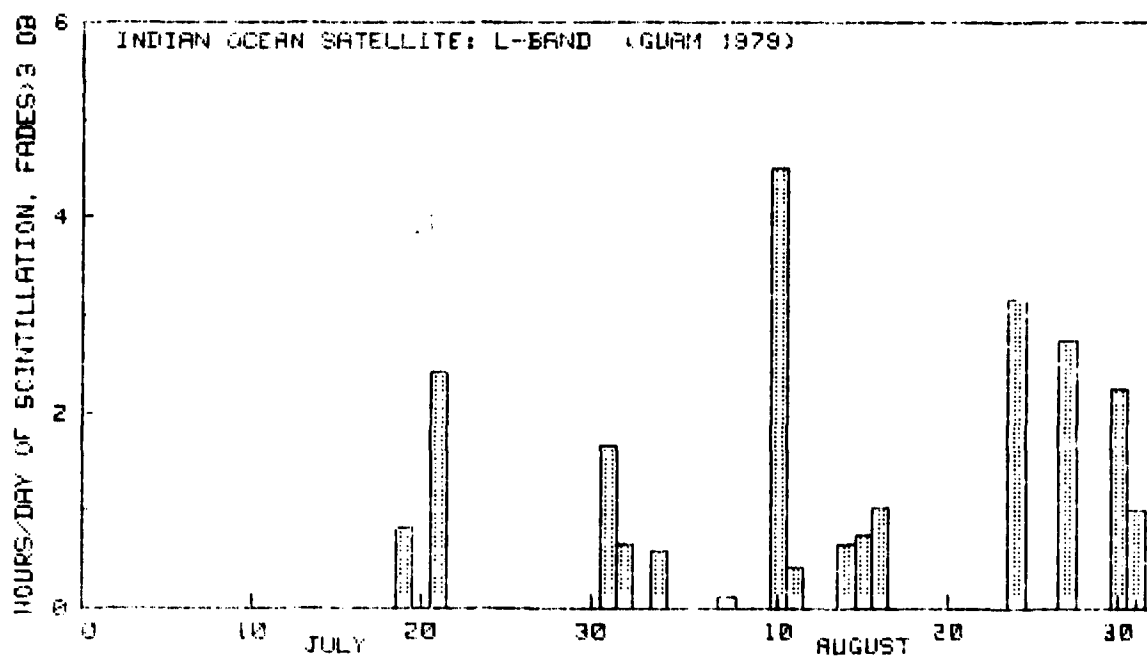


Figure A2. Total hours each day that L-band scintillation fading exceeded 3 dB.

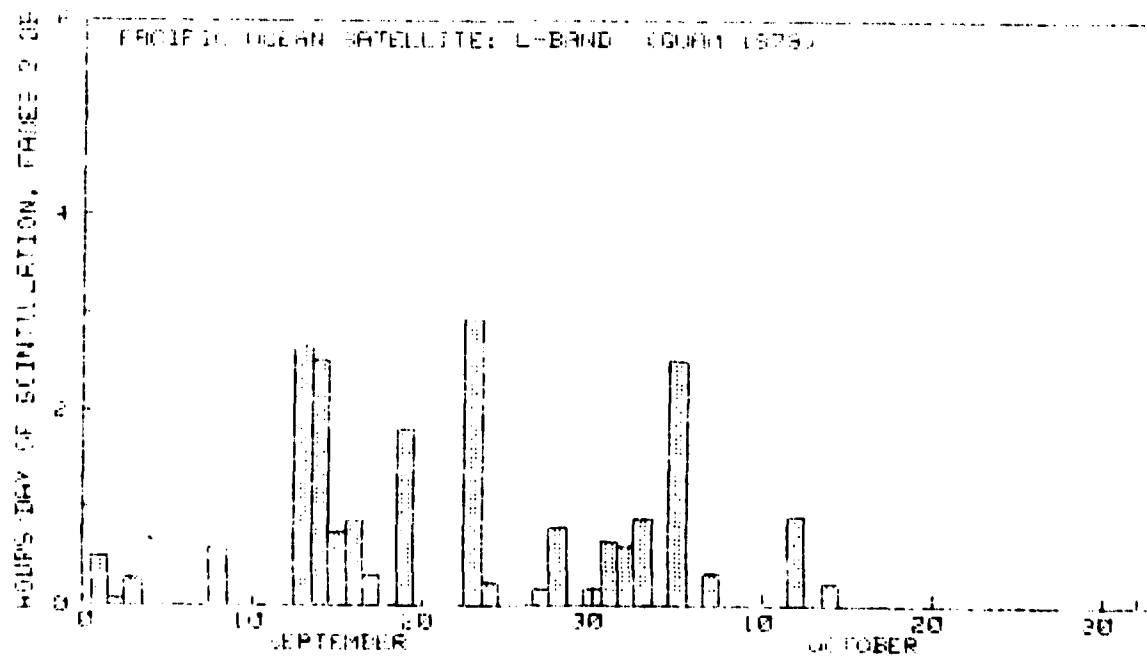
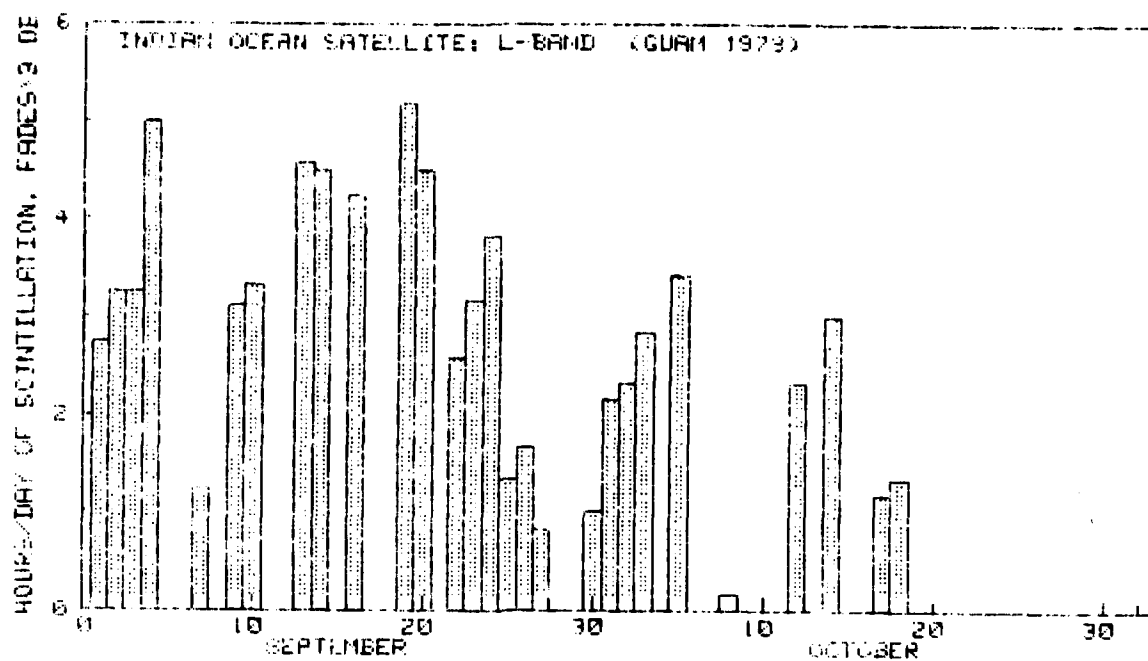


A2 (continued)

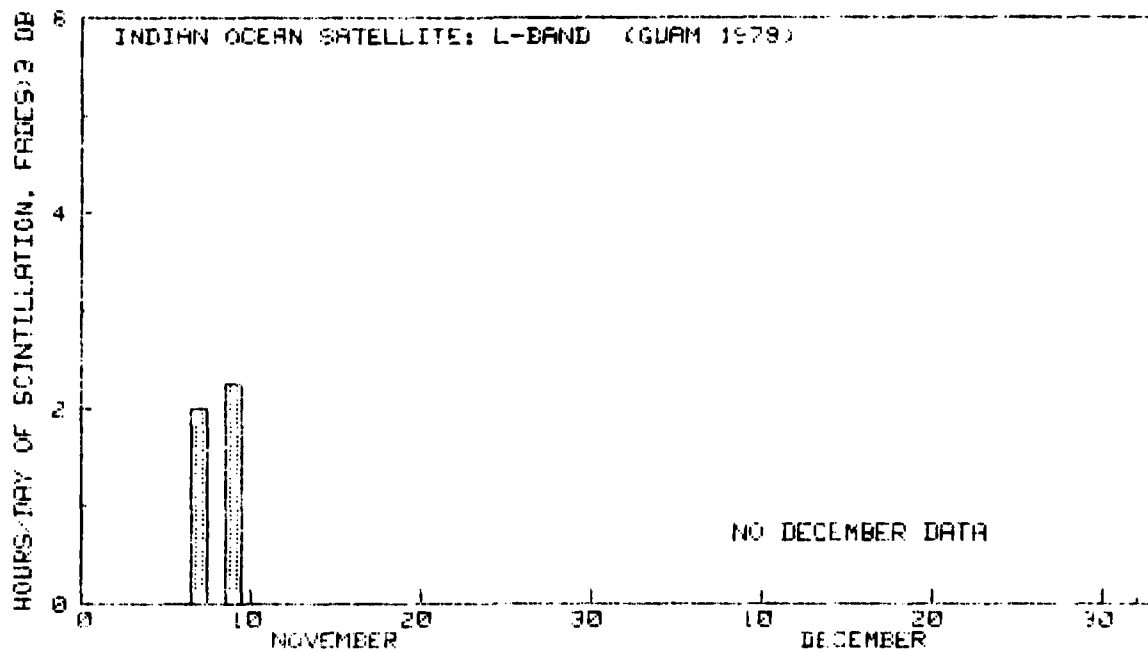


A2 (continued)

A-10

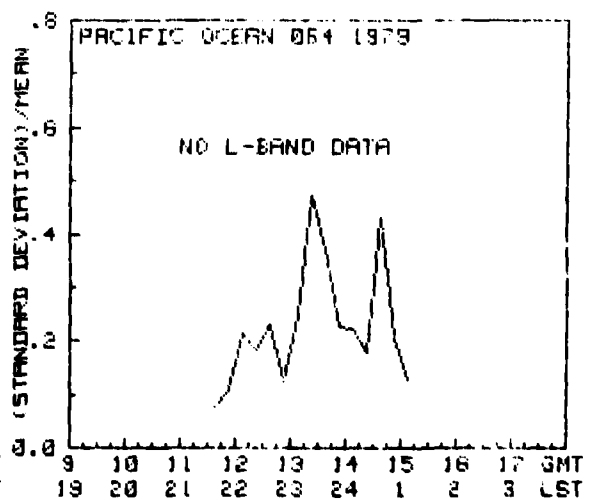
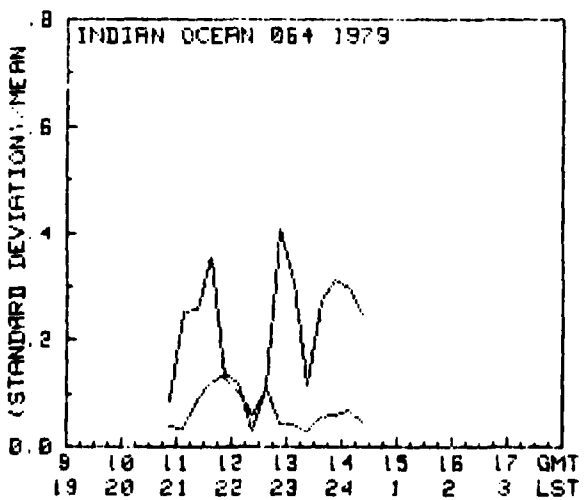
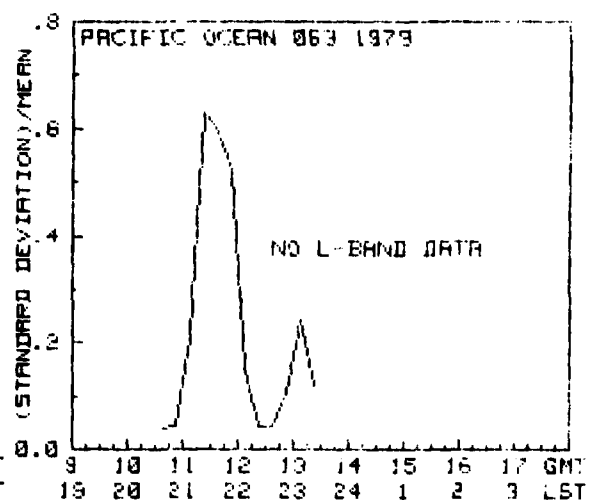
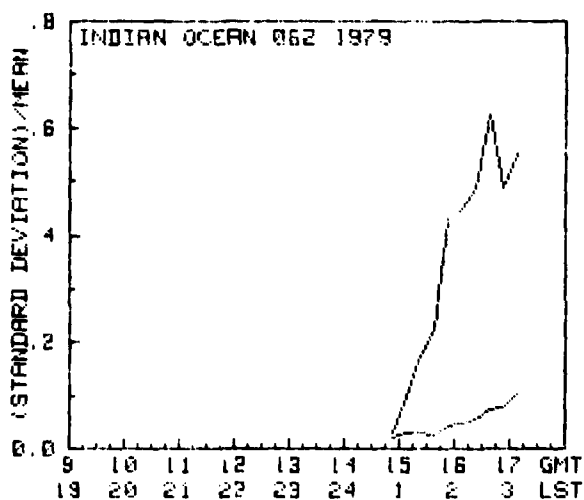
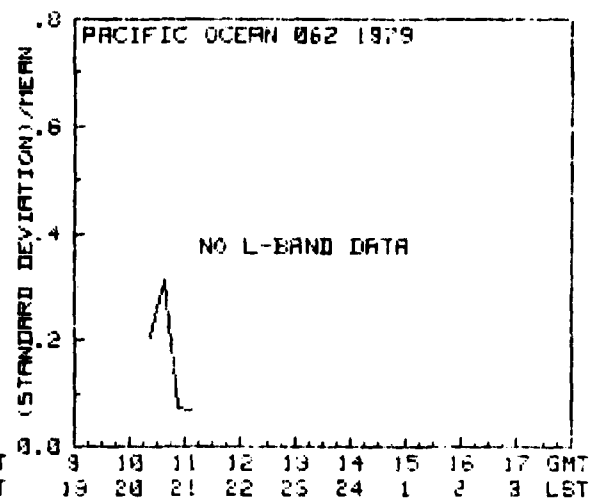
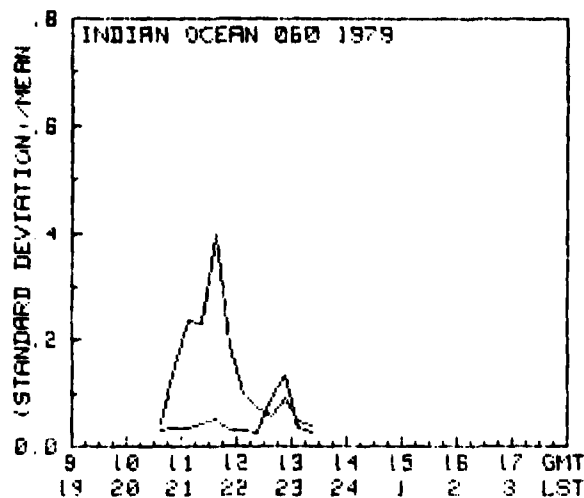


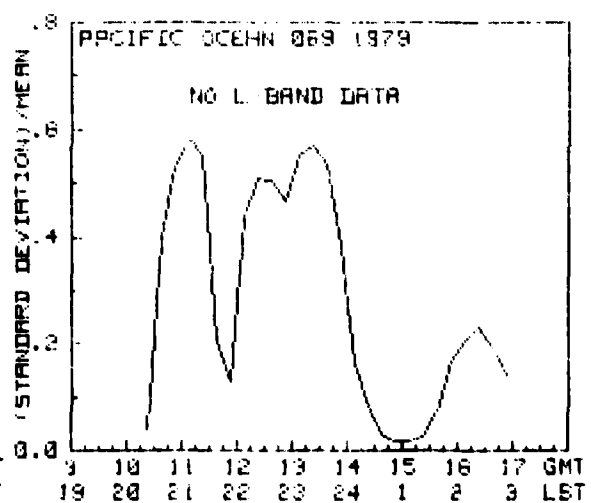
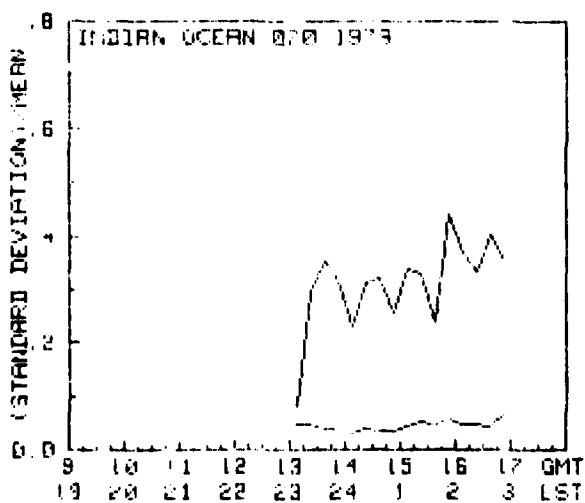
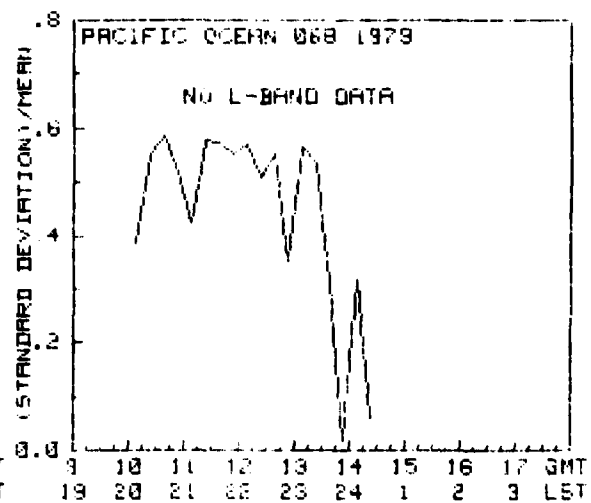
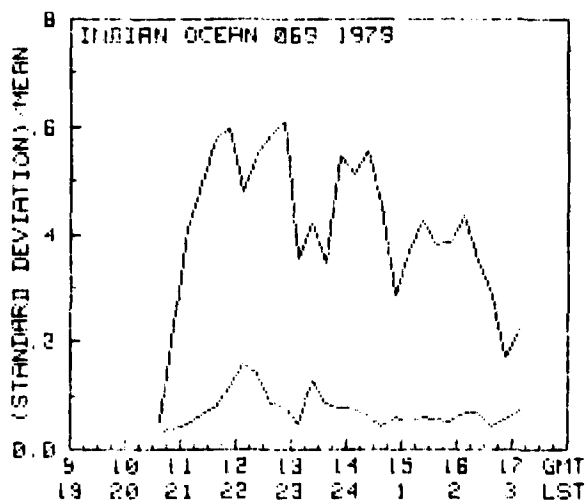
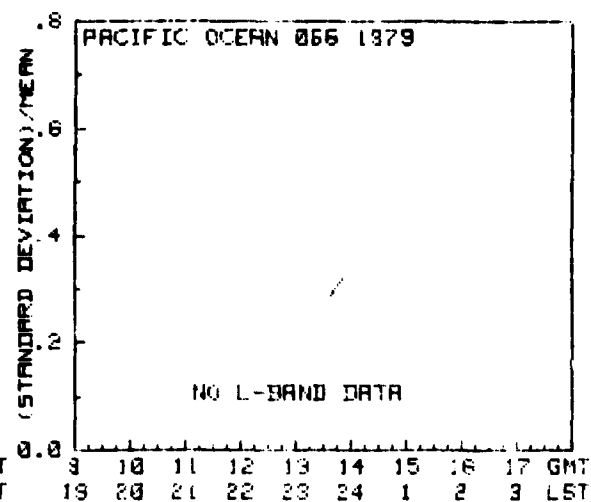
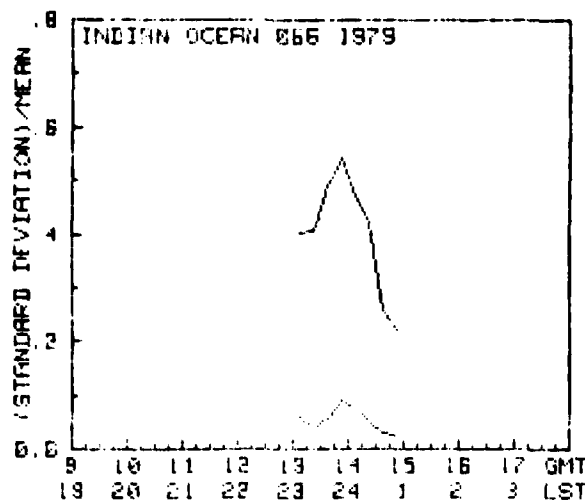
A2 (continued)

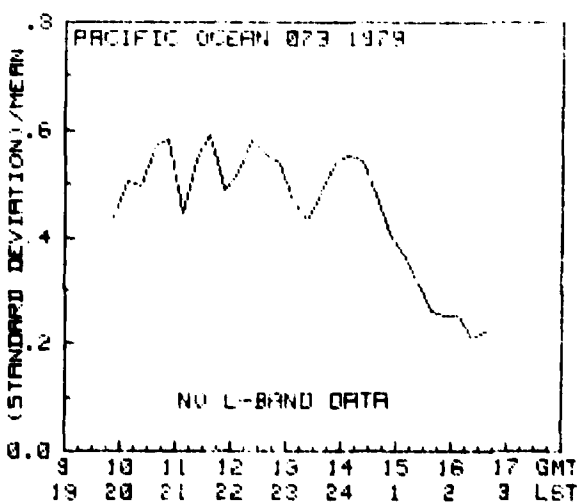
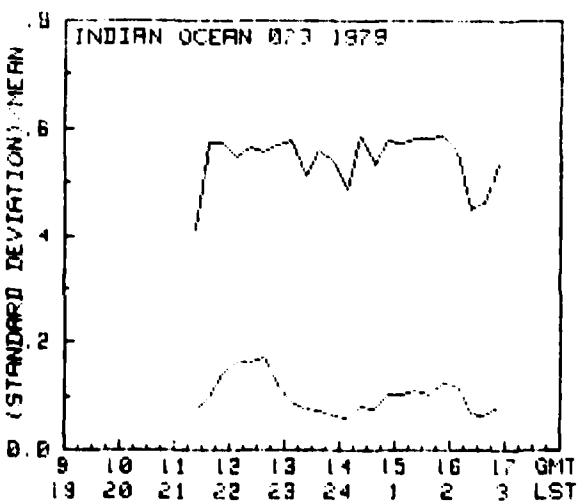
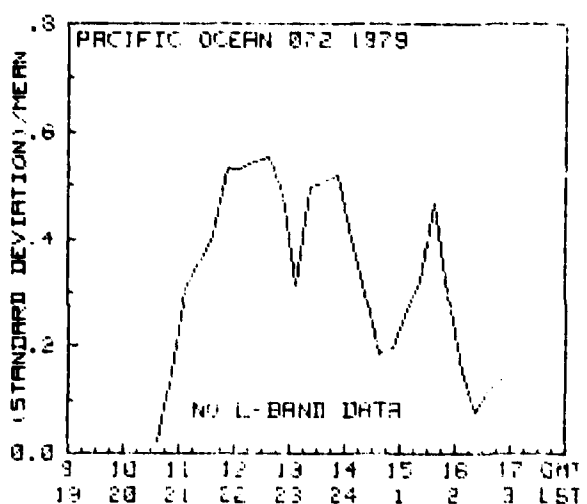
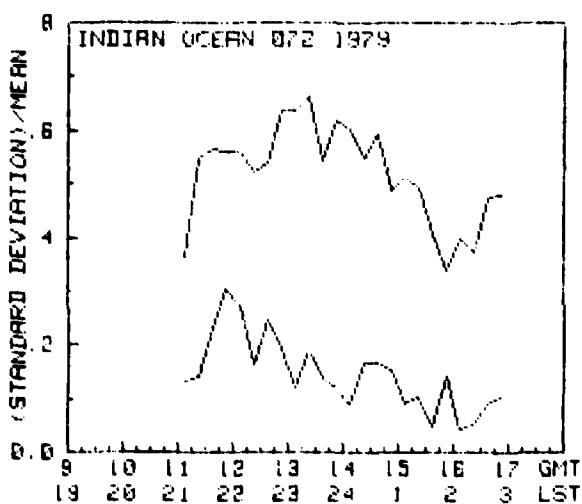
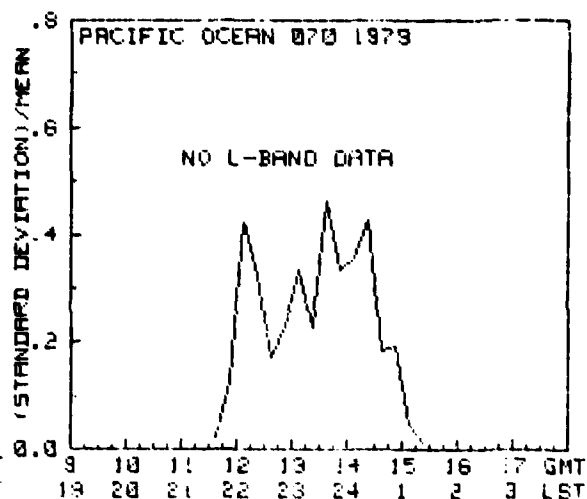
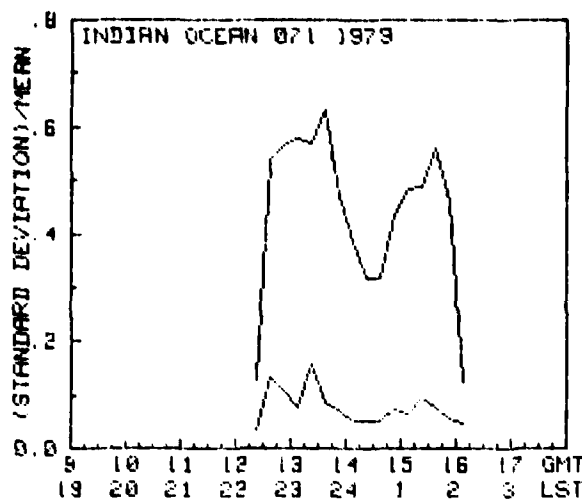


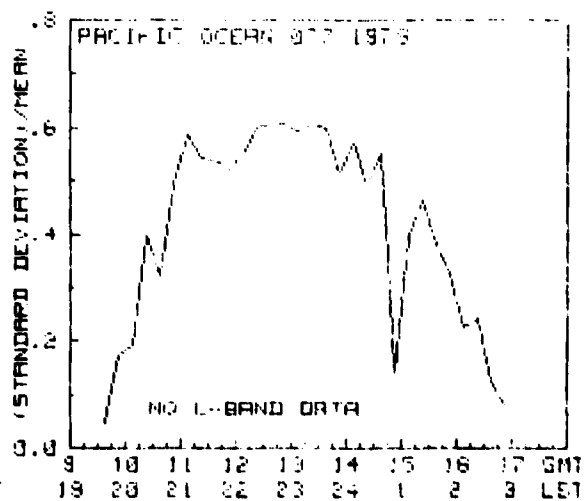
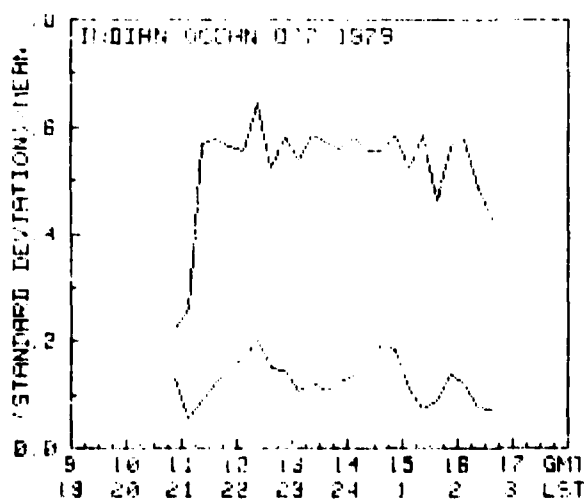
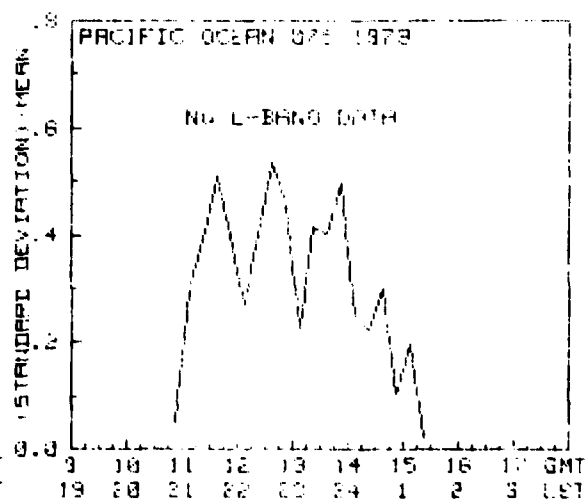
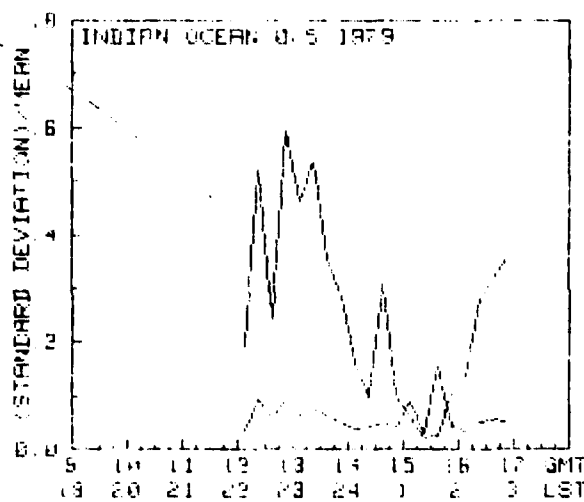
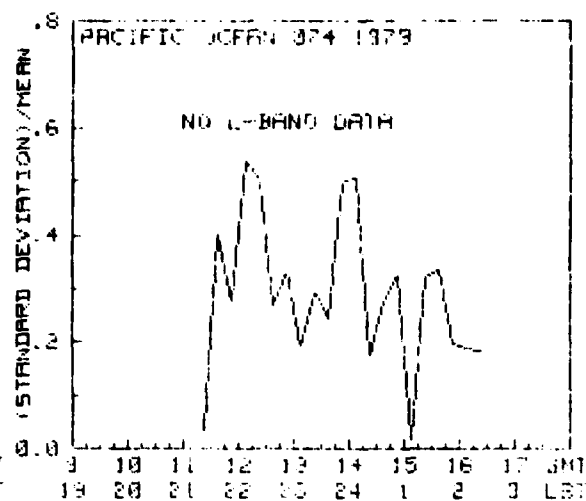
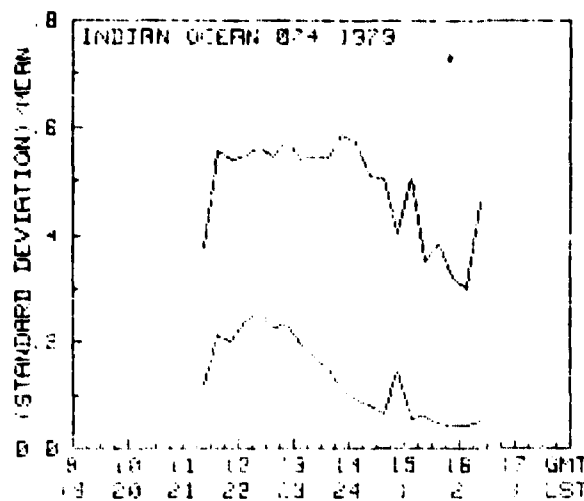


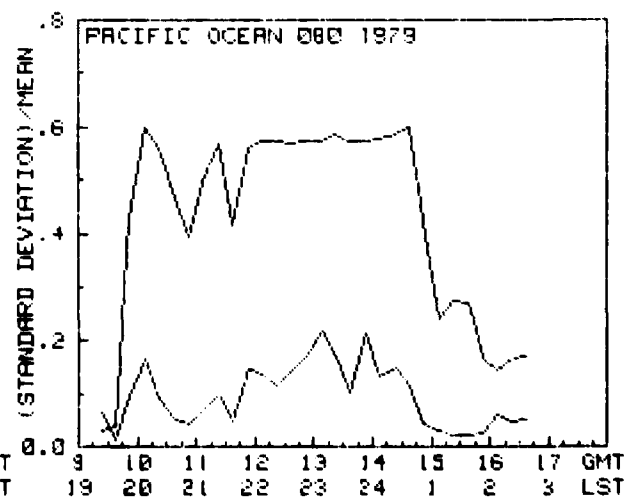
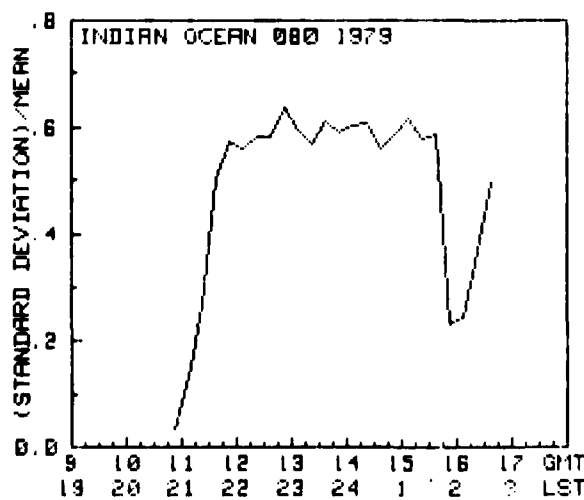
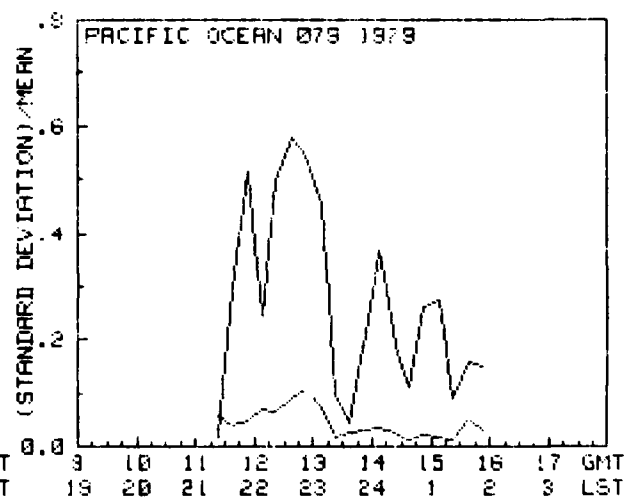
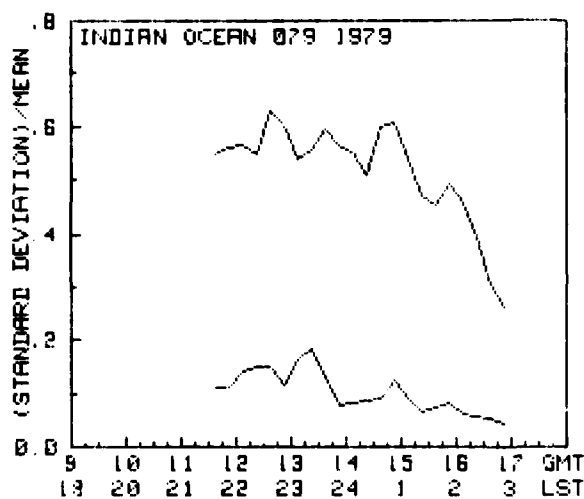
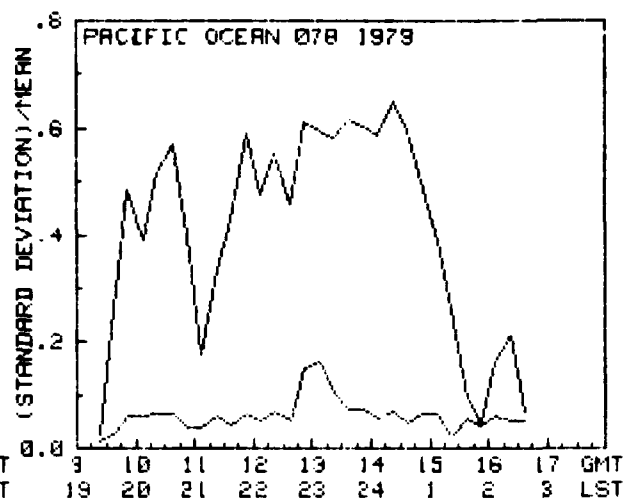
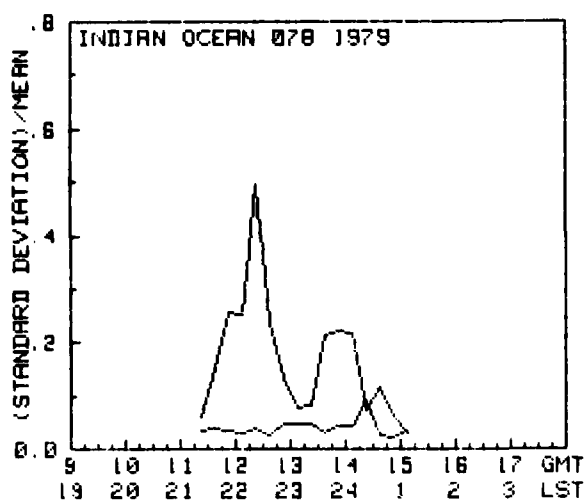
**APPENDIX B**  
**DAILY DIURNAL VARIATION OF STANDARD DEVIATION/MEAN**  
**RESULTING FROM EQUATORIAL SCINTILLATION**  
**AT UHF AND L-BAND**

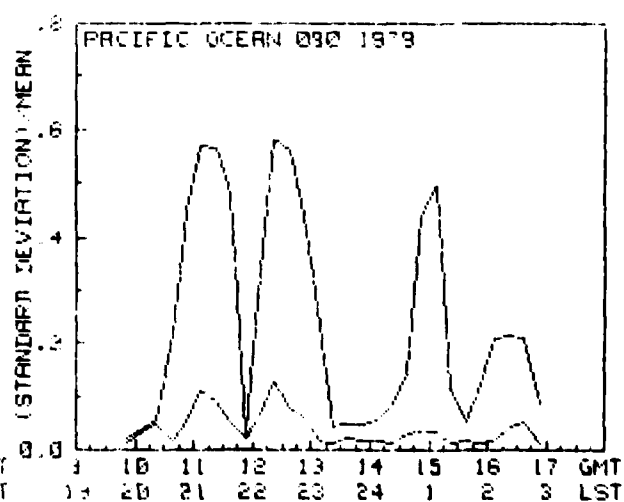
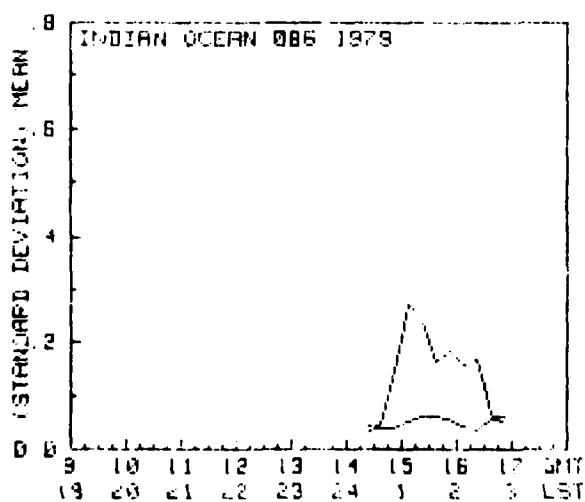
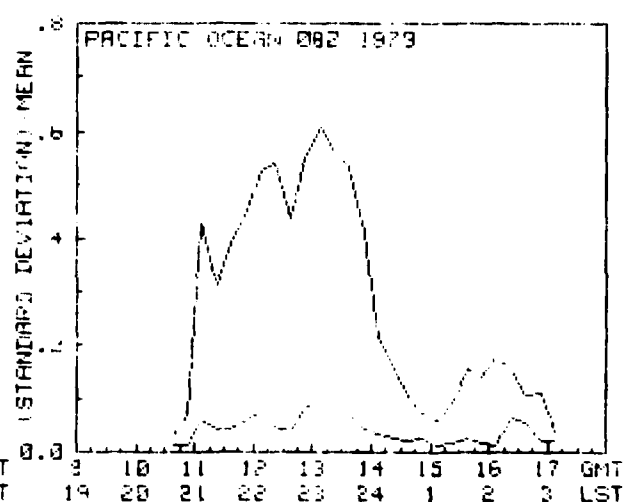
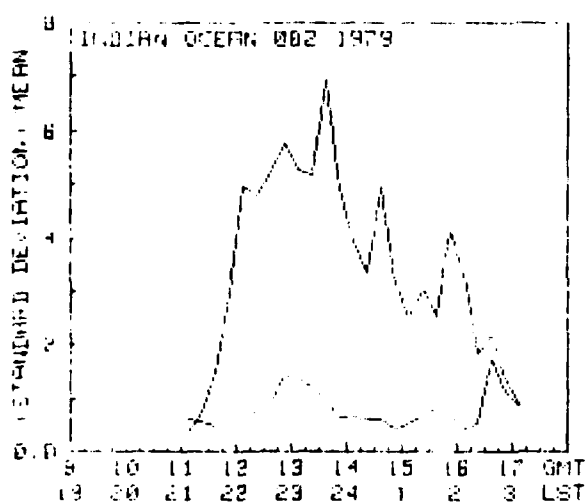
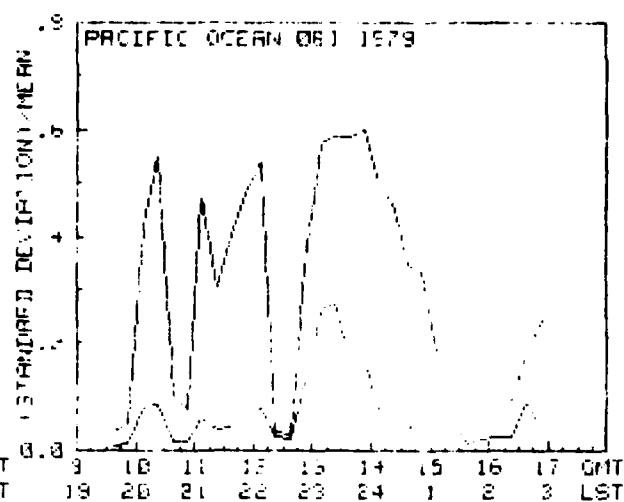
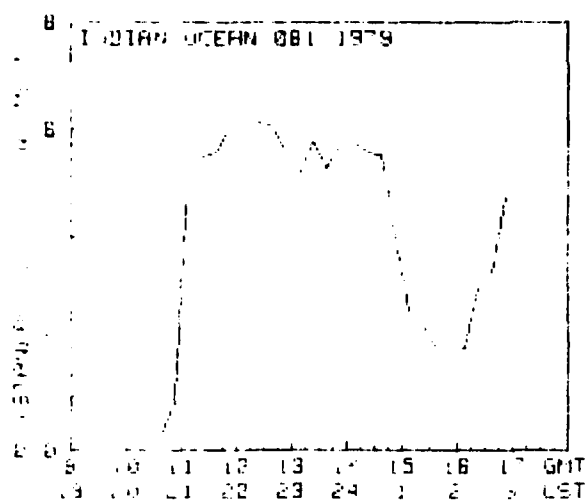


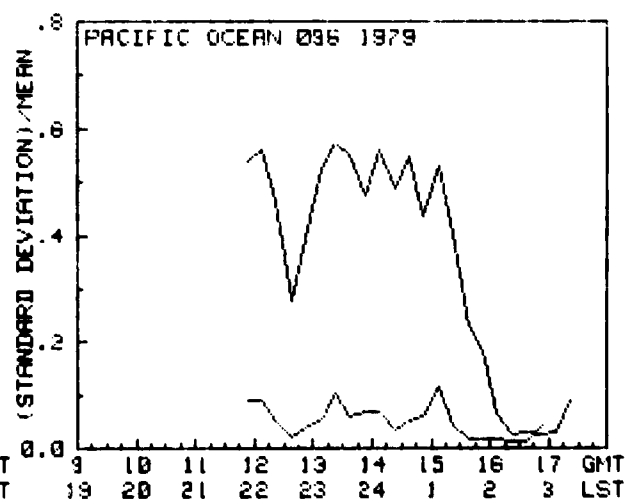
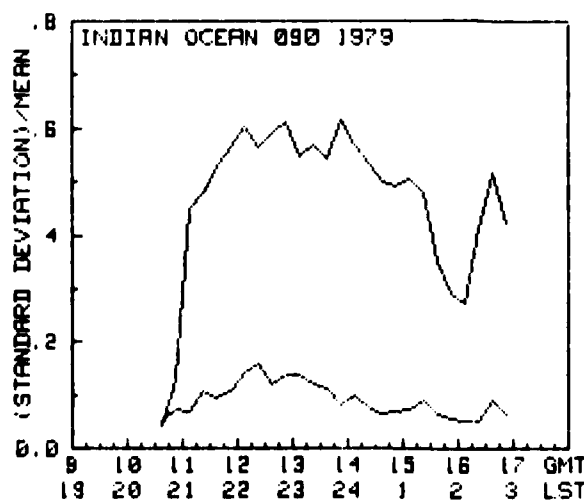
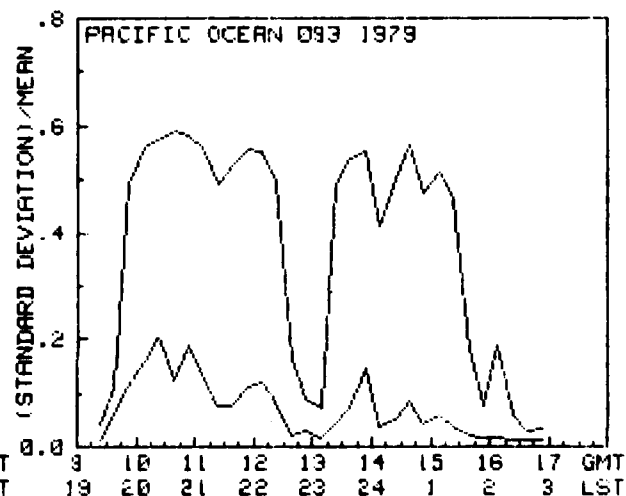
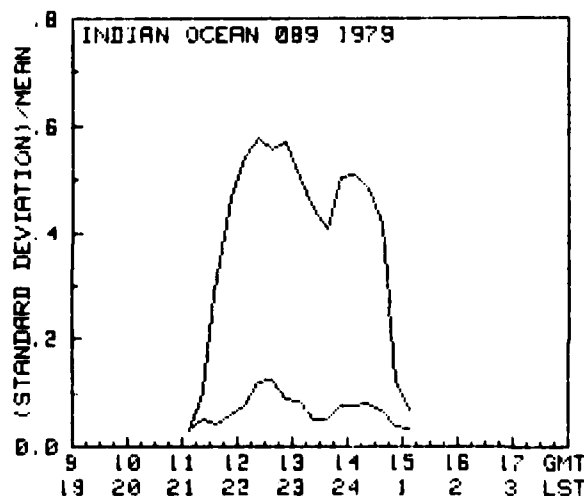
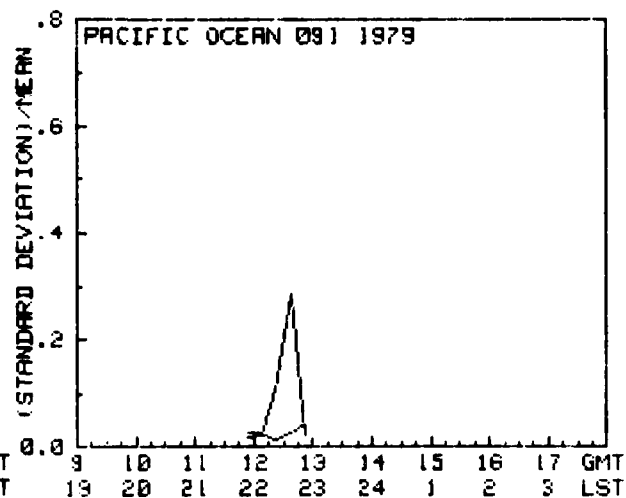
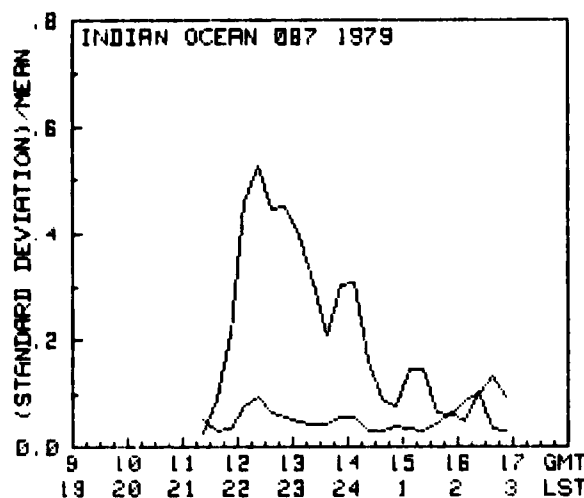




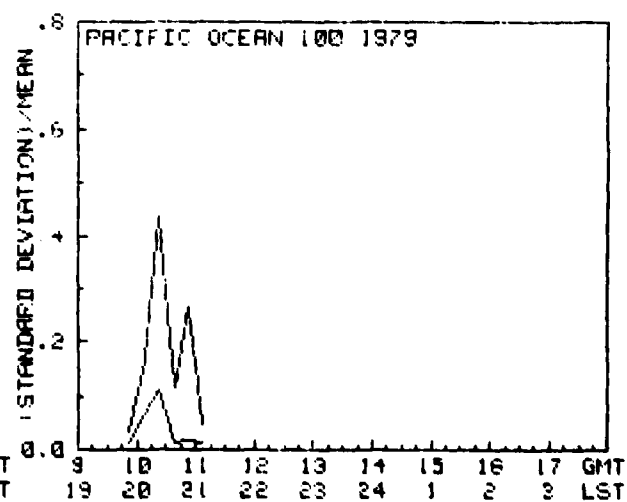
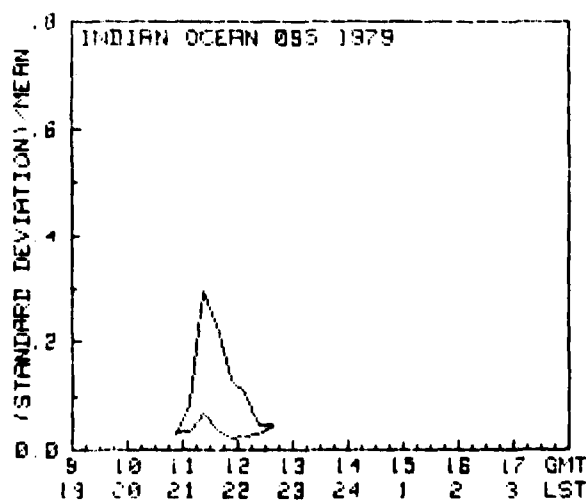
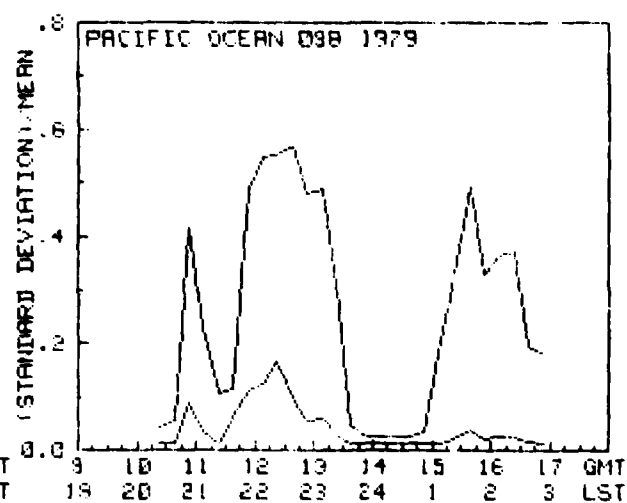
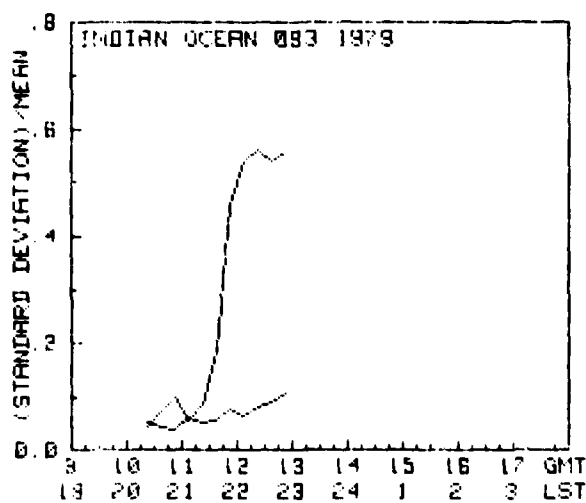
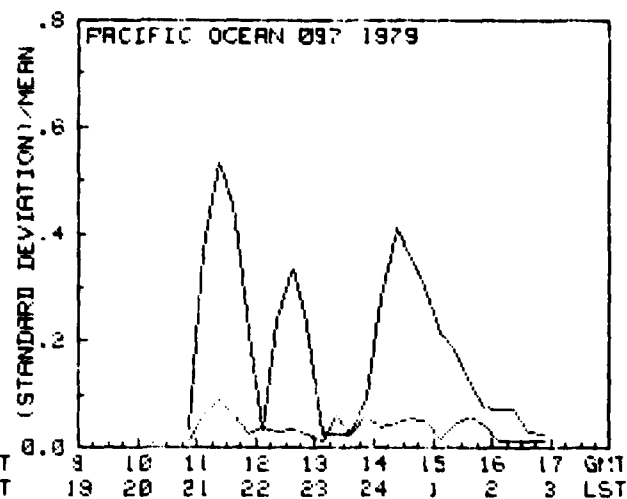
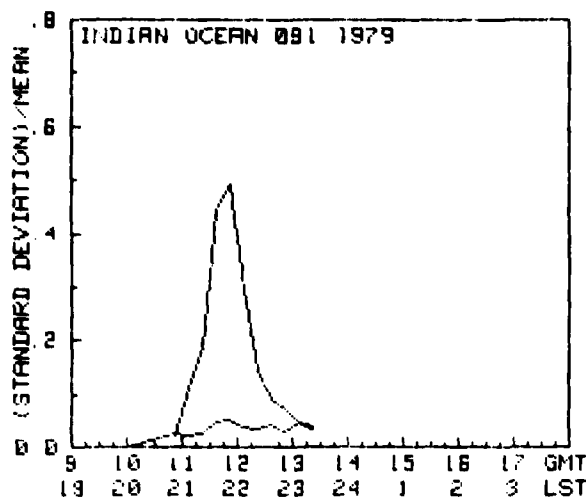


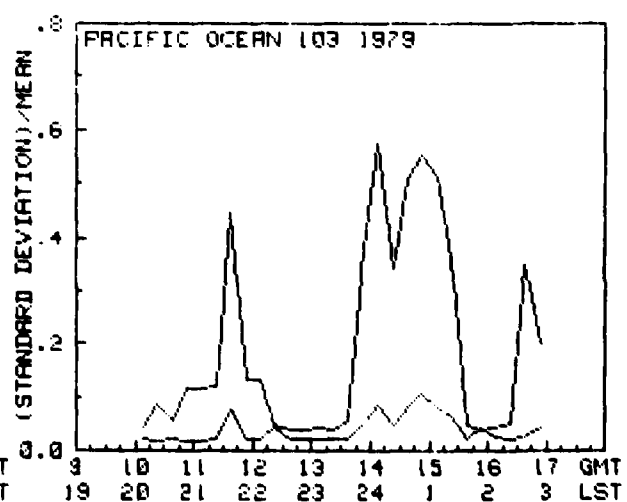
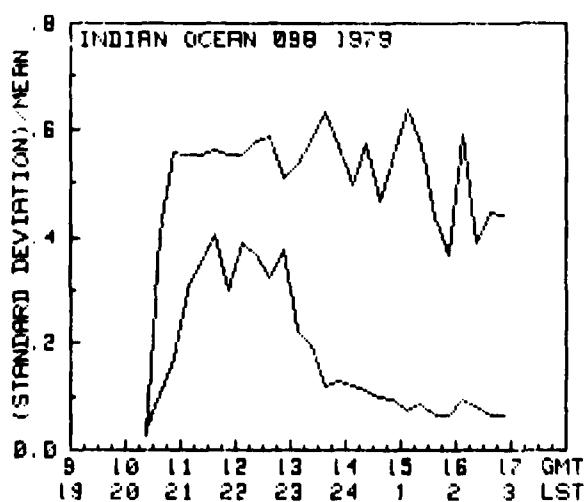
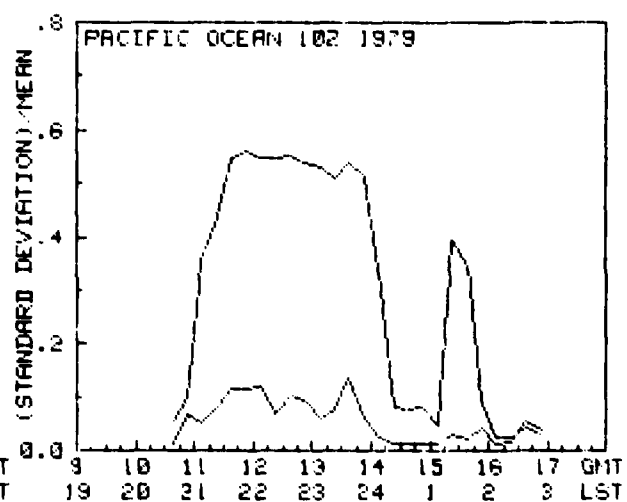
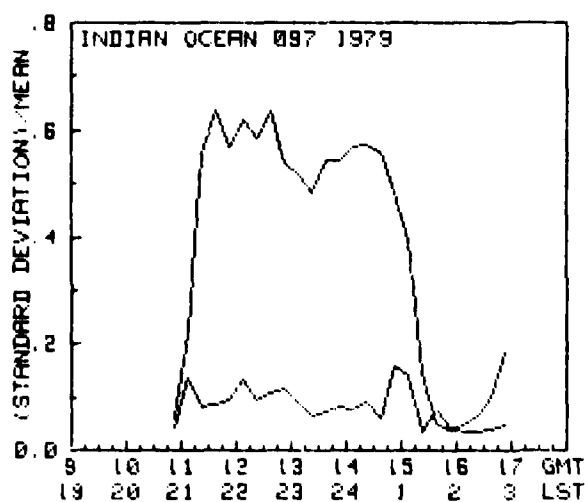
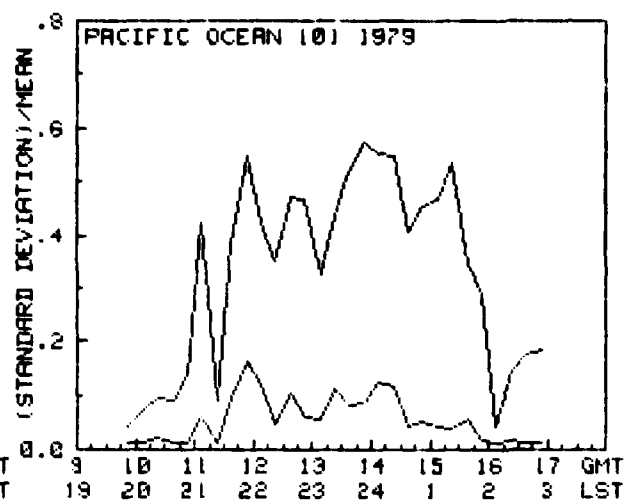
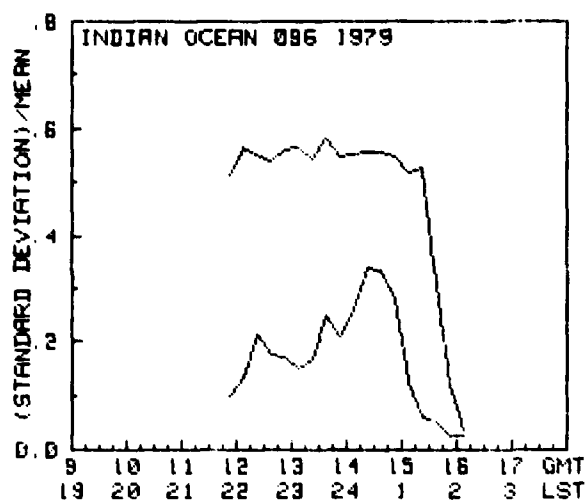


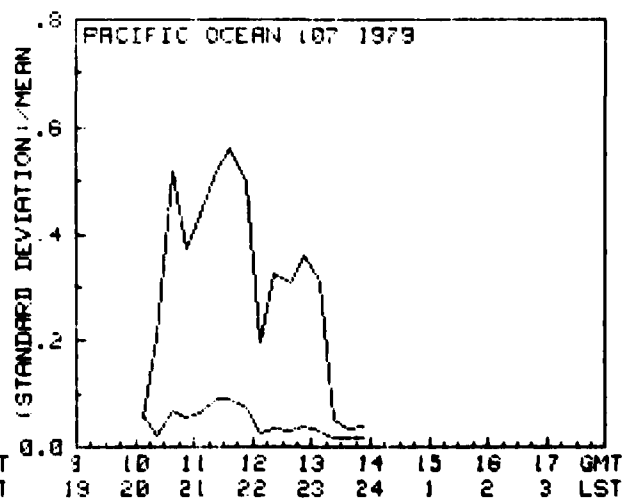
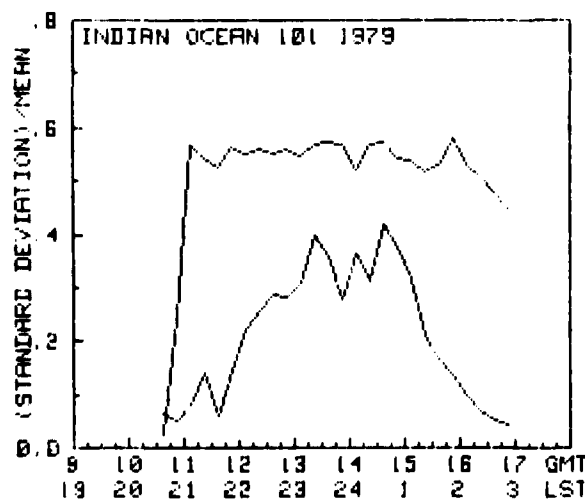
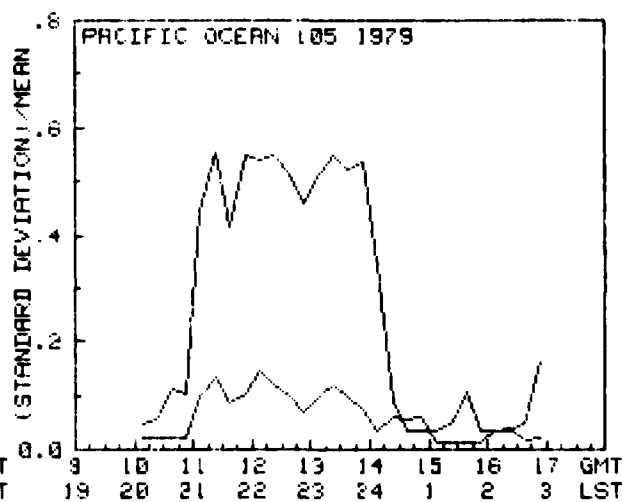
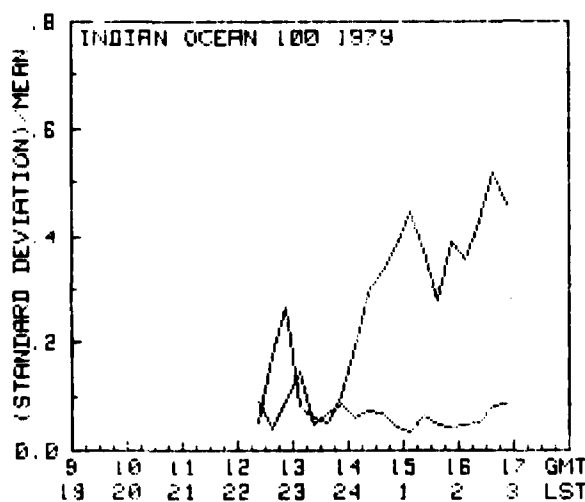
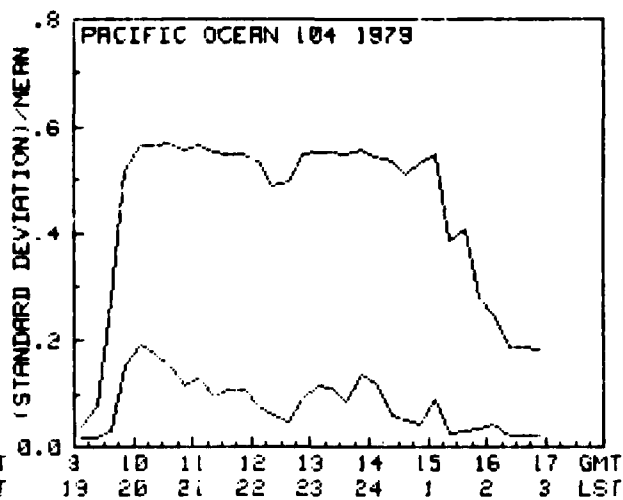
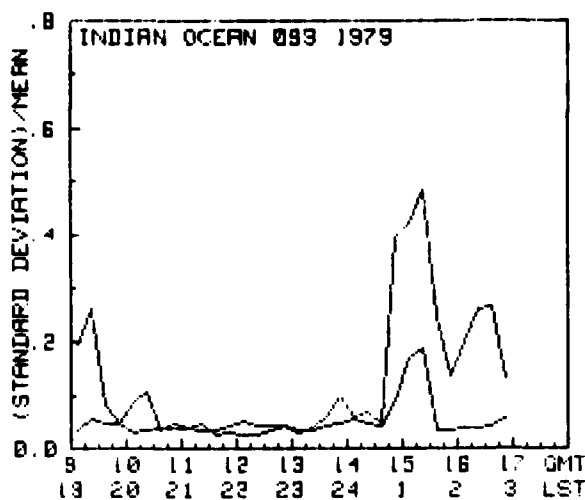


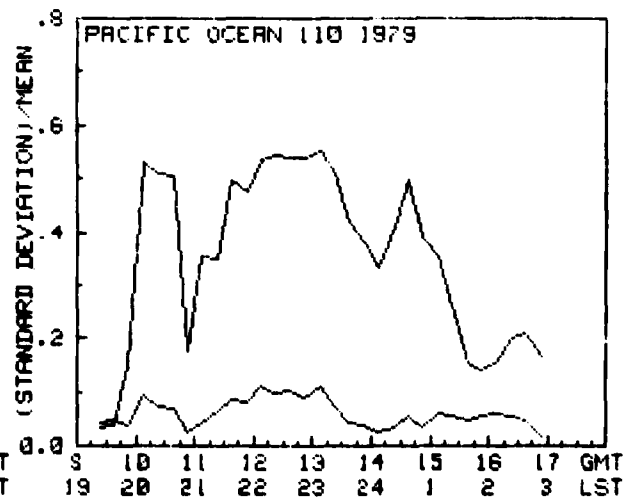
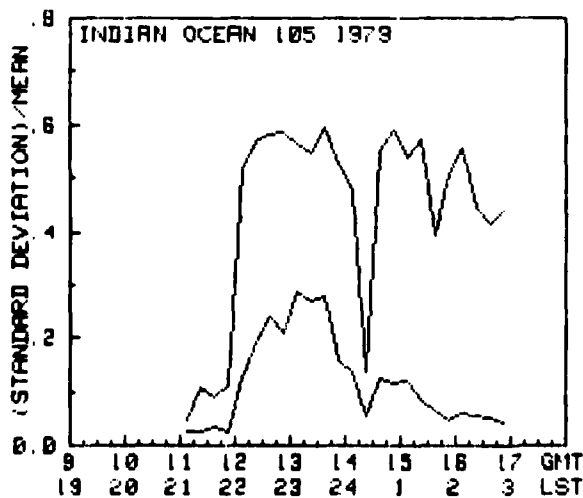
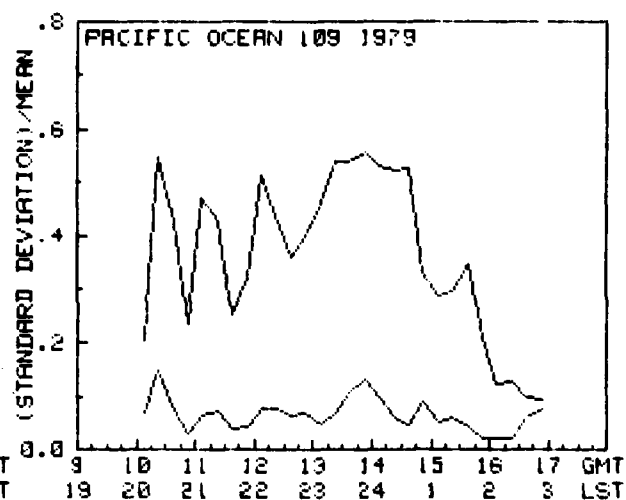
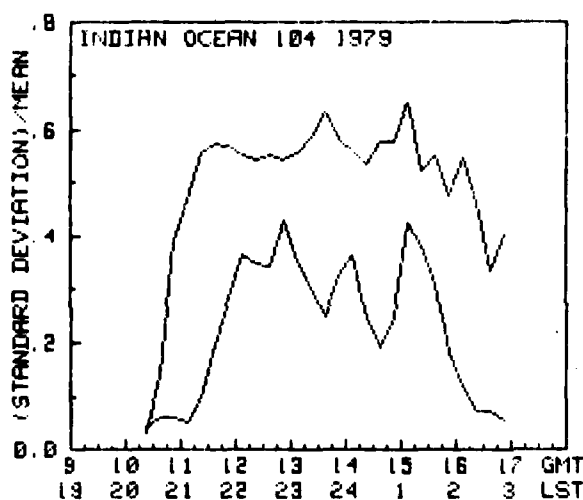
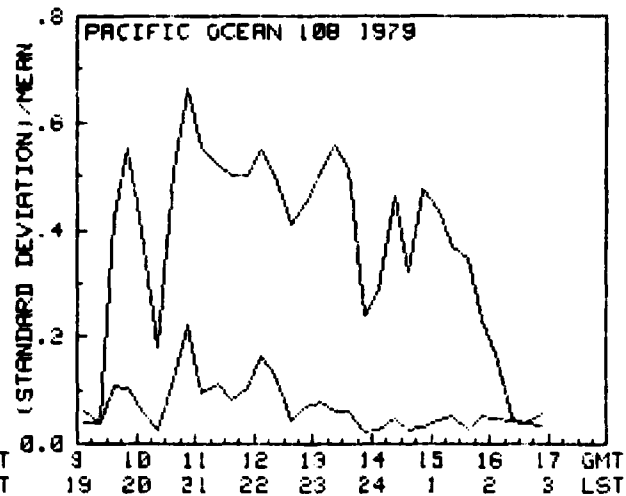
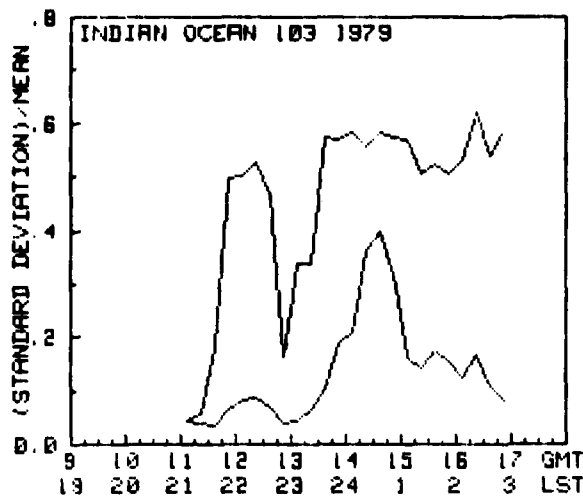


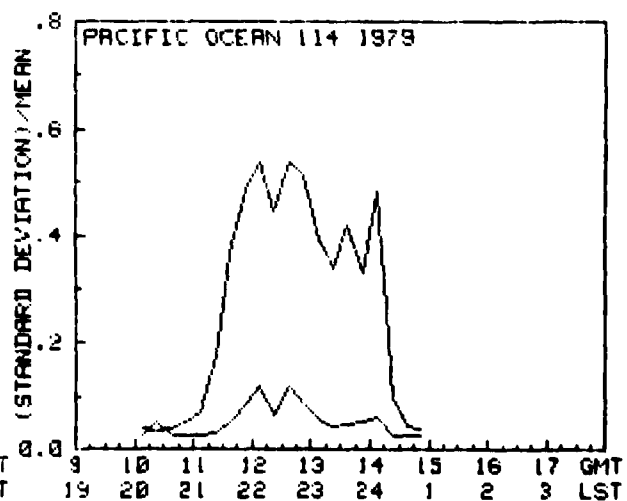
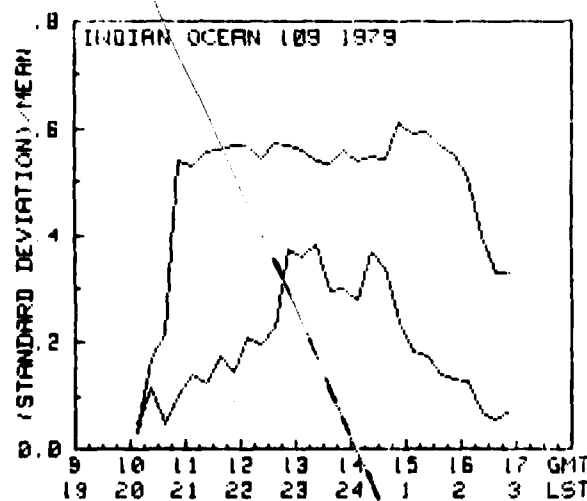
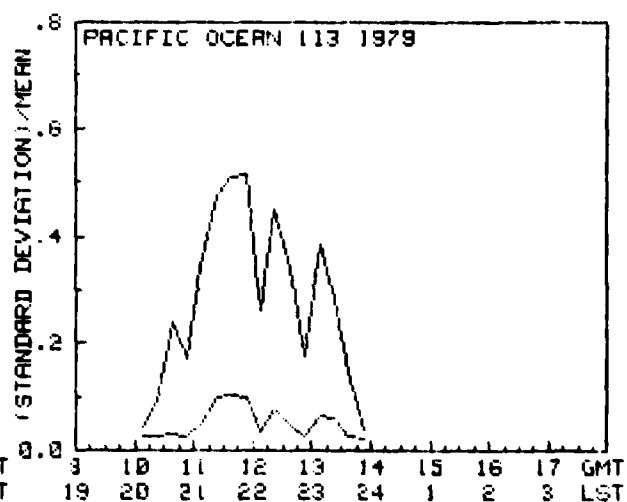
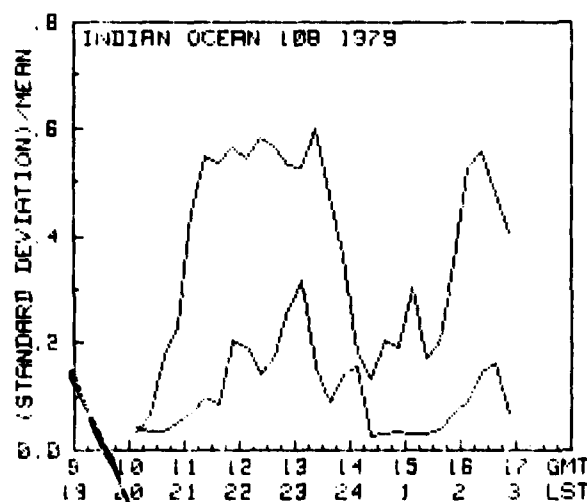
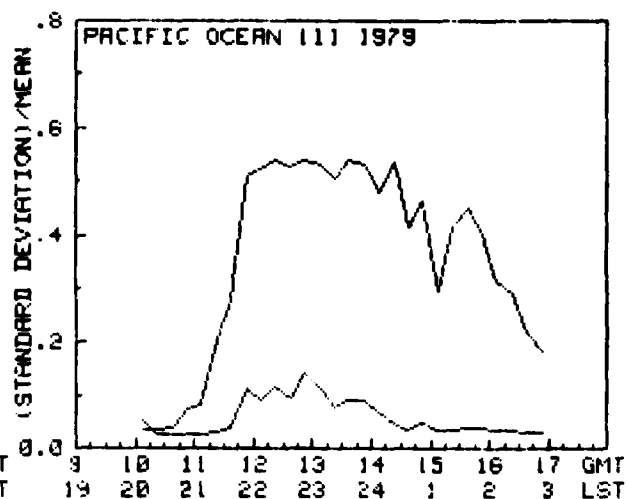
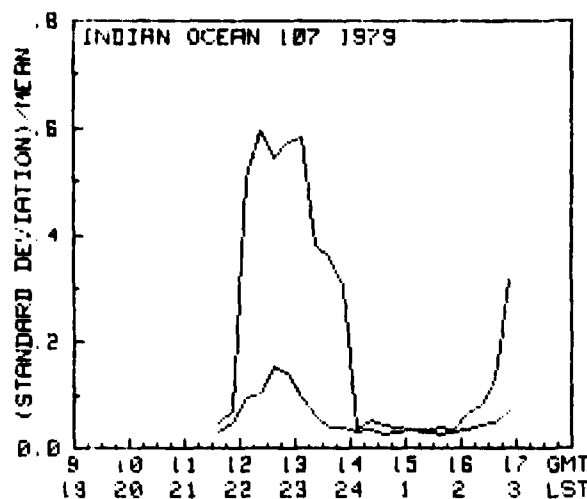


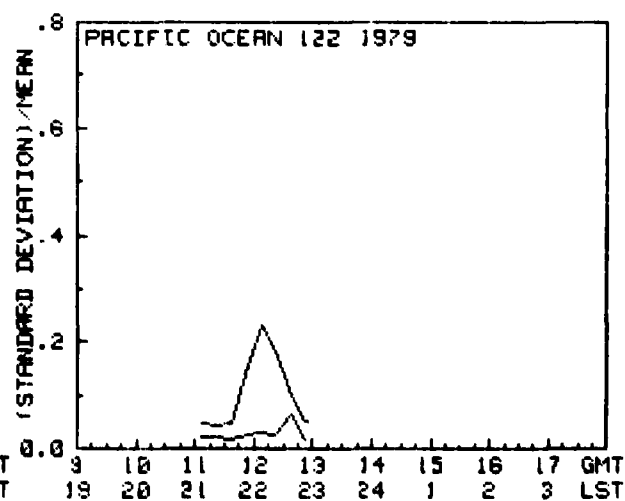
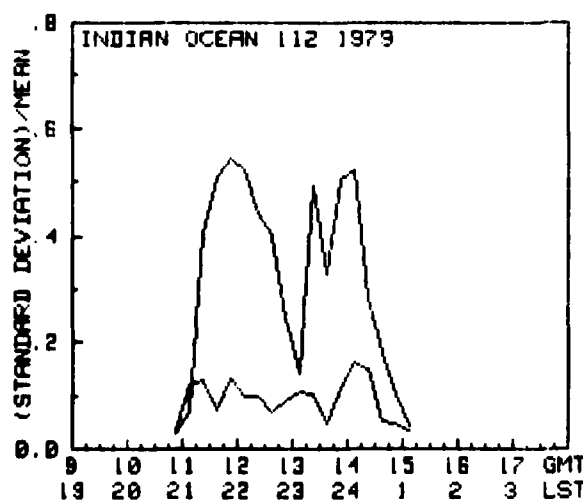
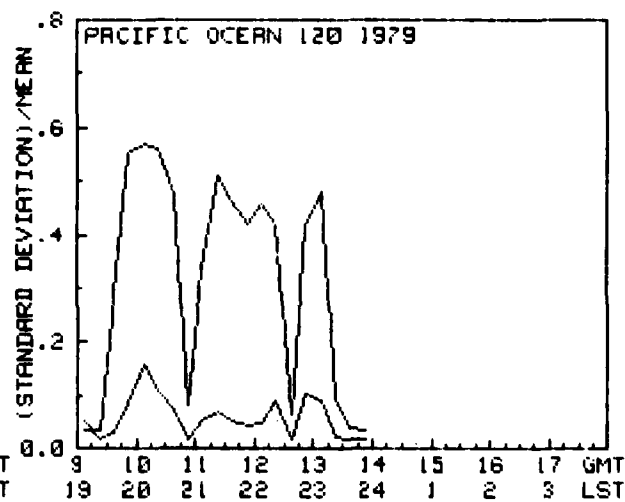
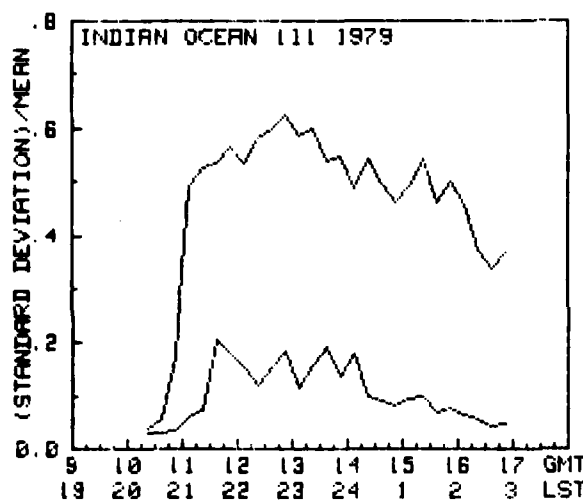
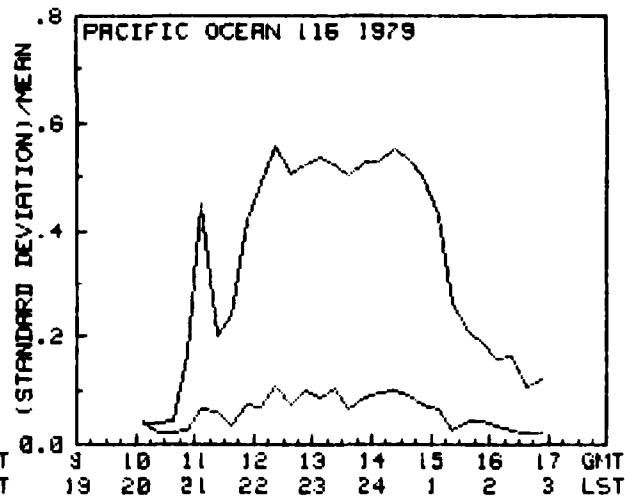
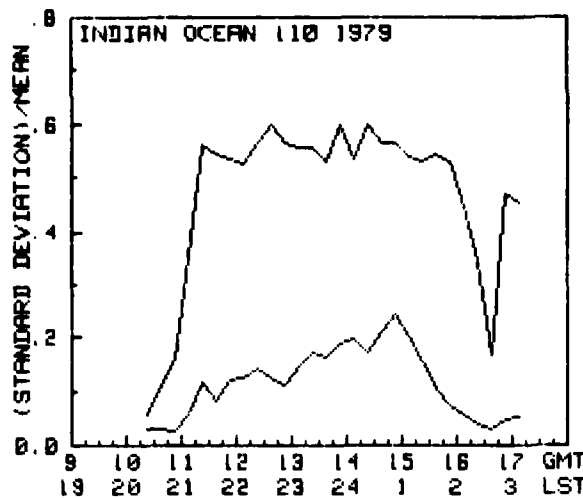


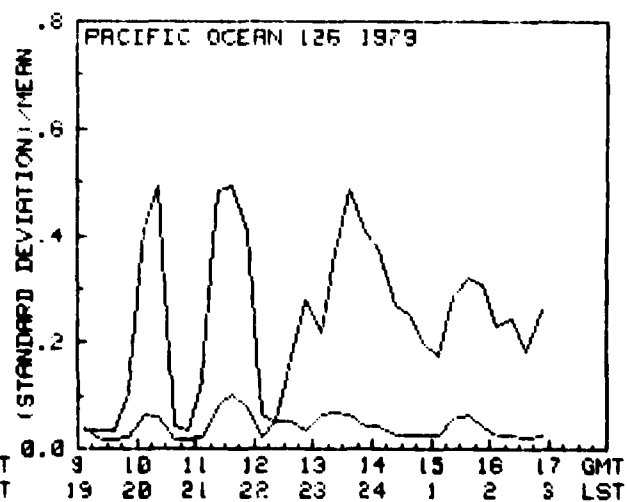
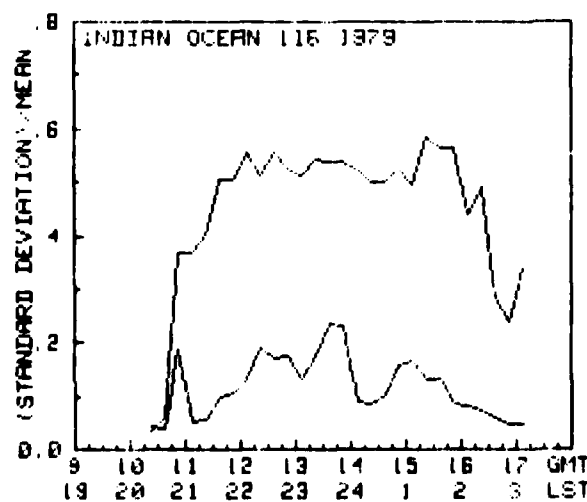
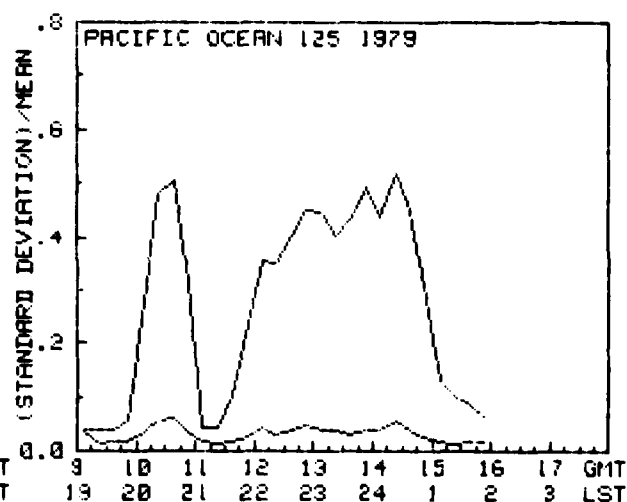
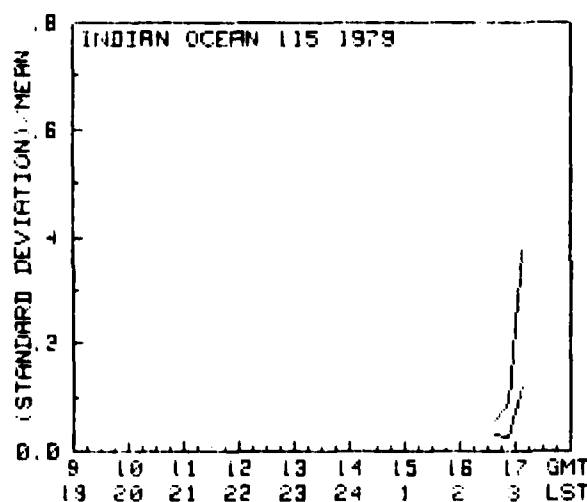
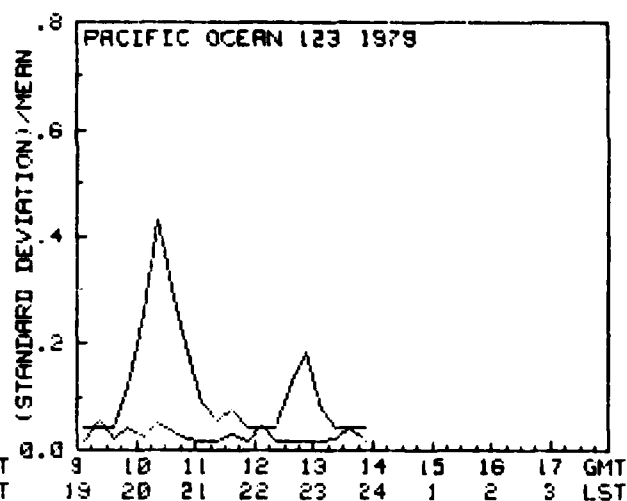
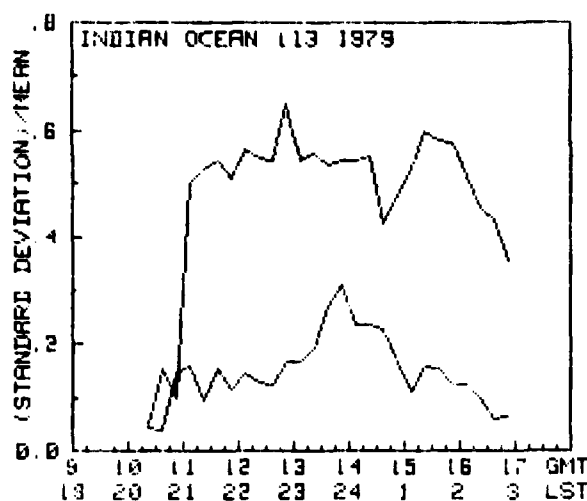


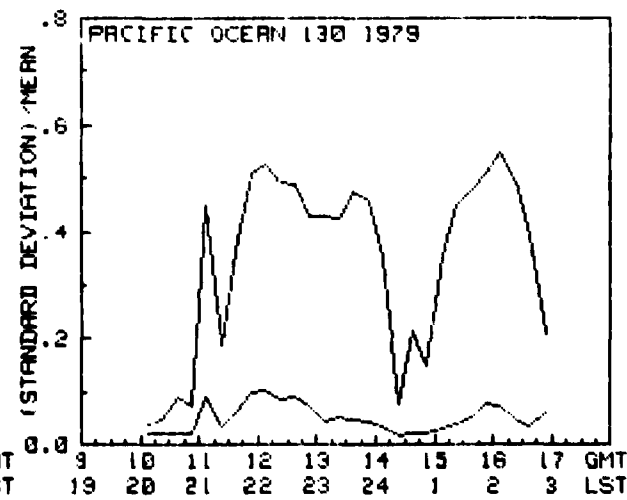
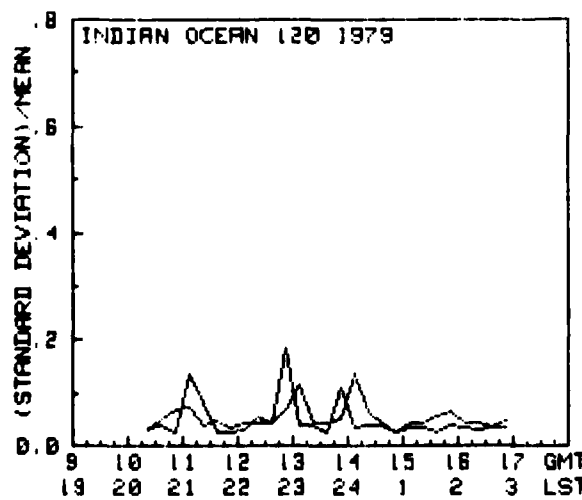
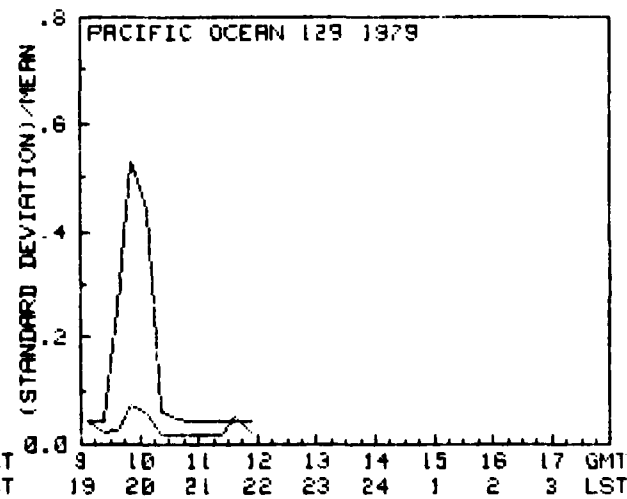
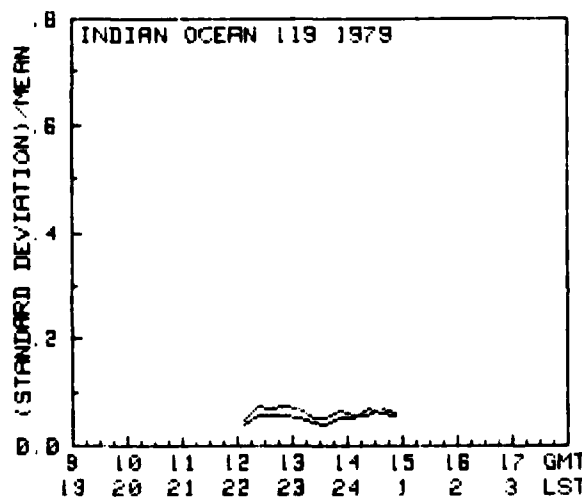
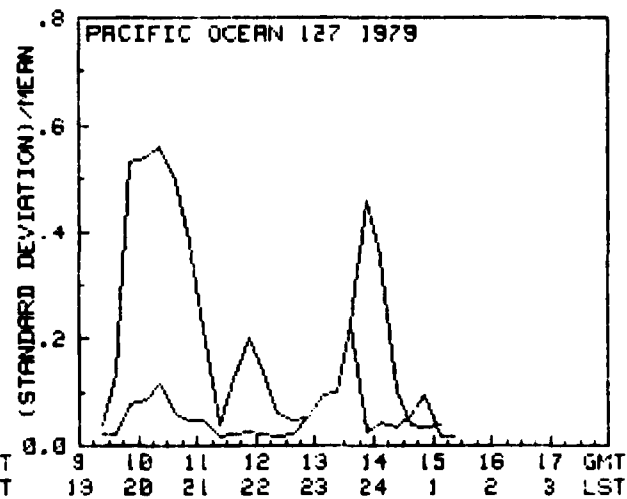
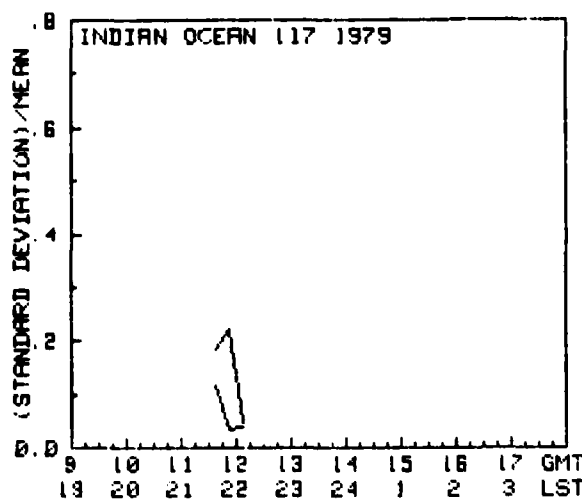




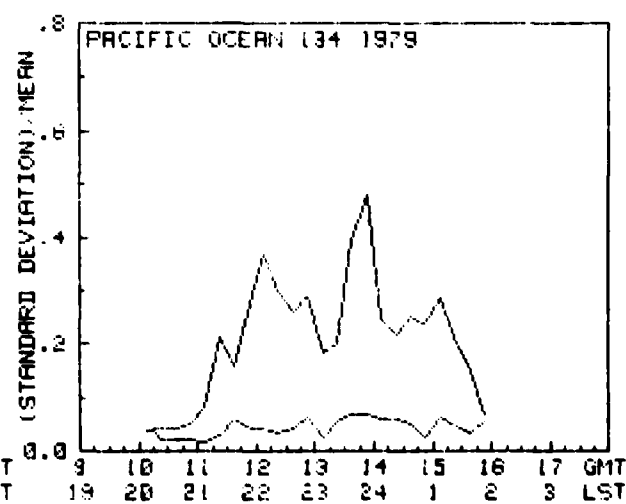
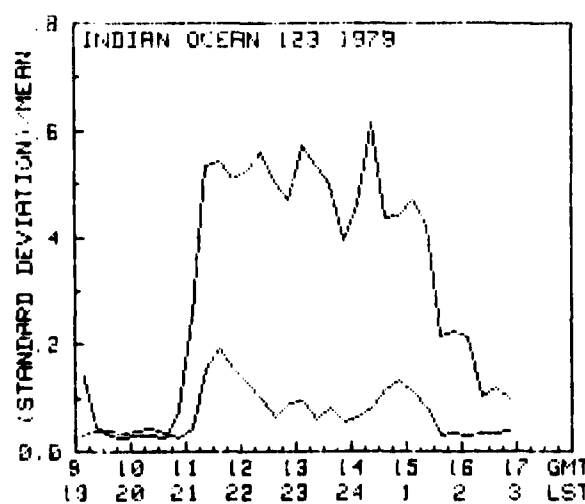
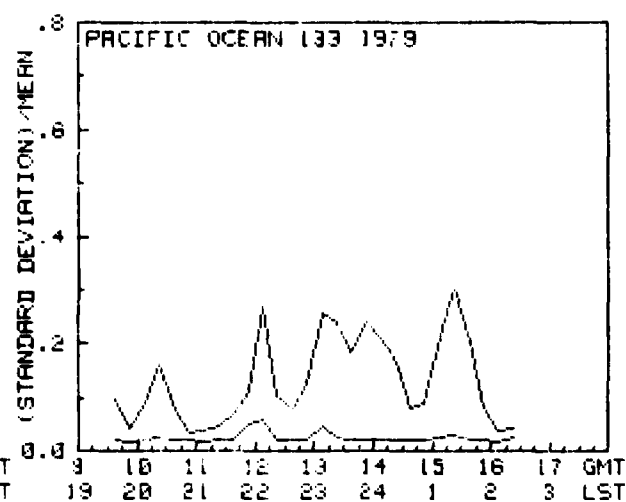
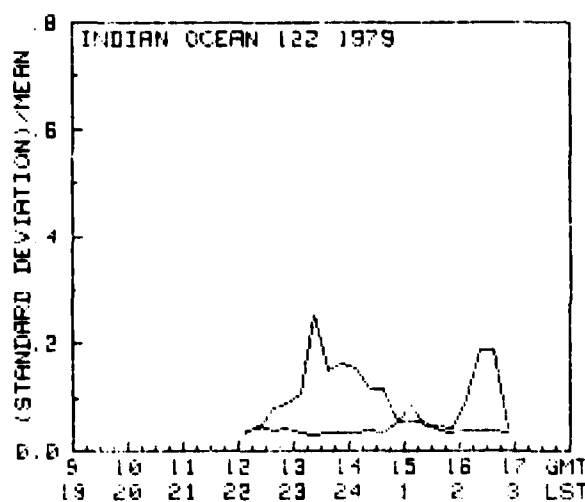
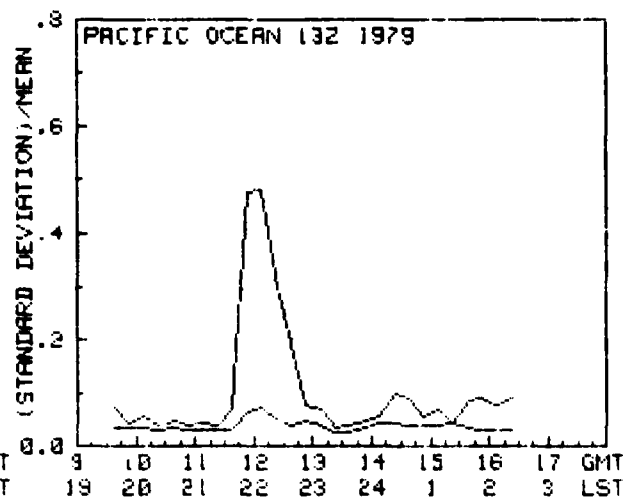
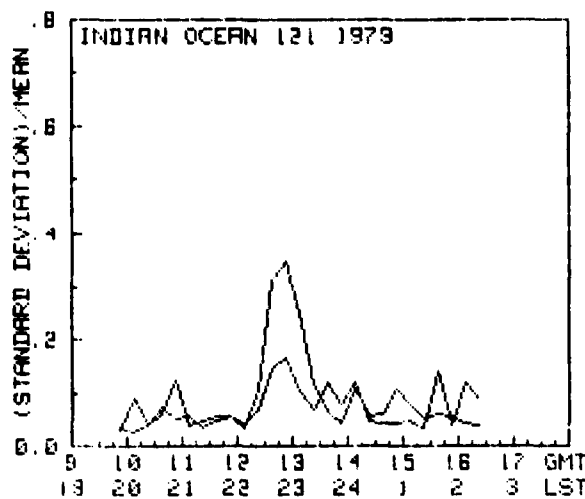


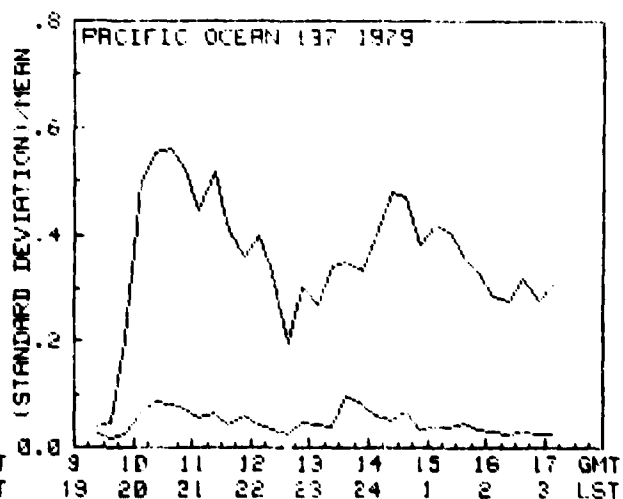
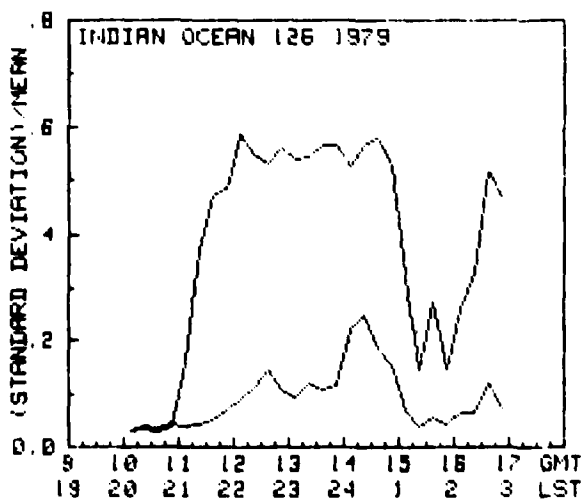
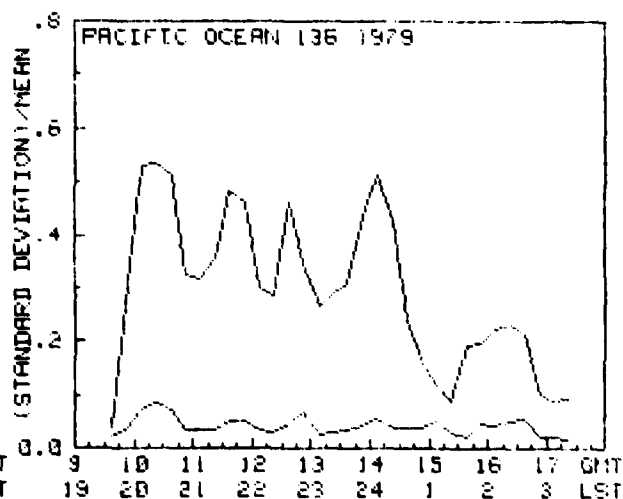
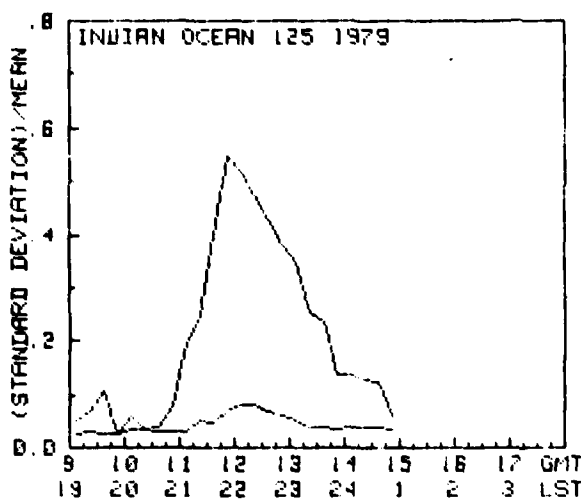
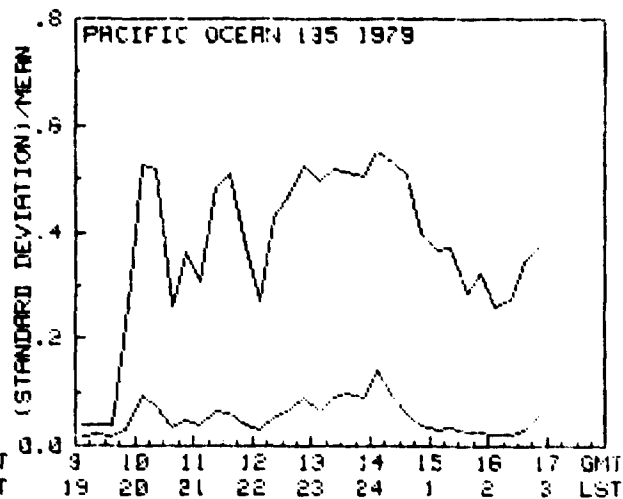
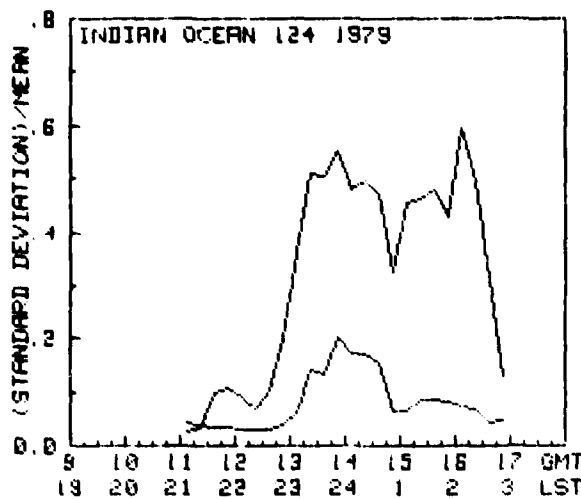


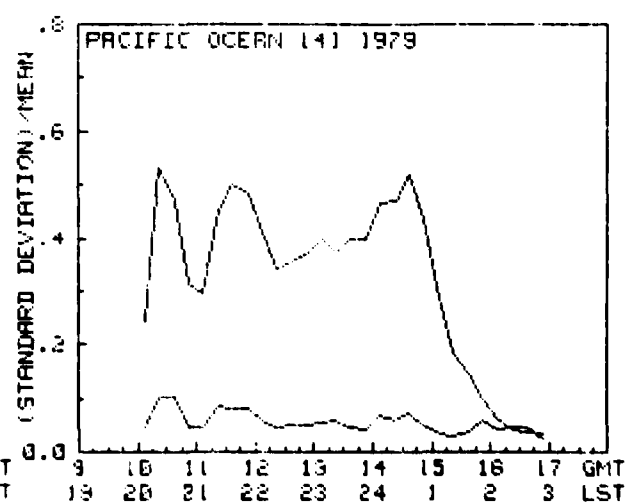
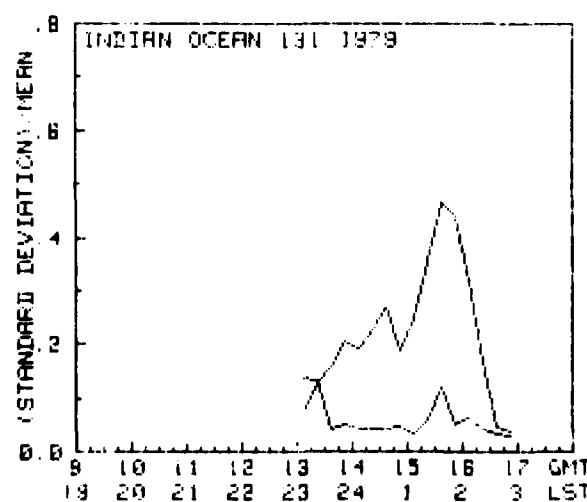
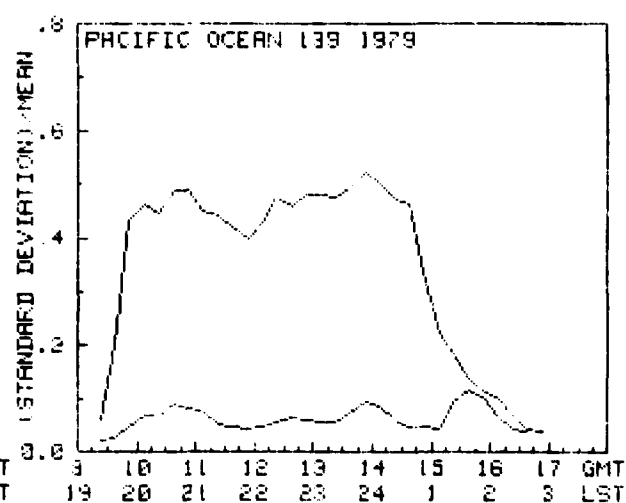
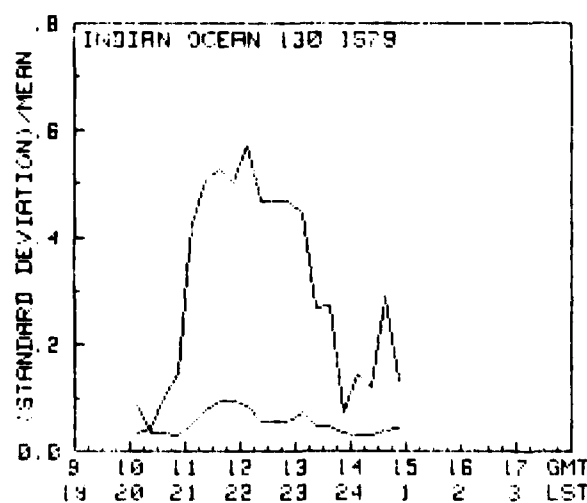
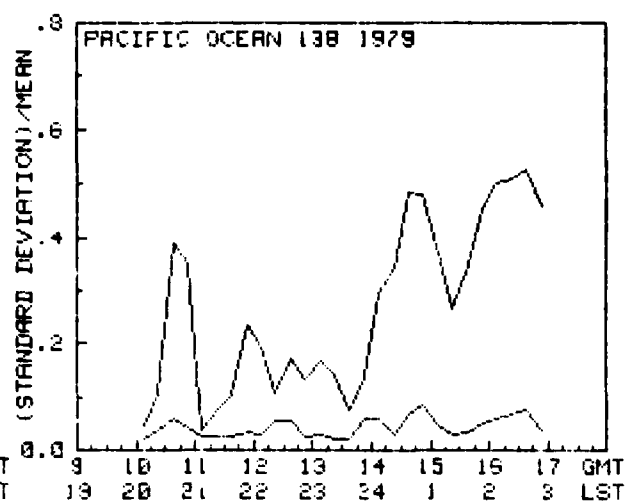
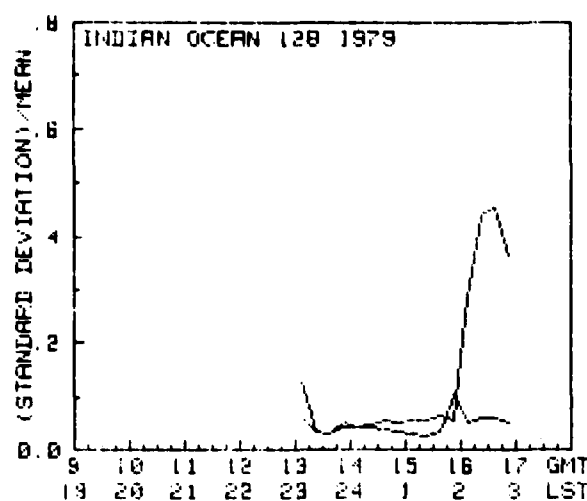


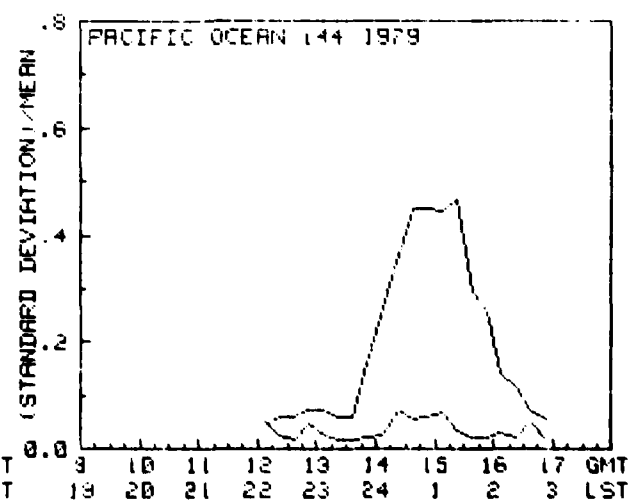
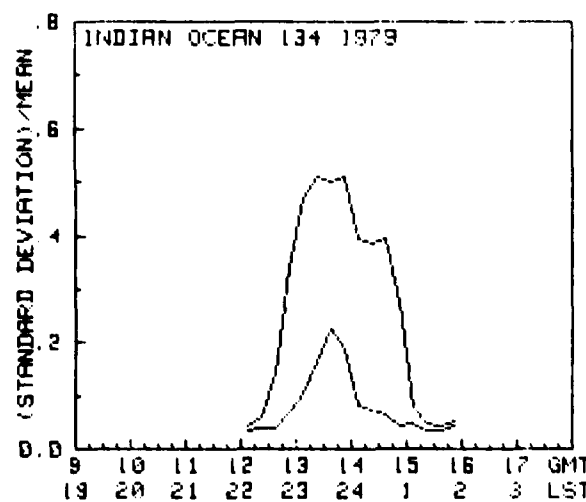
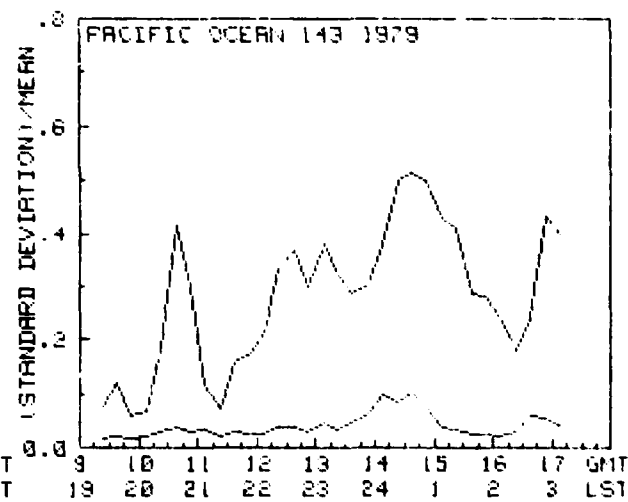
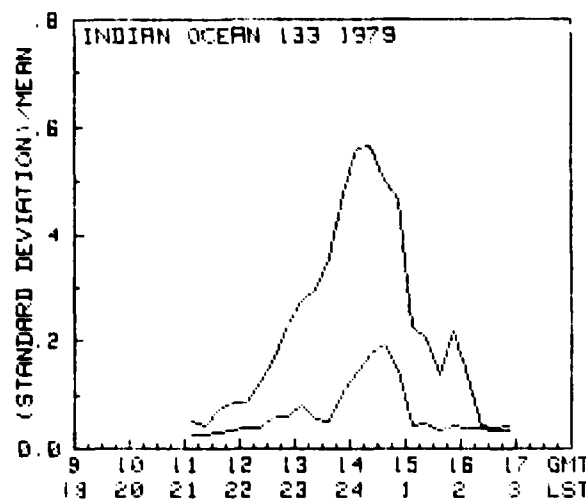
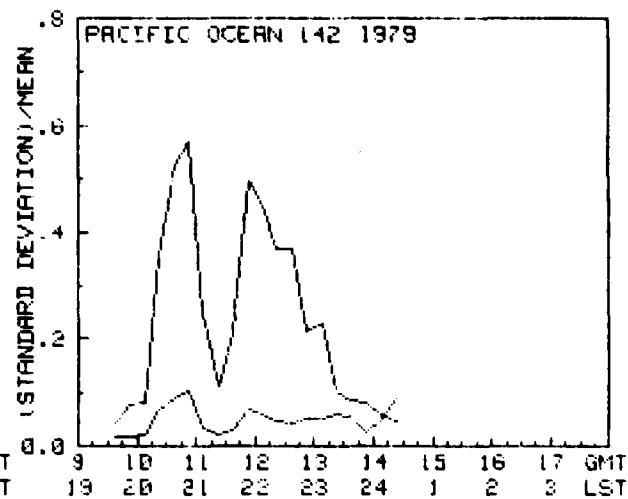
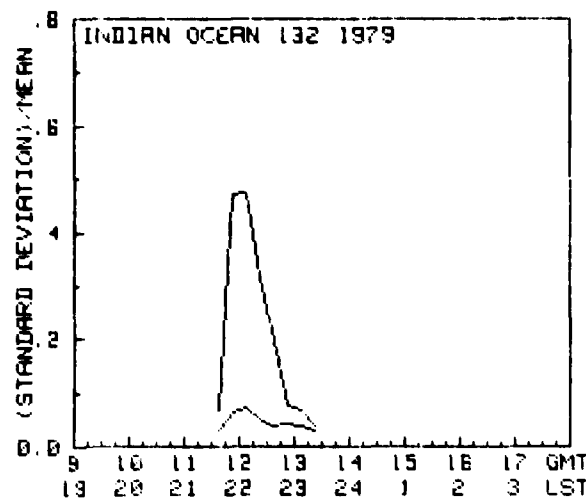


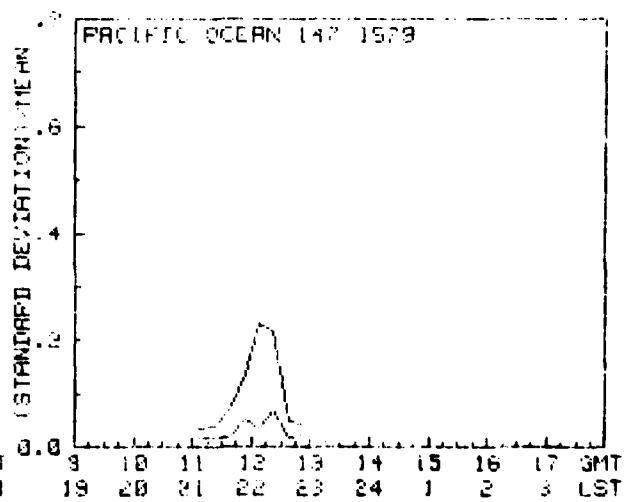
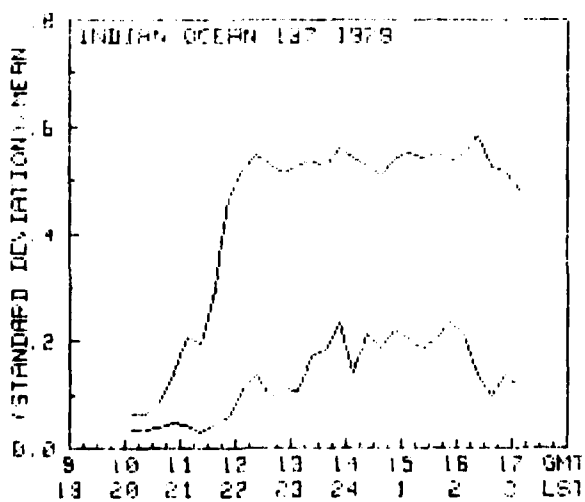
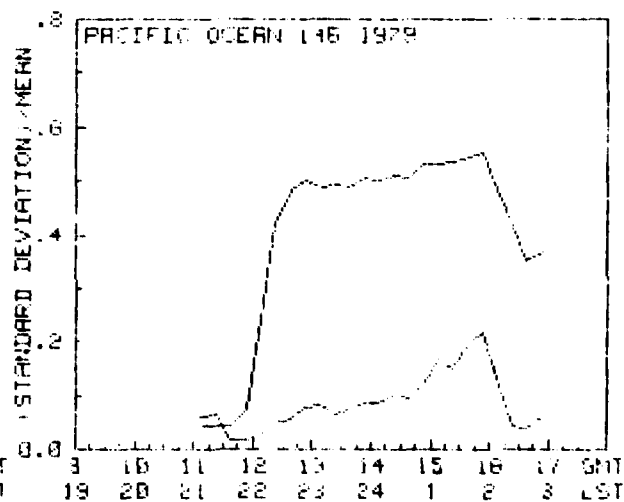
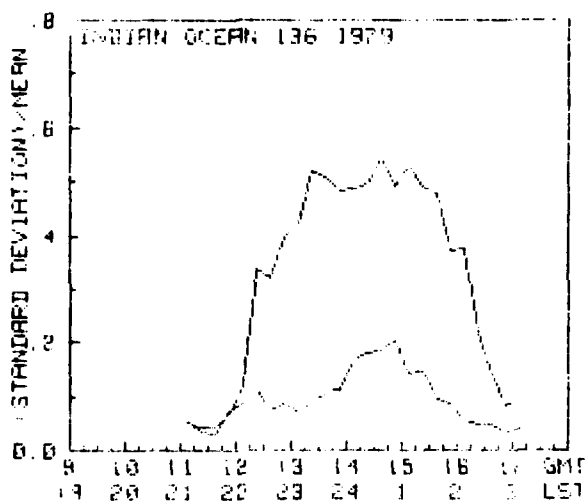
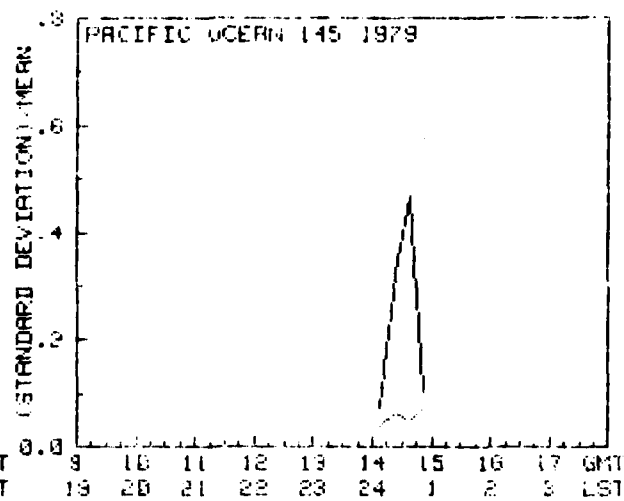
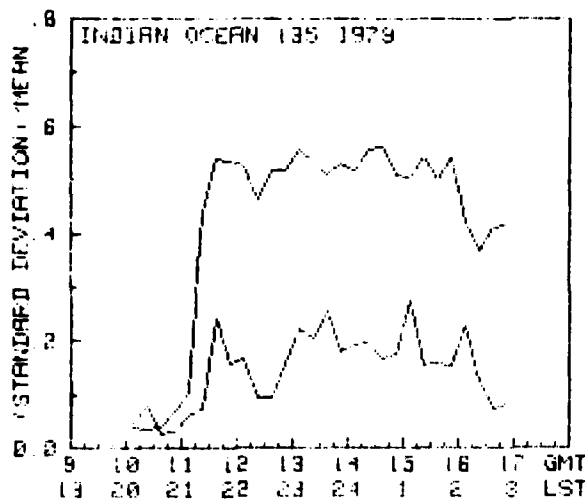


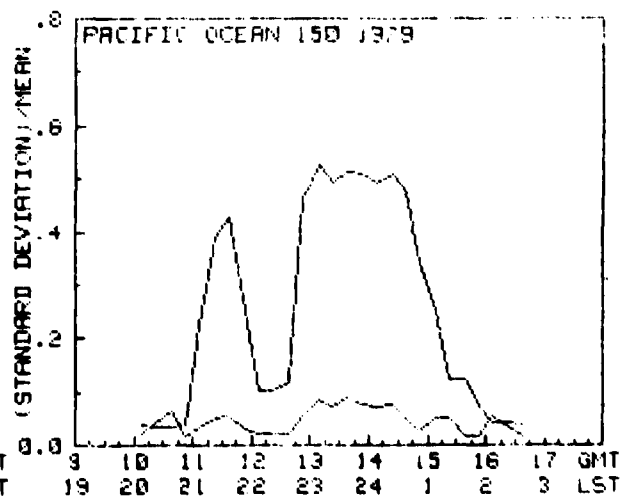
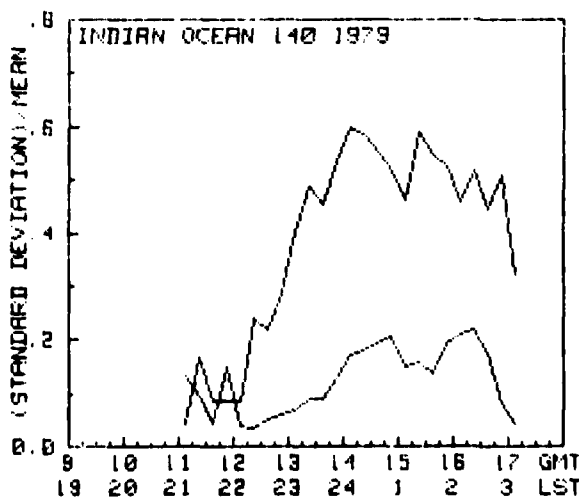
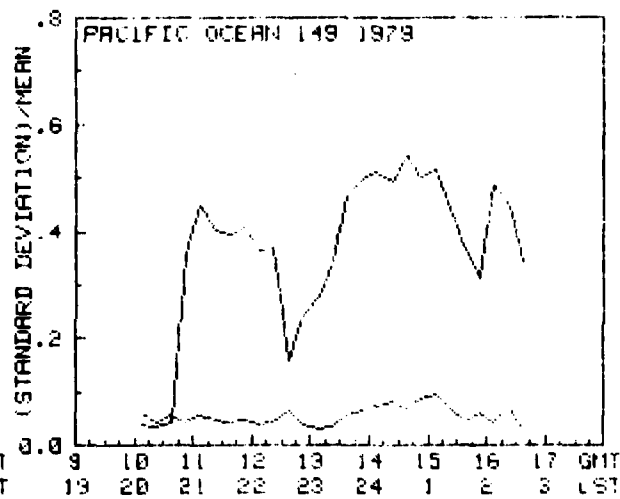
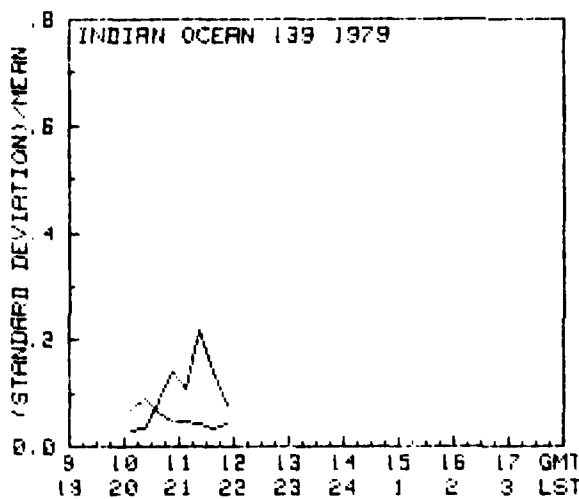
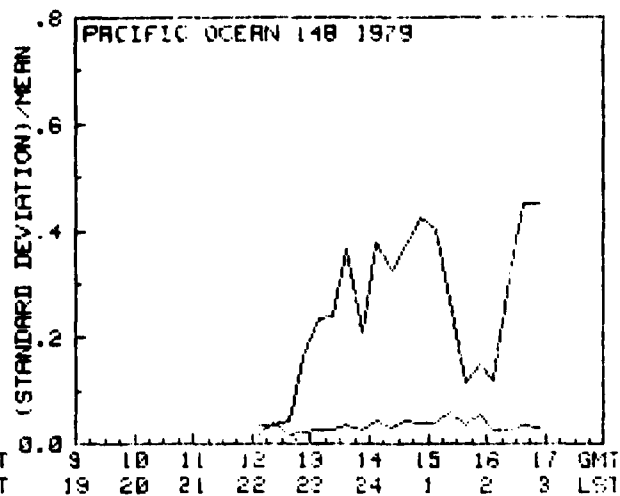
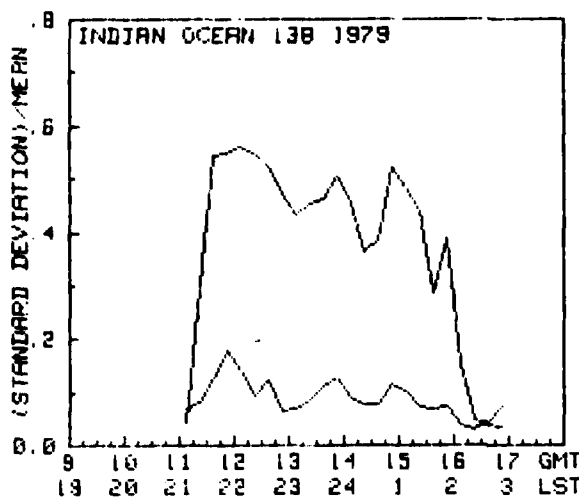


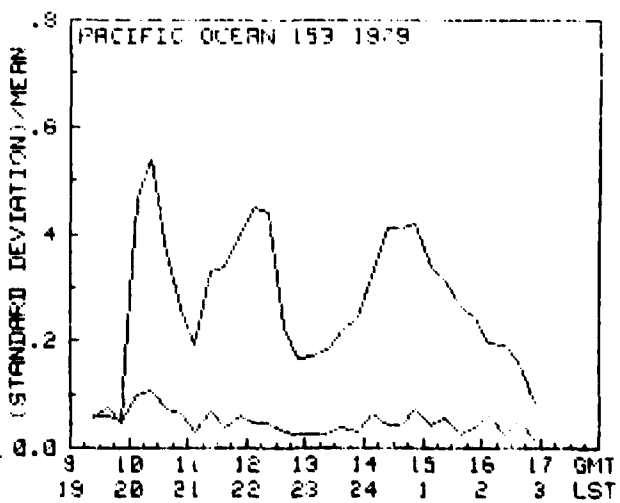
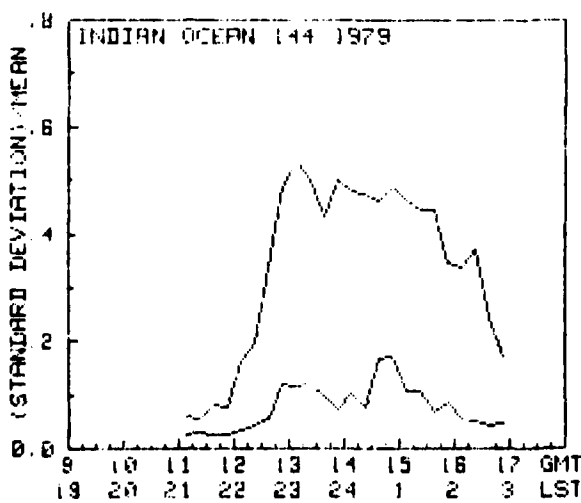
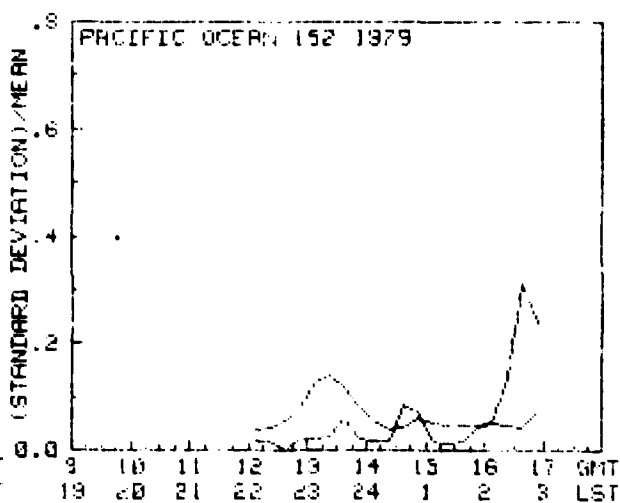
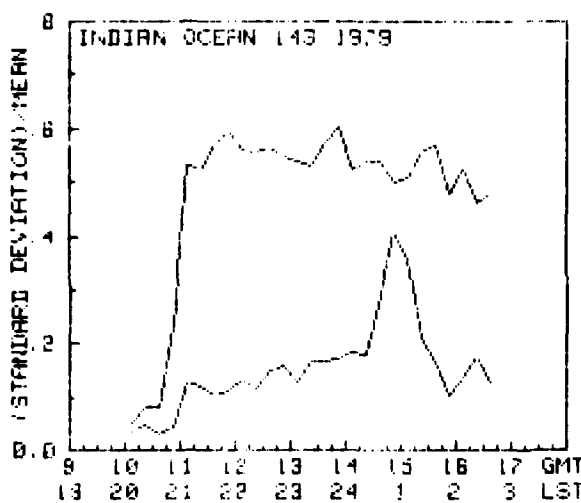
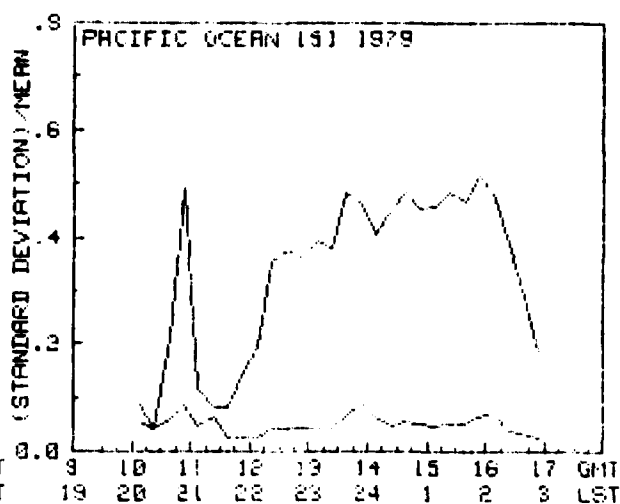
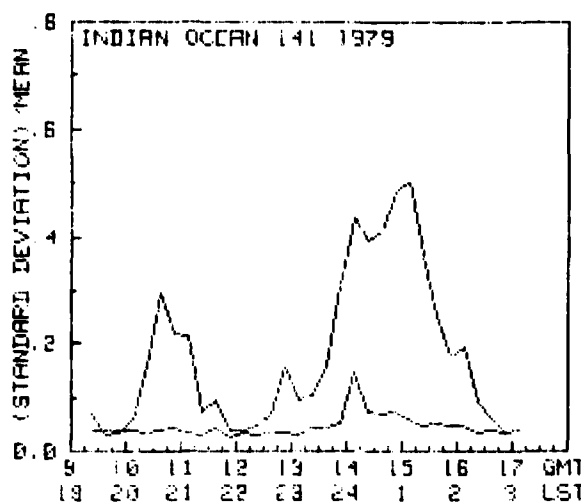


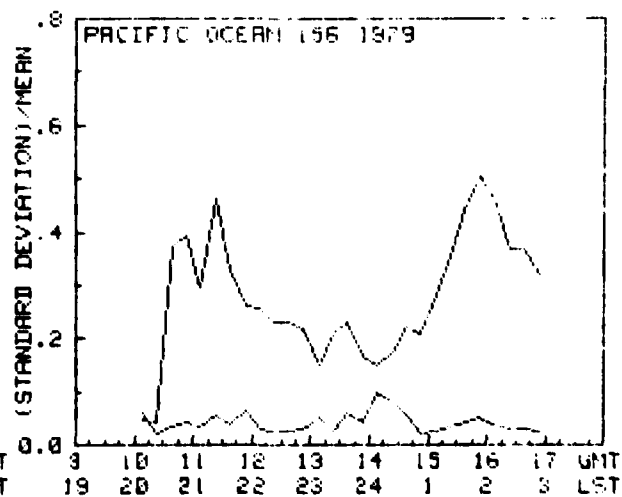
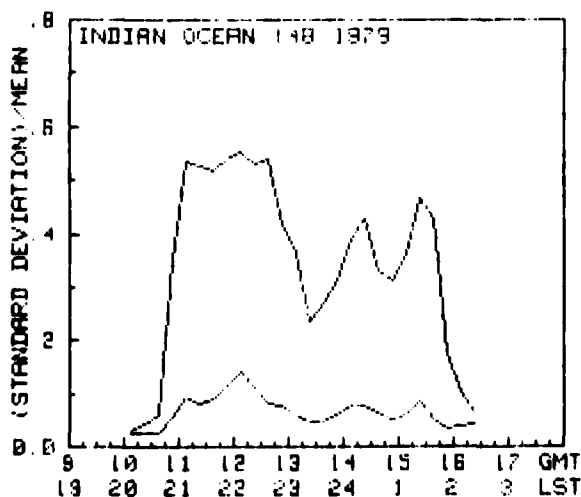
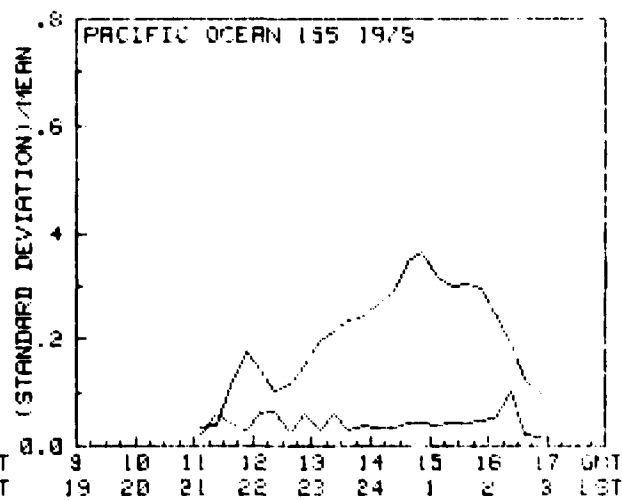
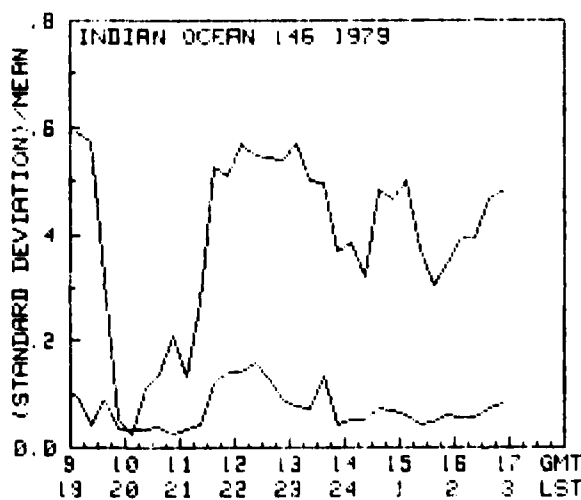
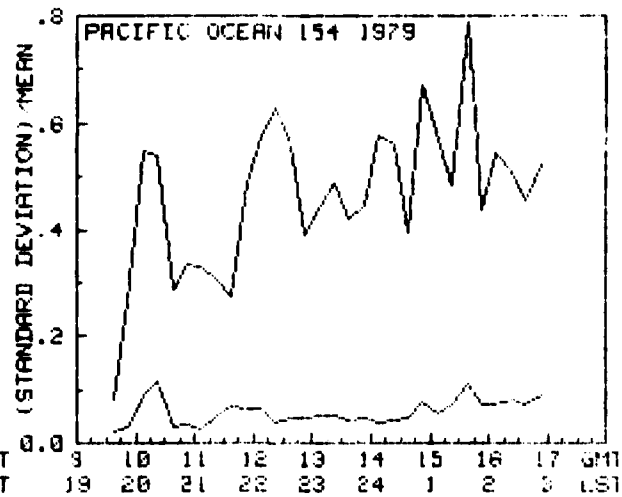
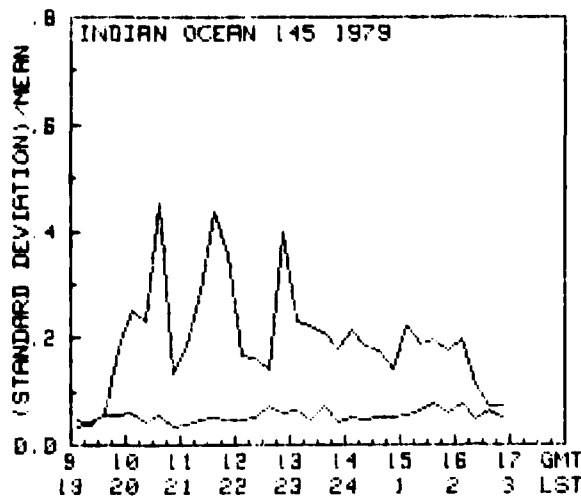




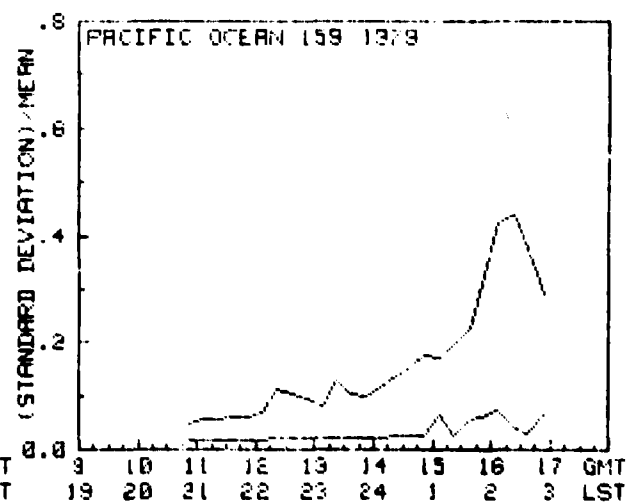
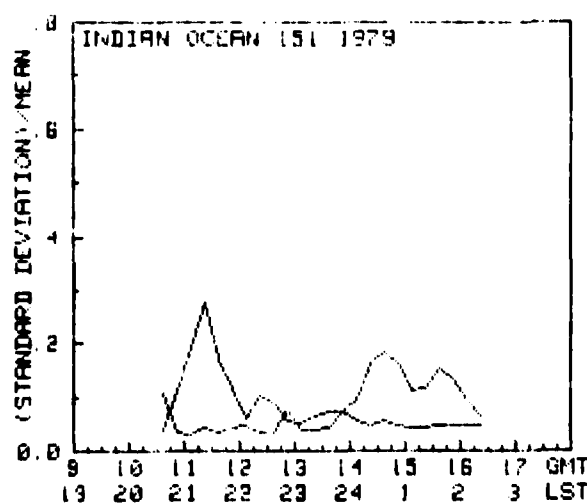
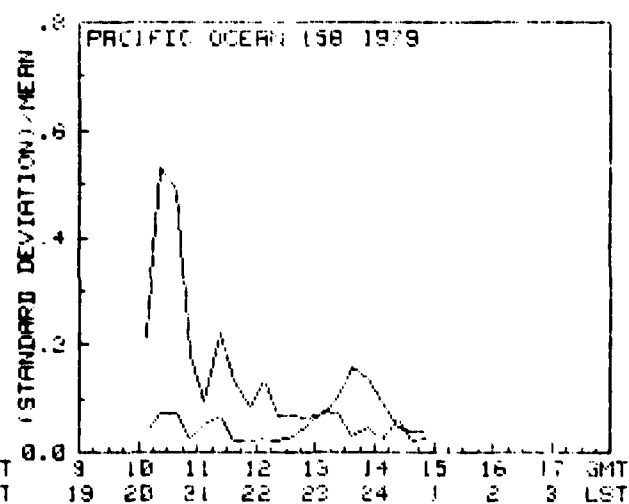
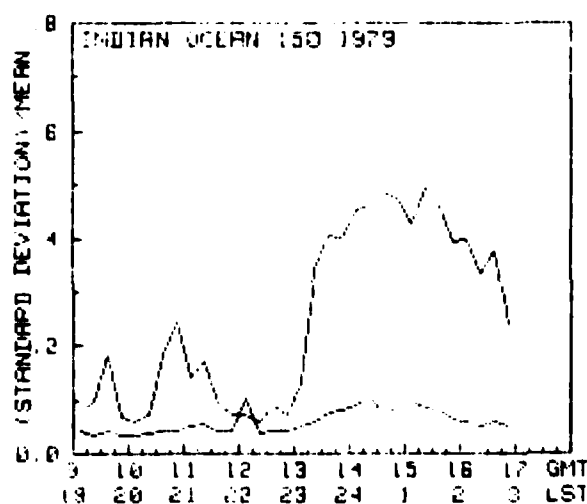
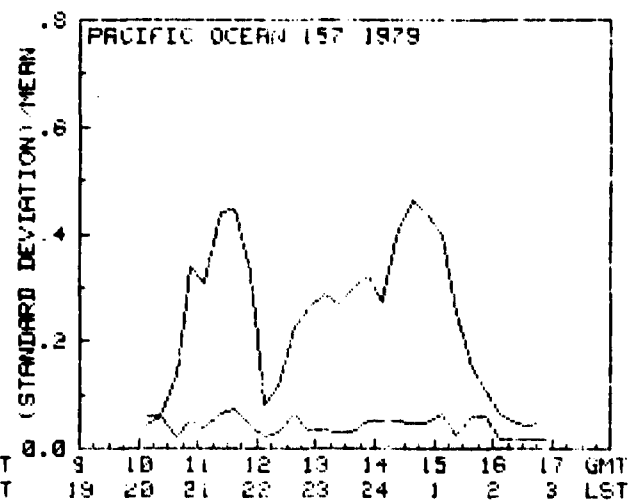
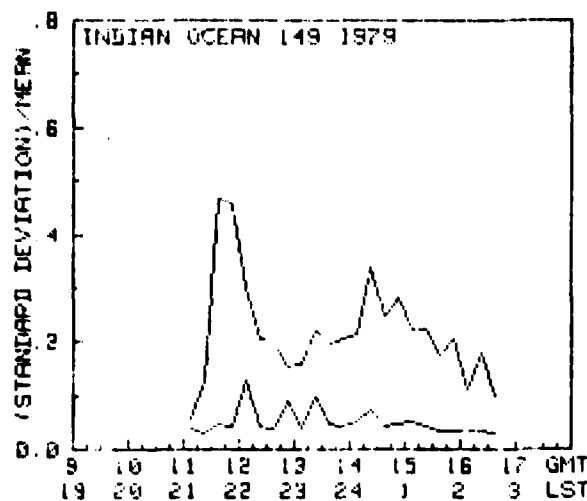


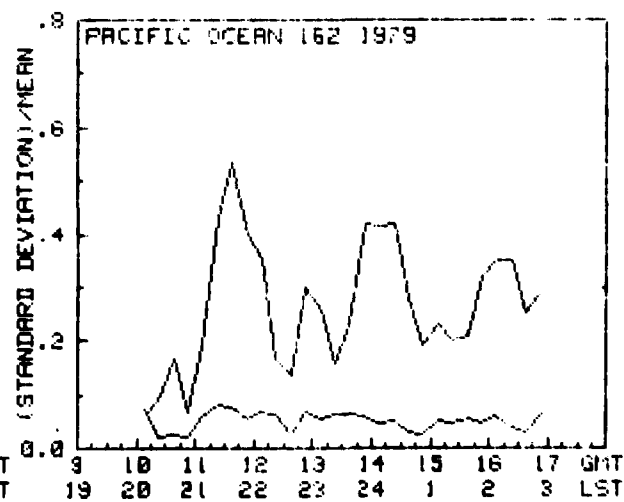
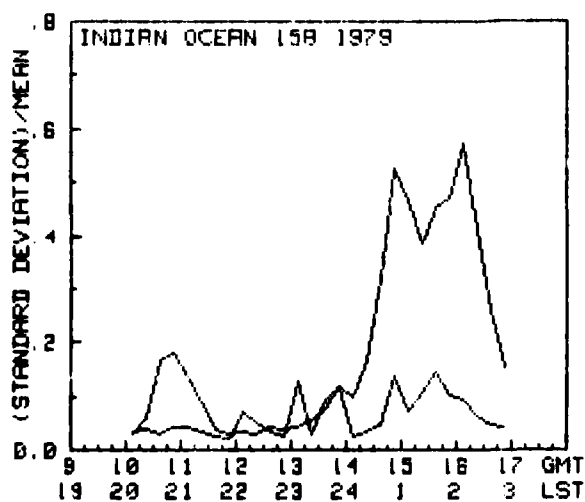
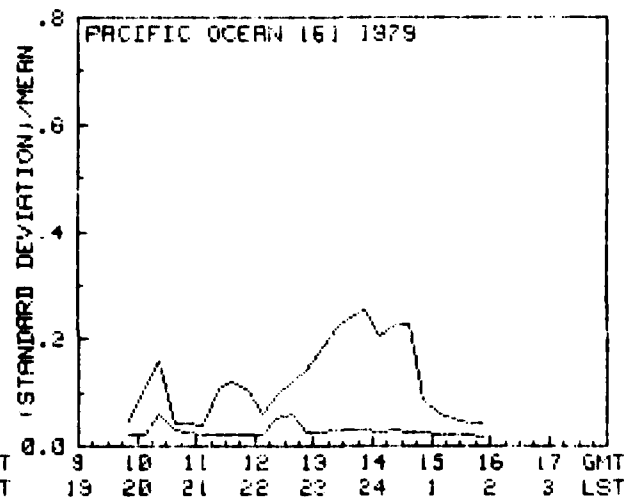
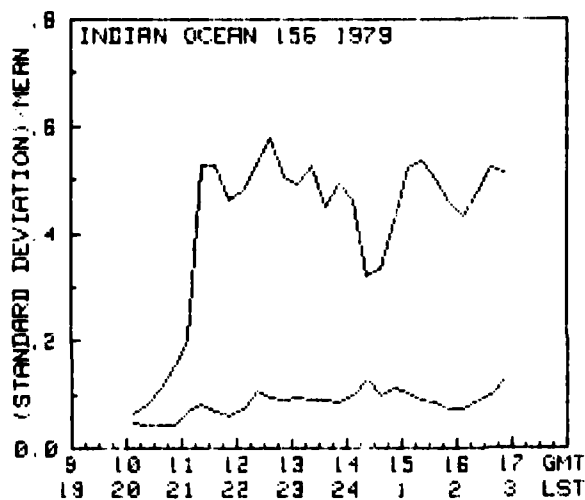
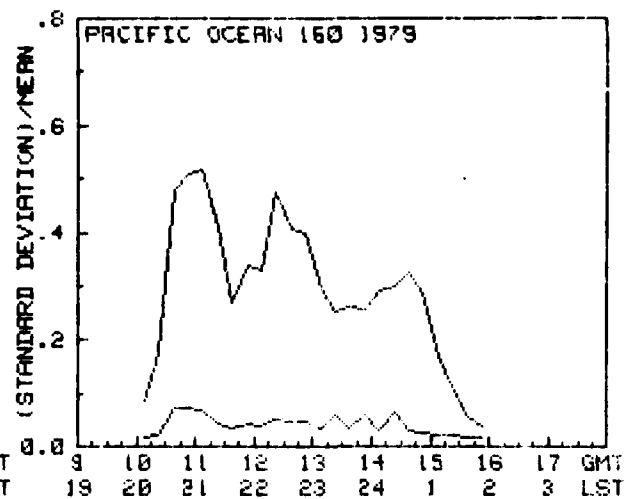
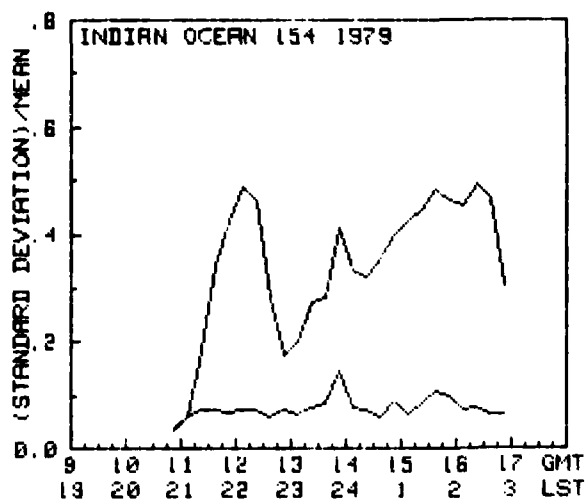


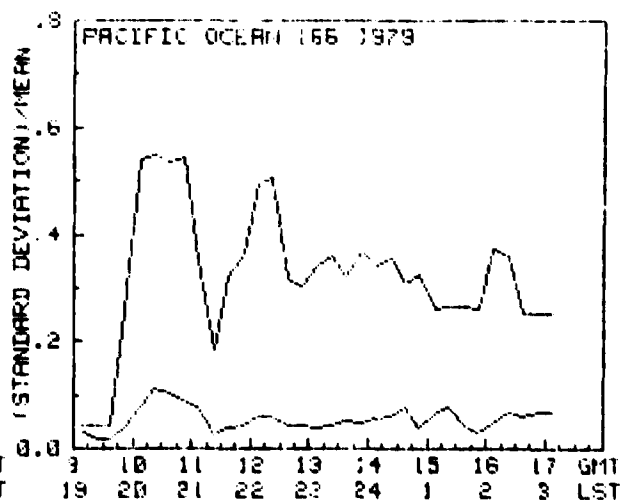
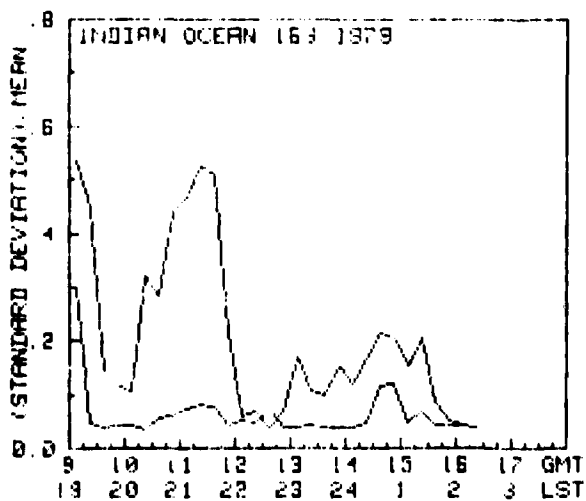
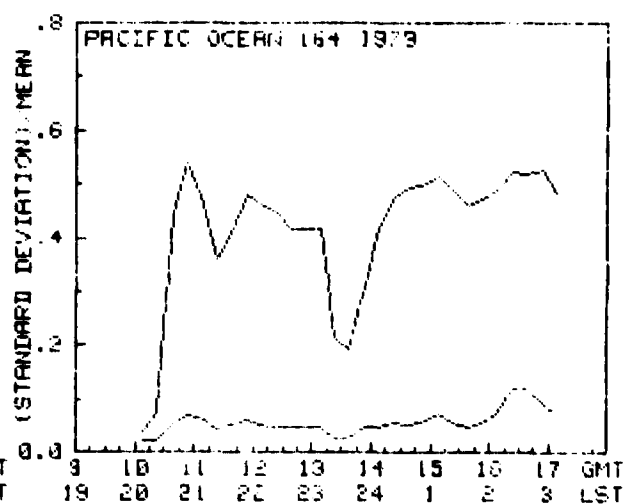
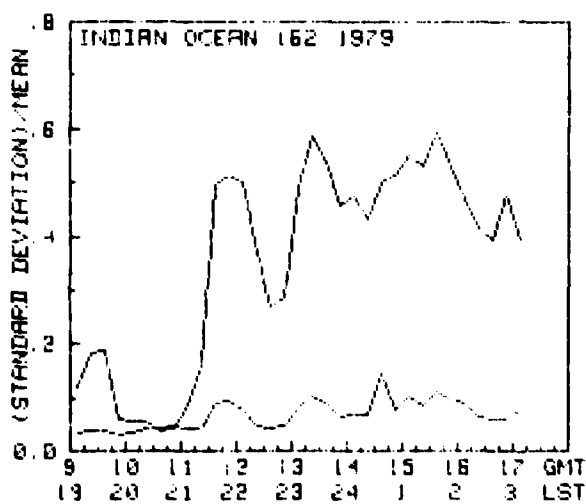
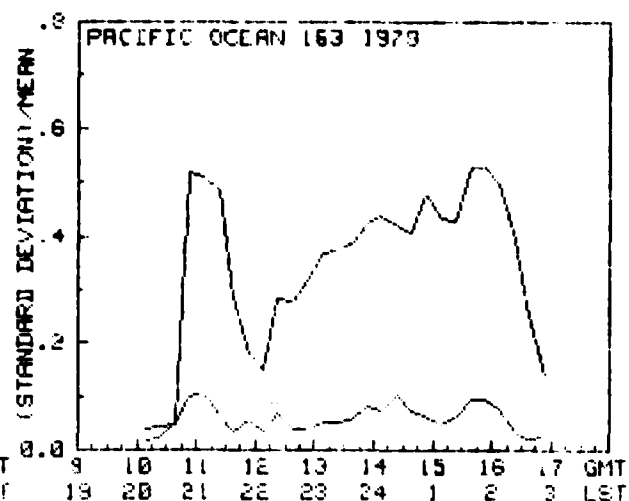
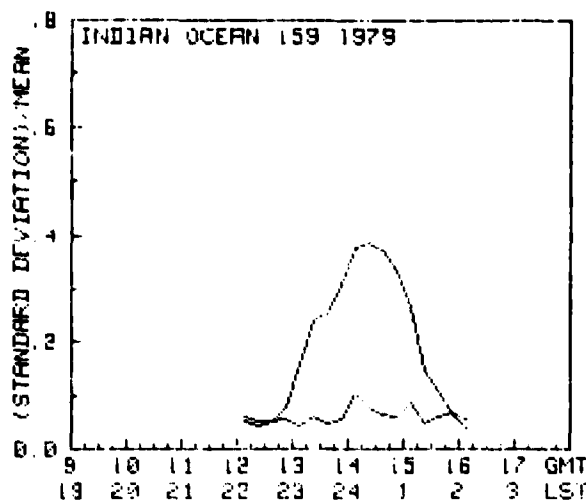


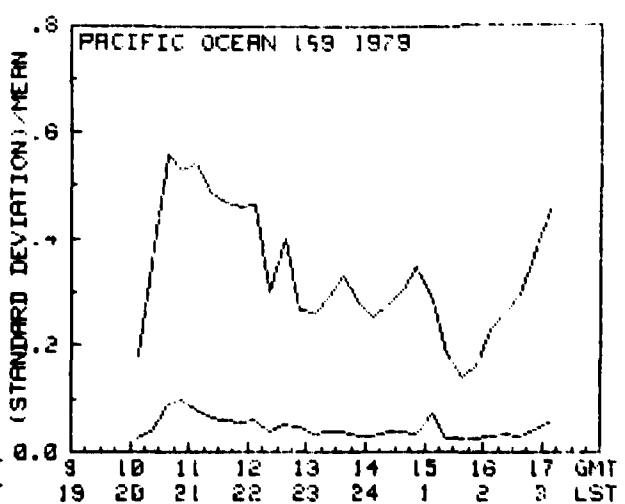
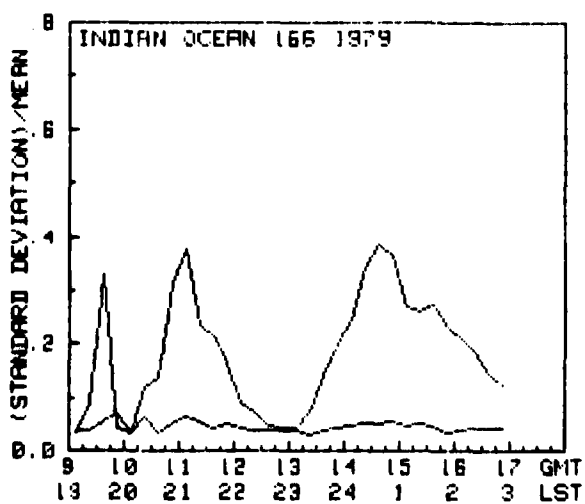
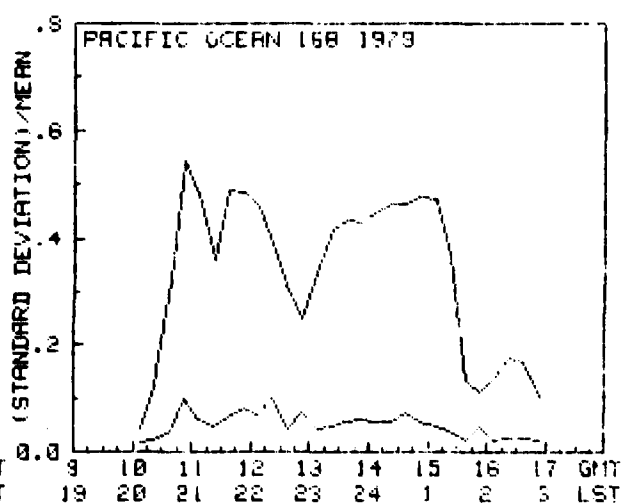
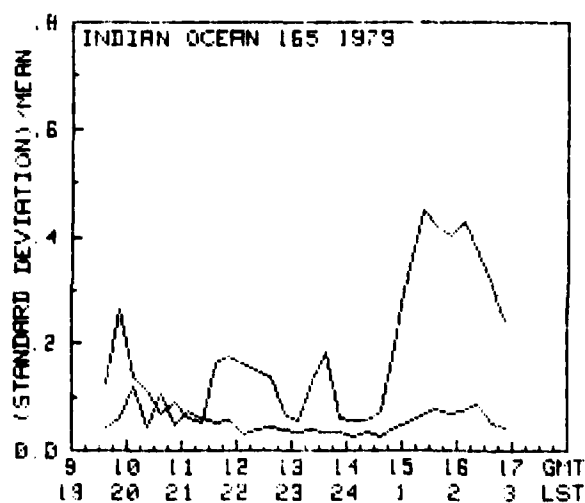
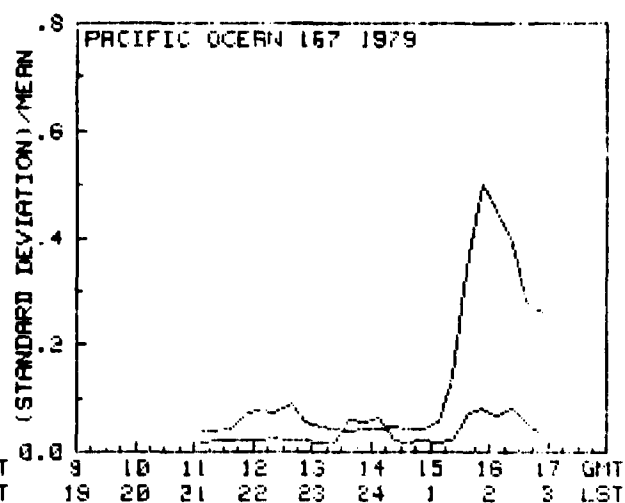
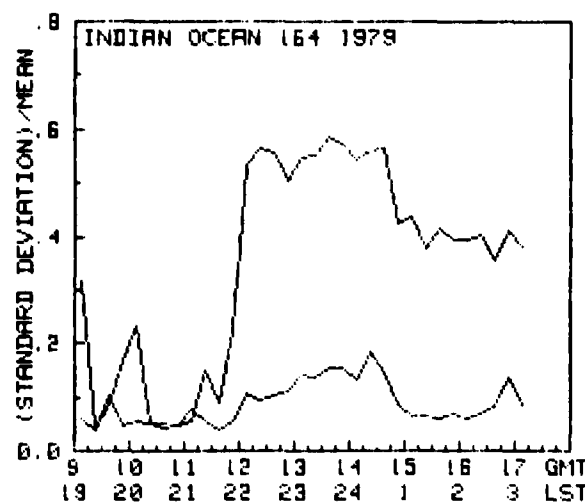


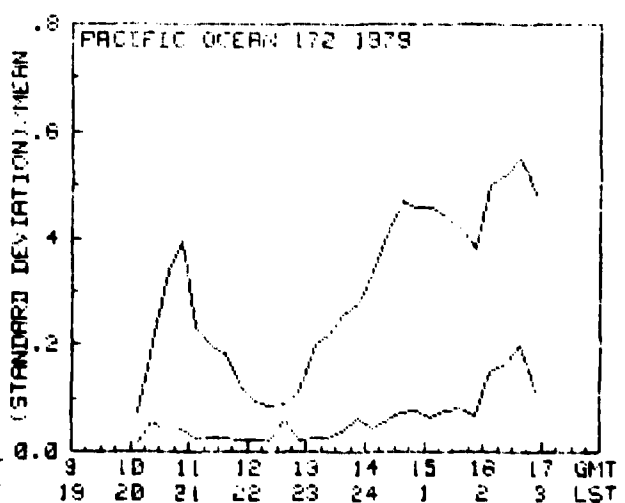
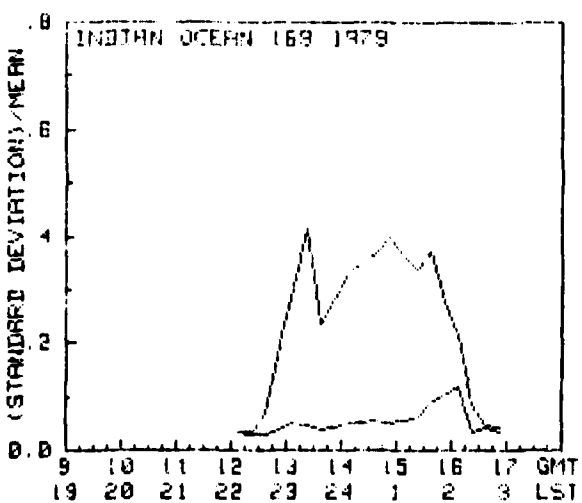
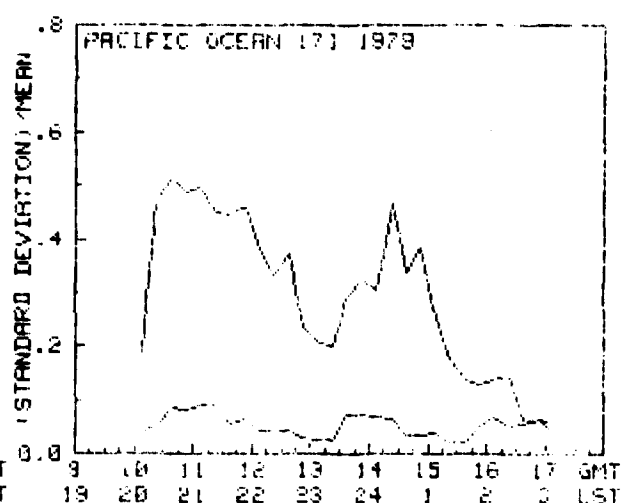
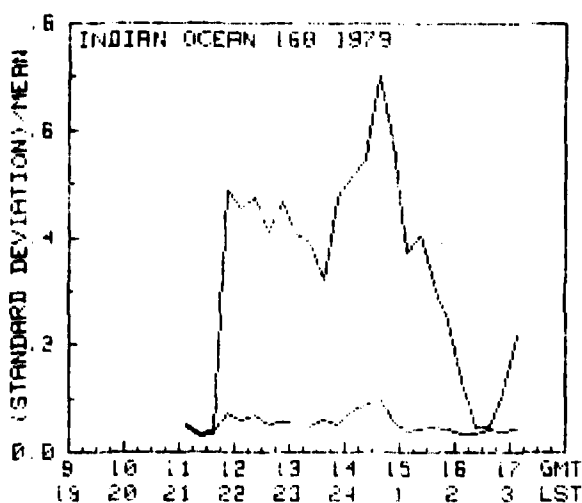
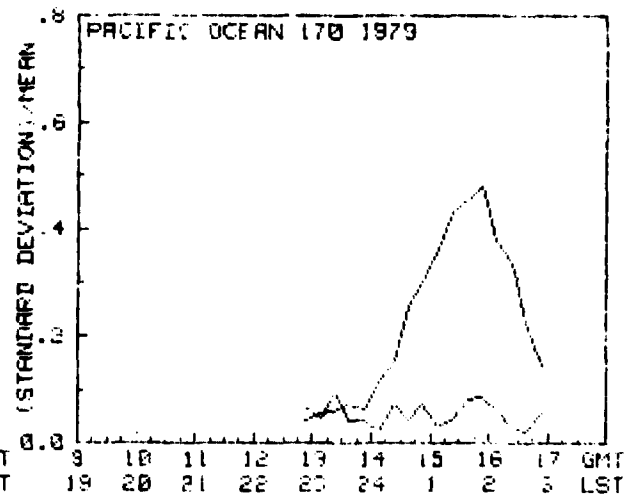
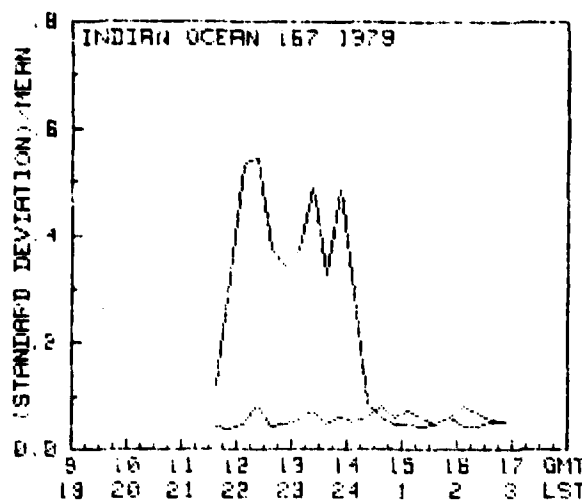


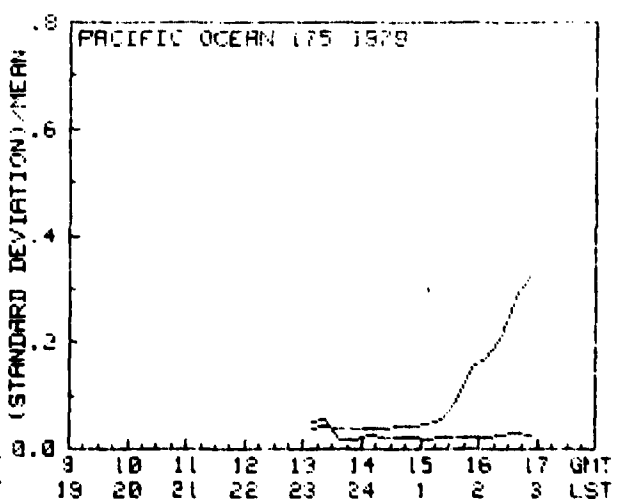
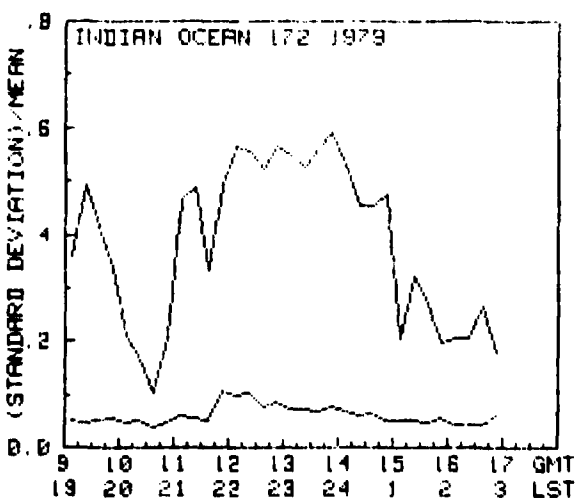
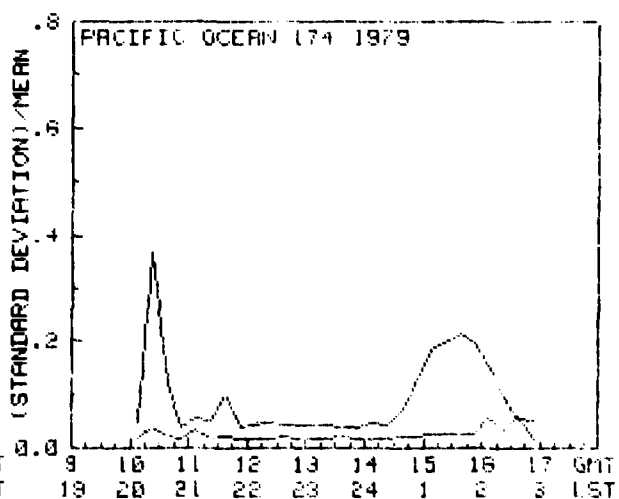
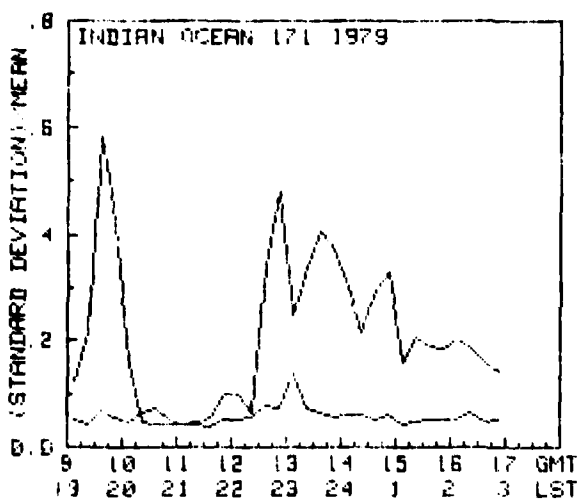
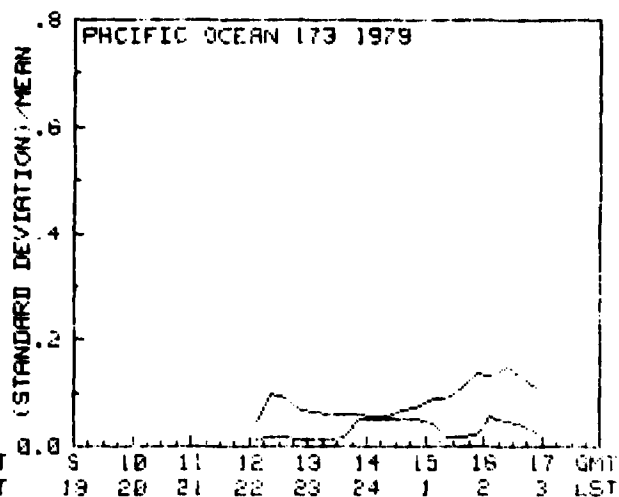
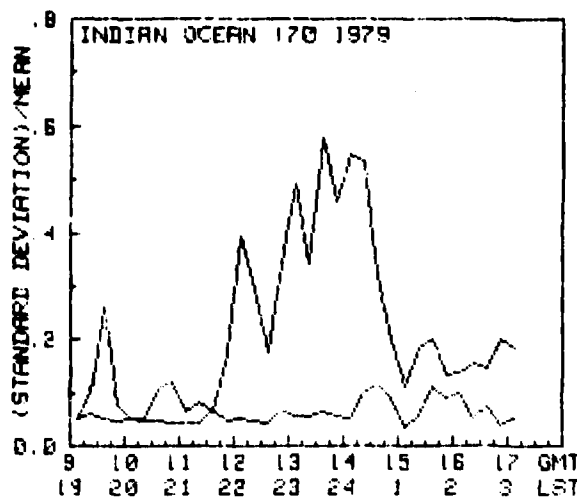


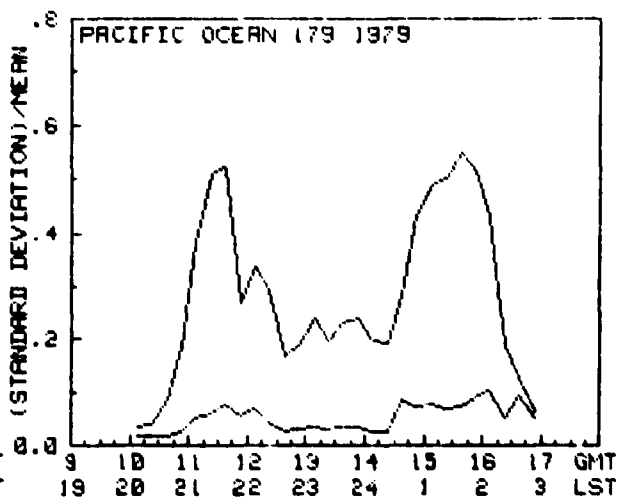
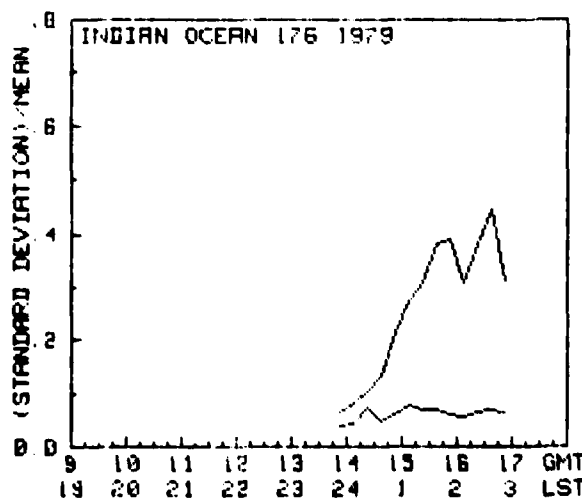
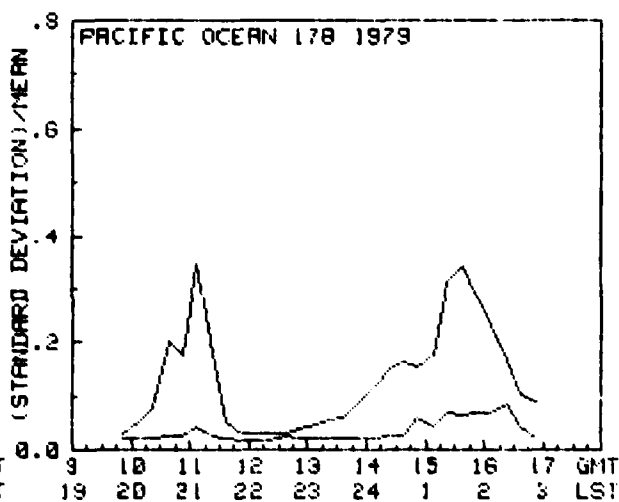
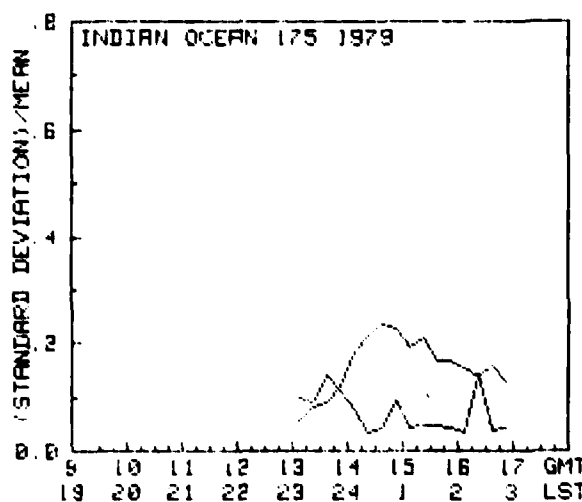
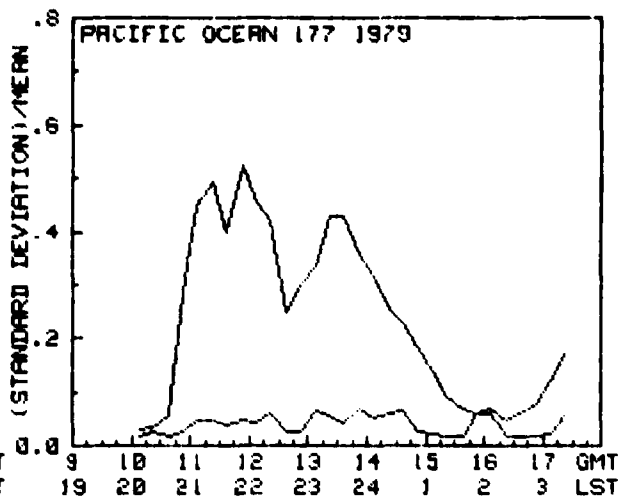
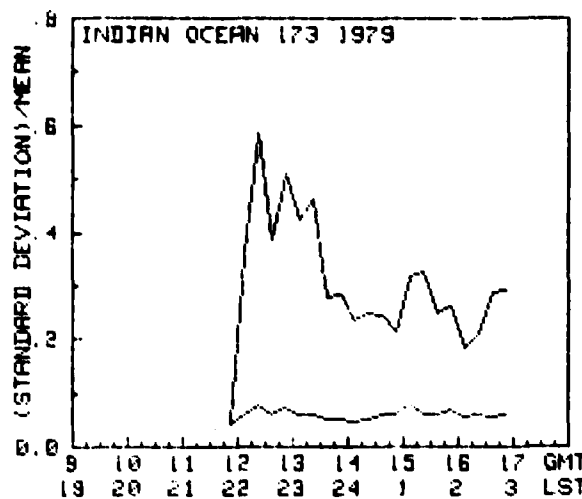


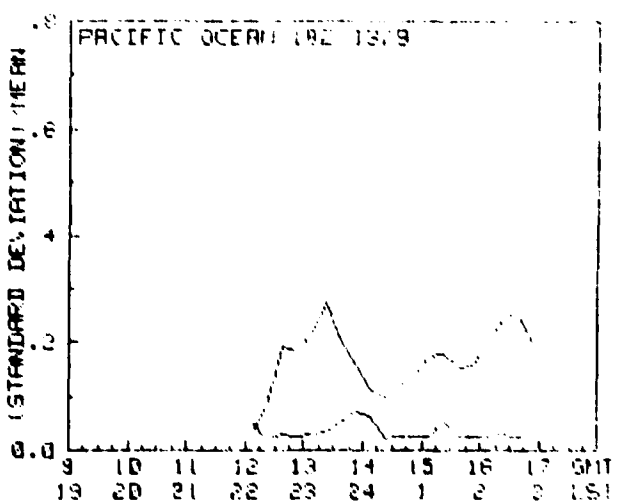
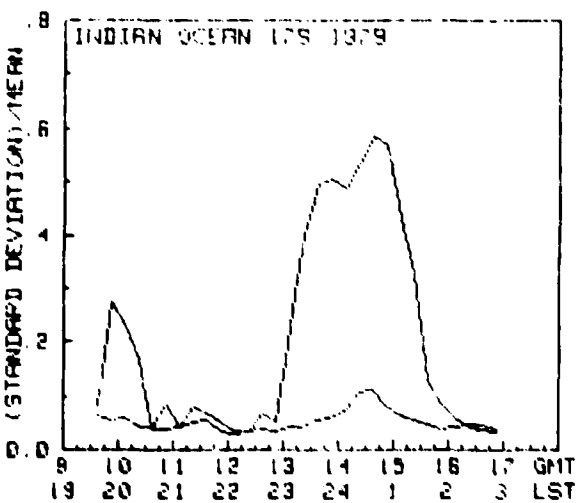
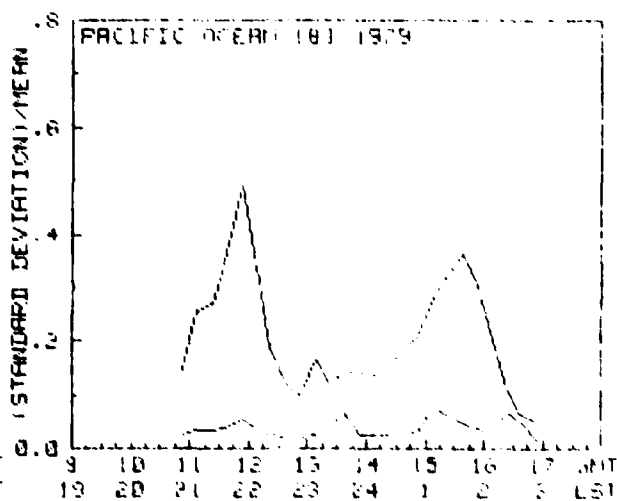
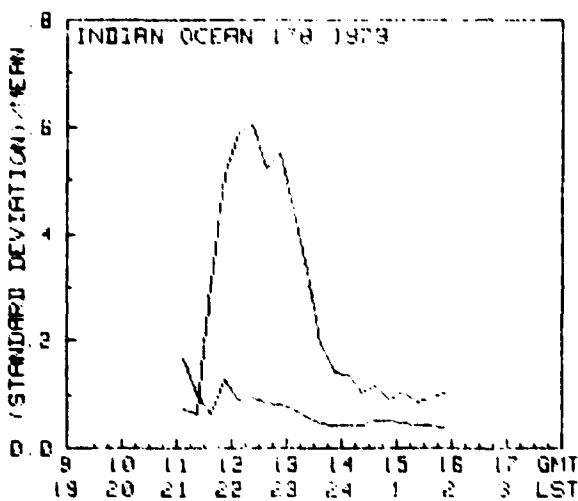
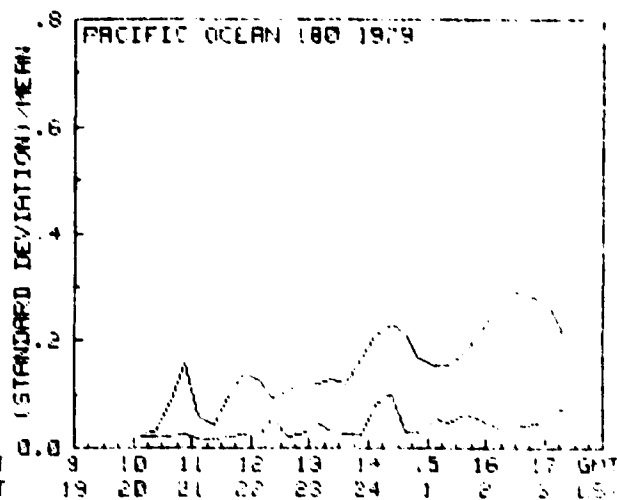
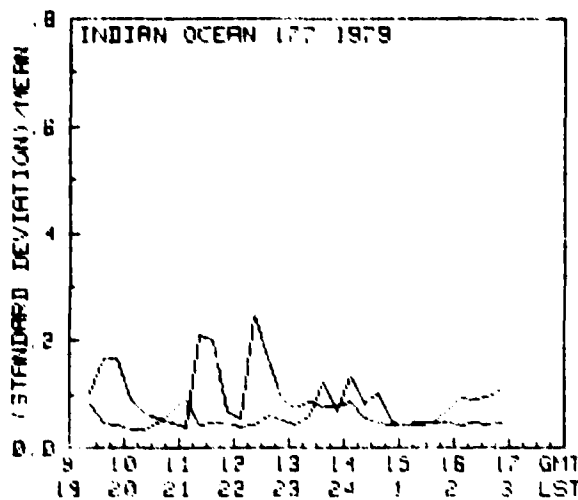




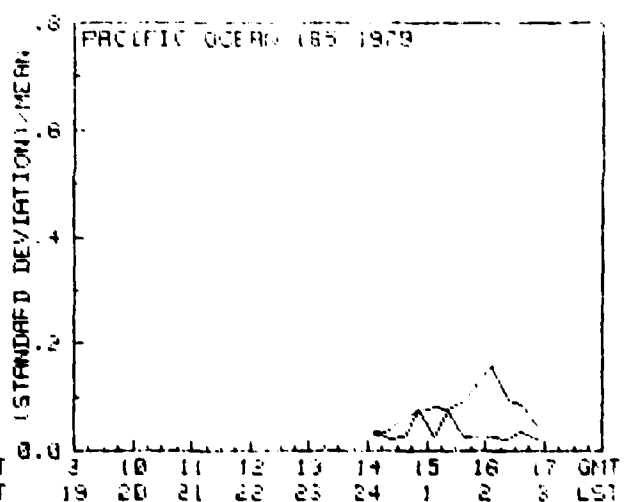
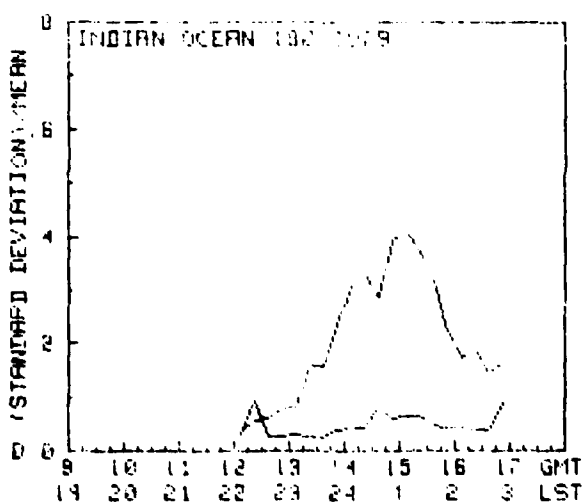
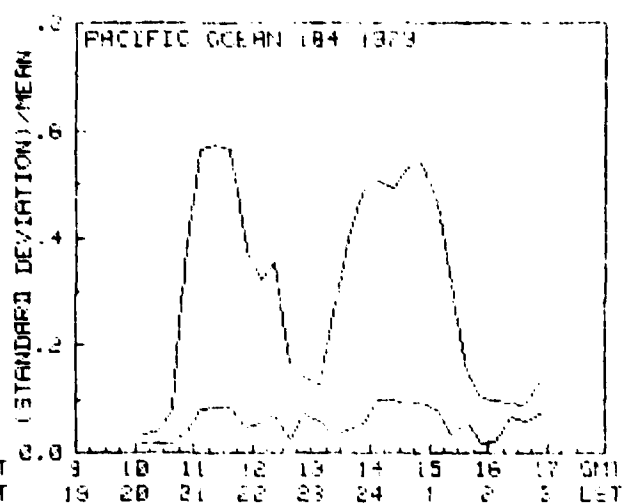
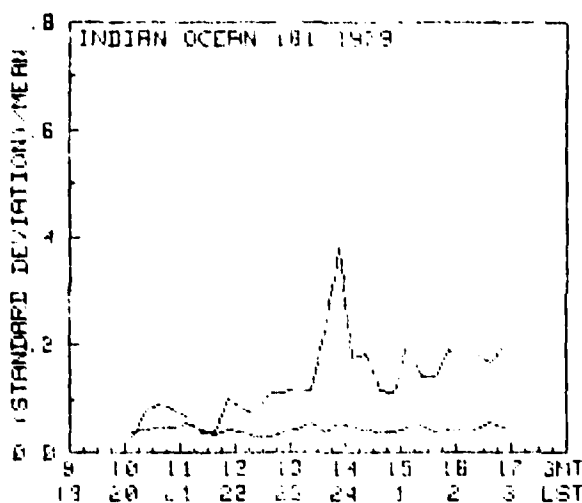
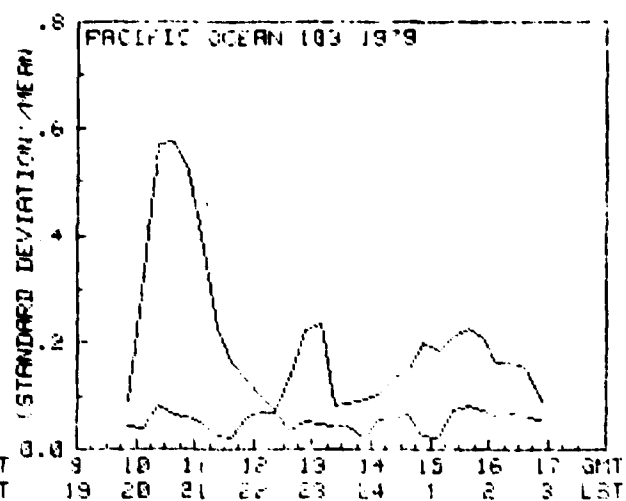
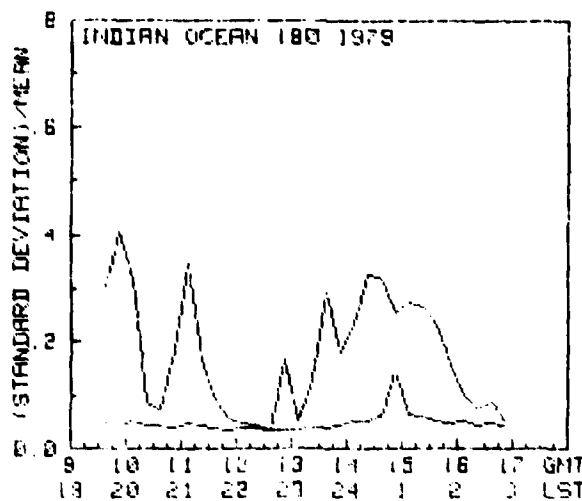


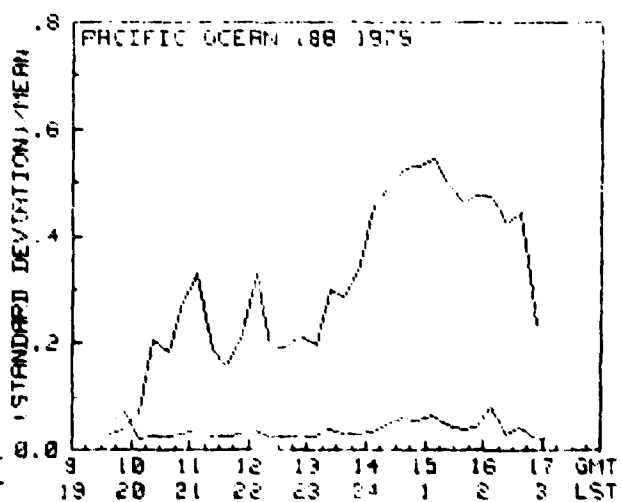
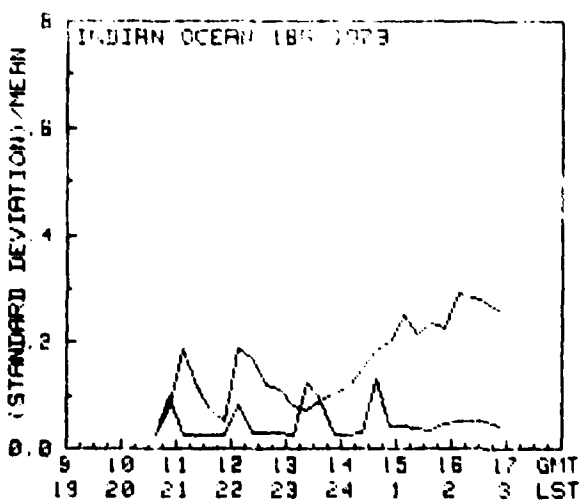
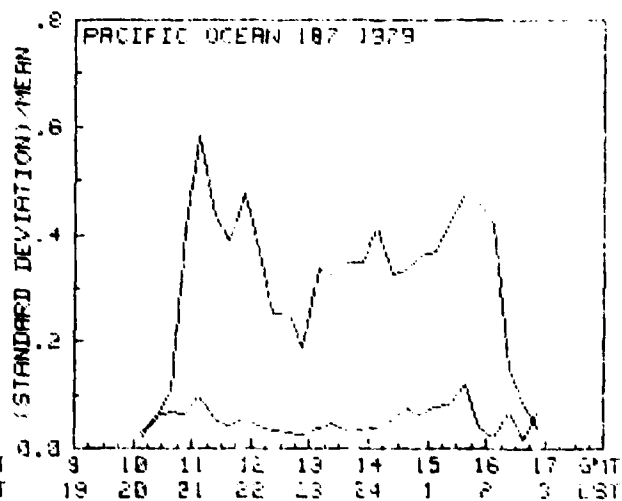
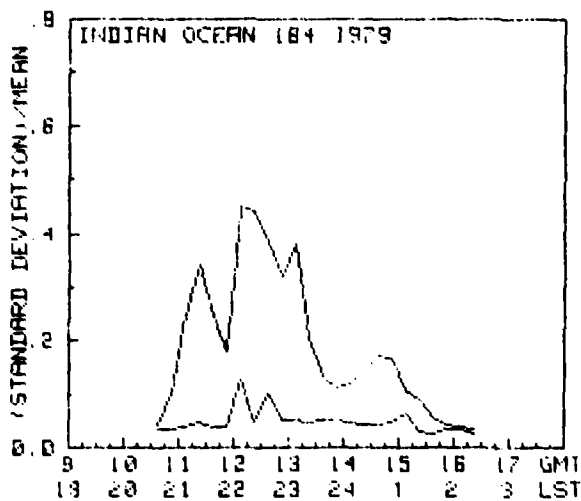
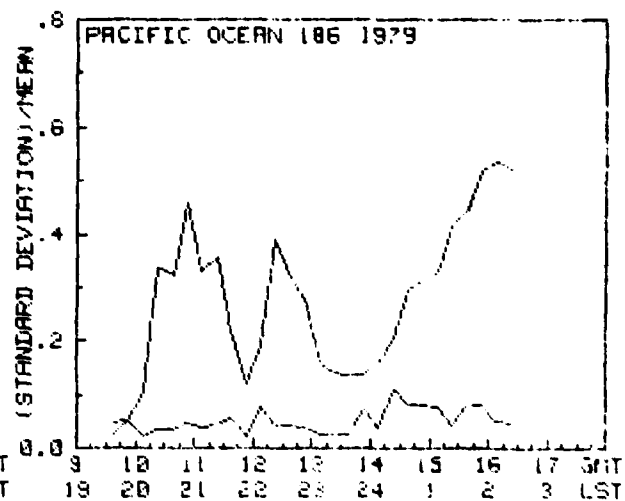
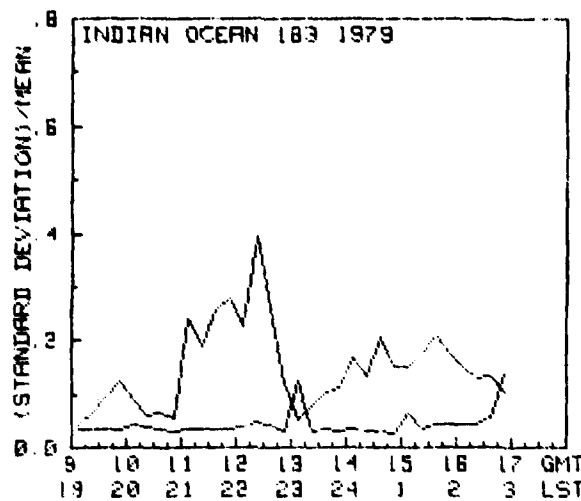


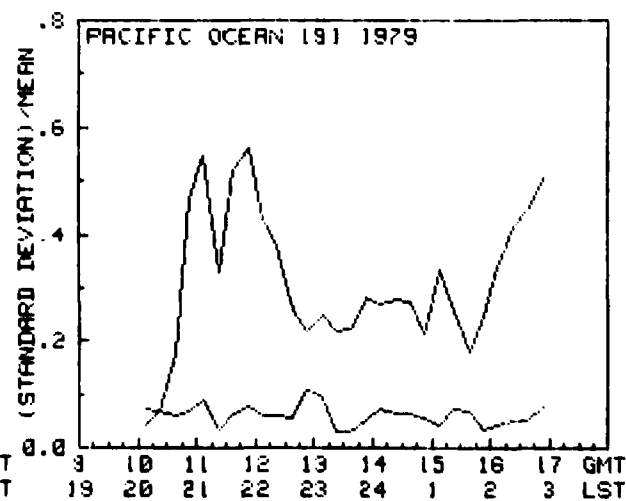
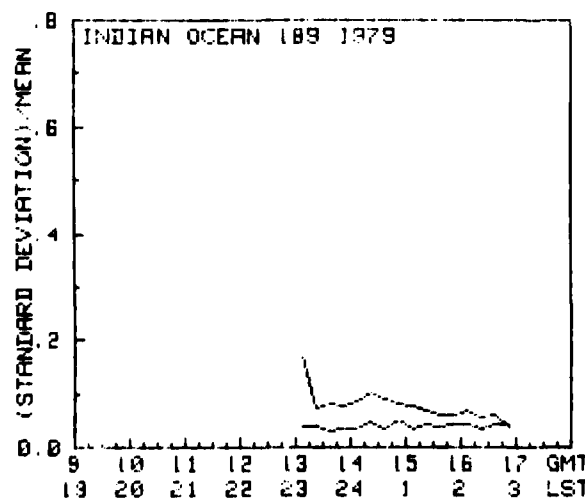
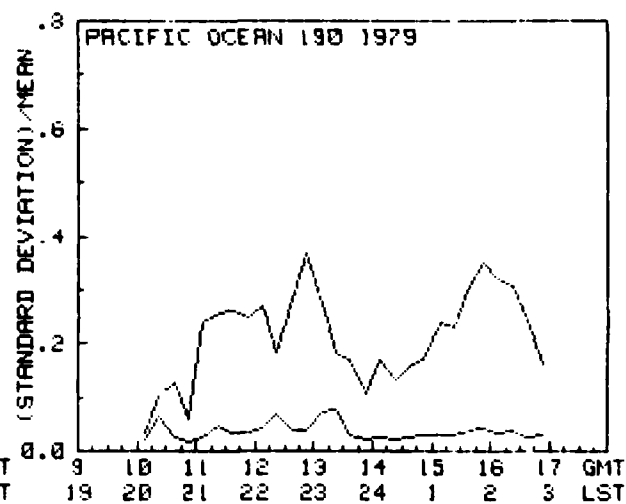
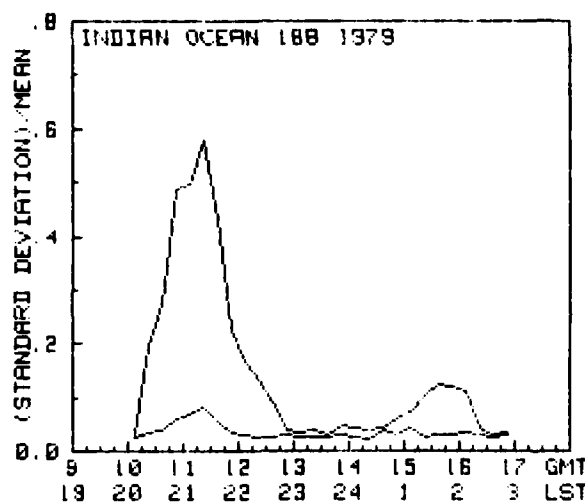
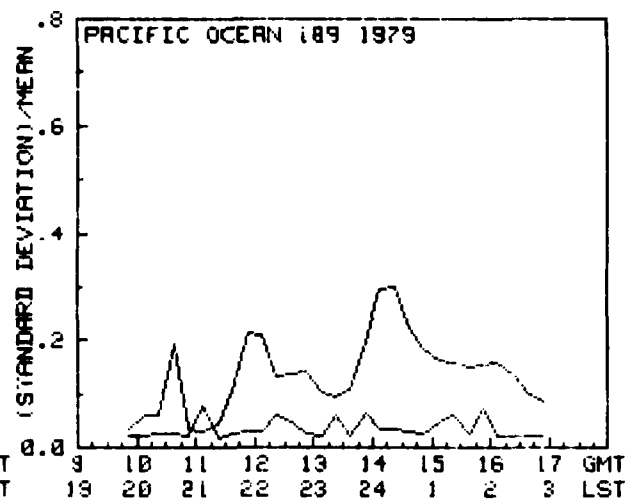
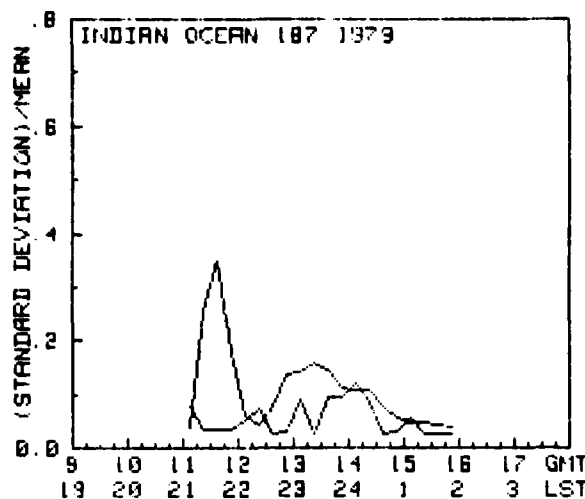


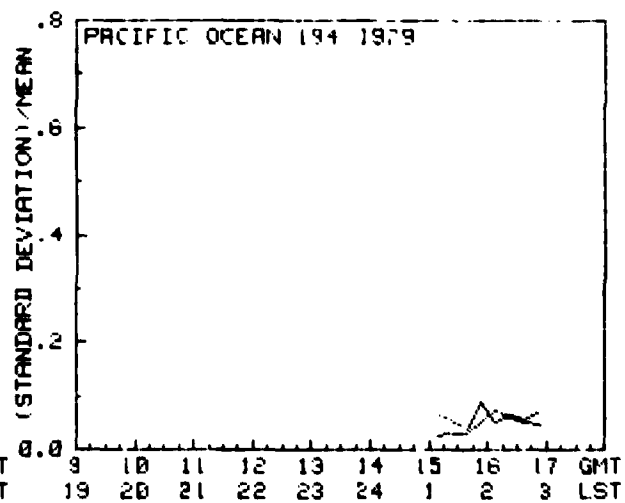
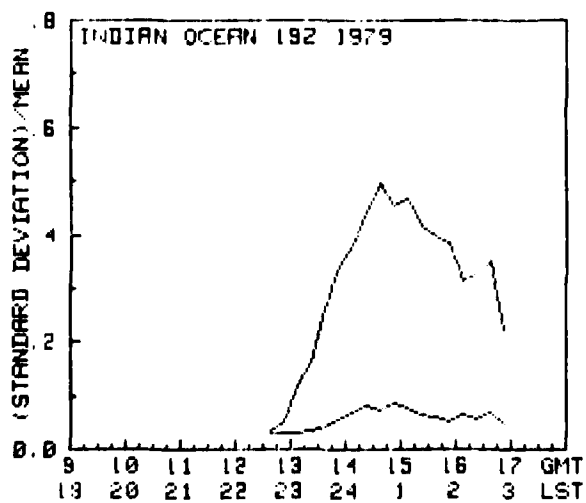
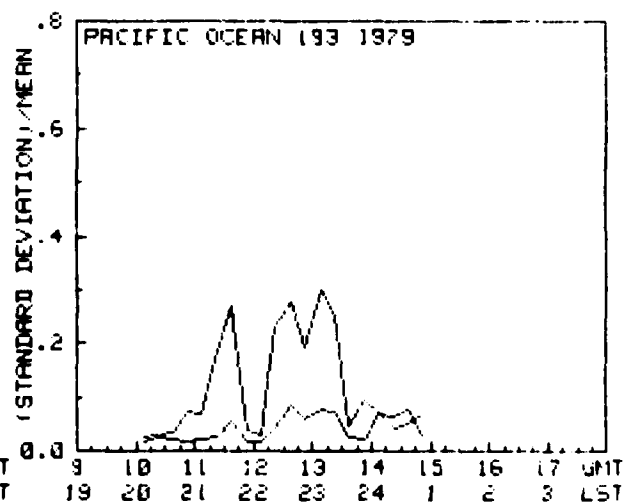
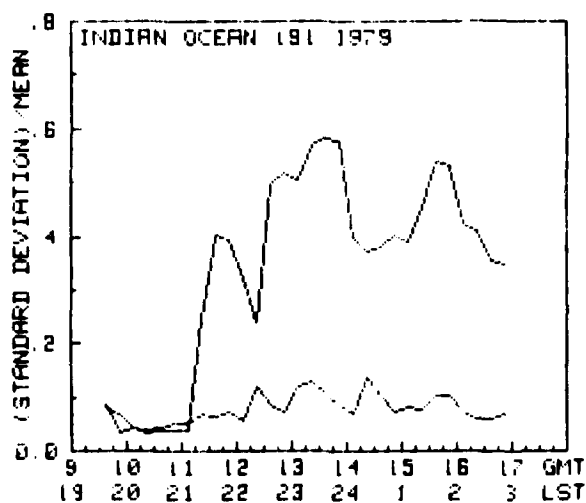
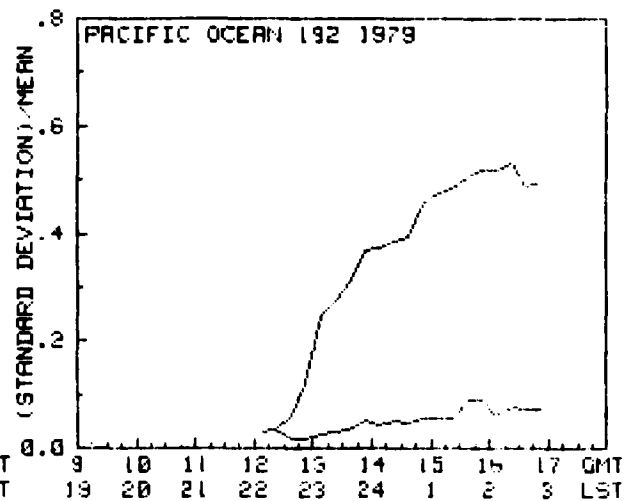
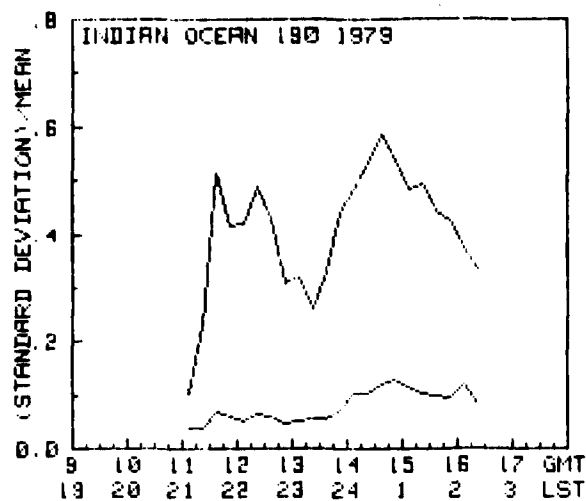


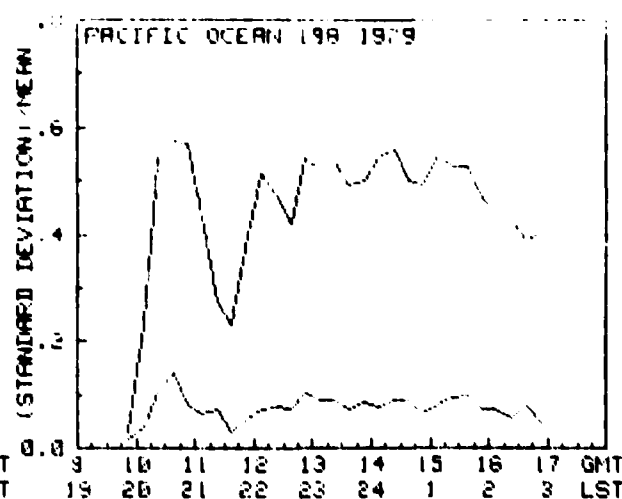
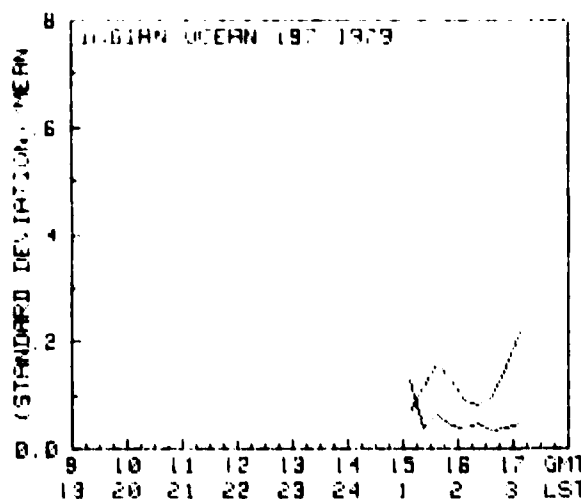
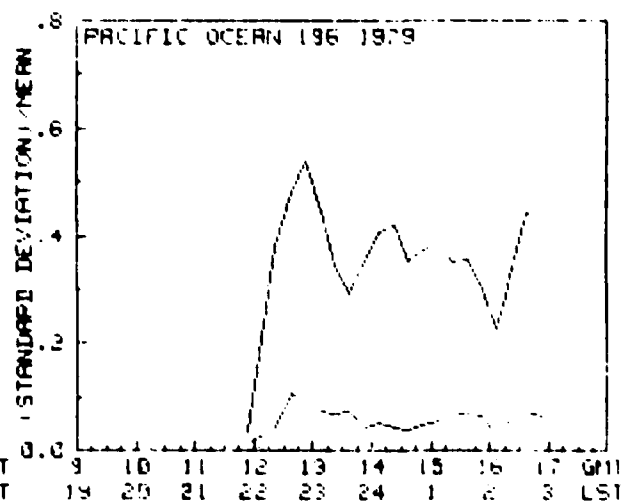
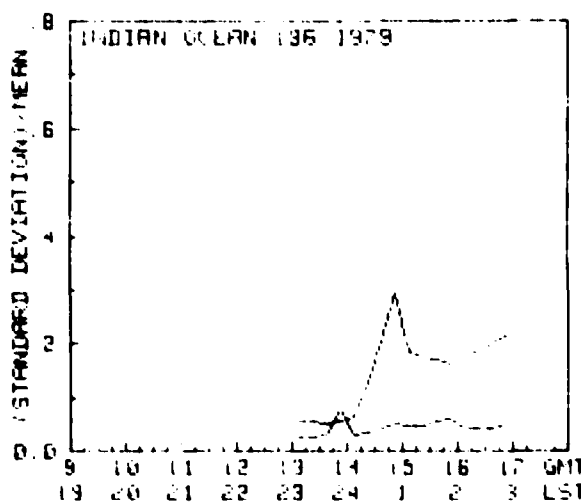
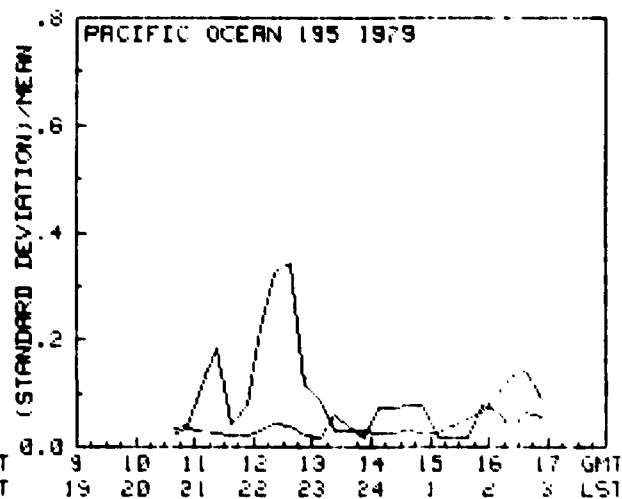
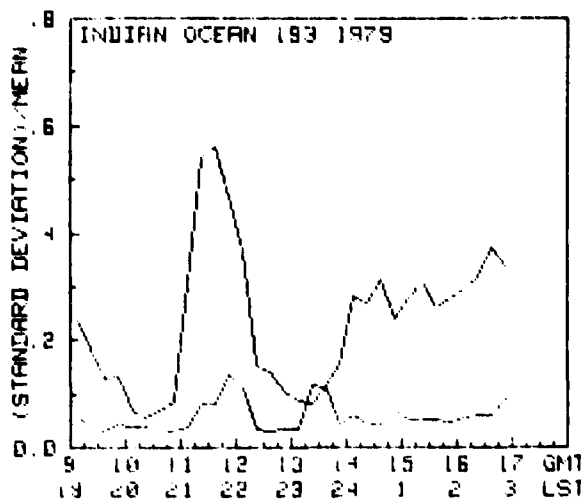


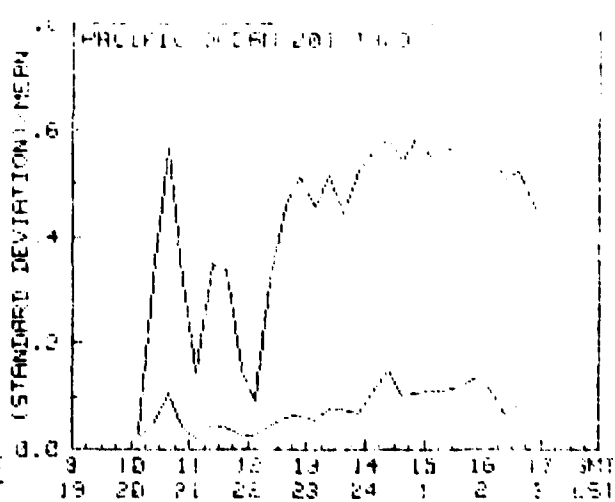
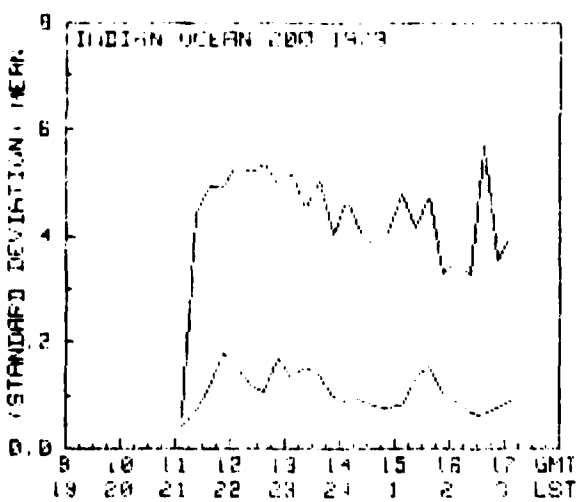
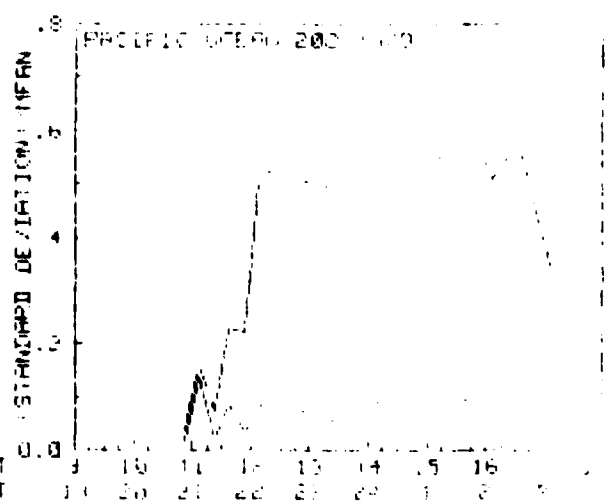
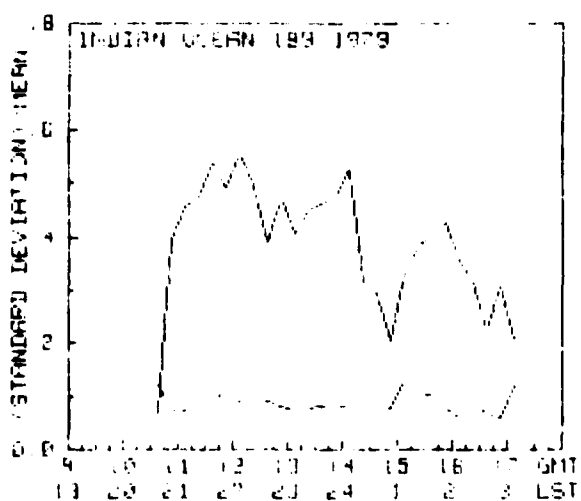
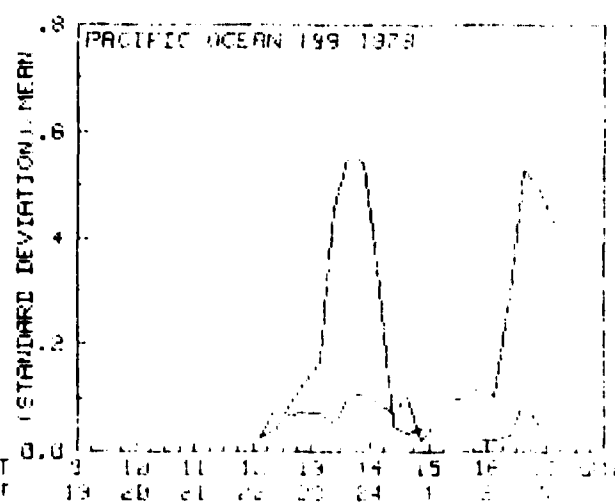
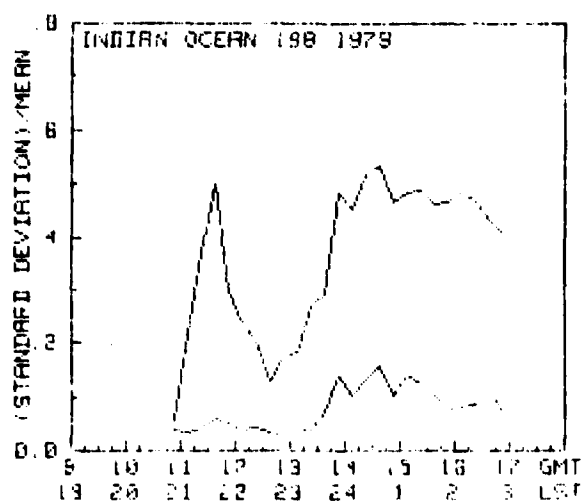


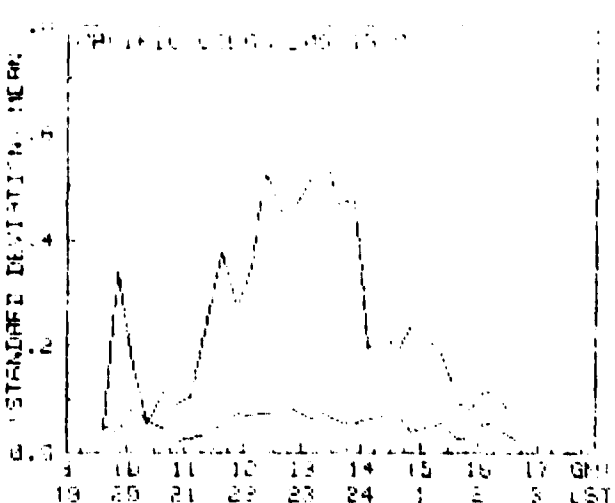
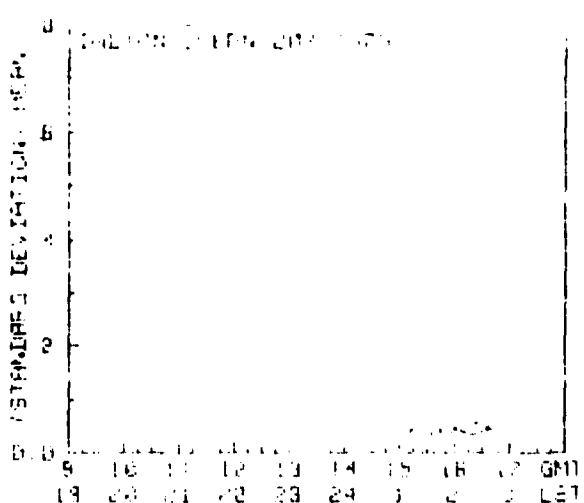
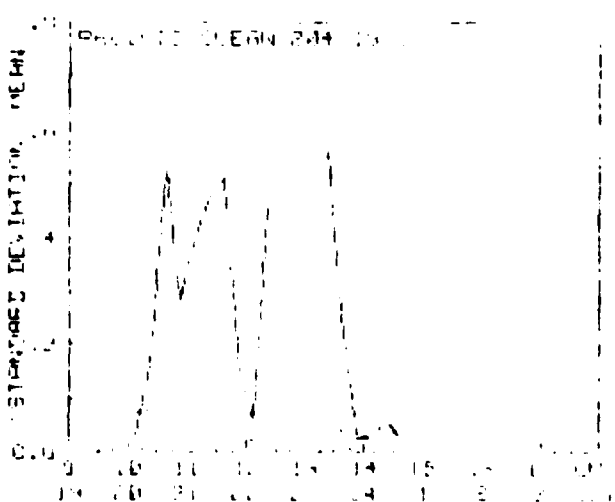
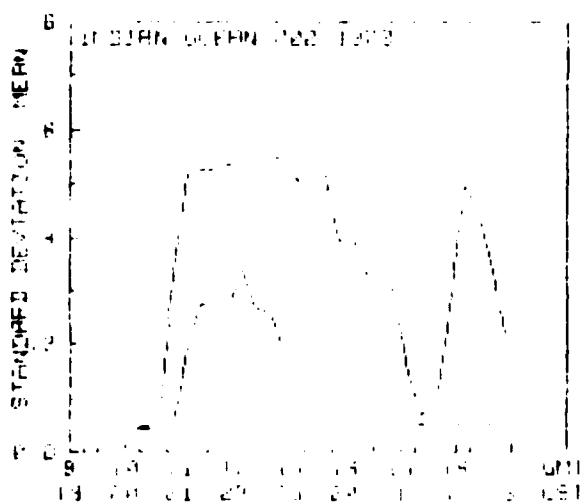
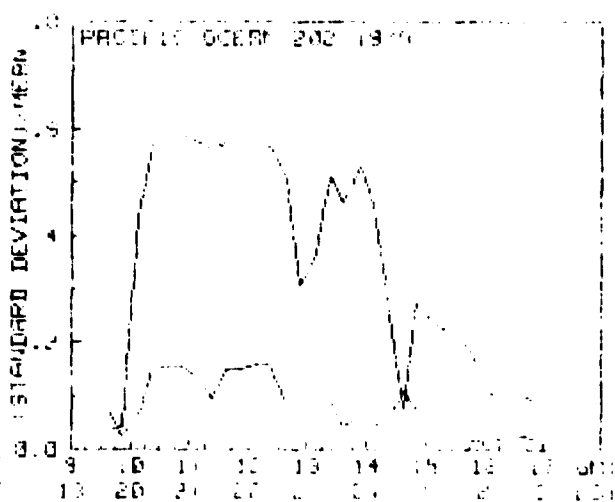
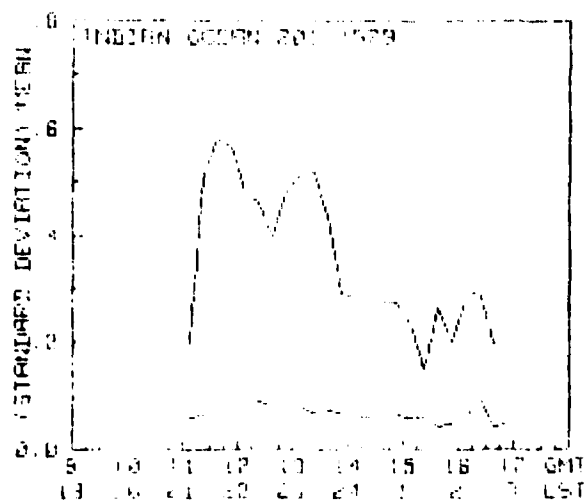


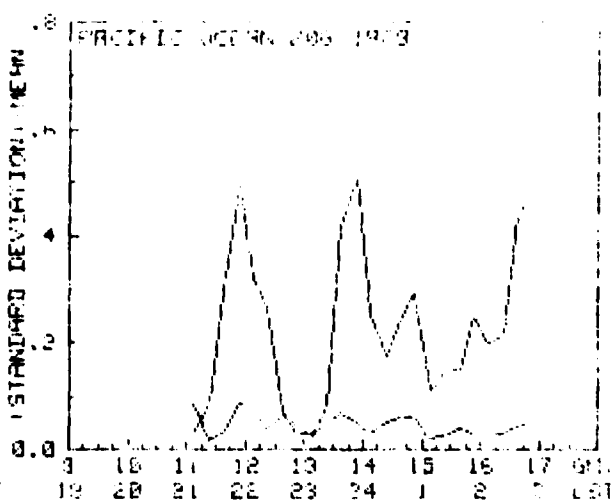
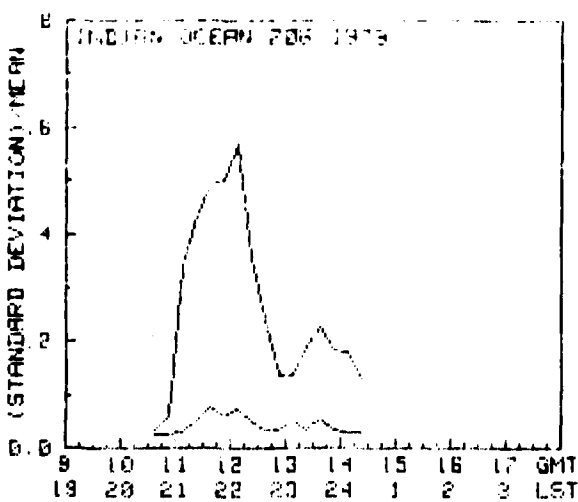
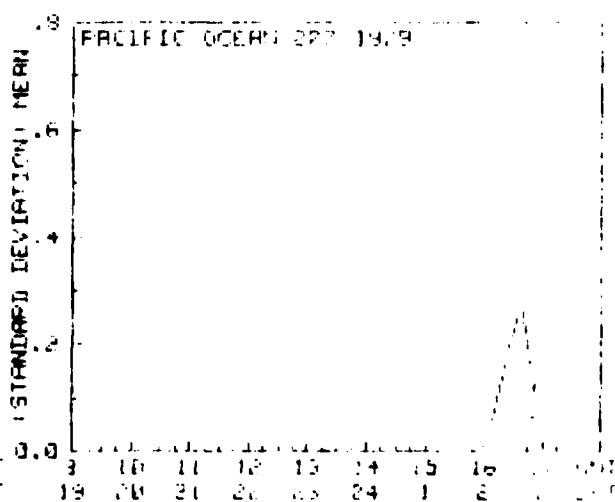
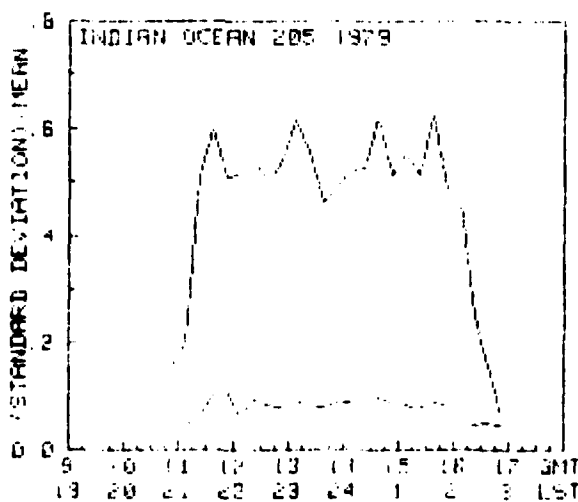
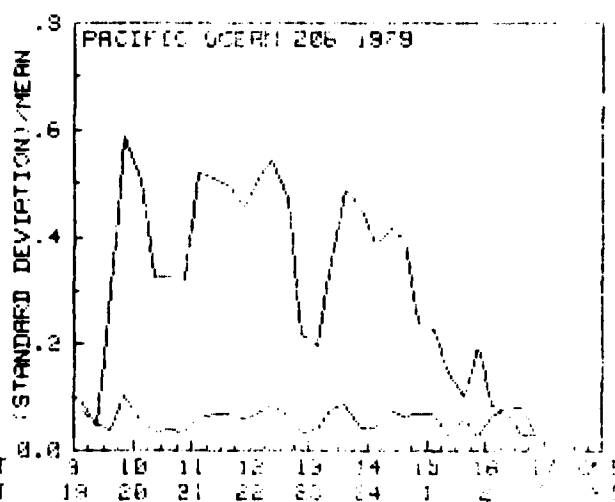
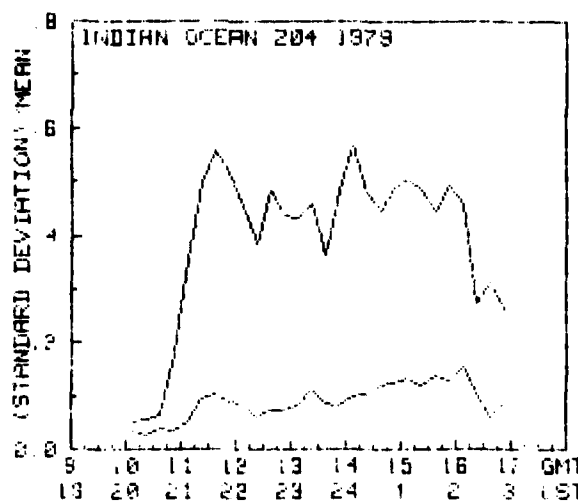




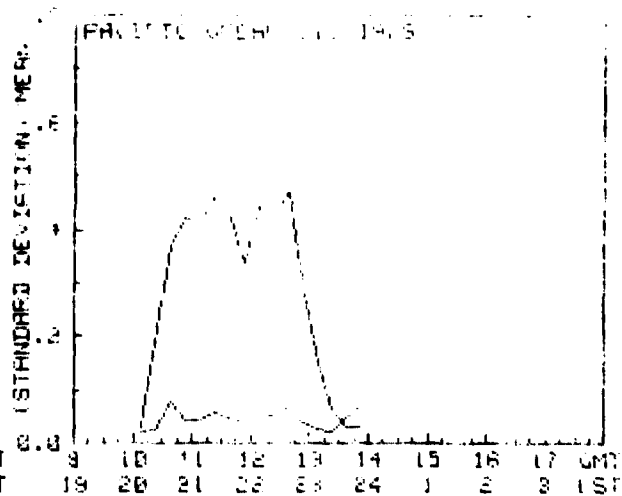
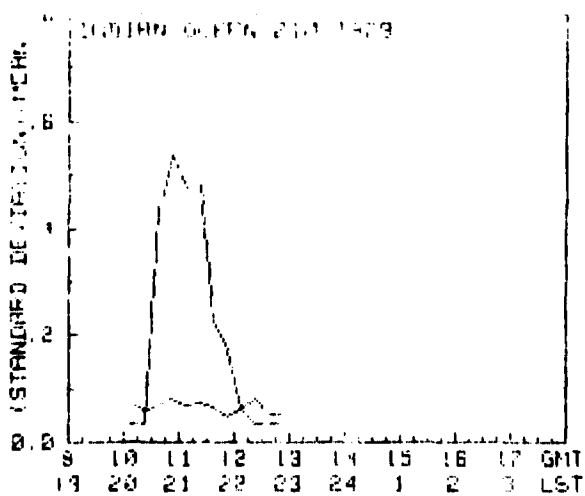
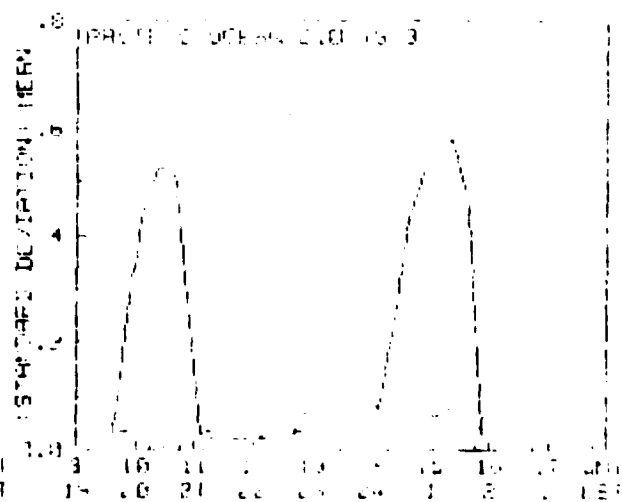
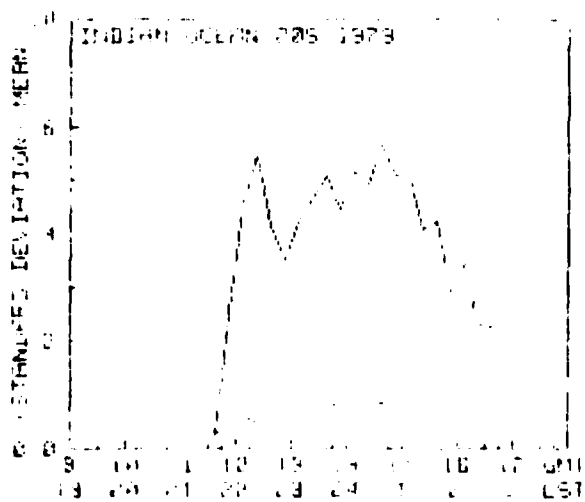
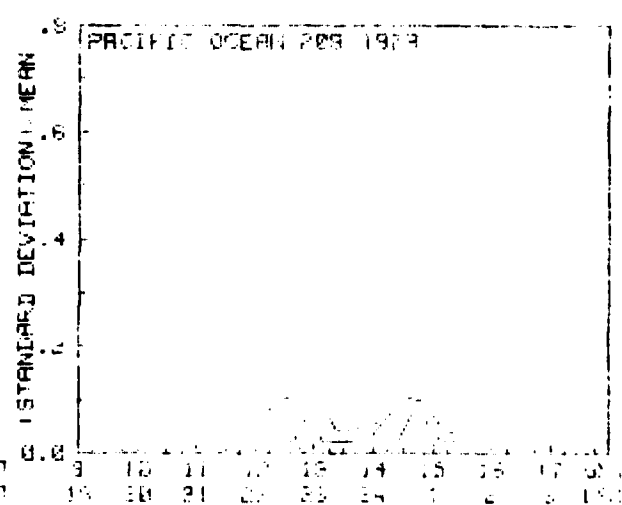
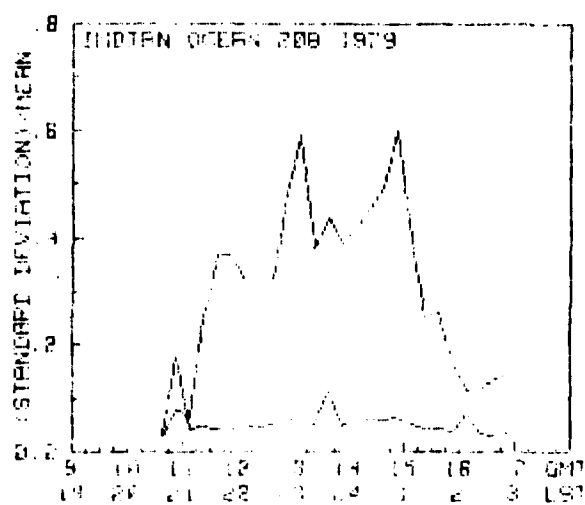


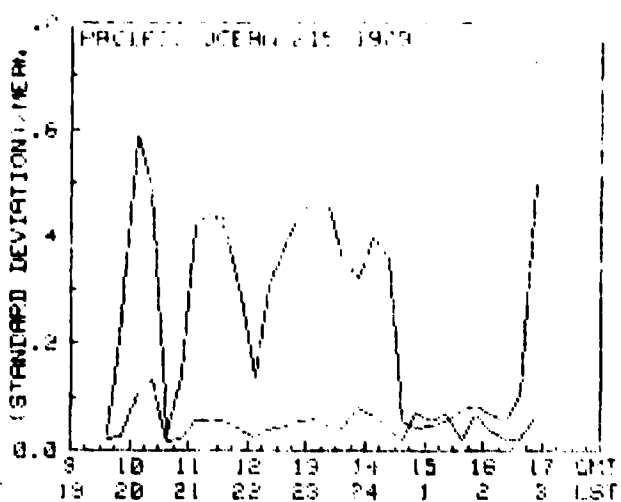
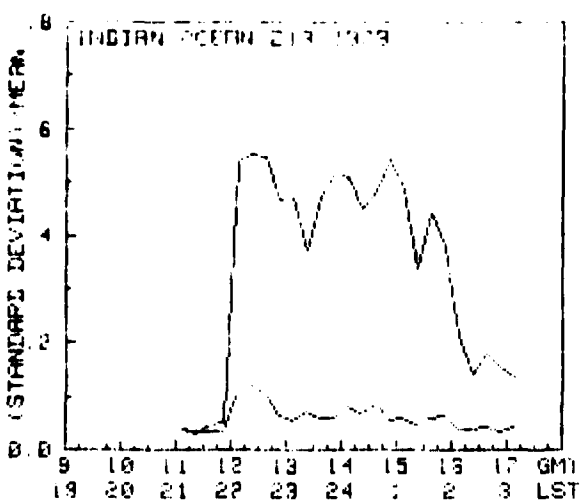
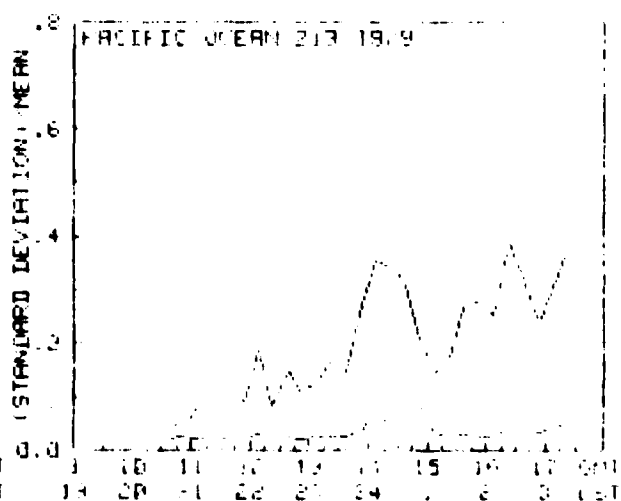
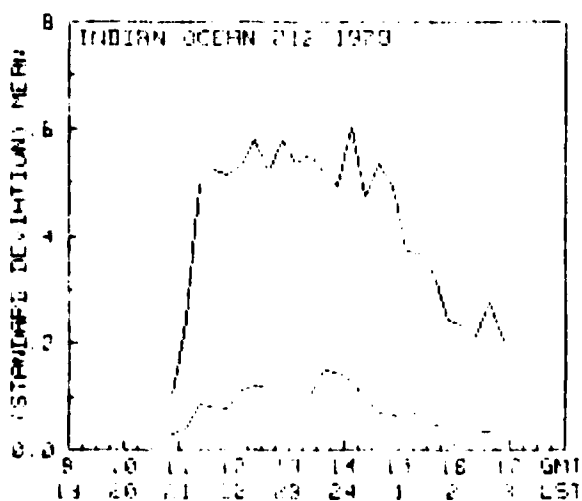
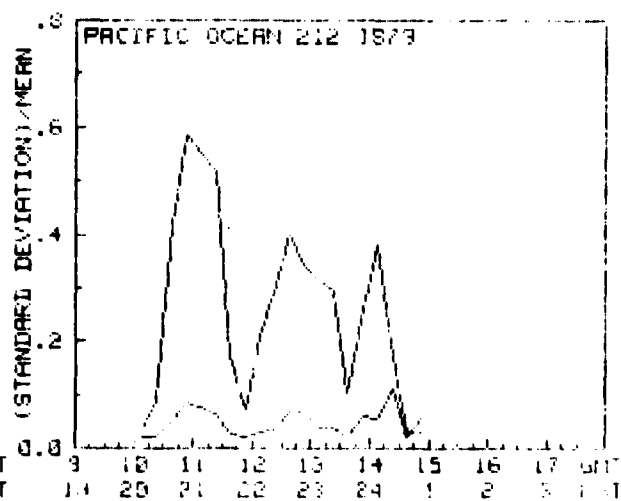
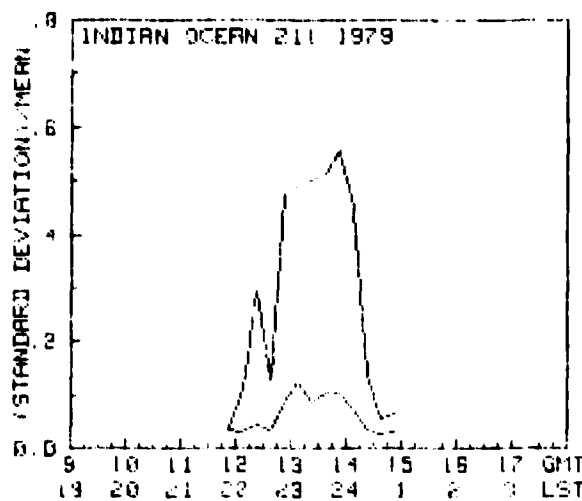


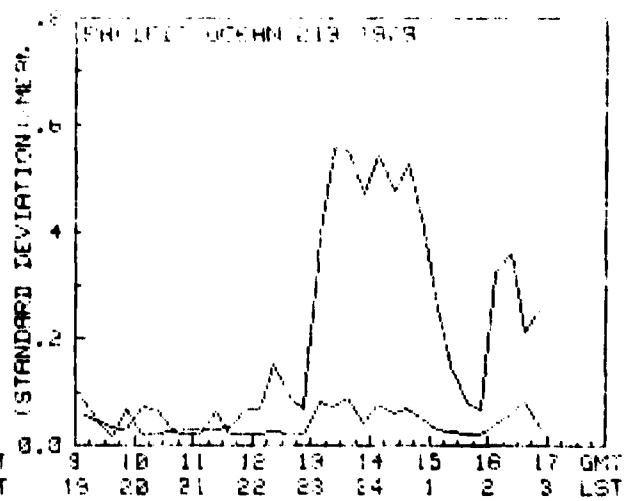
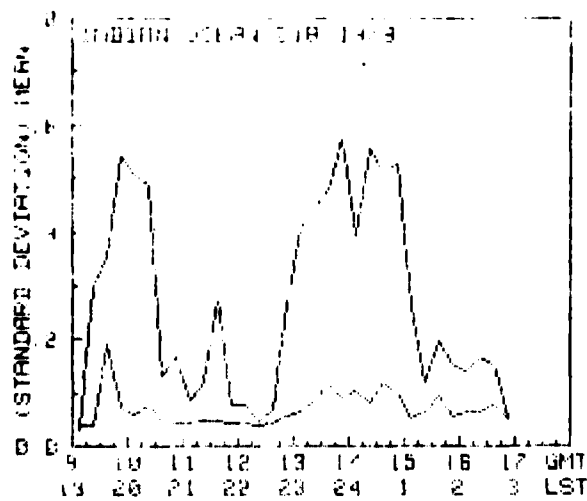
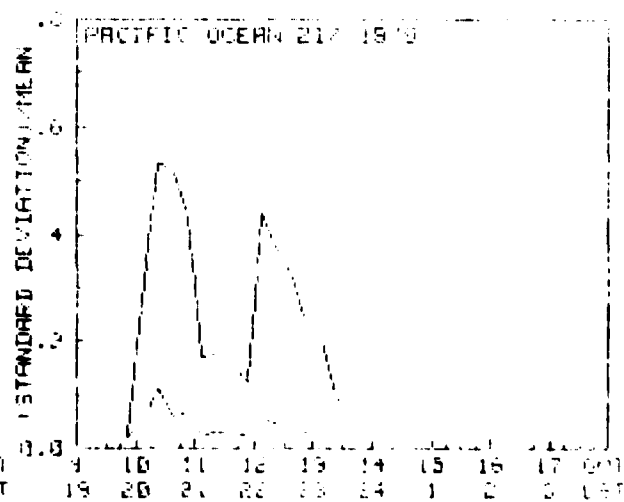
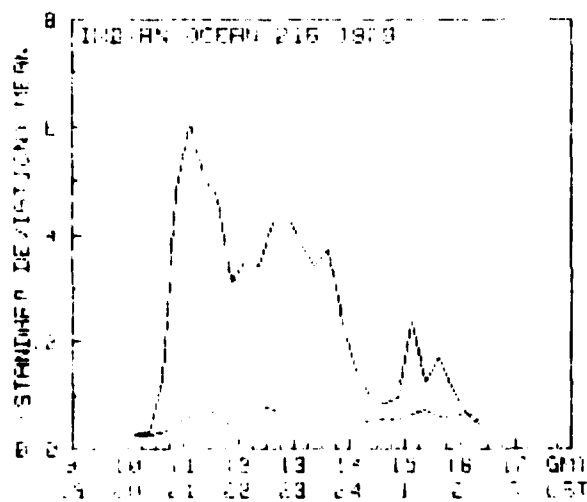
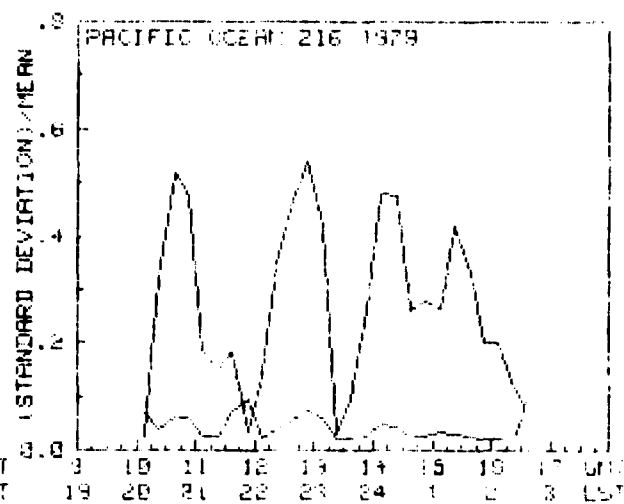
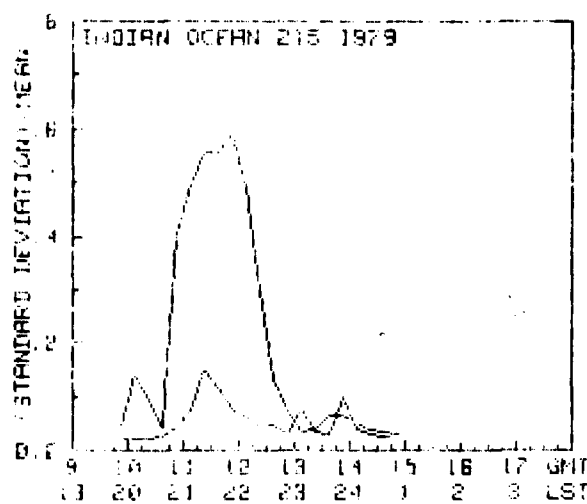


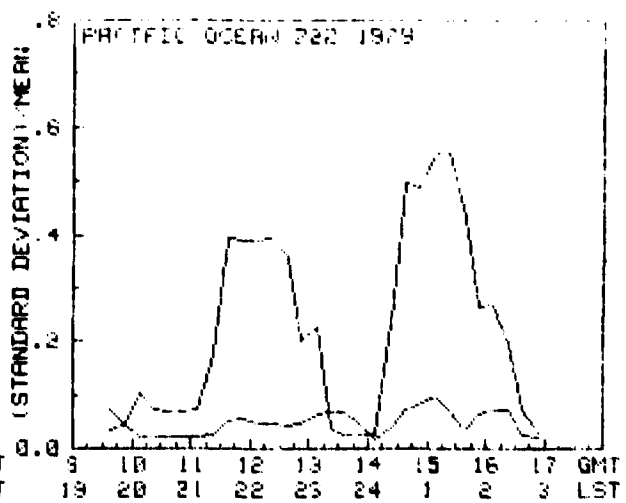
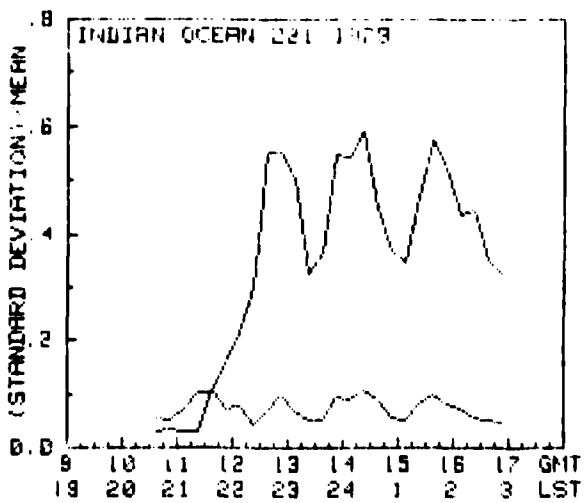
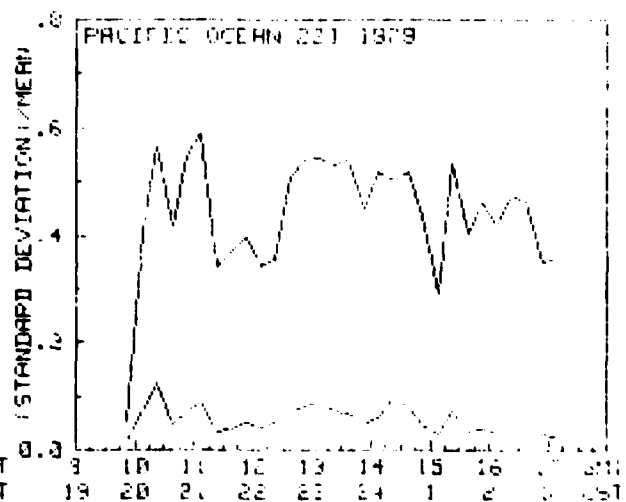
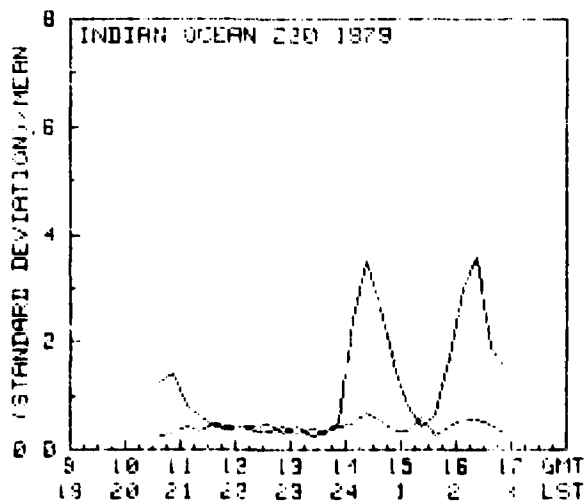
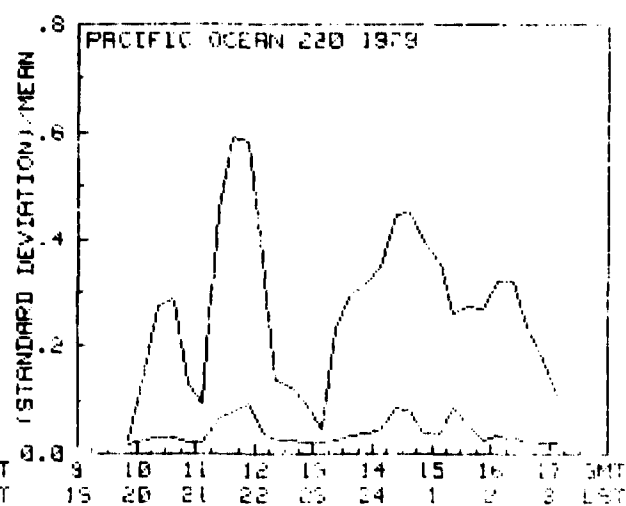
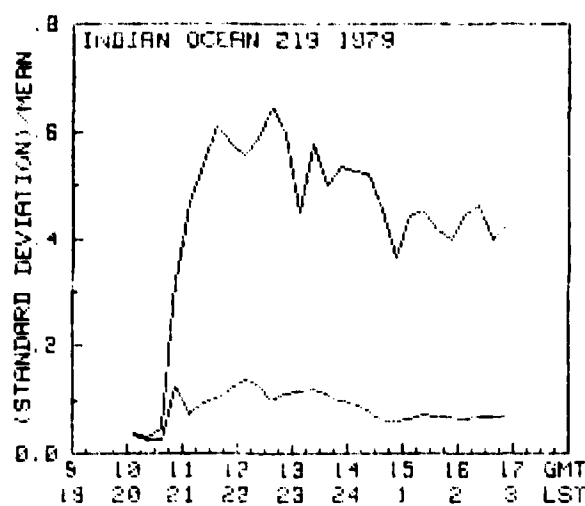


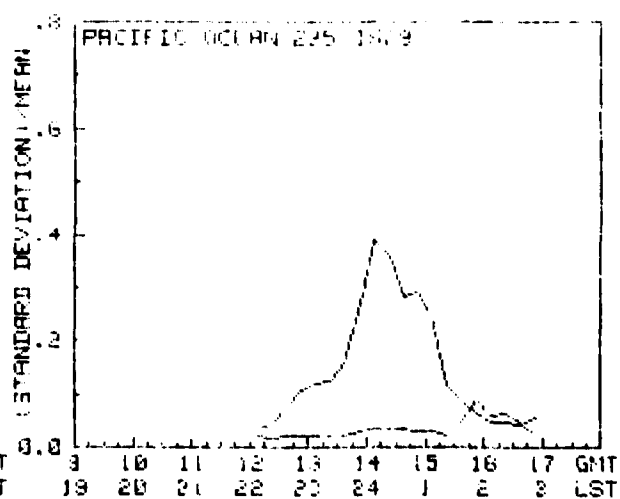
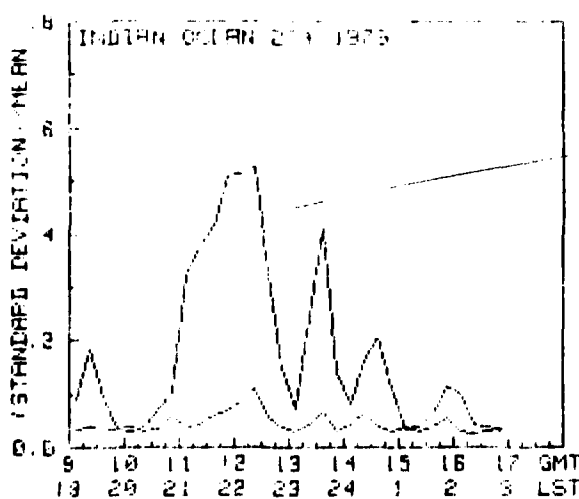
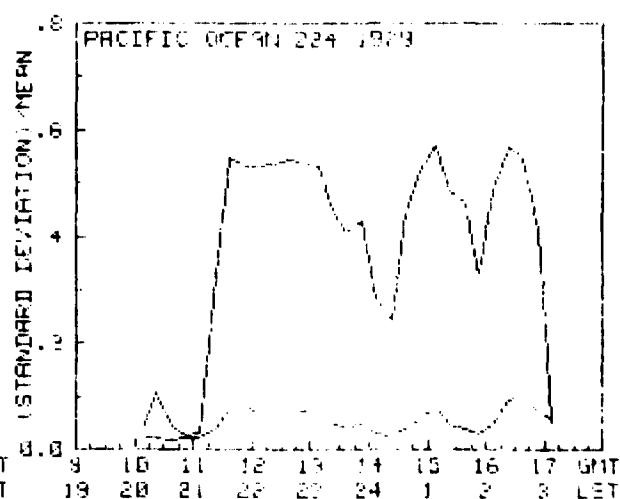
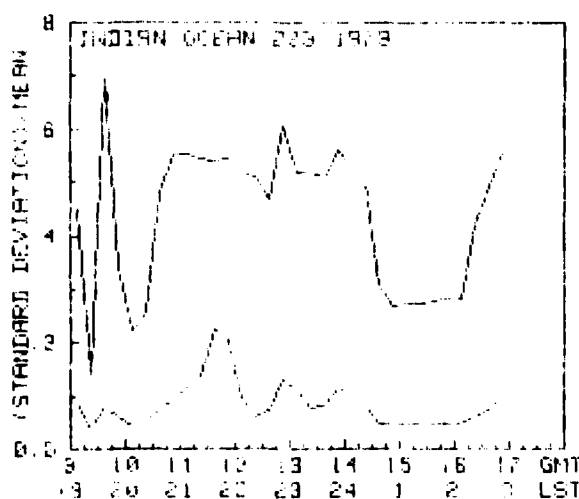
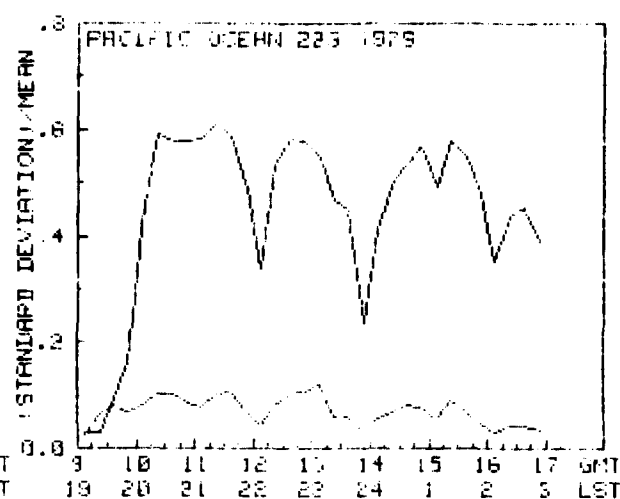
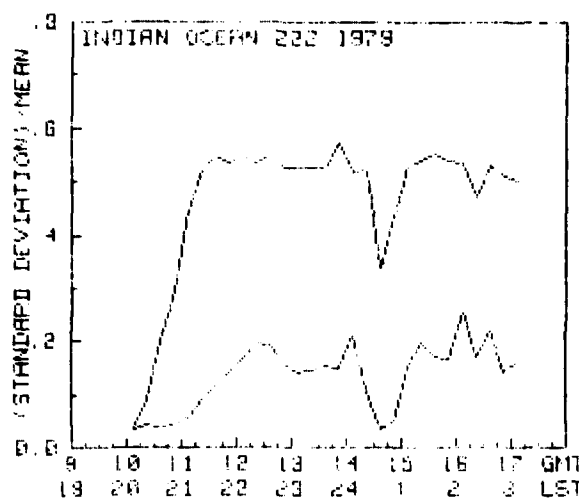


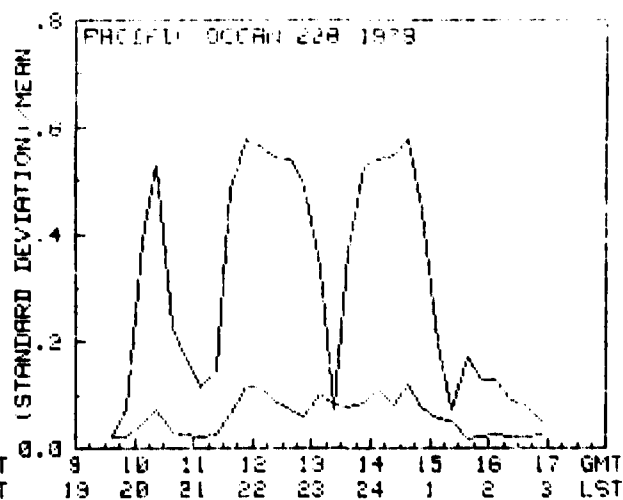
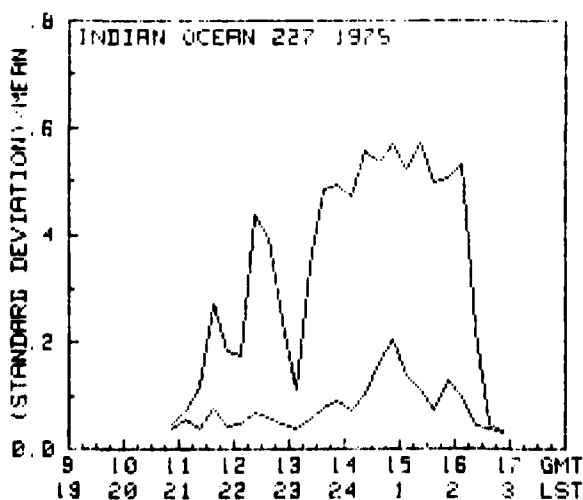
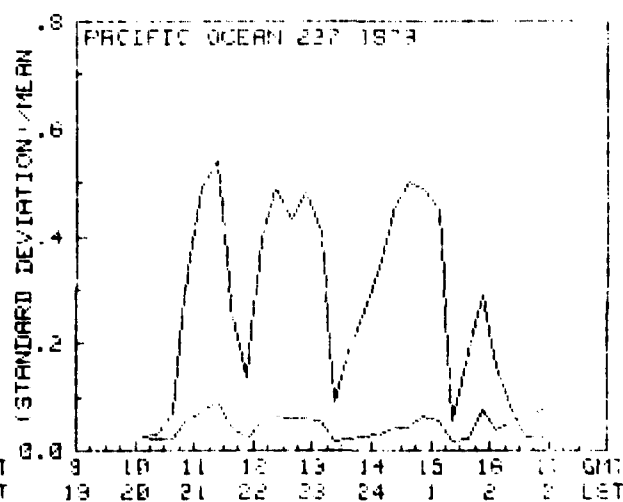
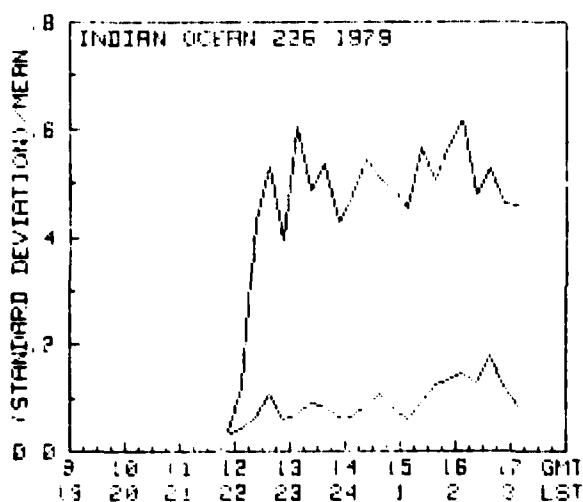
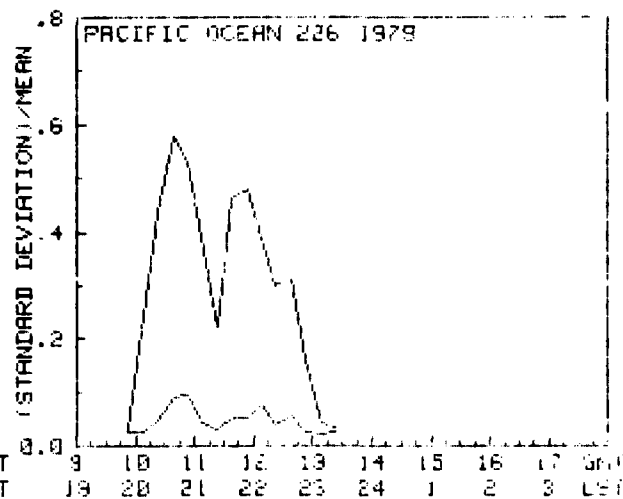
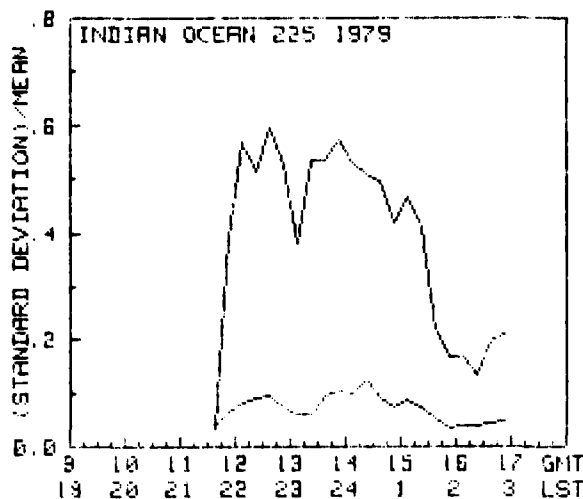


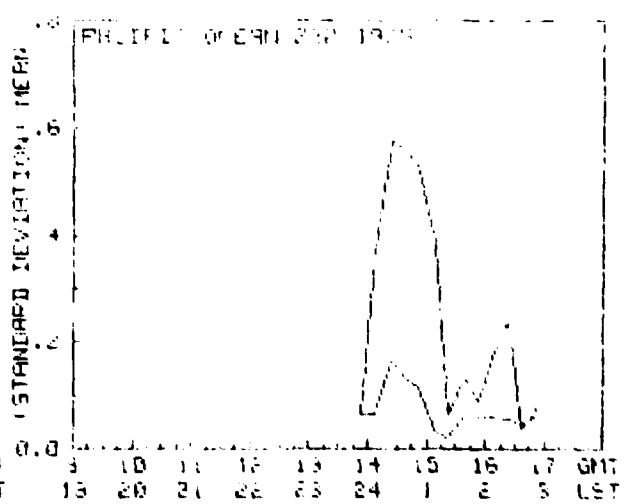
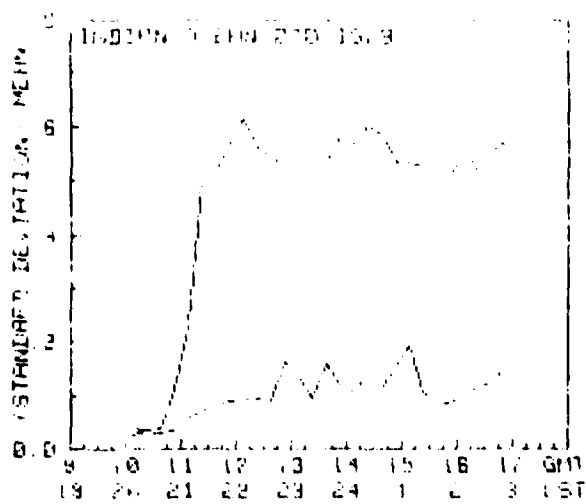
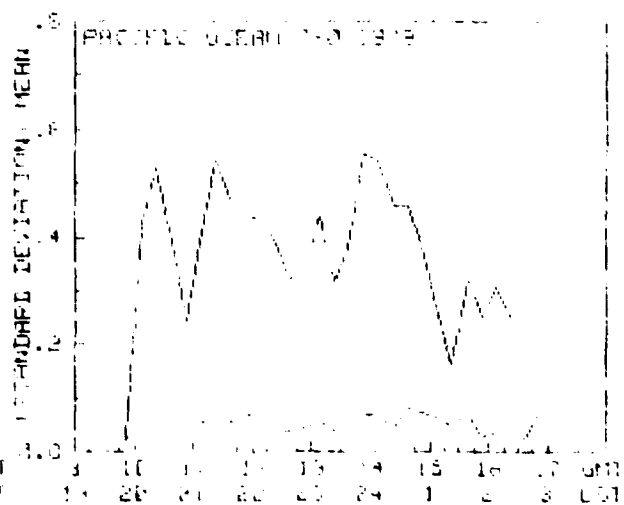
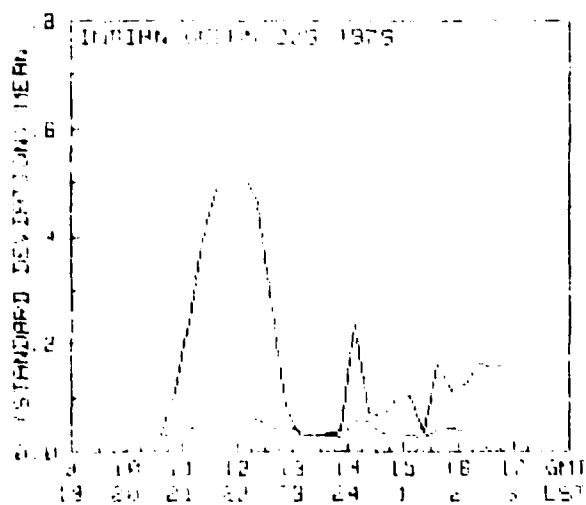
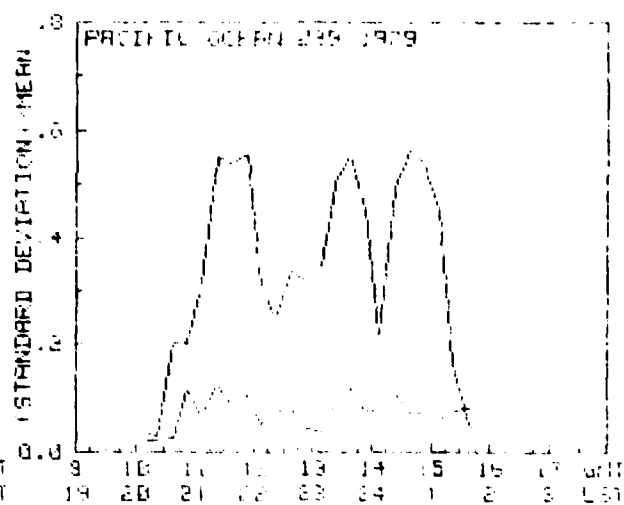
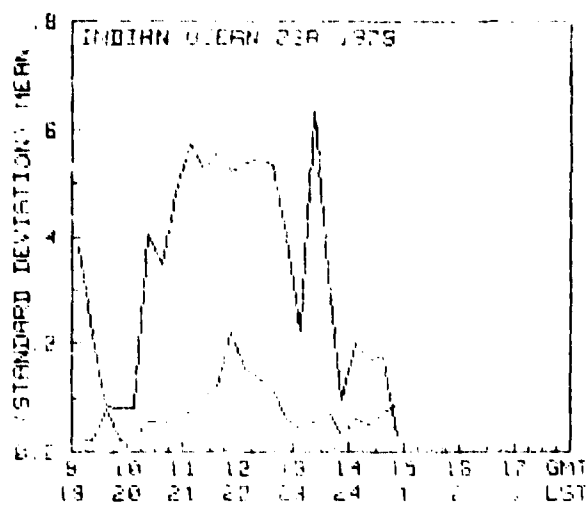


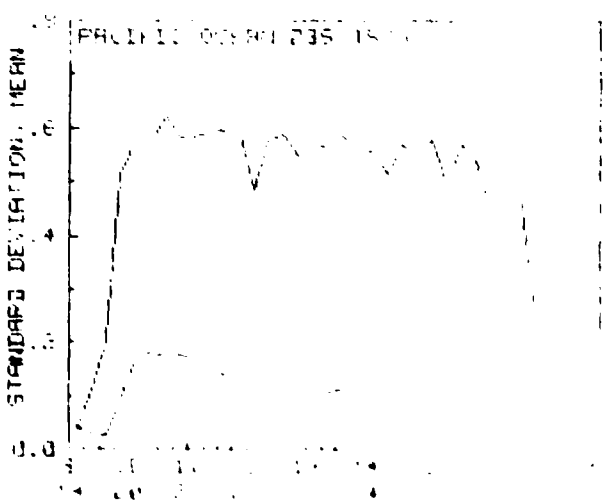
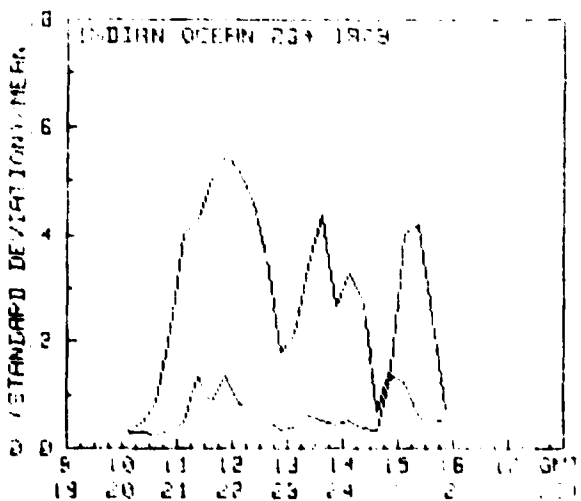
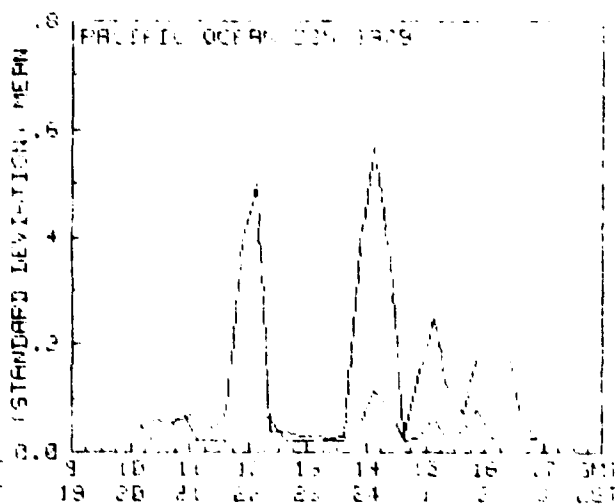
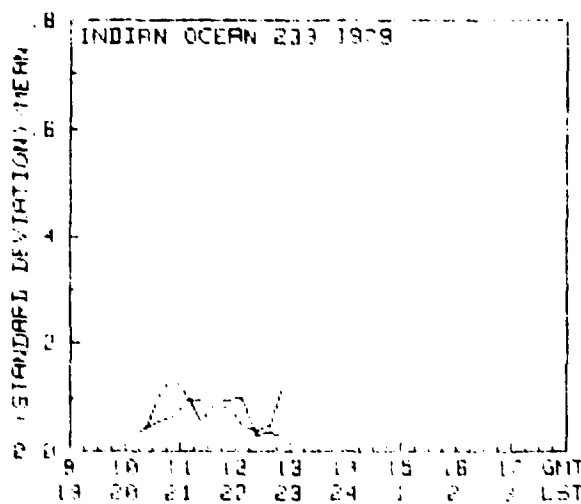
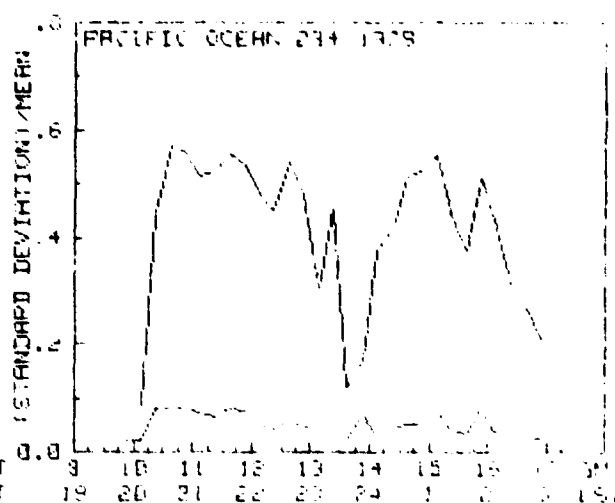
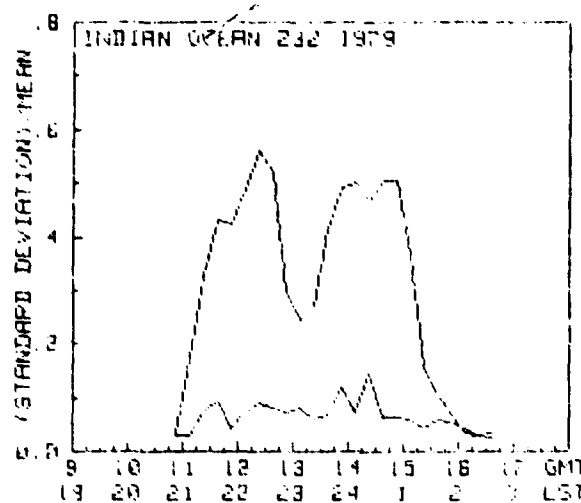




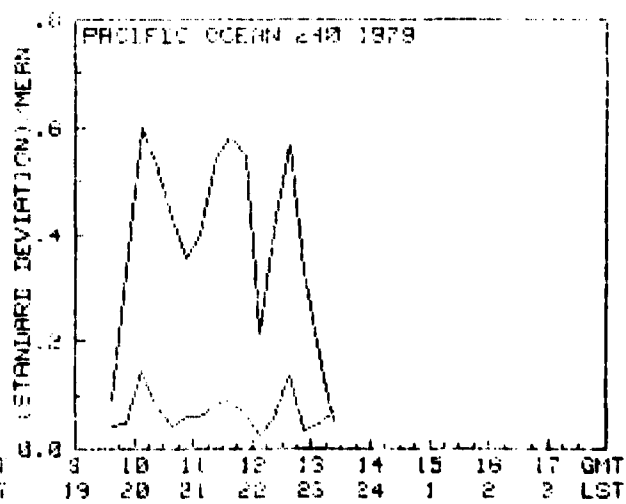
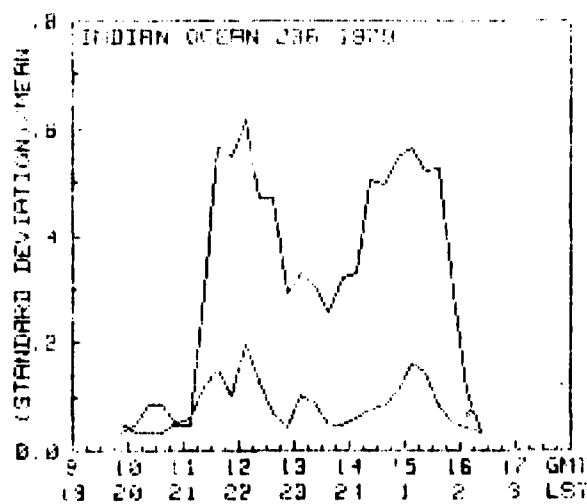
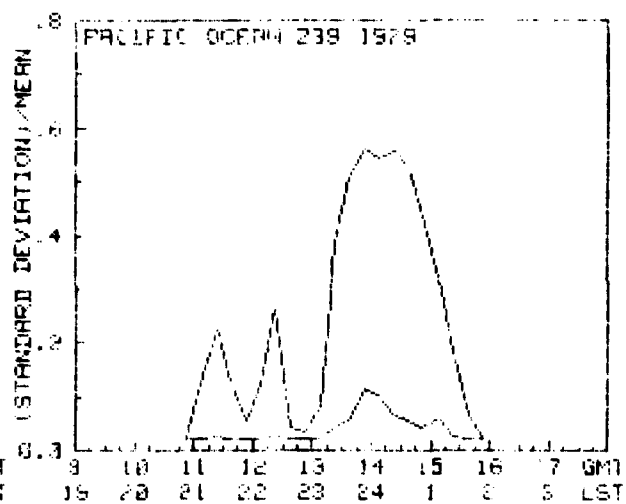
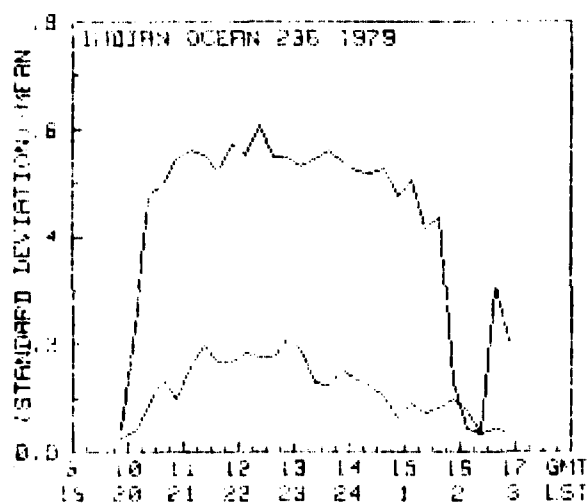
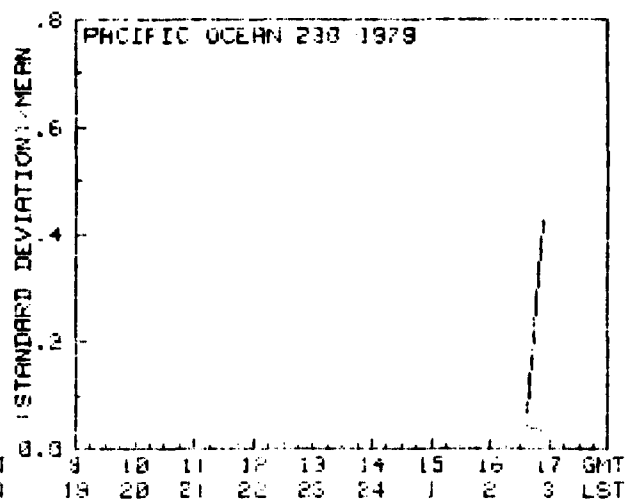
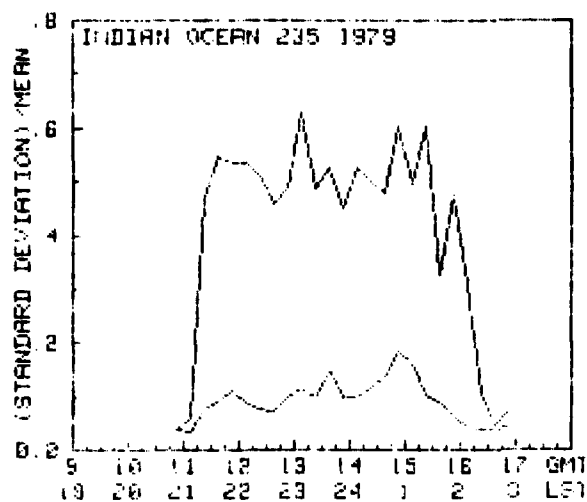


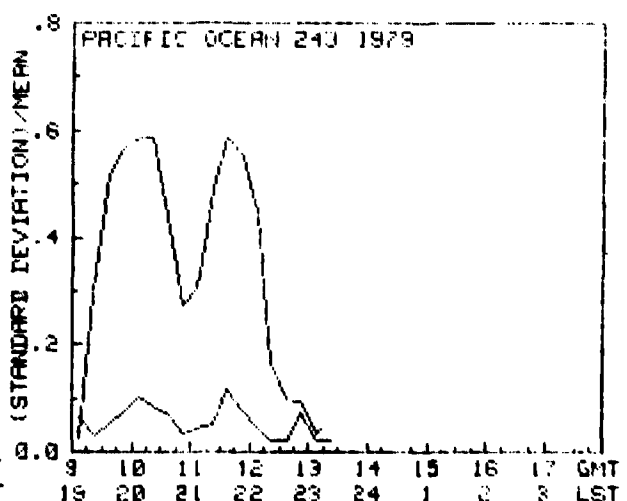
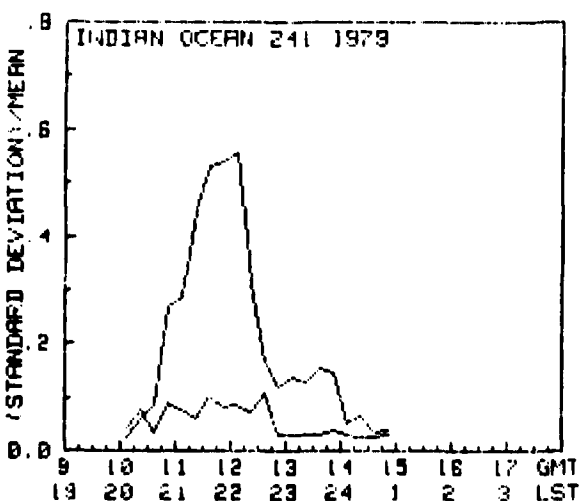
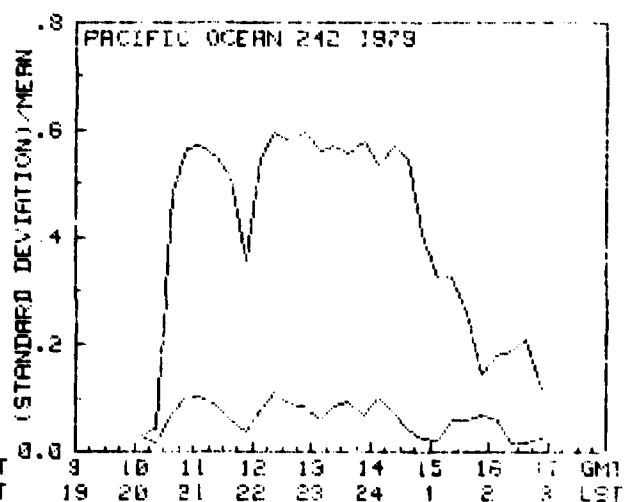
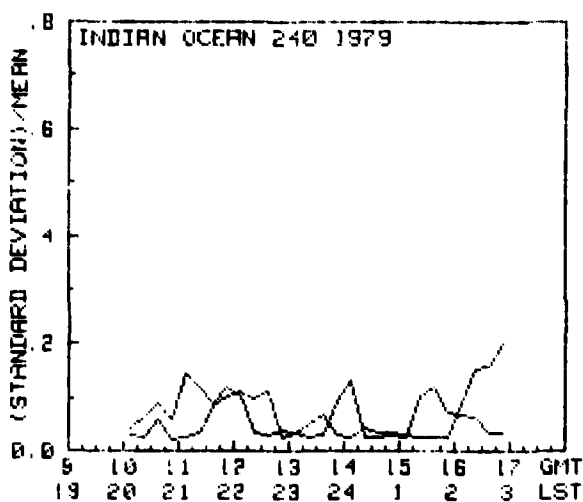
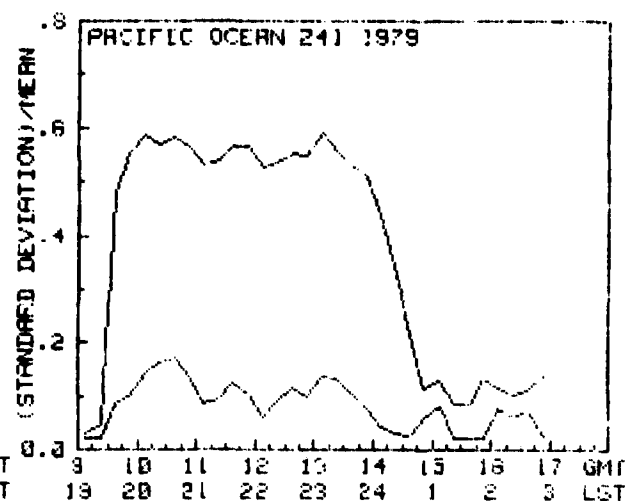
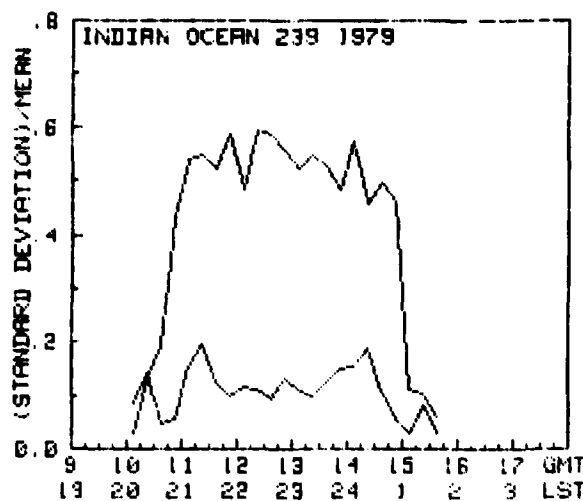


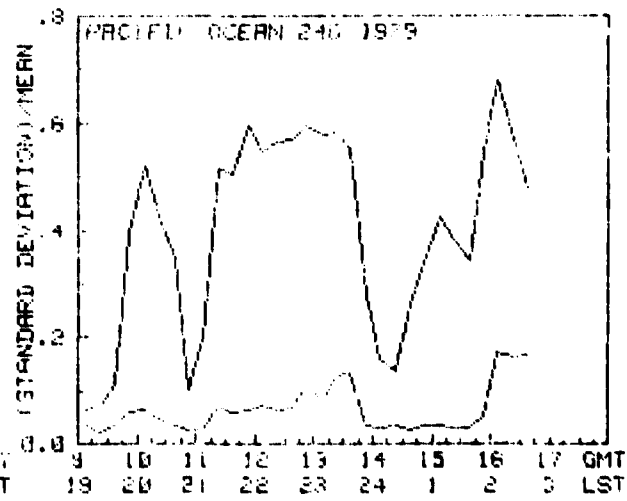
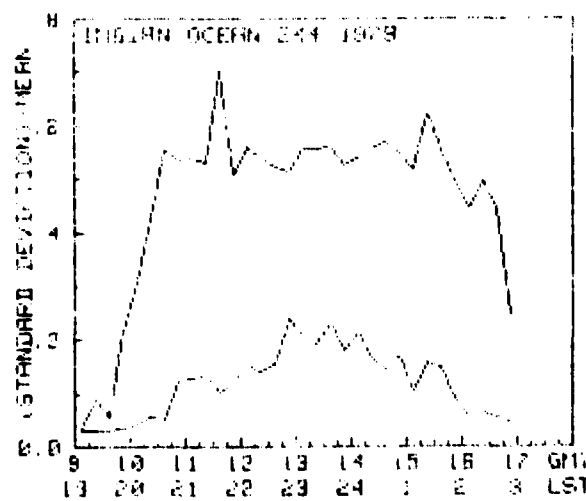
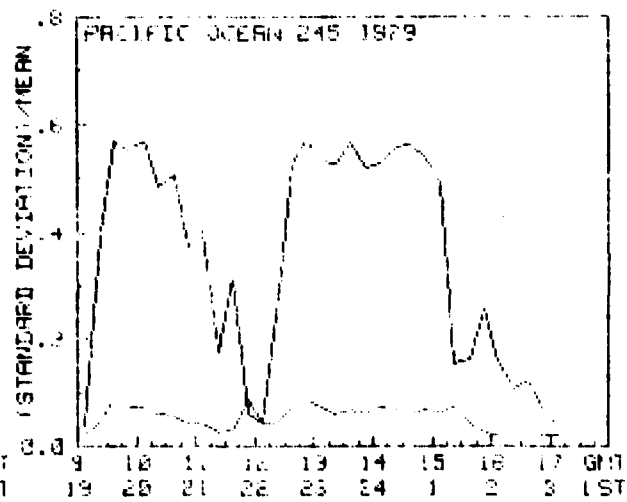
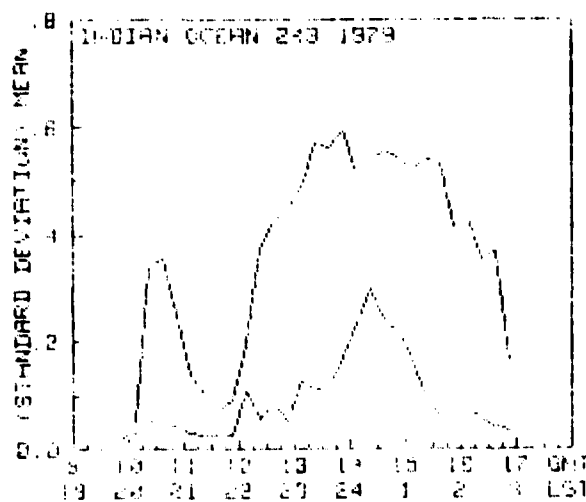
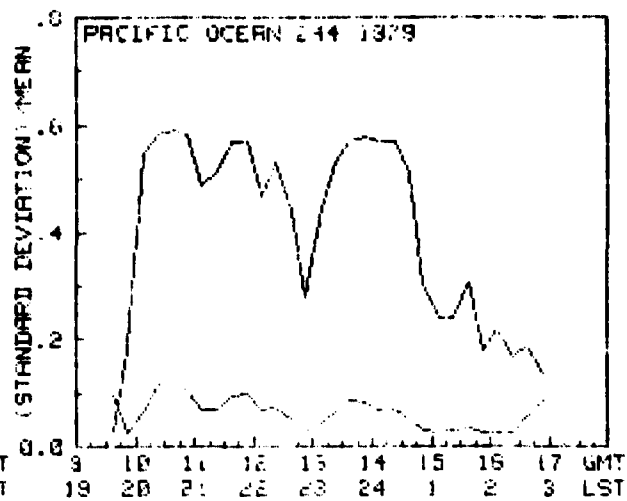
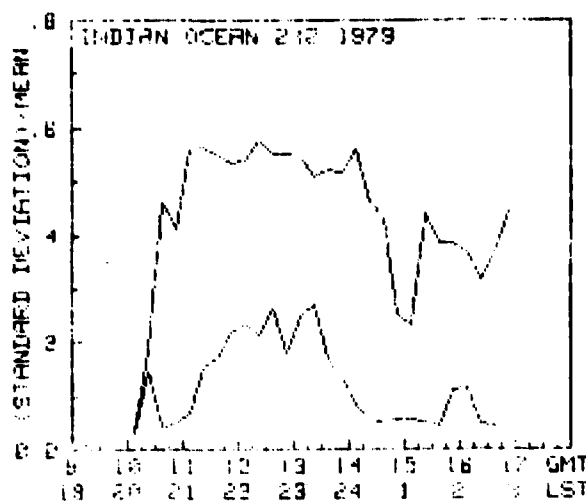


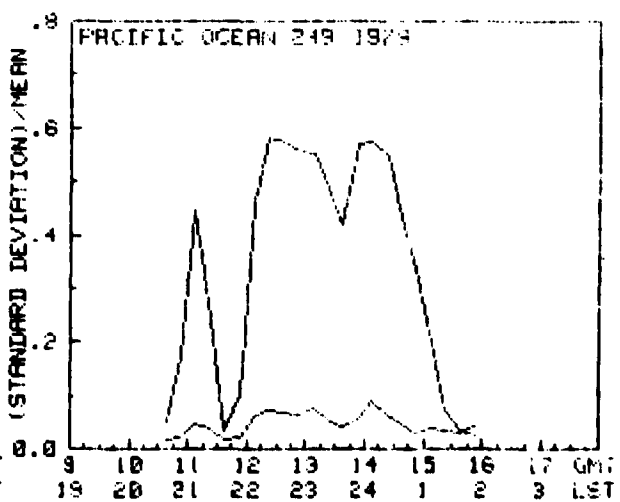
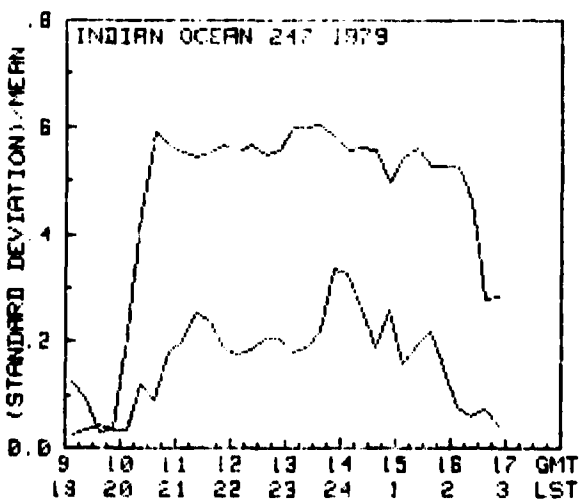
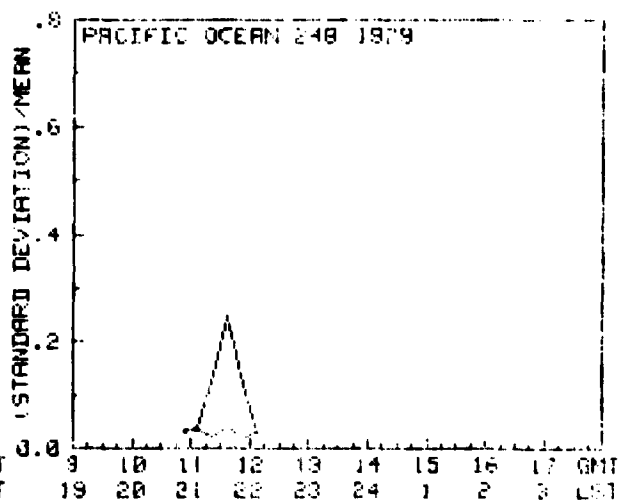
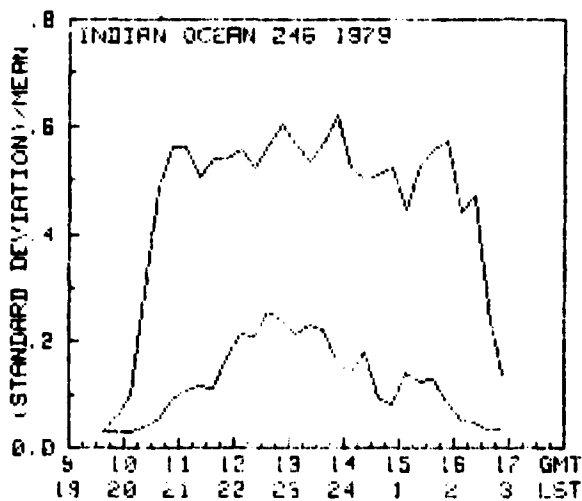
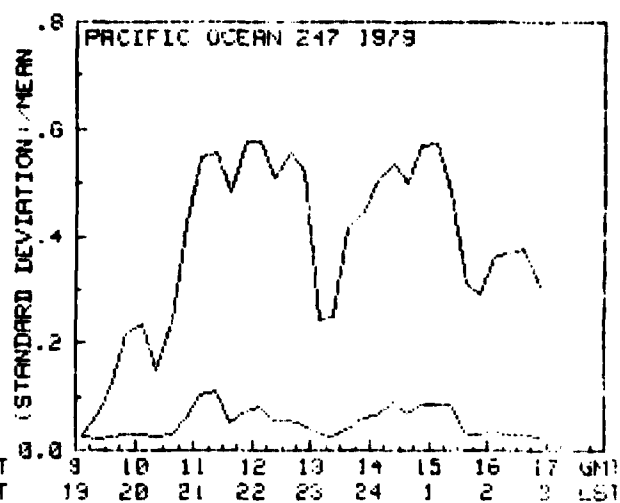
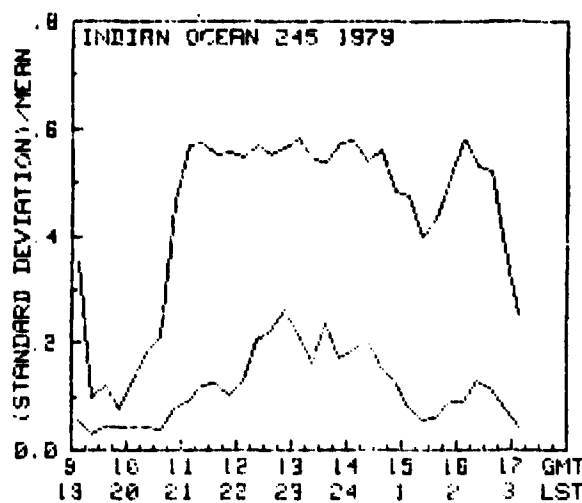


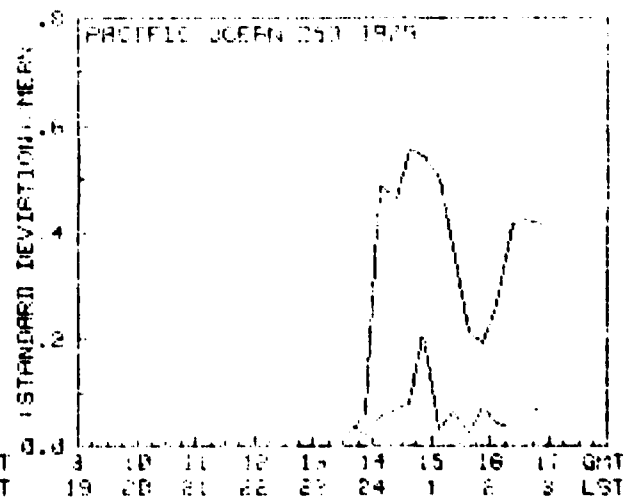
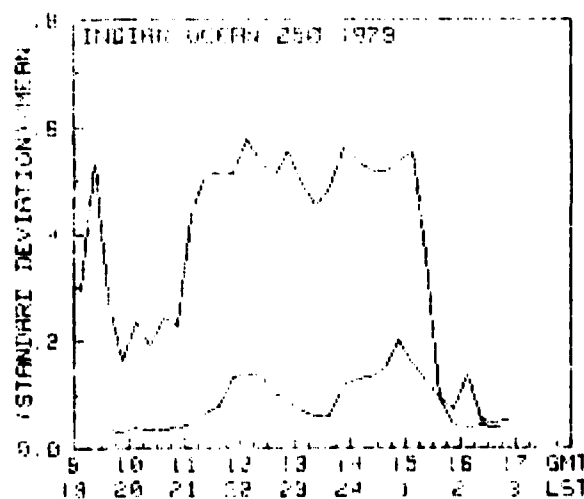
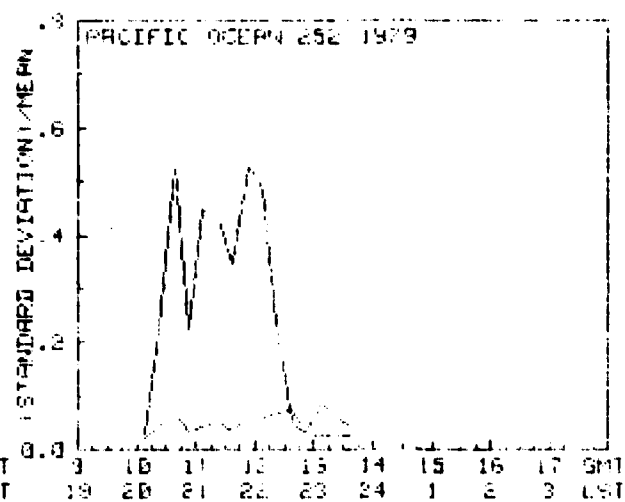
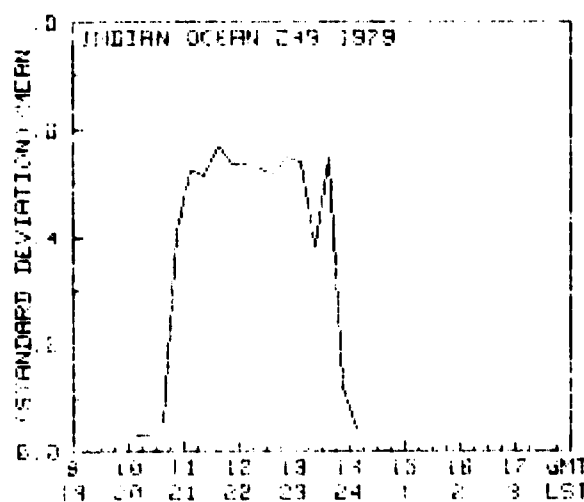
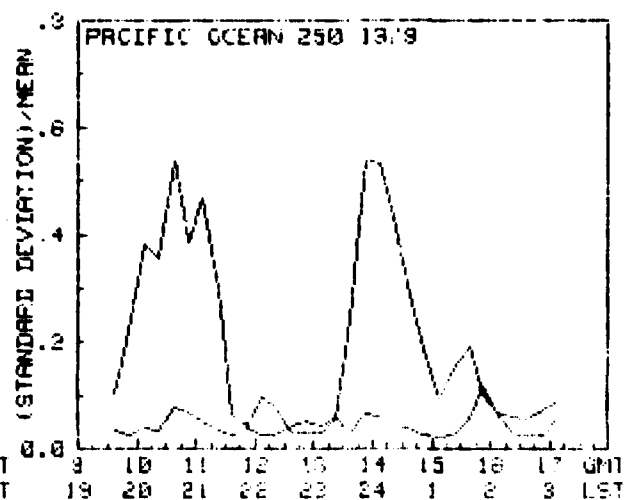
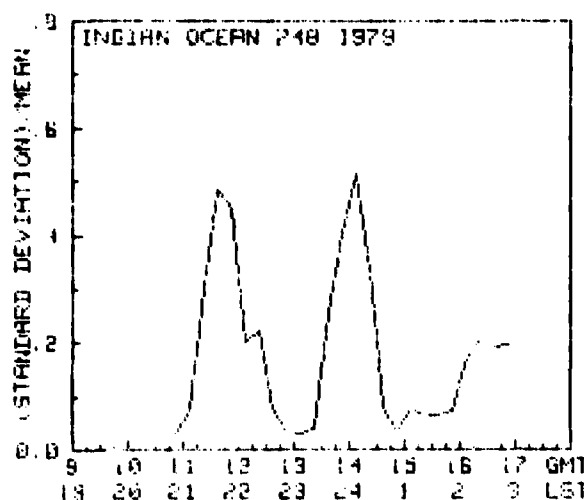


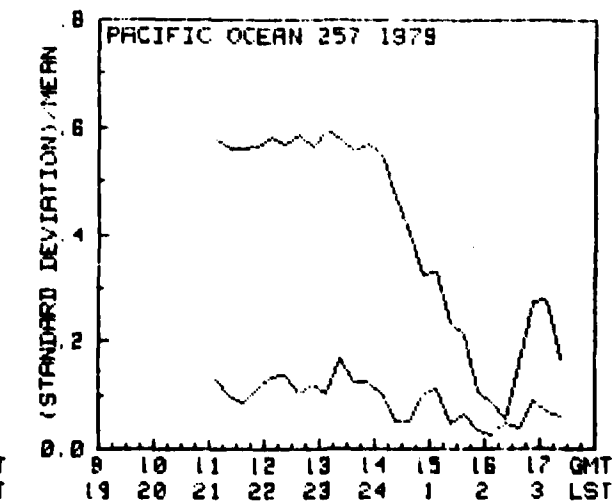
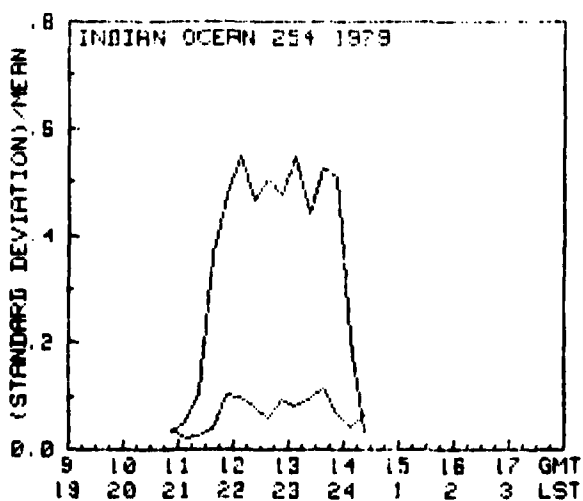
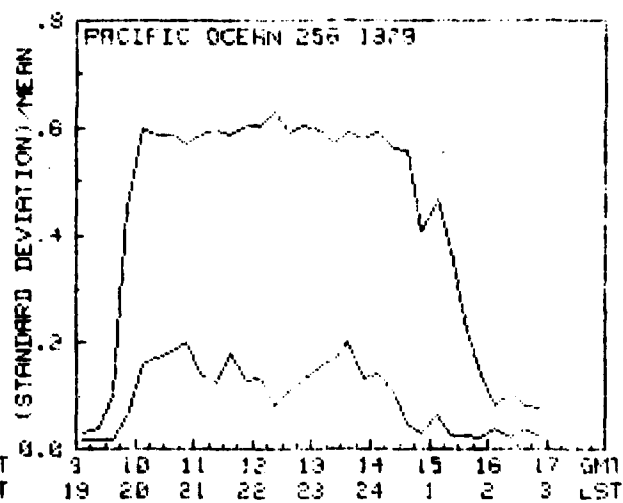
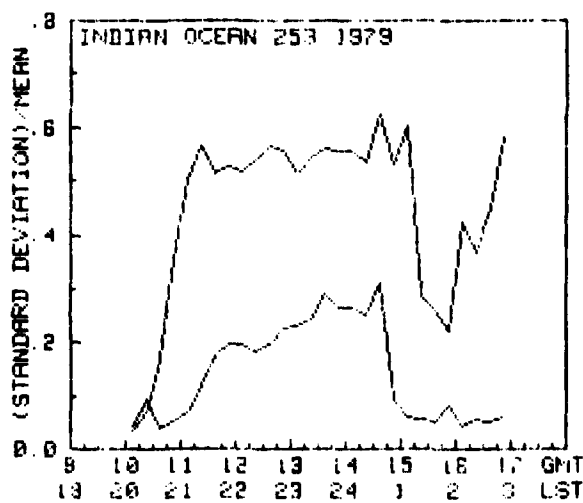
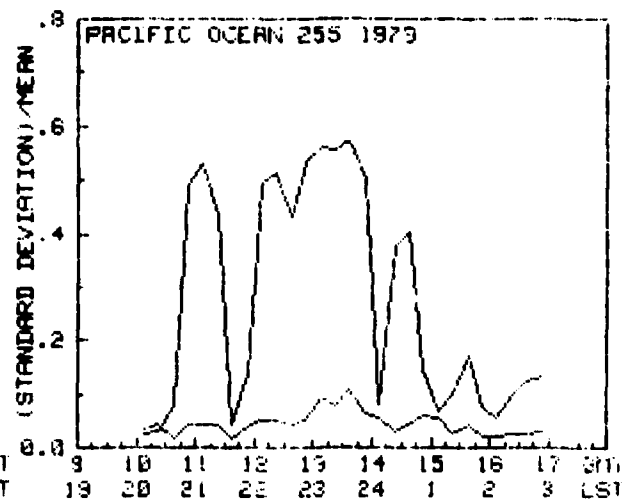
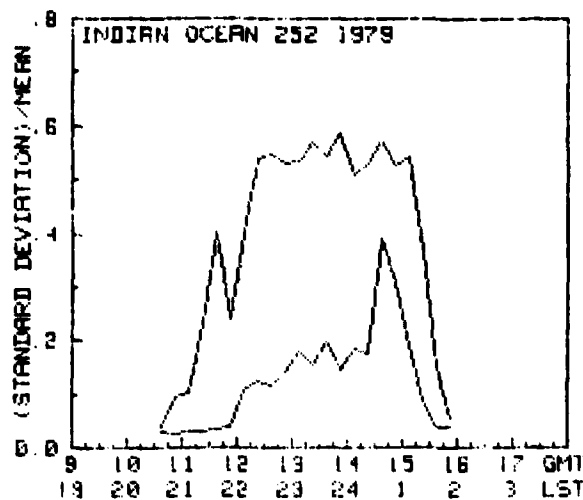


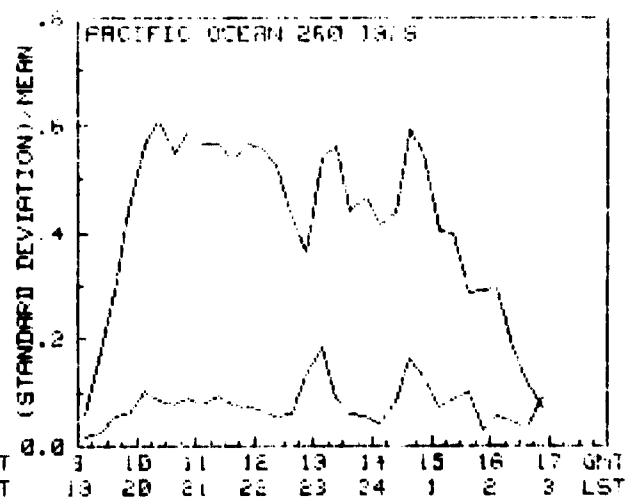
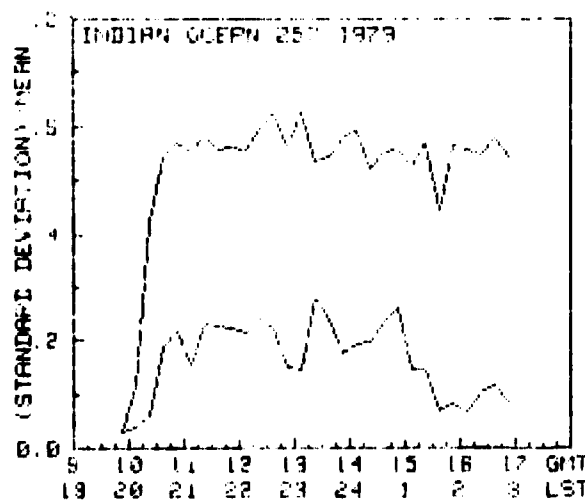
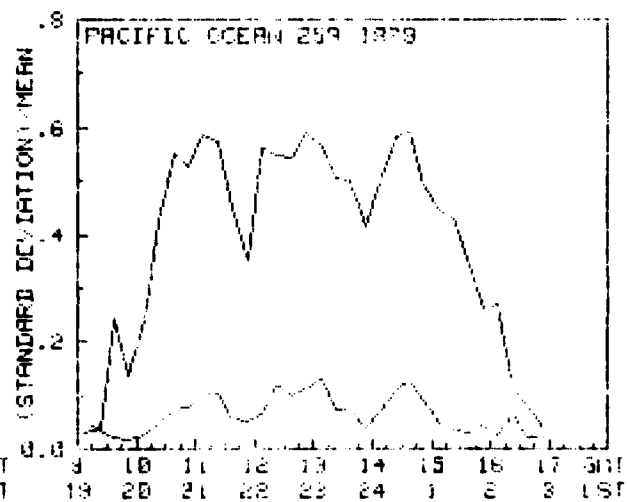
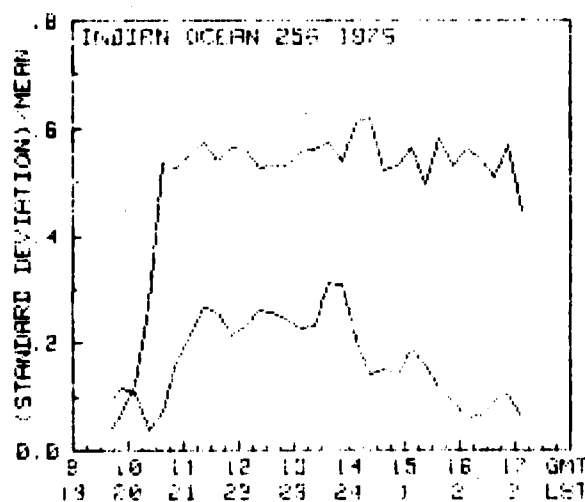
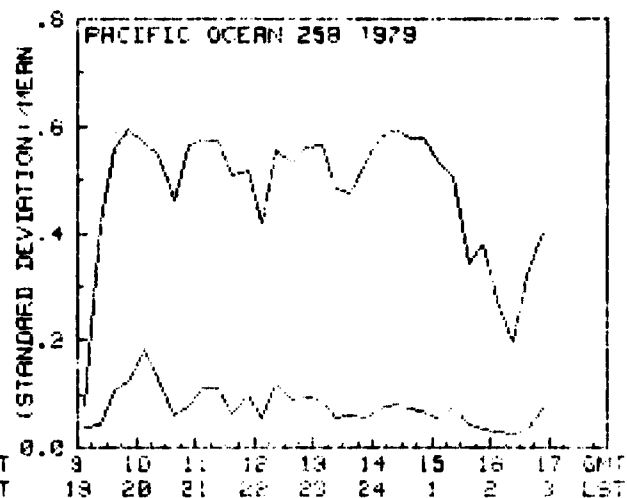
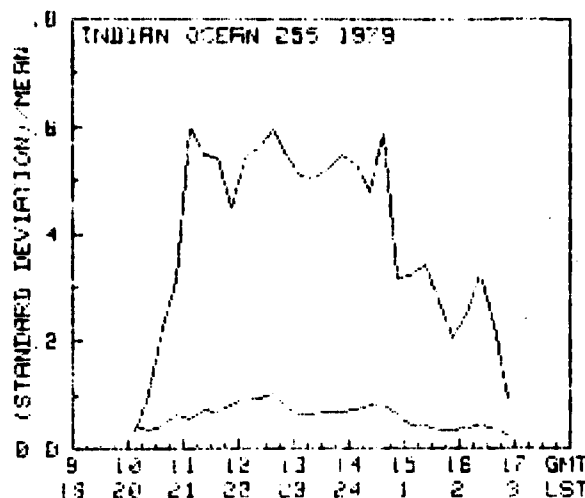


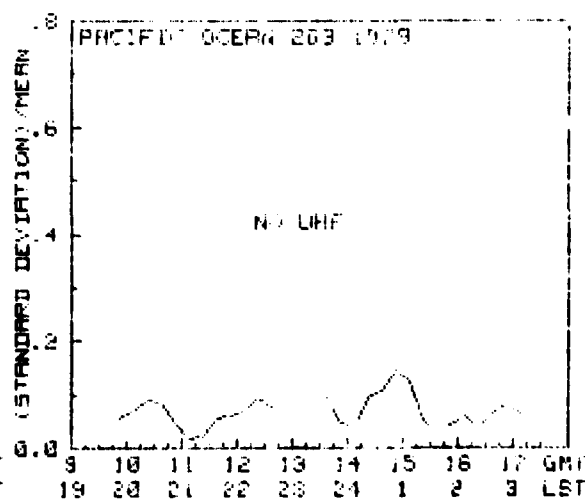
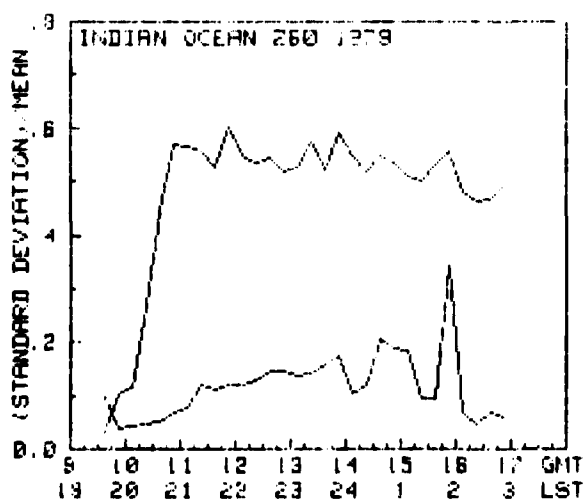
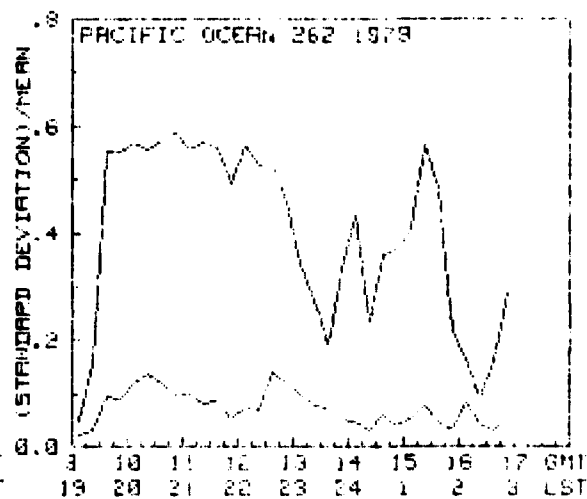
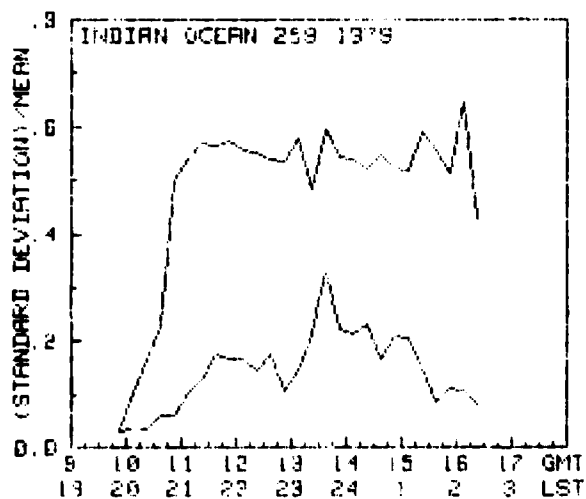
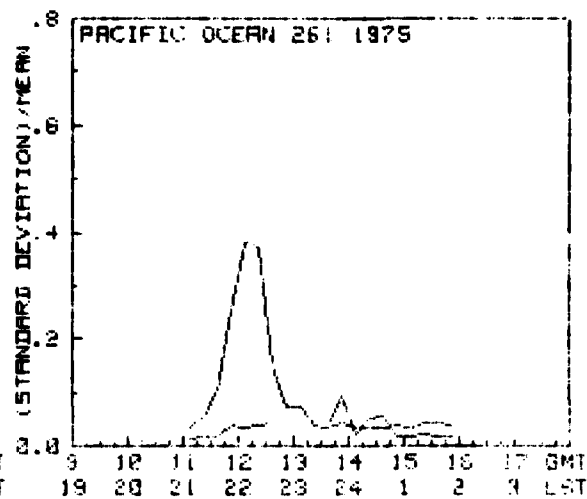
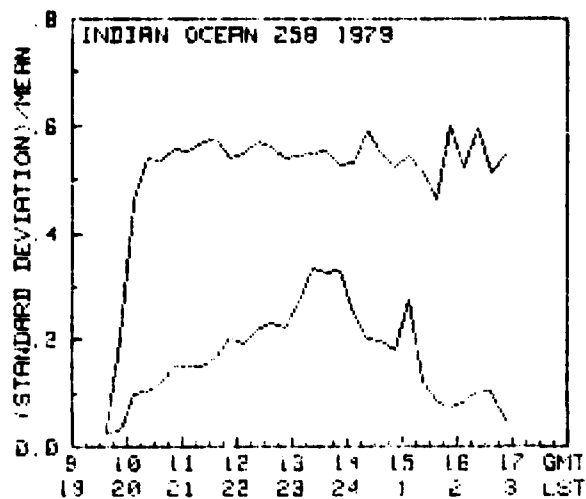




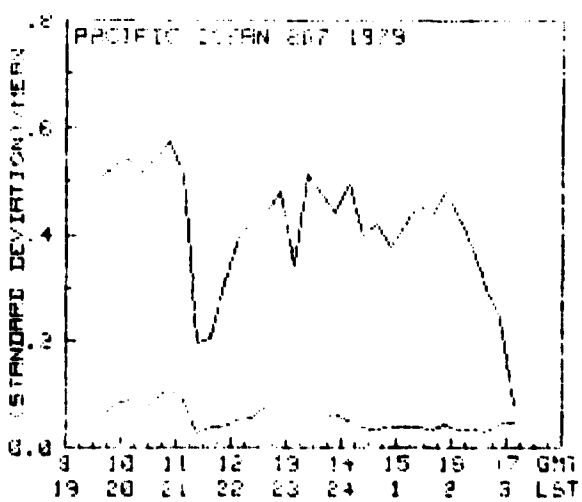
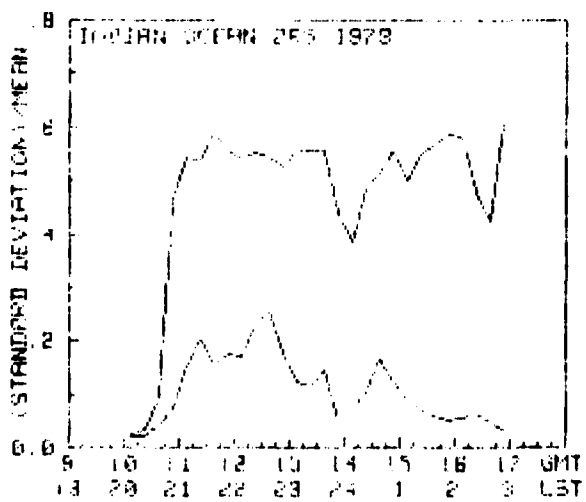
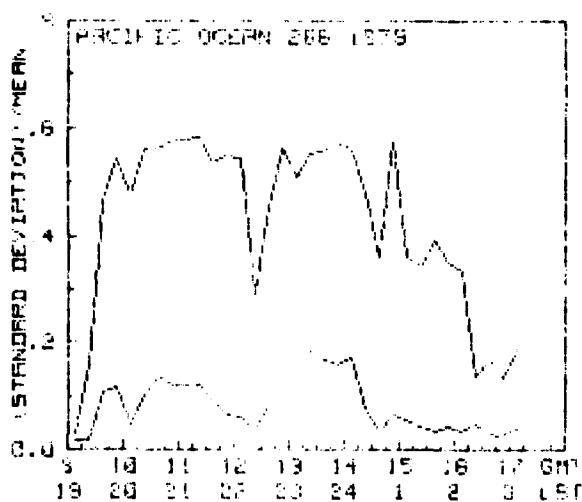
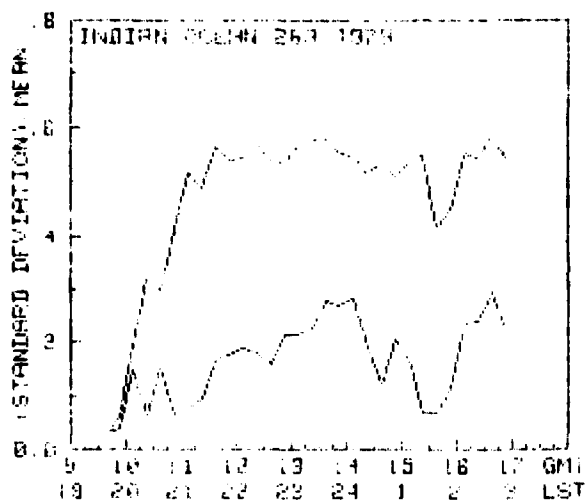
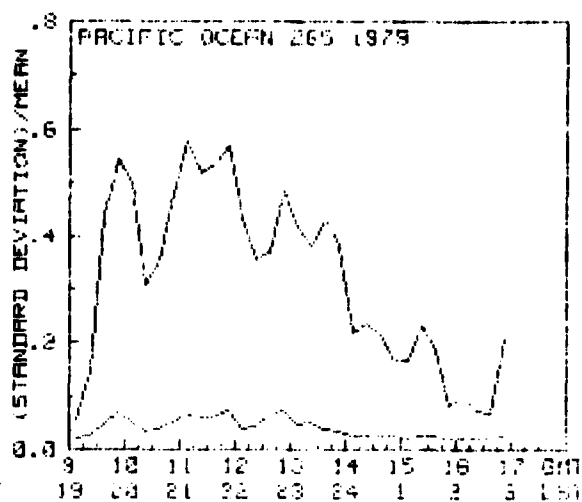
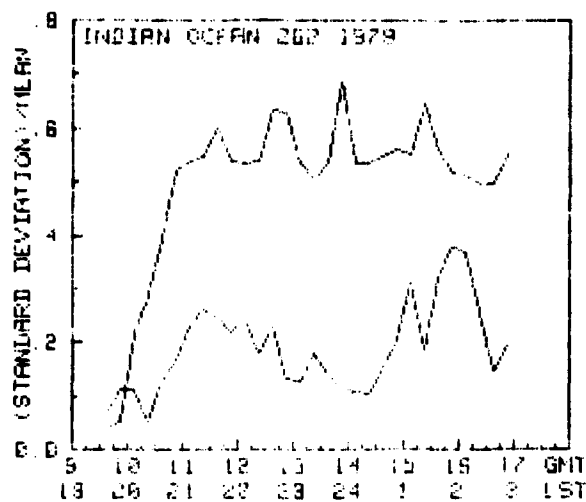


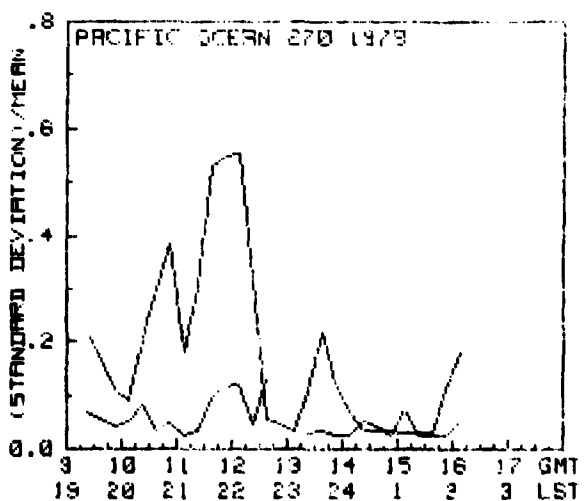
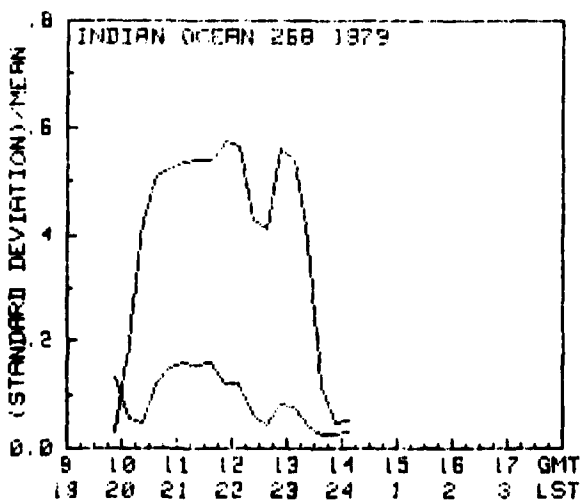
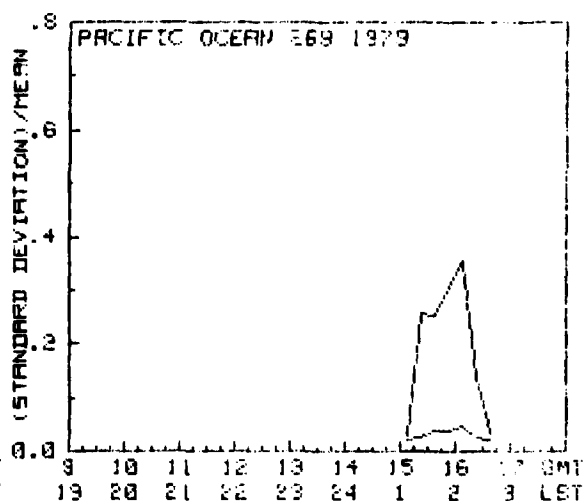
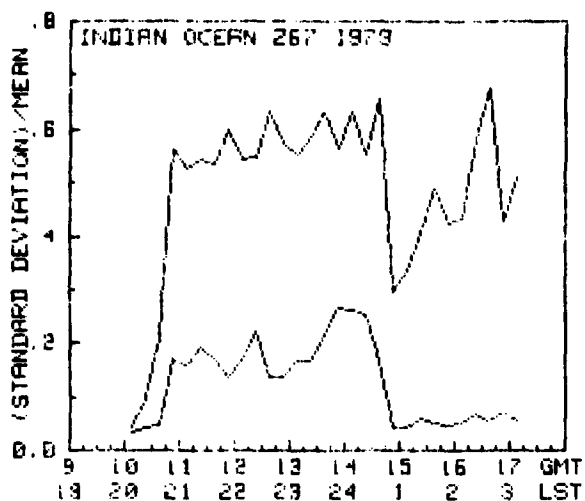
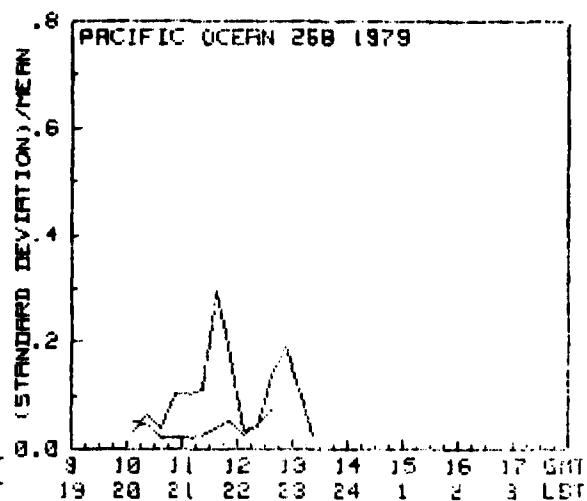
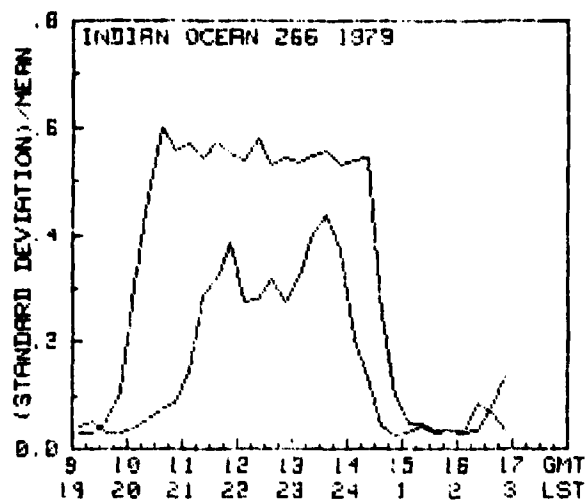


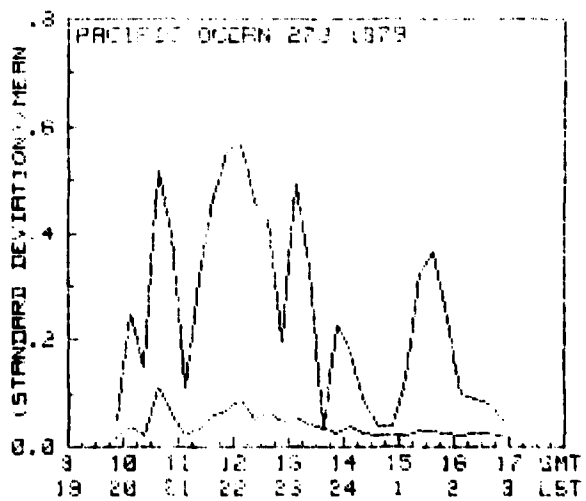
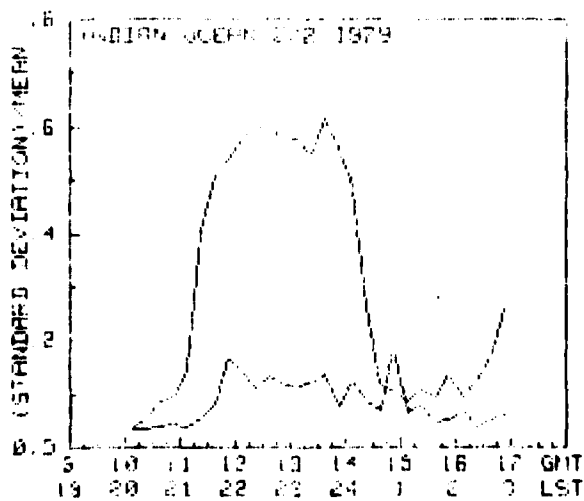
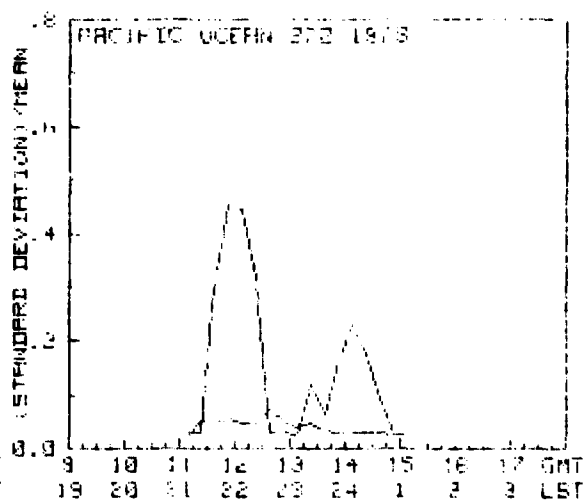
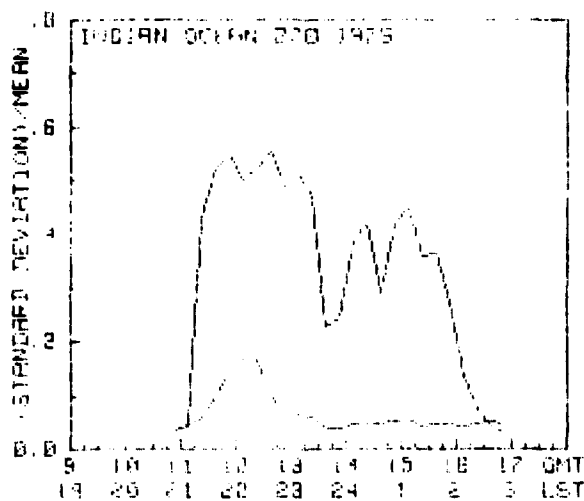
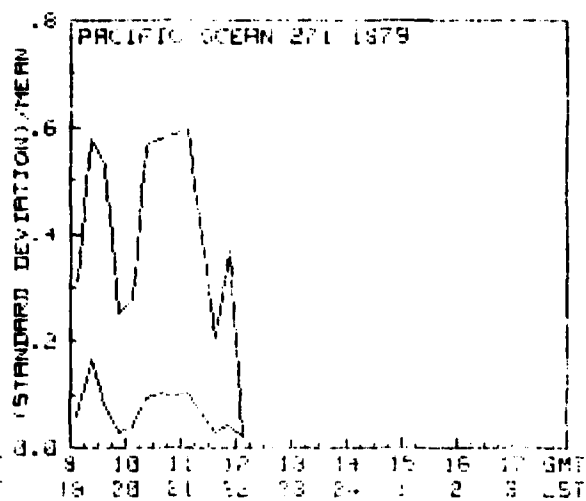
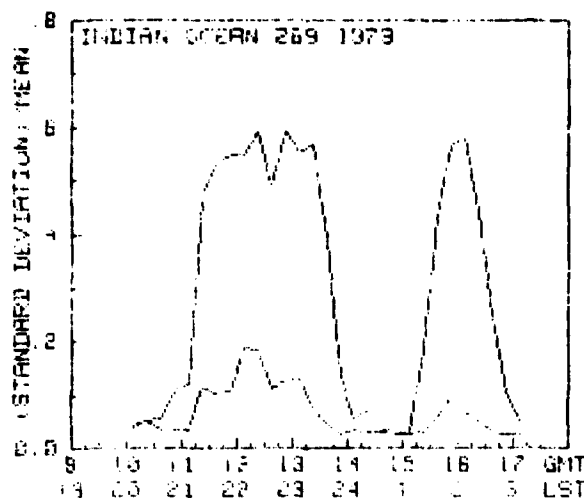


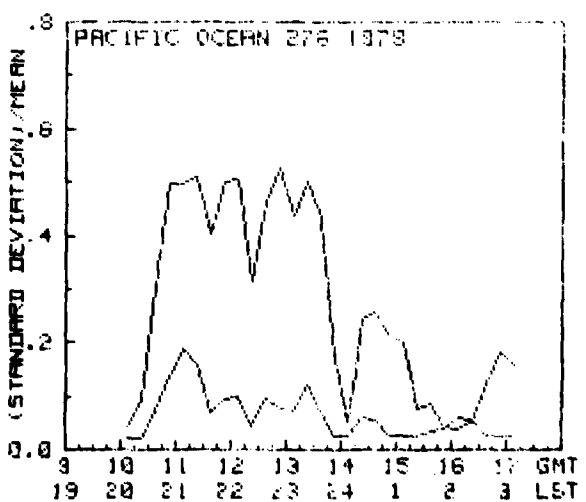
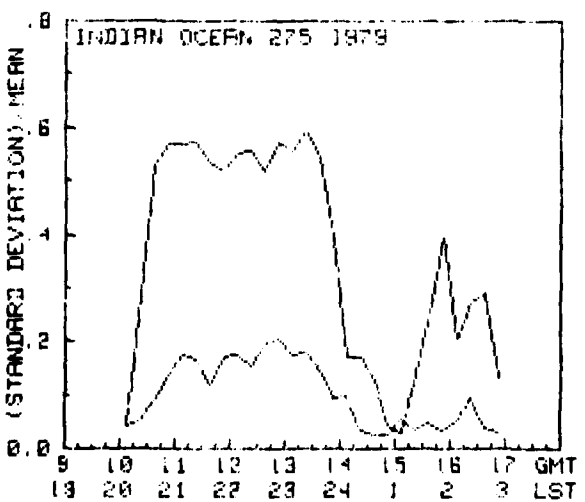
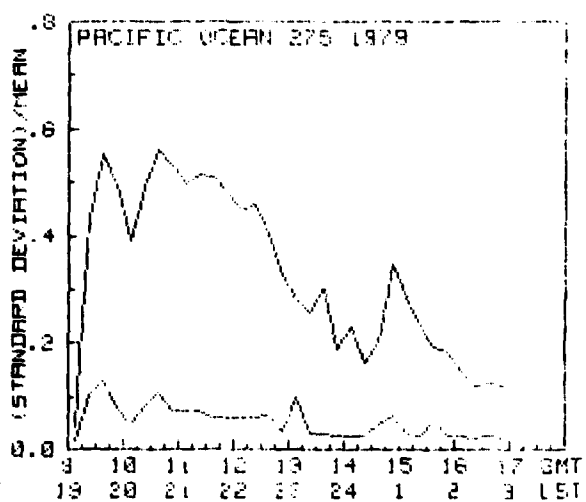
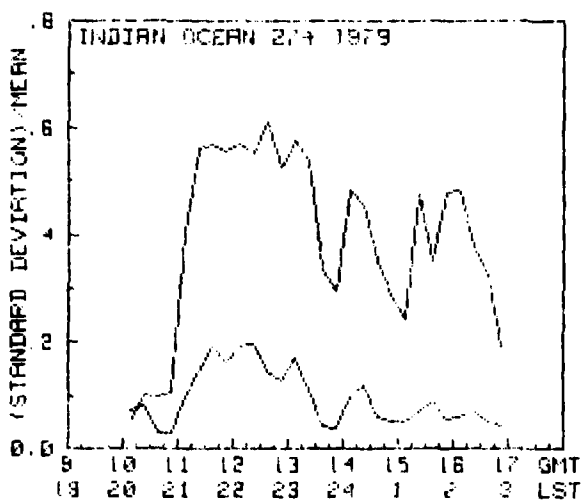
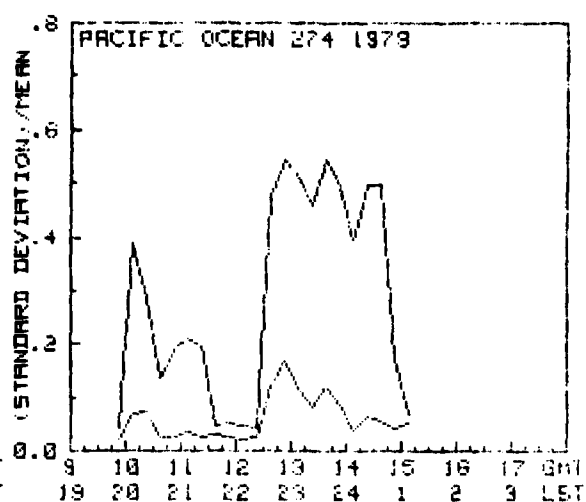
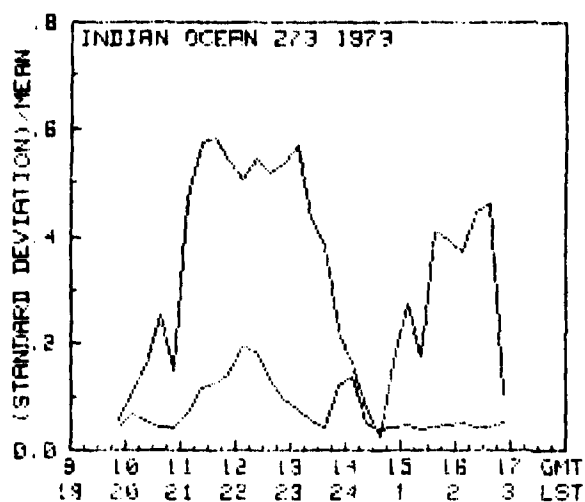


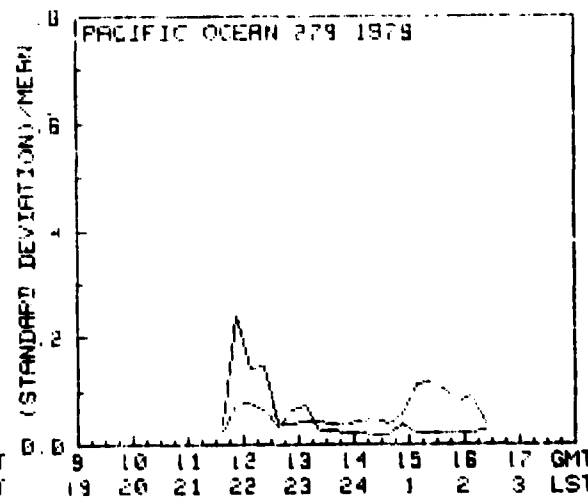
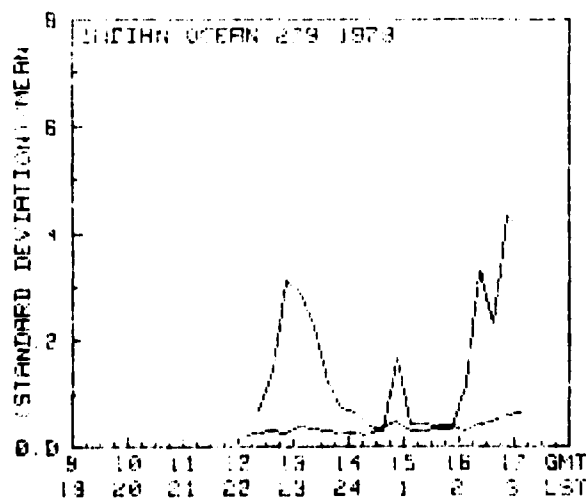
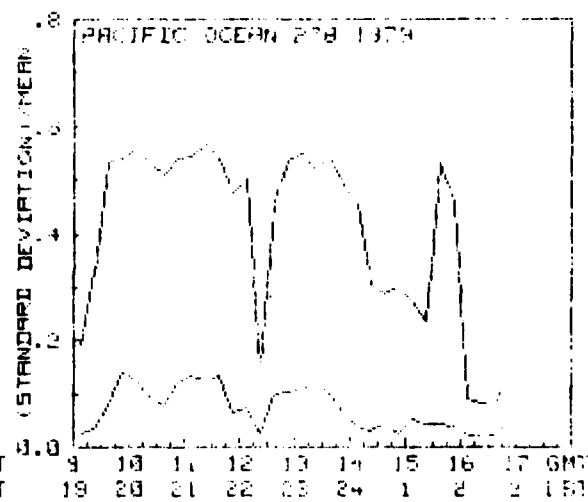
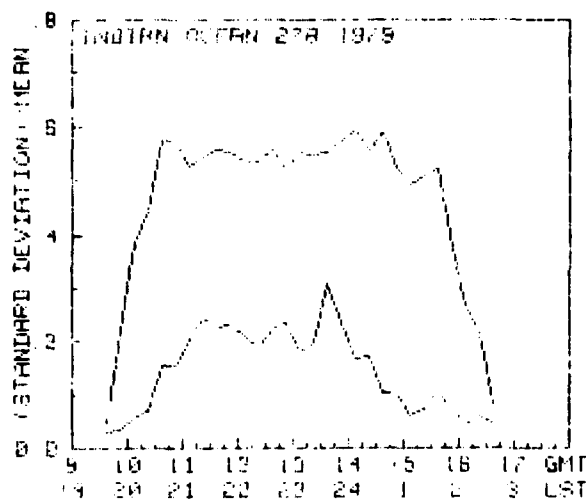
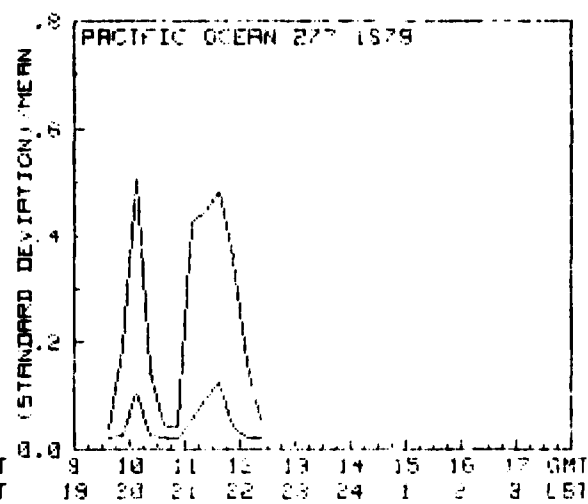
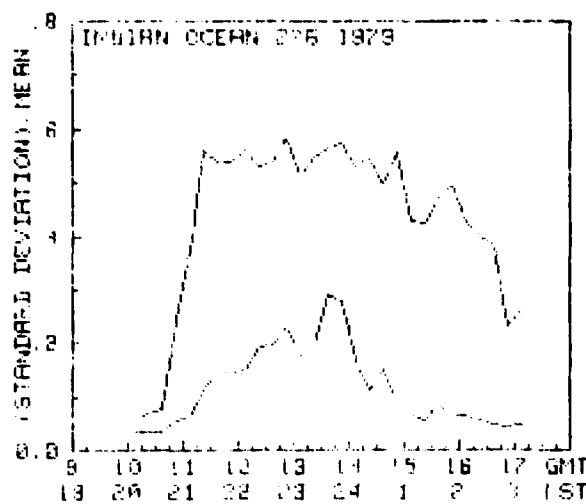


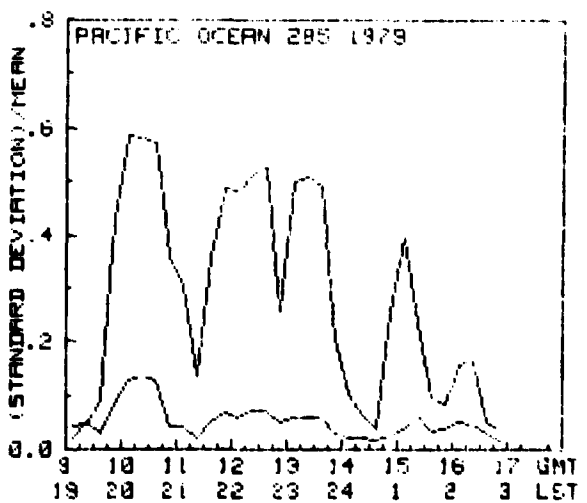
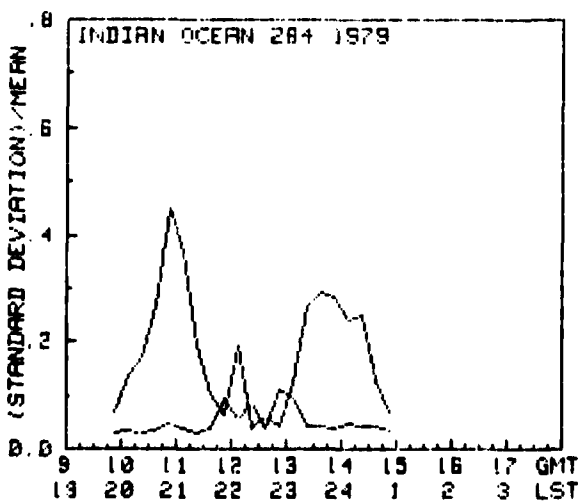
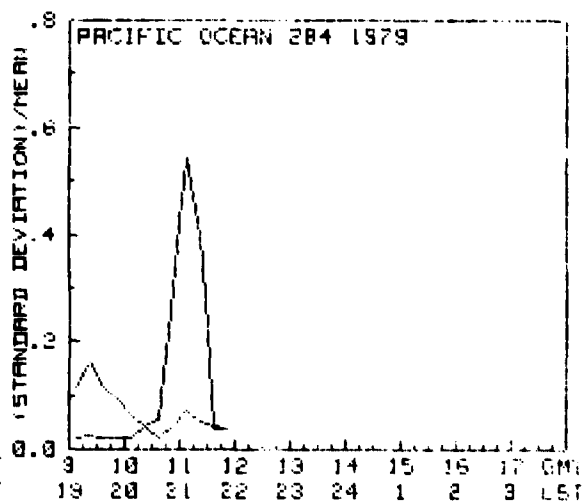
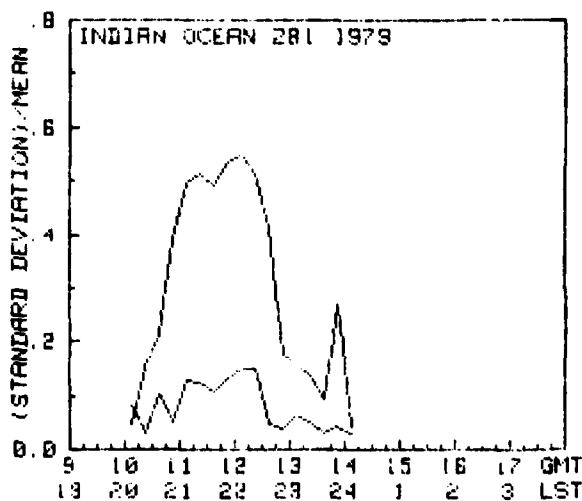
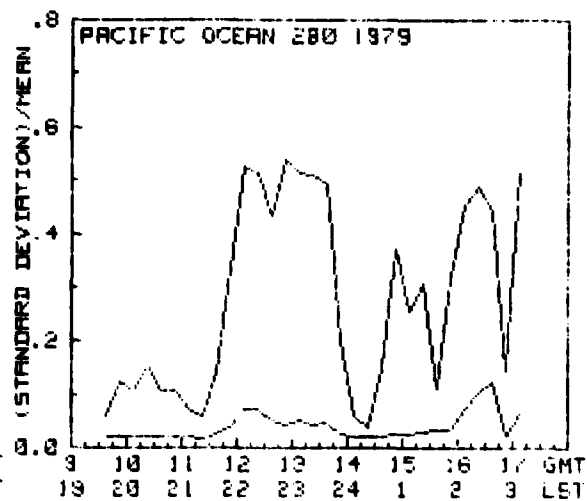
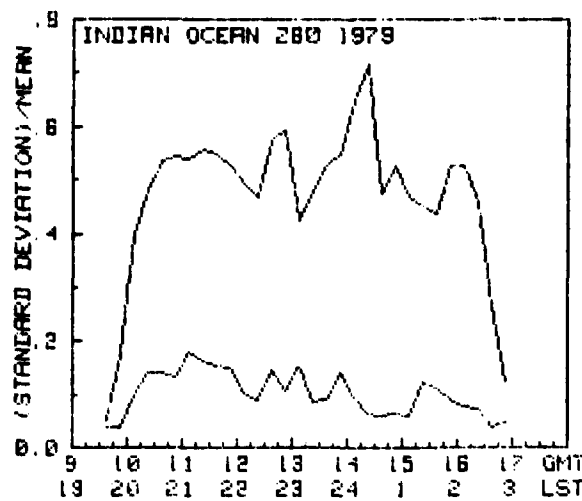


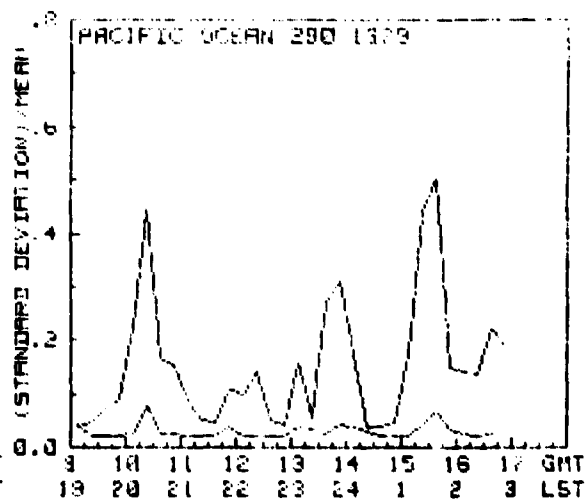
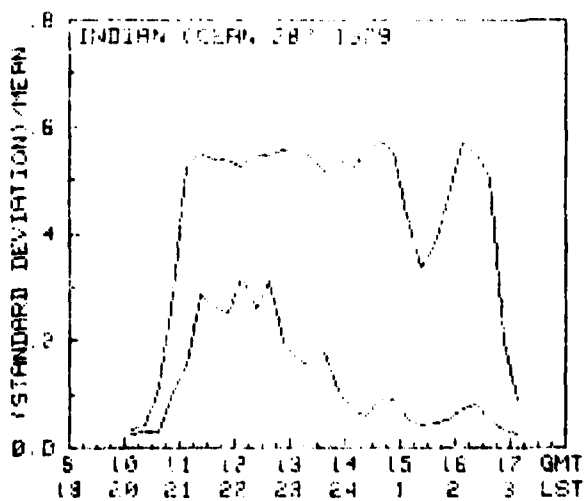
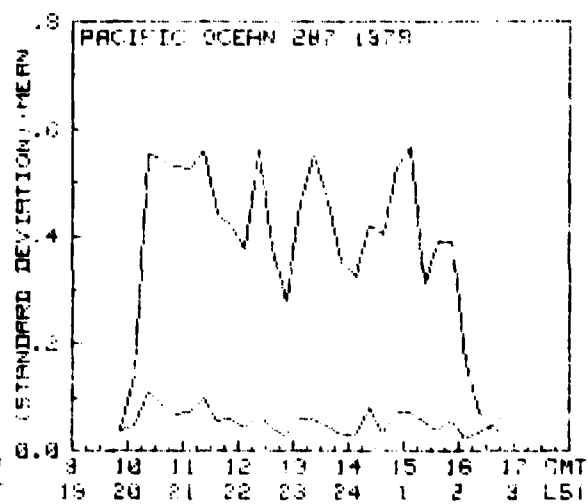
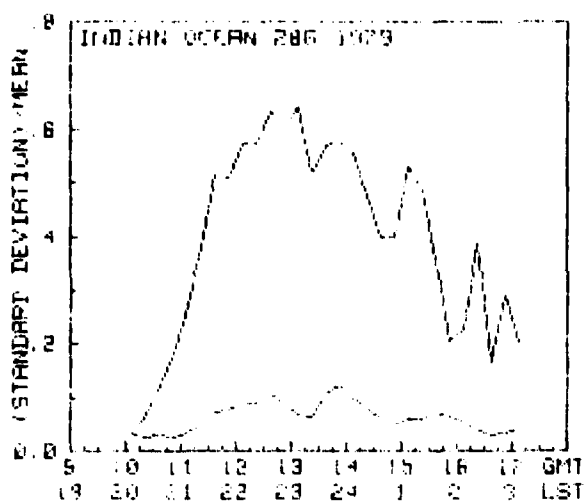
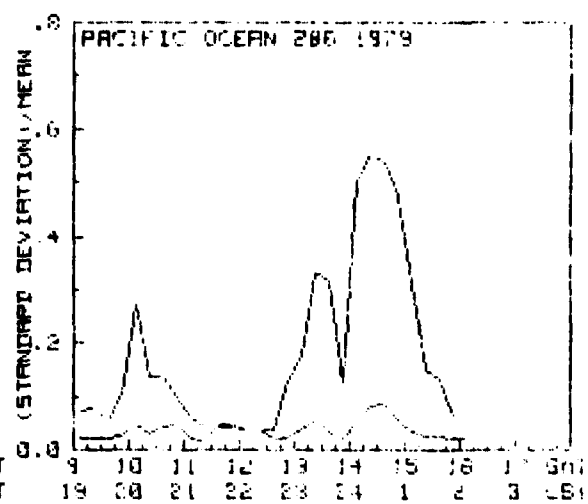
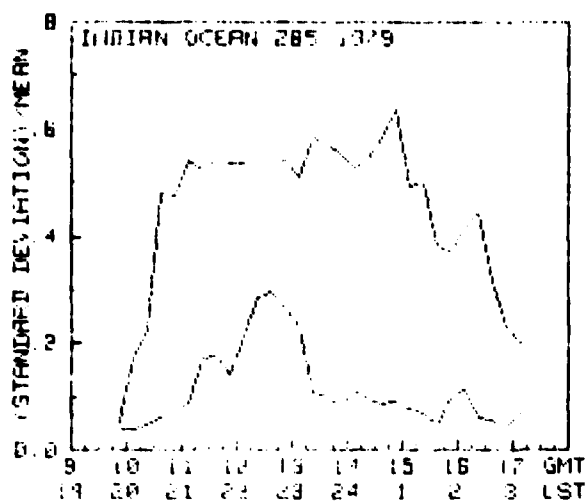


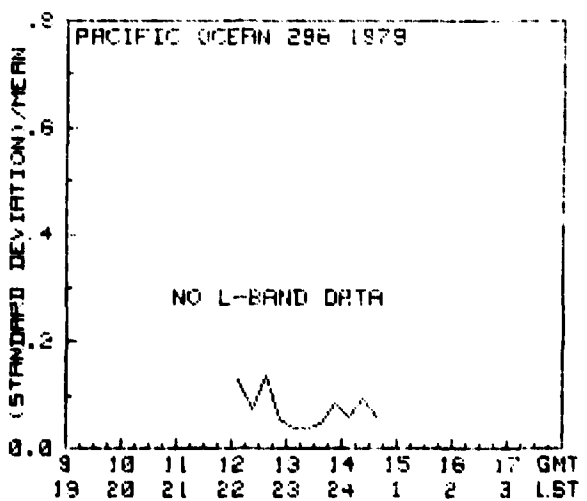
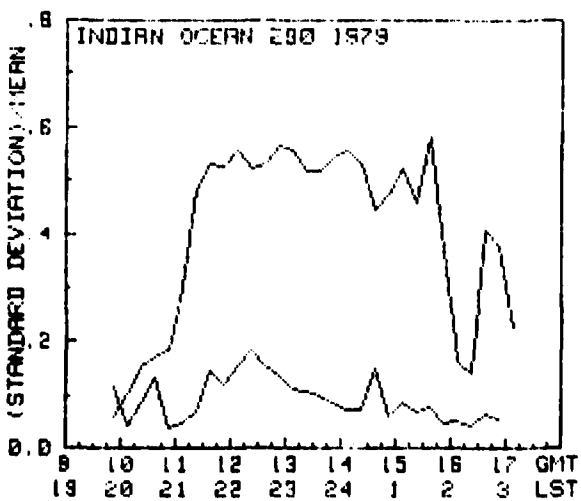
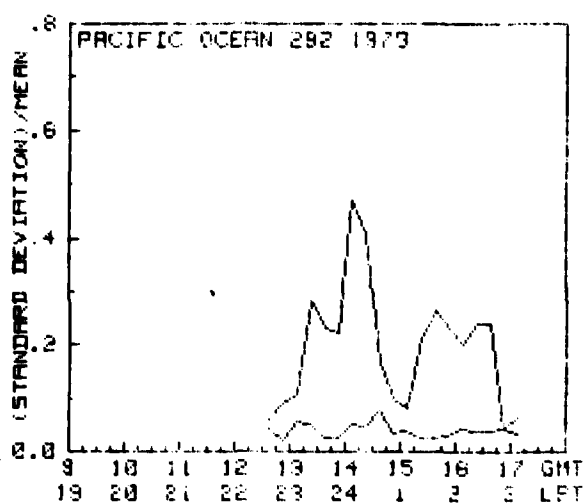
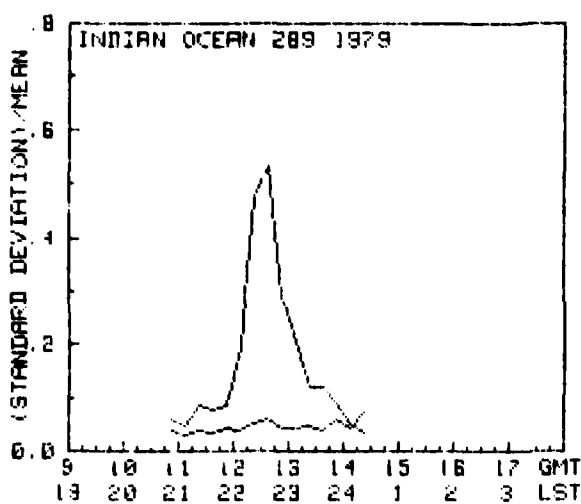
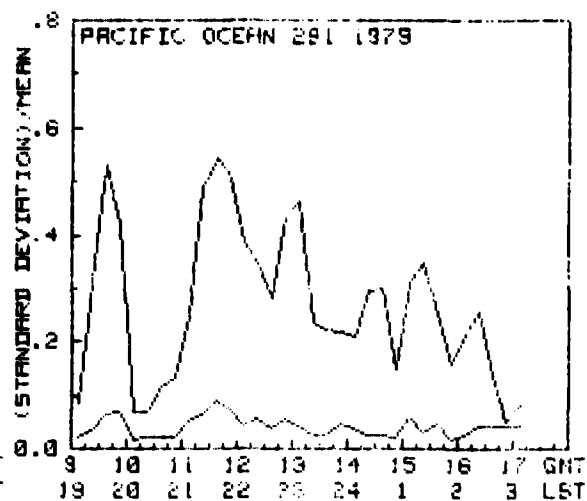
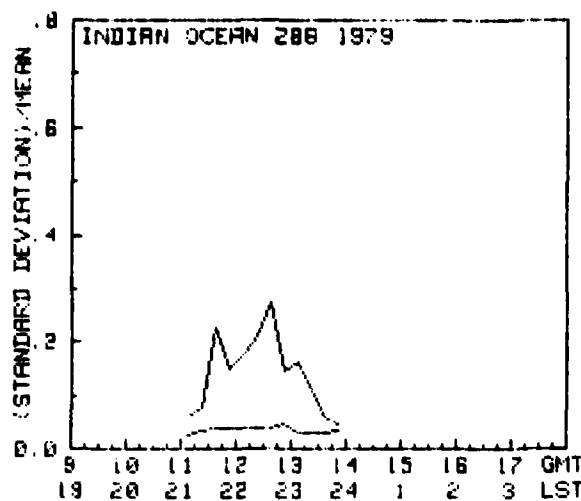




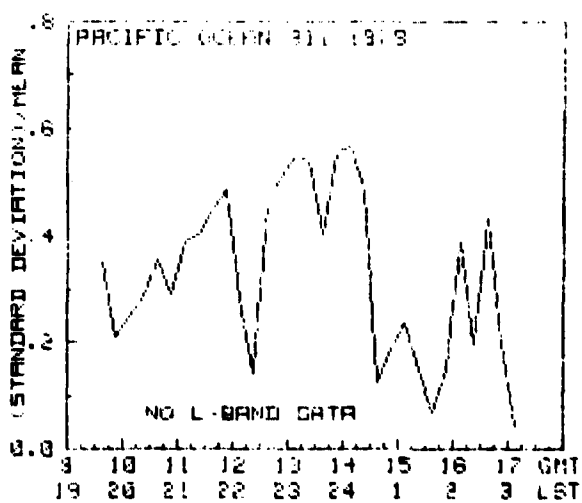
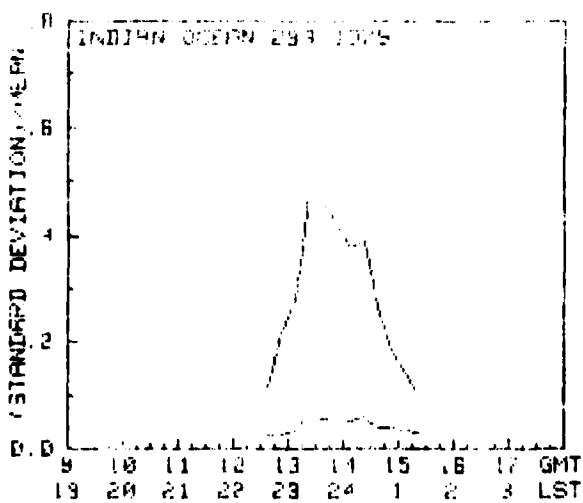
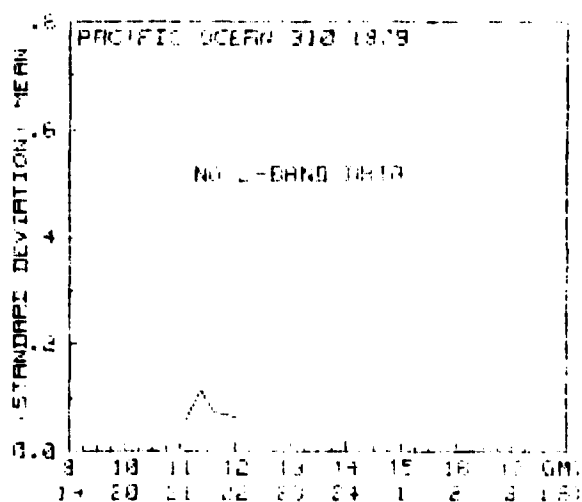
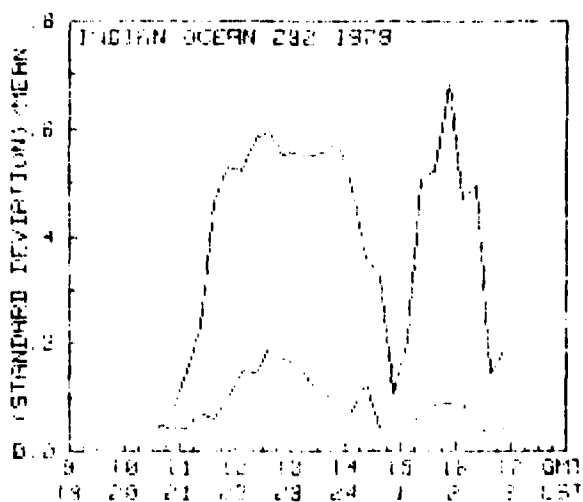
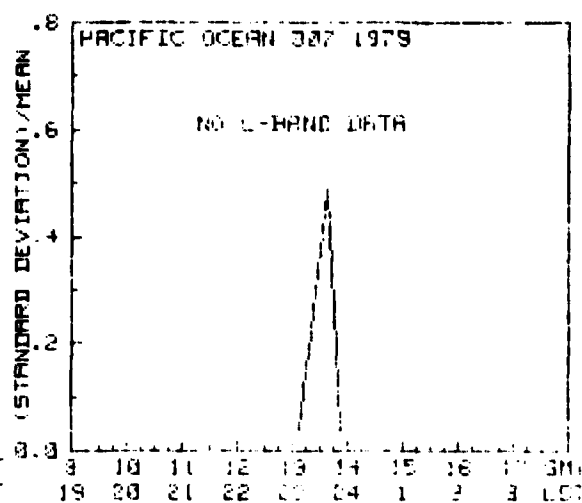
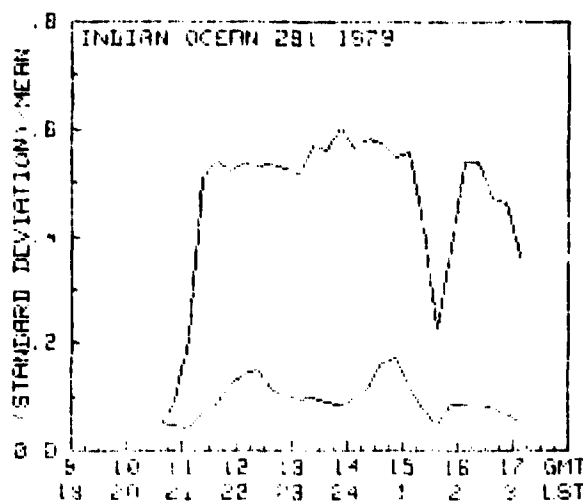


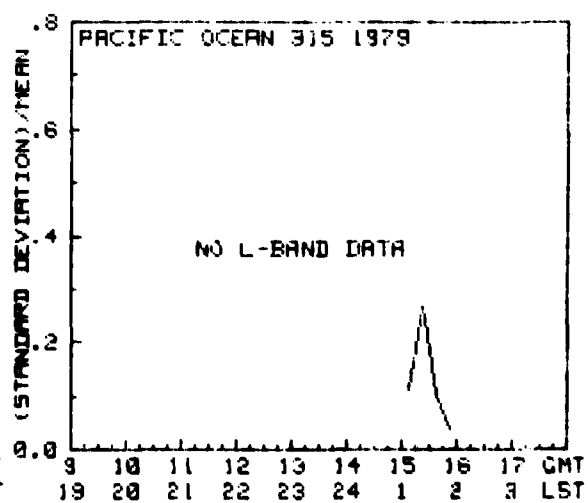
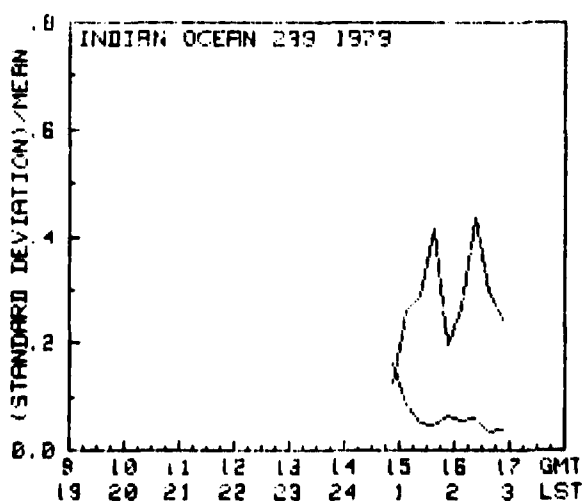
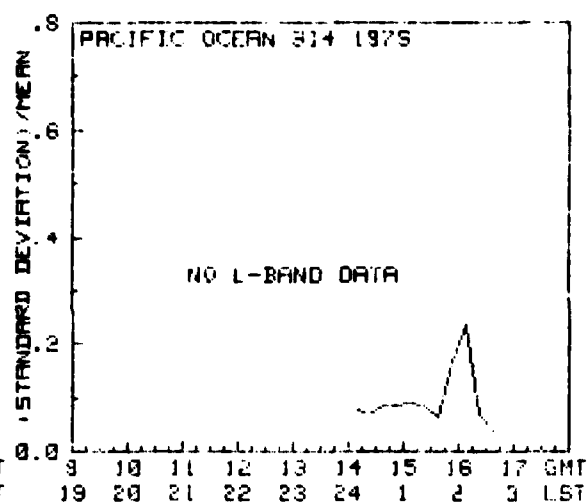
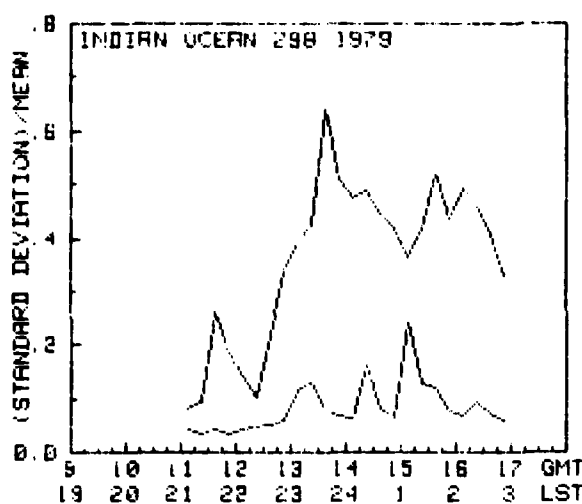
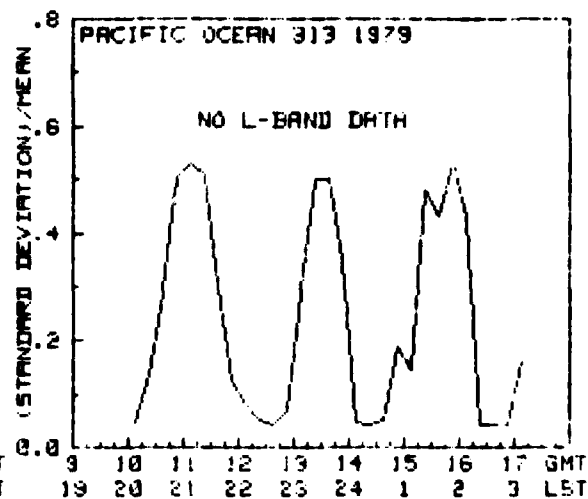
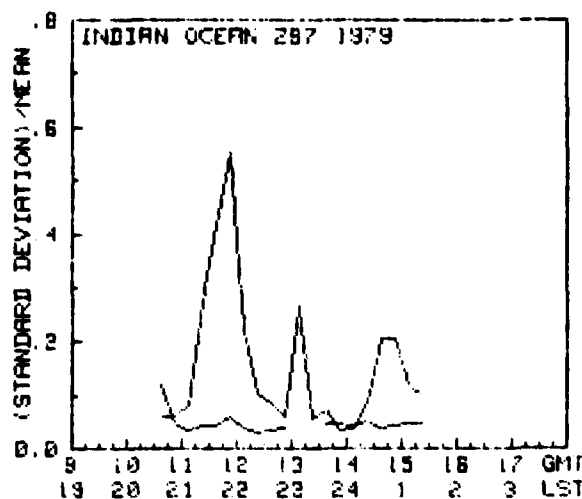


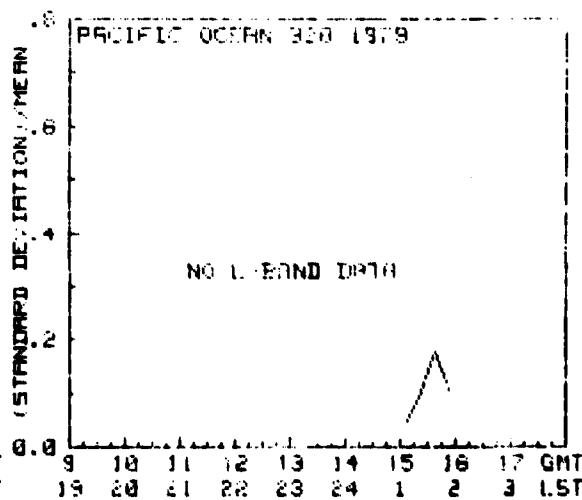
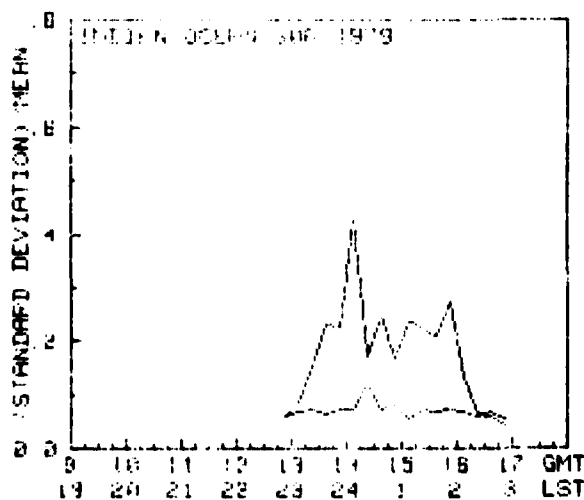
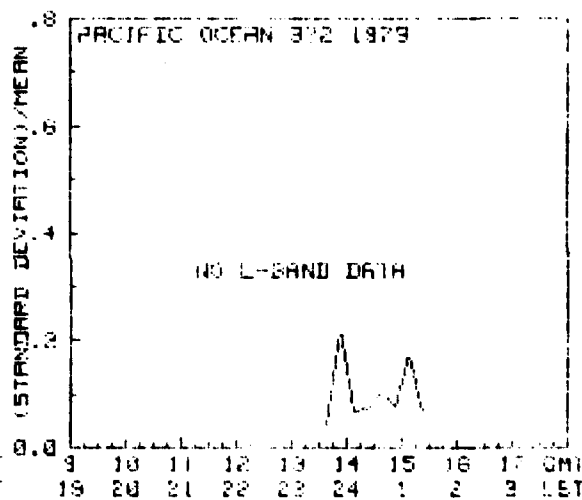
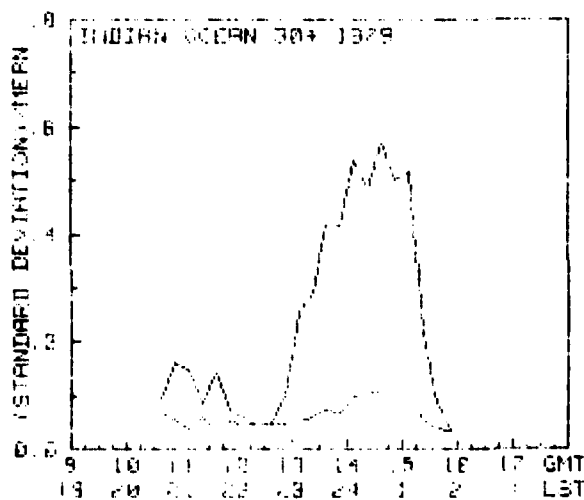
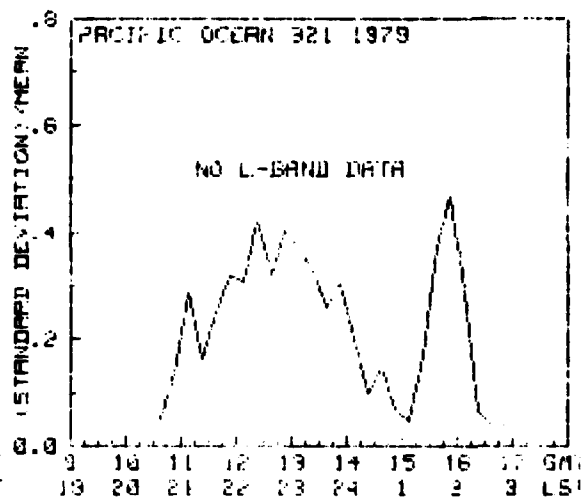
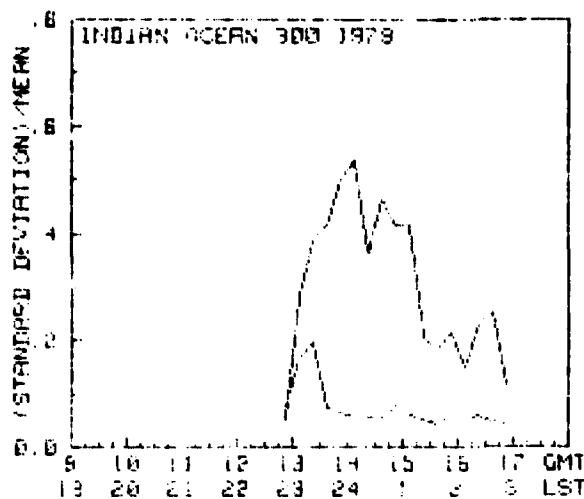


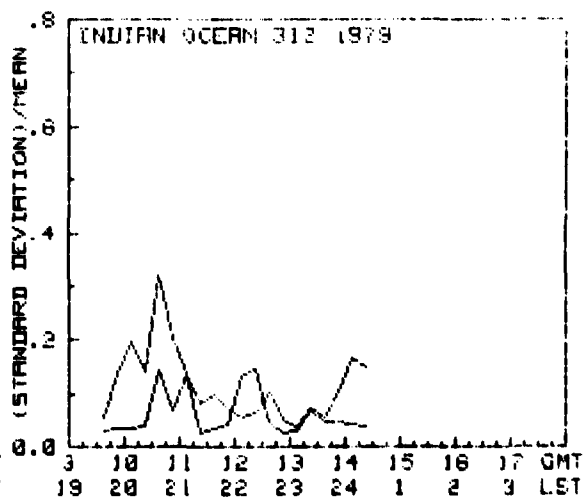
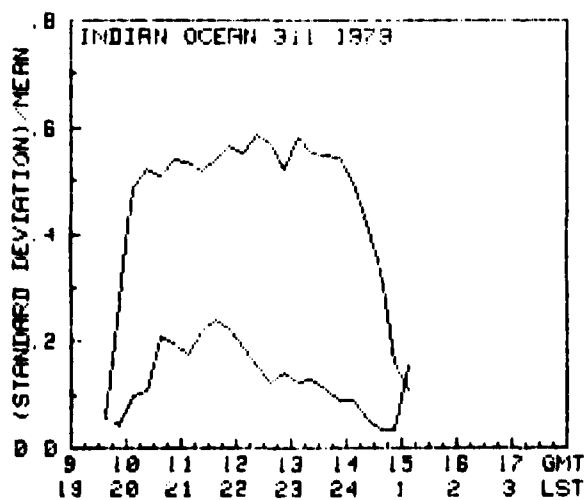
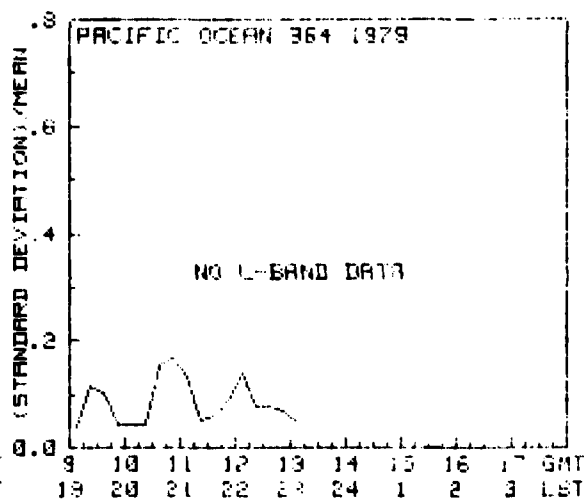
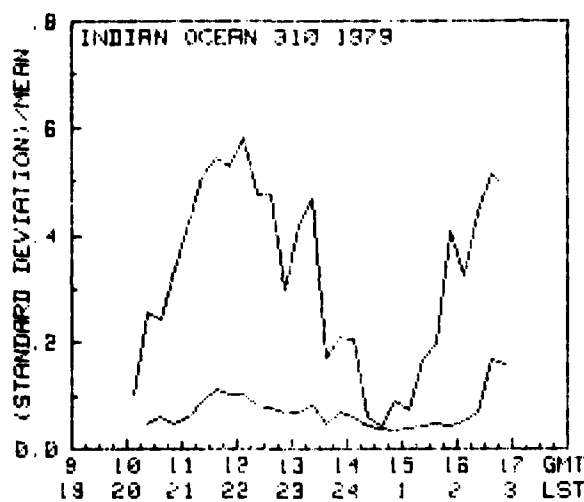
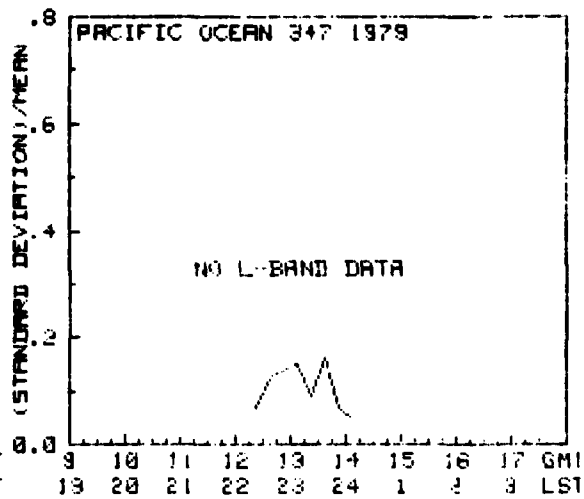
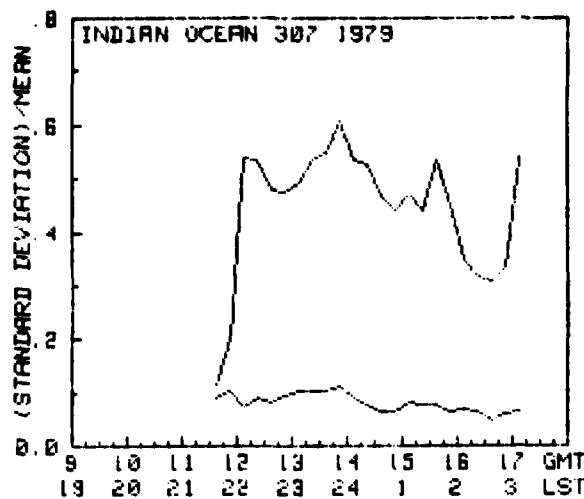


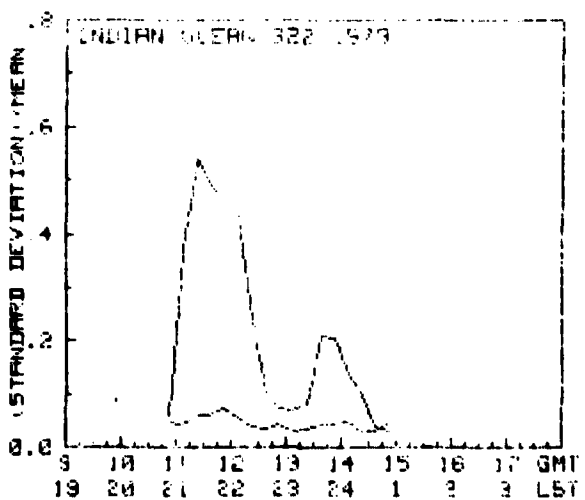
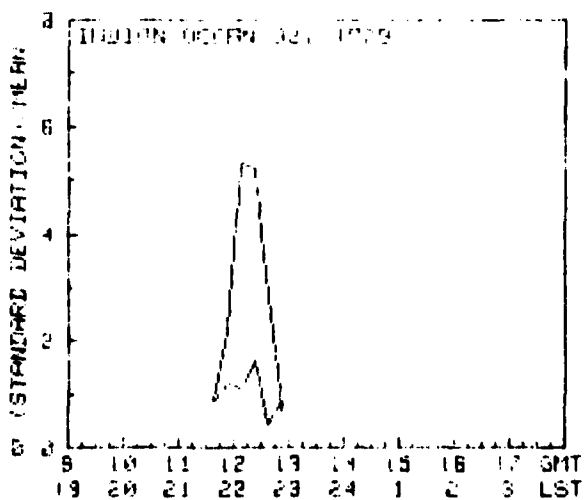
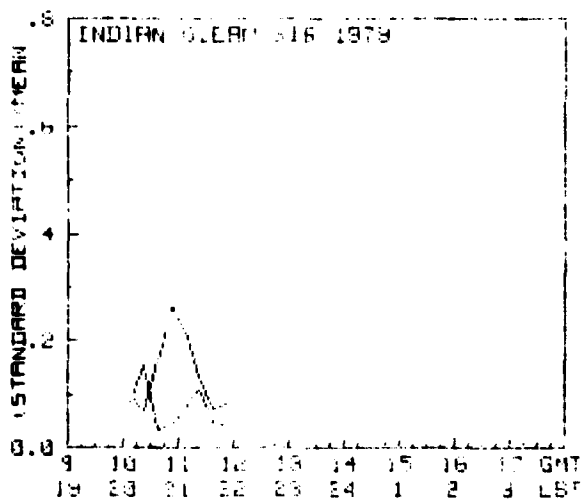
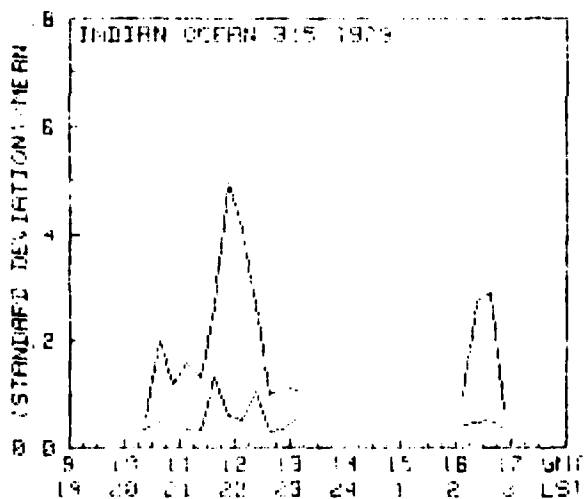
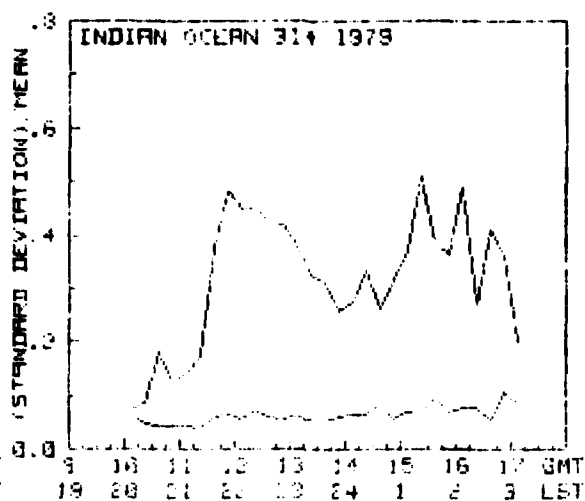
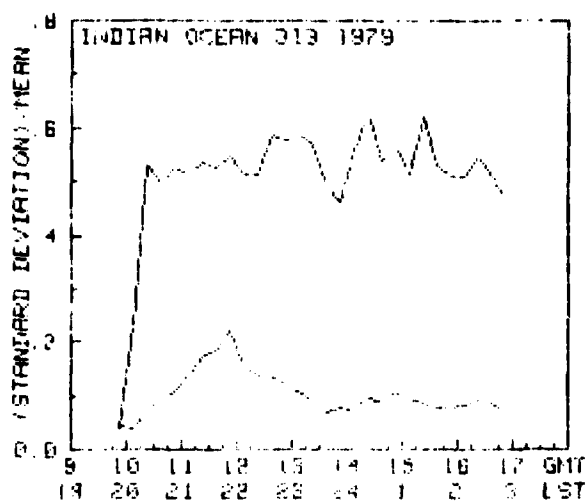


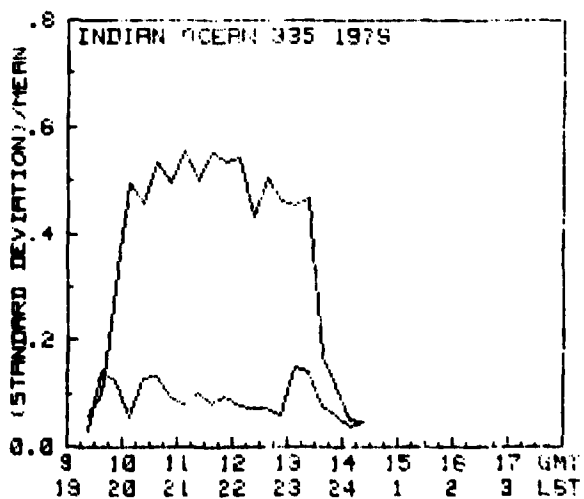
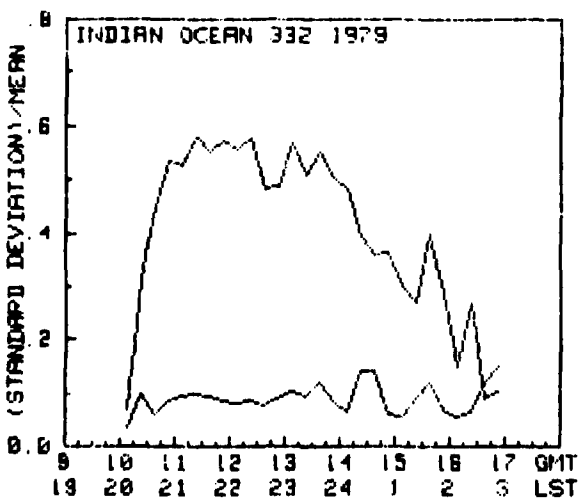
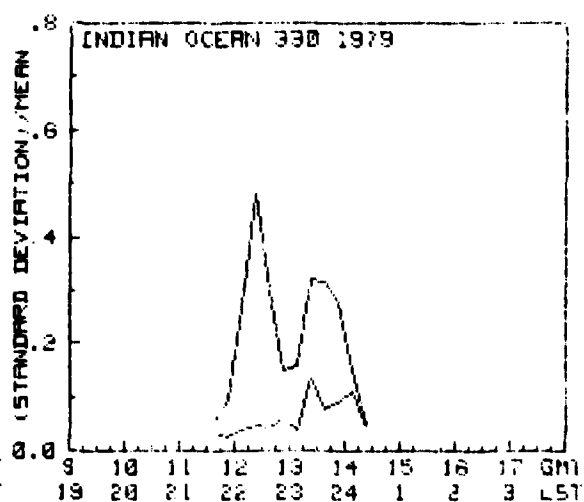
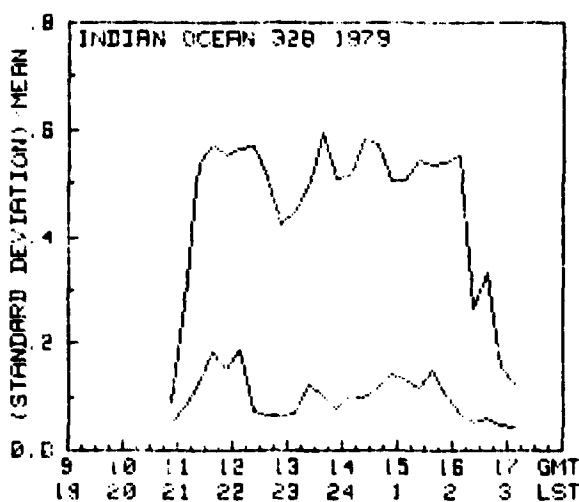
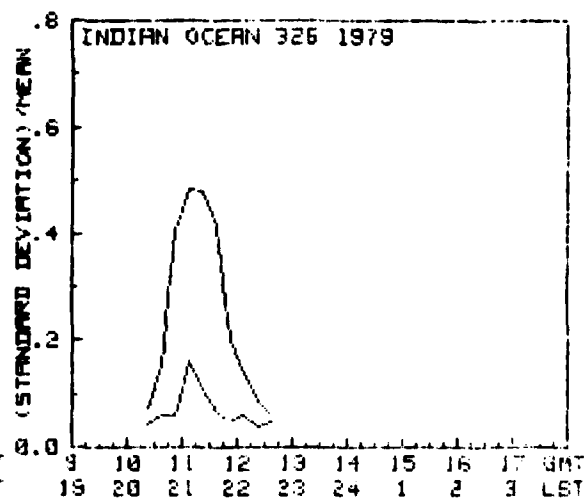
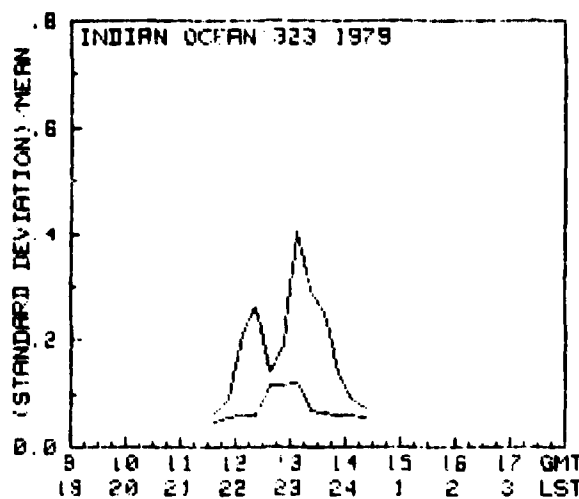


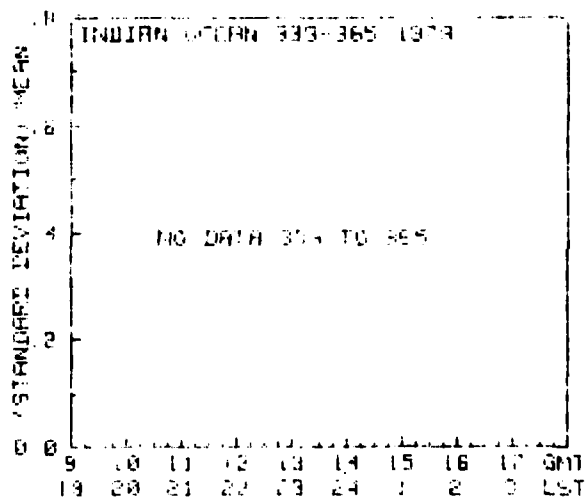
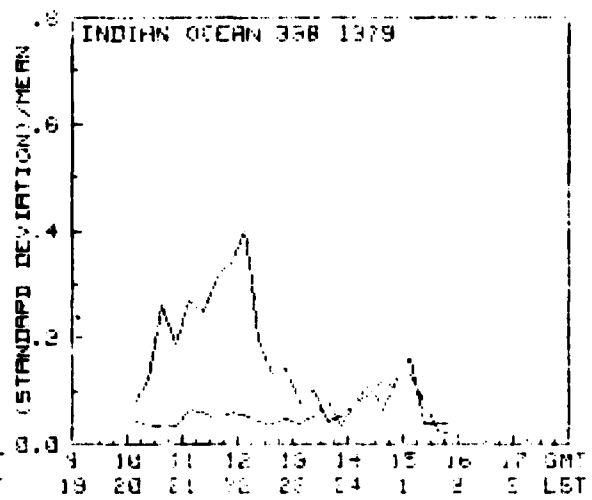
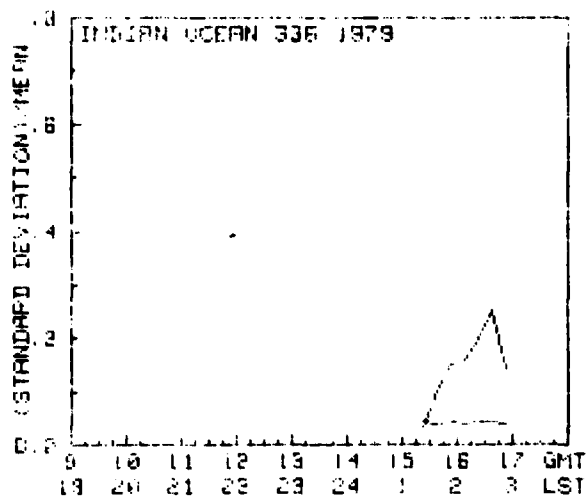












**APPENDIX C**  
**CUMULATIVE FADE DURATION DISTRIBUTIONS**  
**AT UHF AND L-BAND FOR SIGNAL LEVELS 6 AND 12 dB**  
**BELOW THE UNDISTURBED SIGNAL**



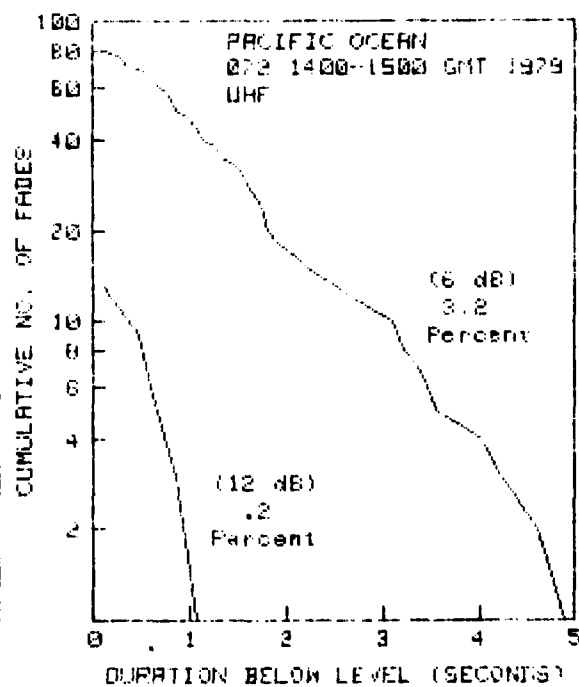
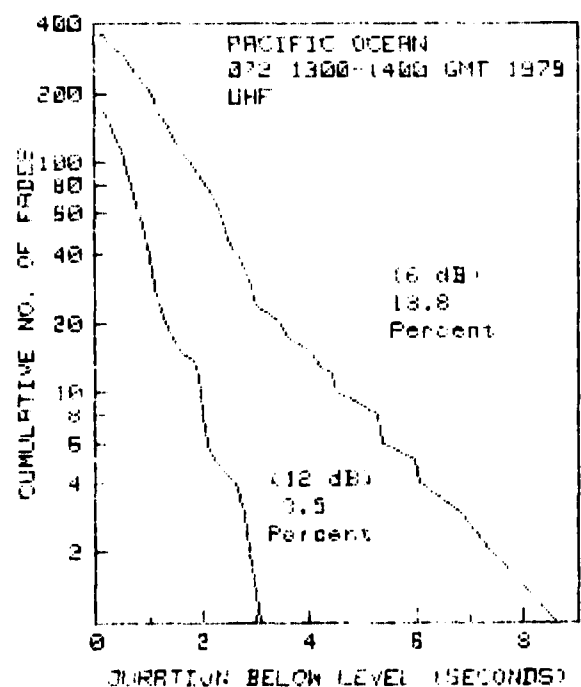
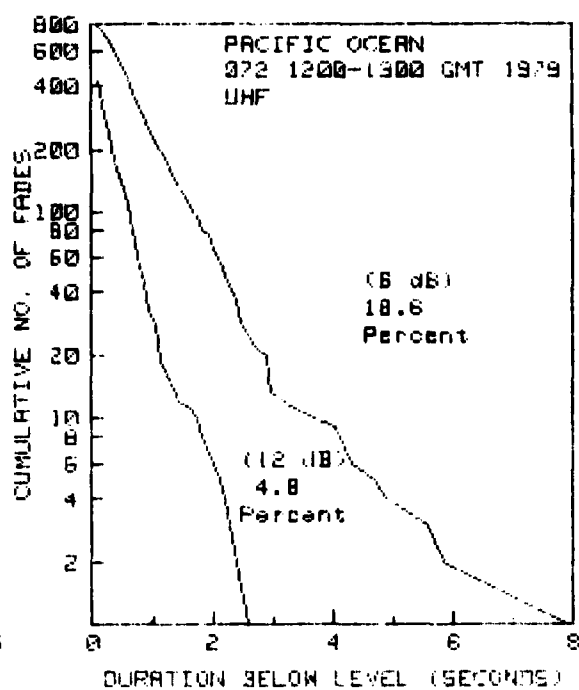
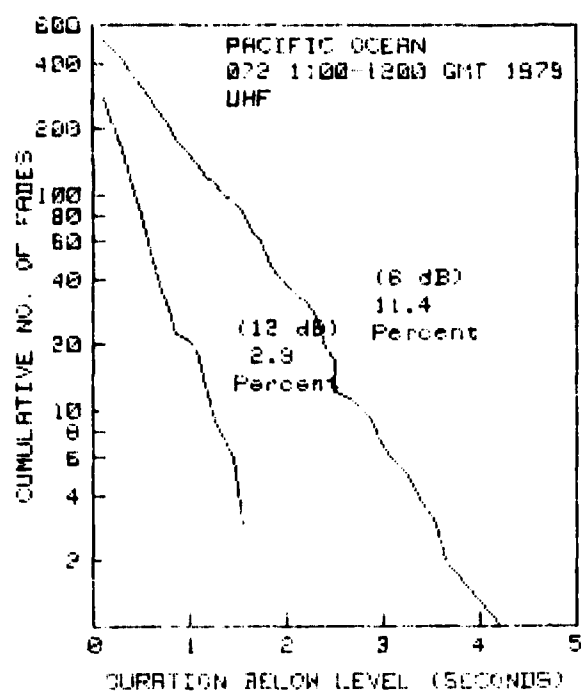
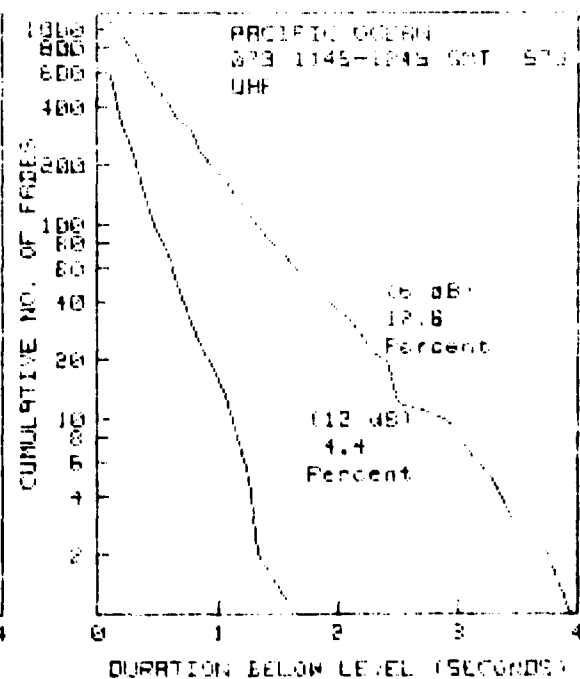
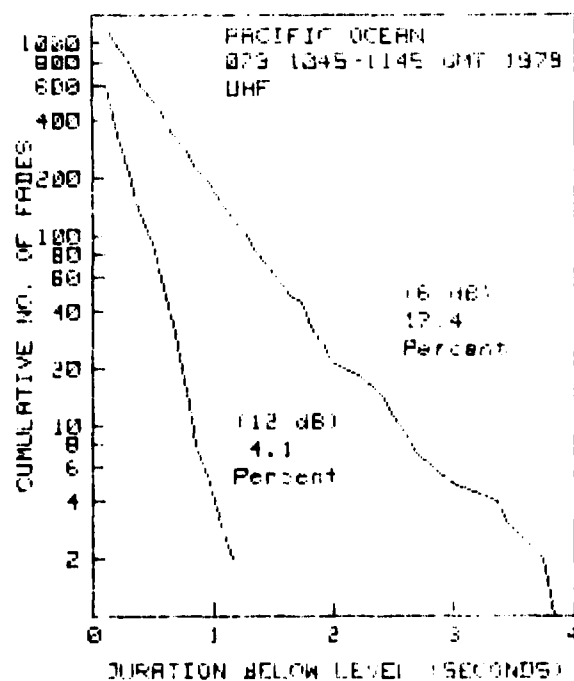
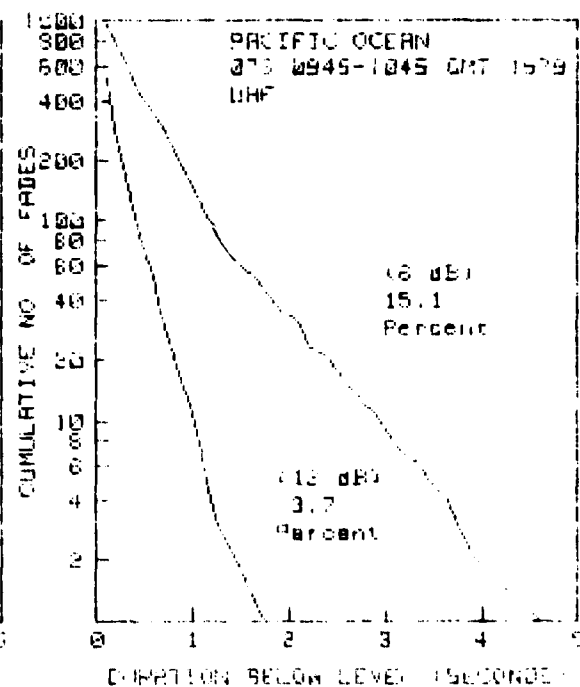
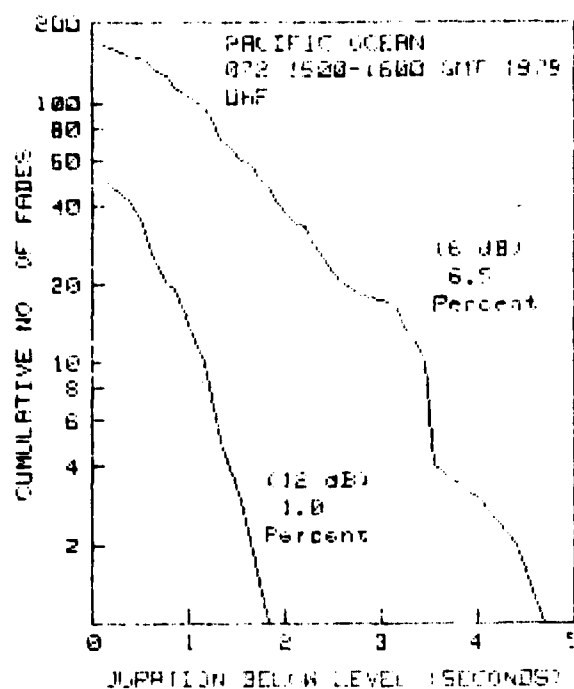
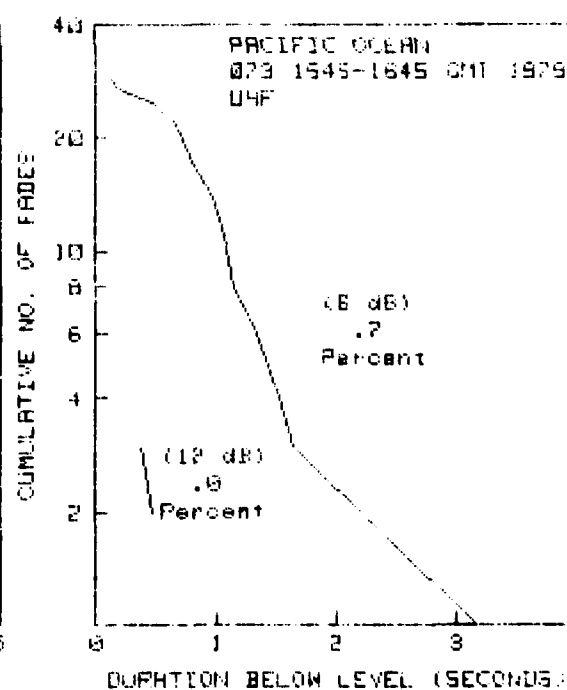
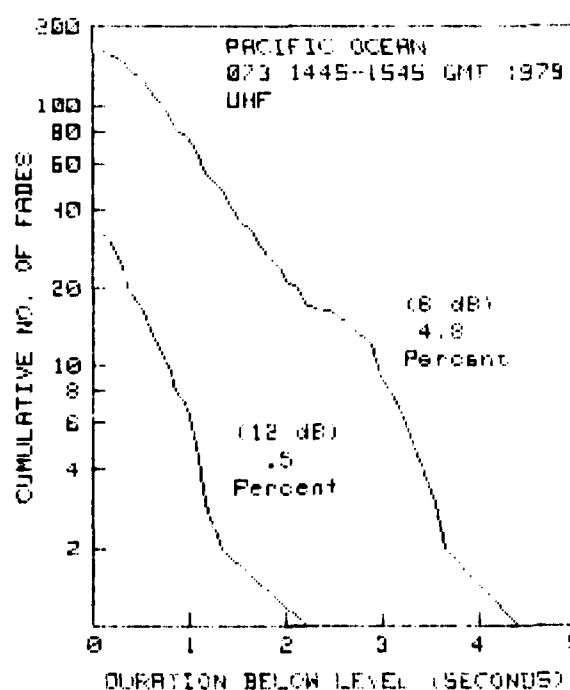
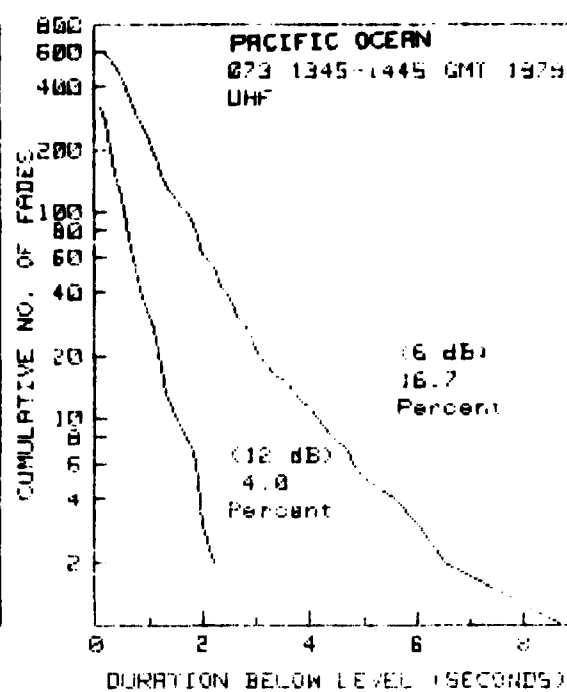
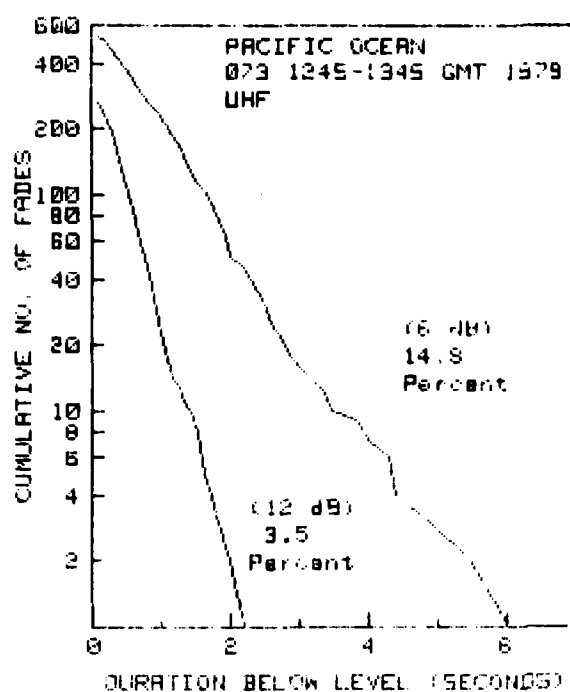


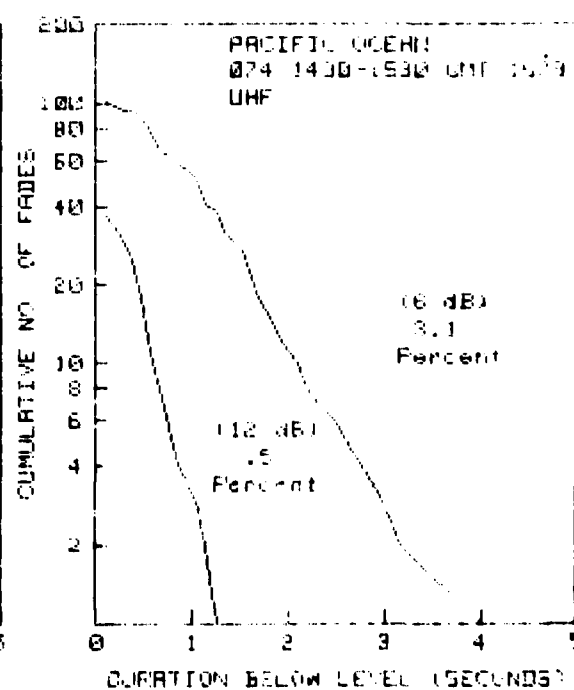
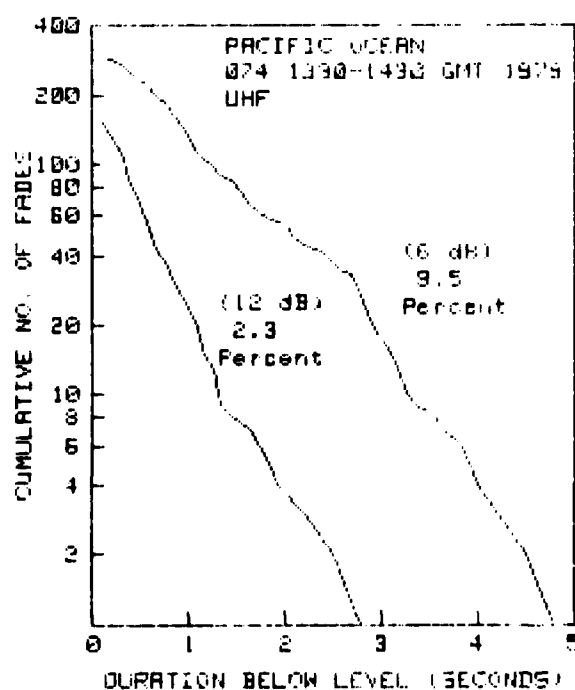
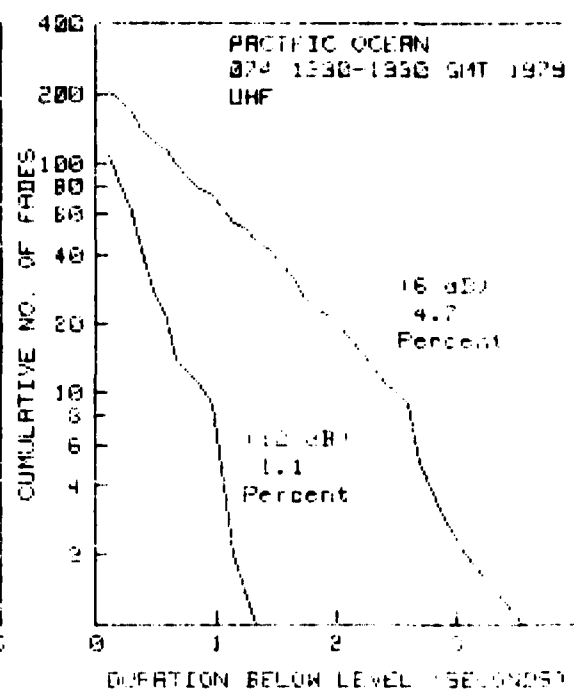
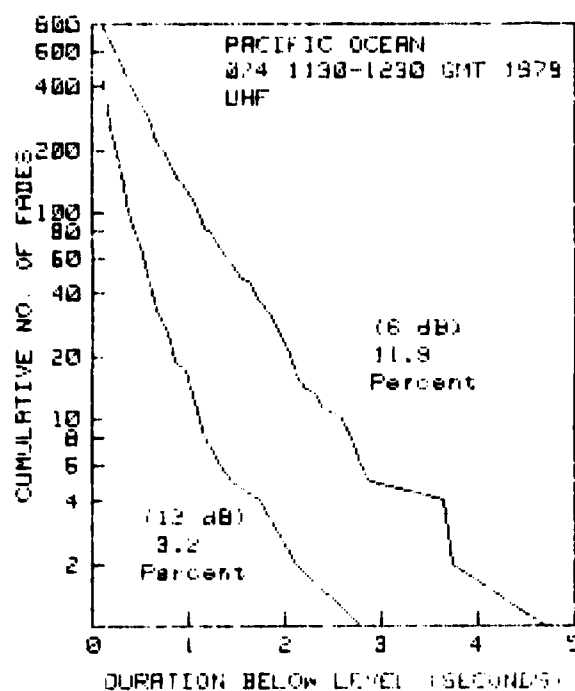
Figure C1. Cumulative uhf fade duration distribution for the Pacific Ocean satellite (elevation angle about 50°).



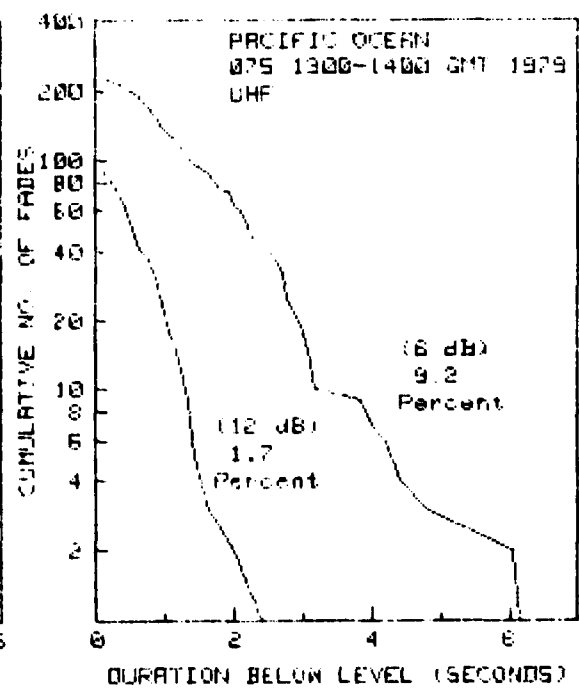
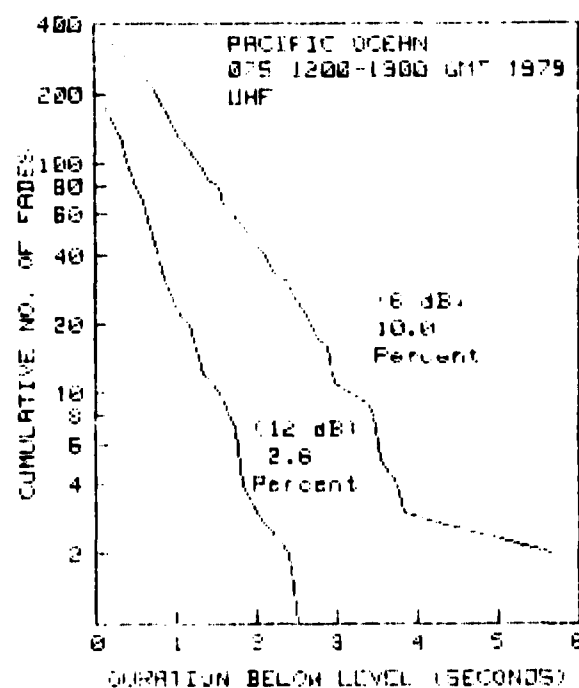
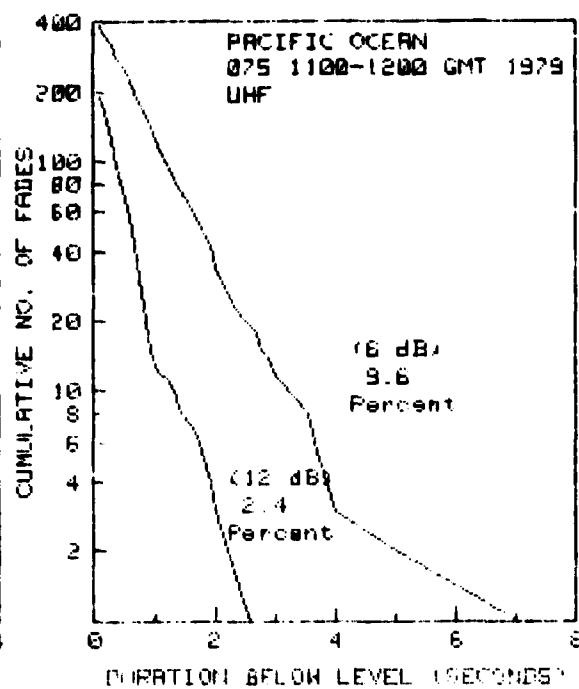
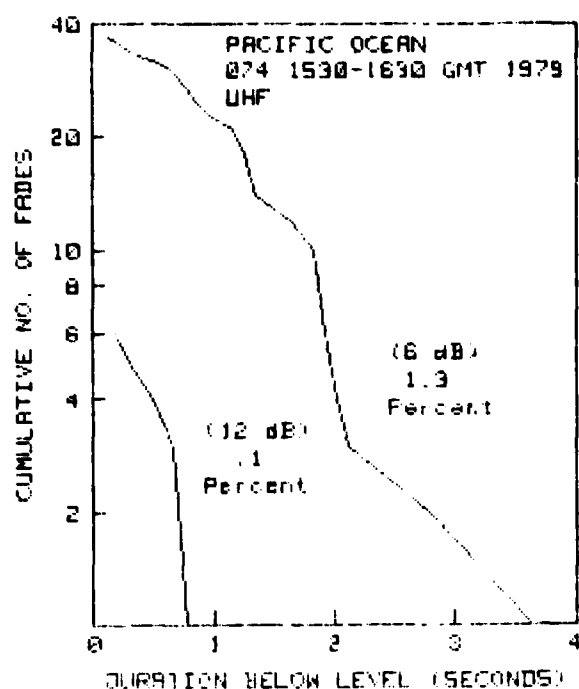
C1 (continued)



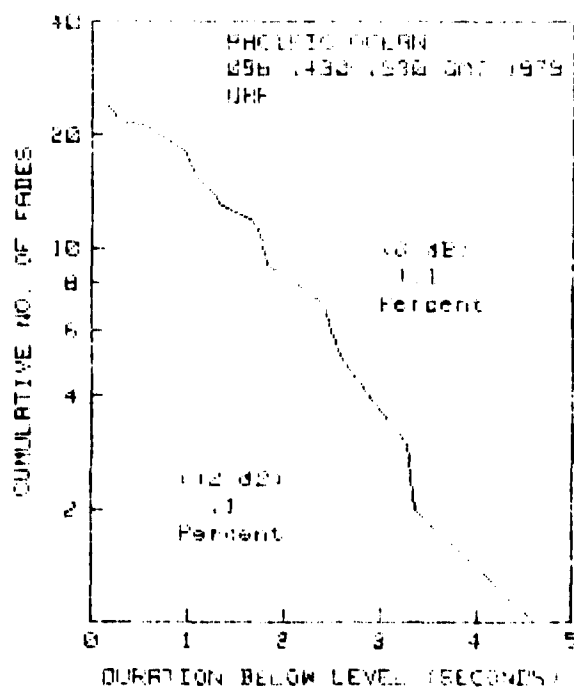
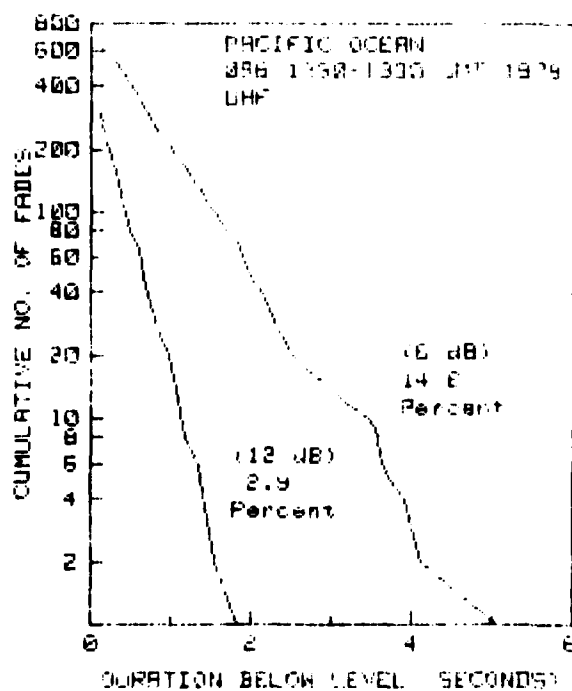
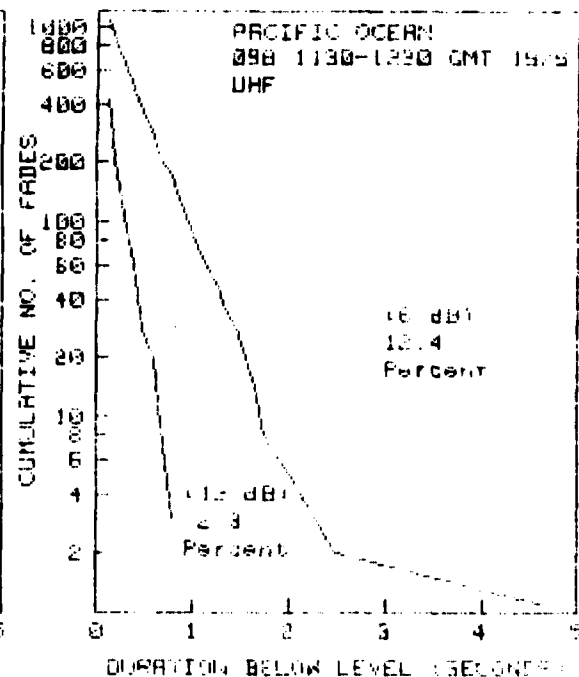
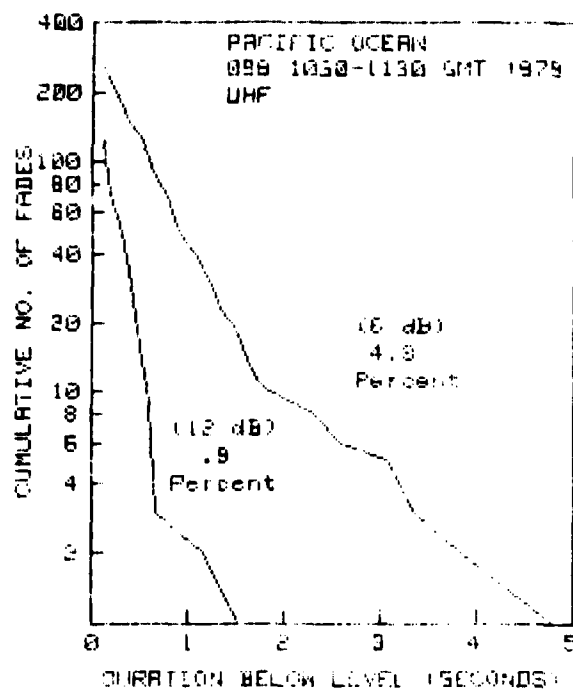
C1 (continued)



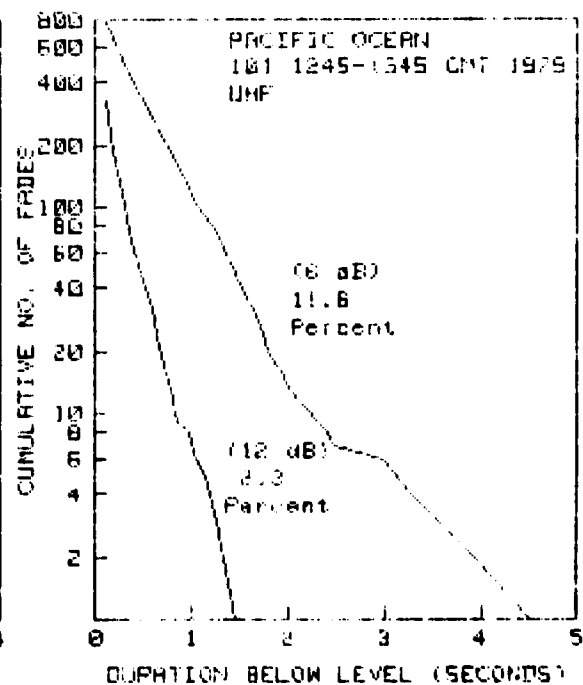
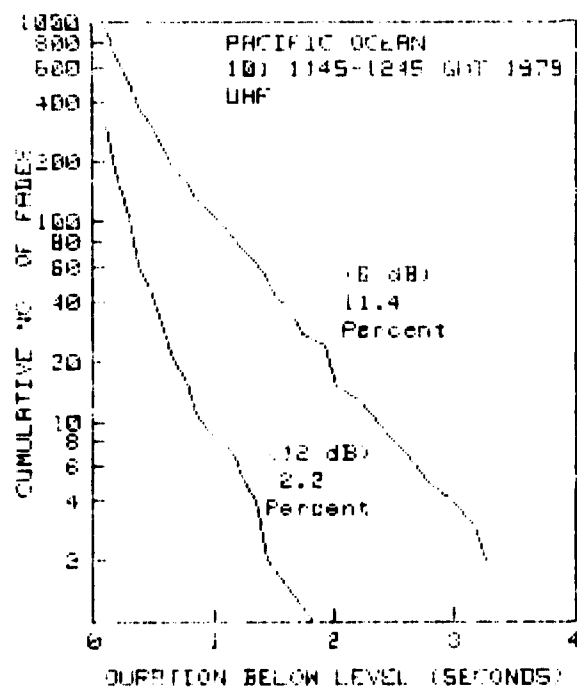
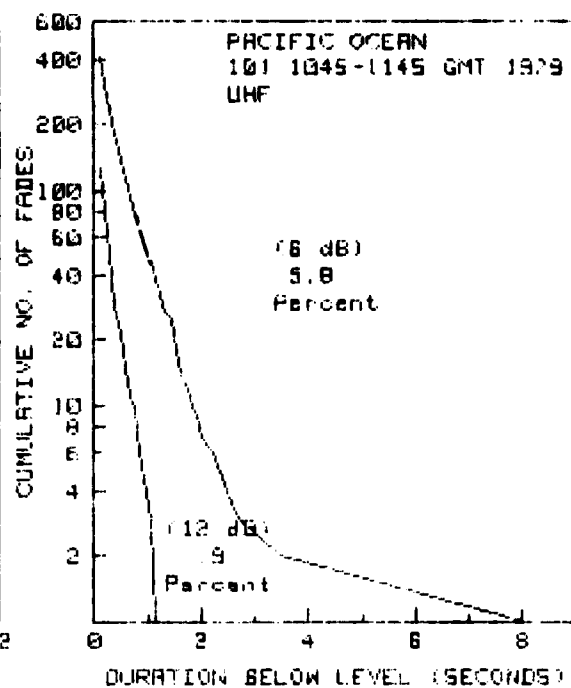
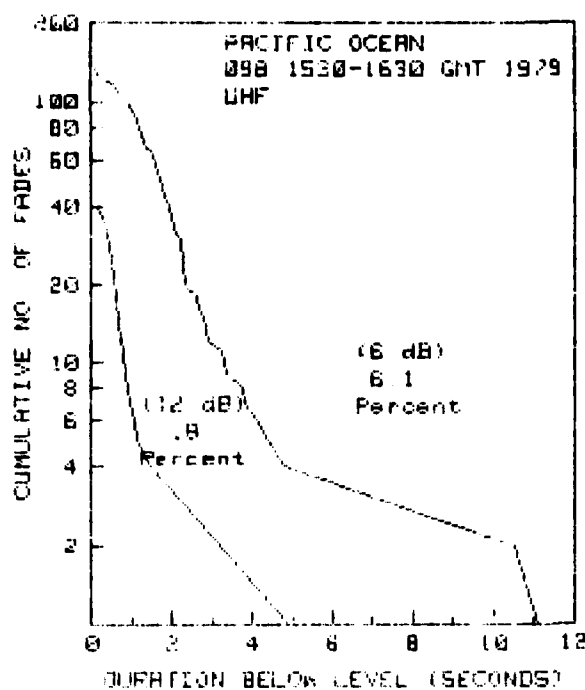
C1 (continued)



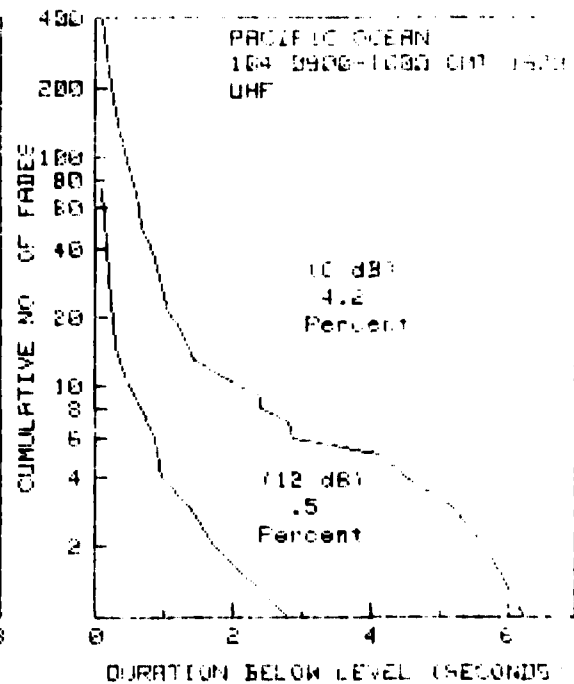
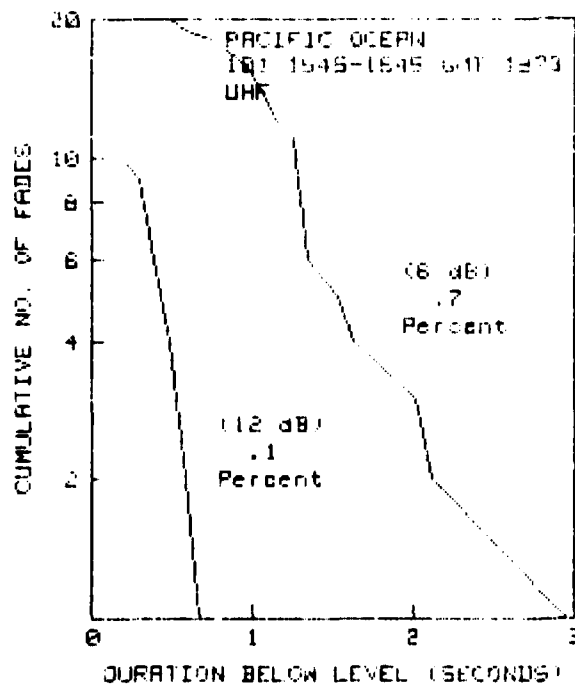
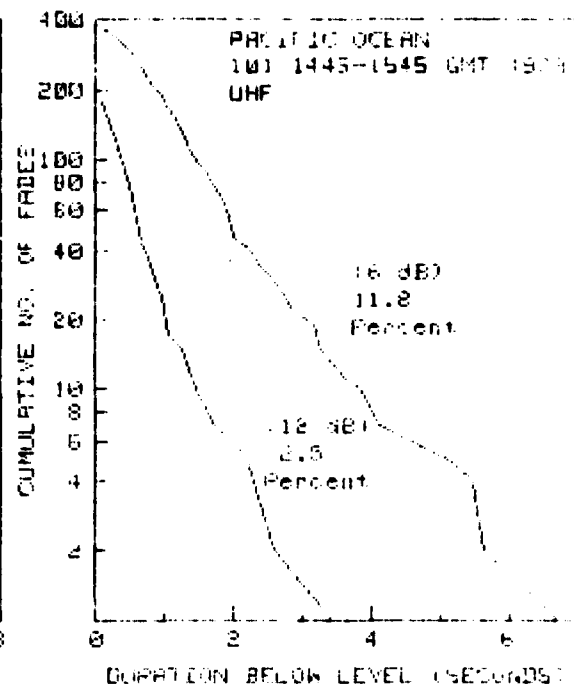
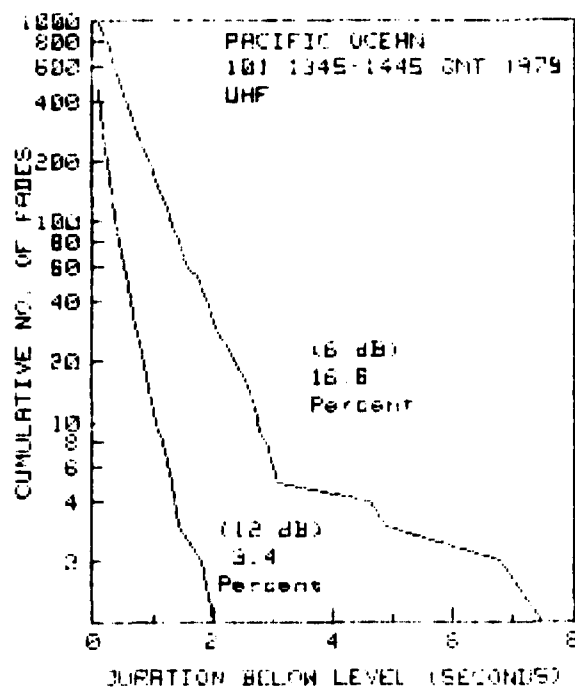
C1 (continued)



C1 (continued)

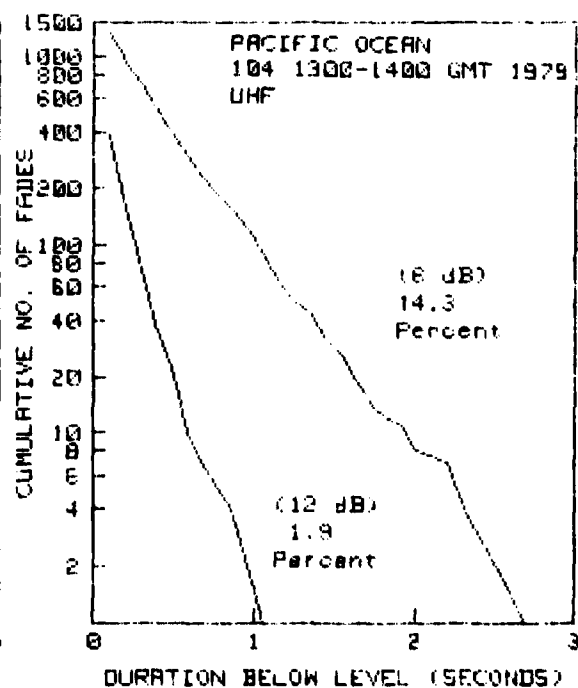
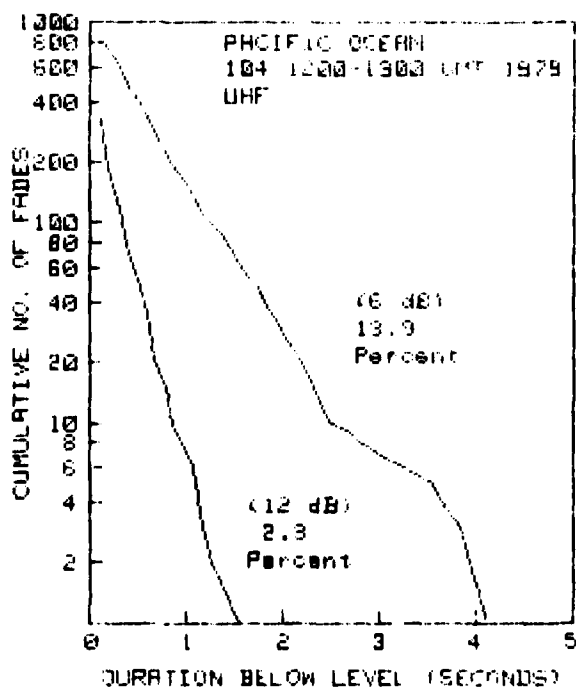
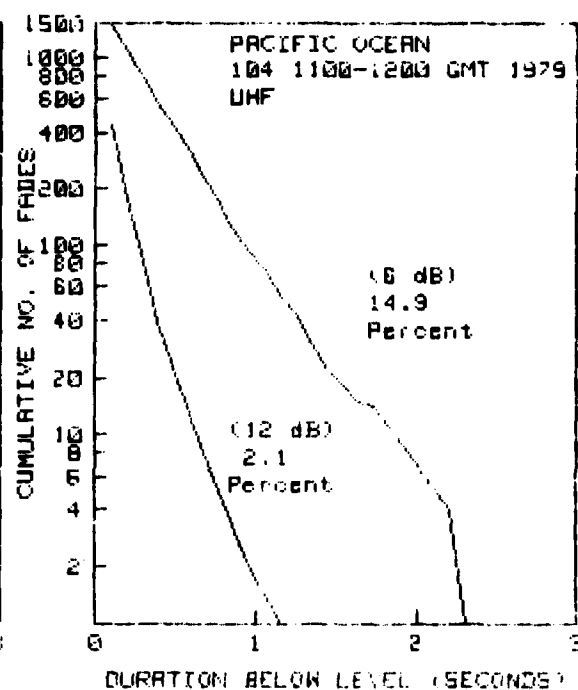
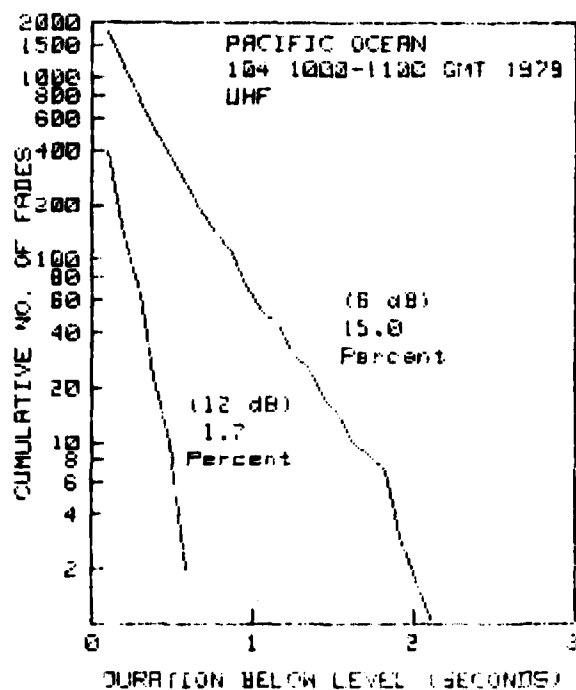


C1 (continued)

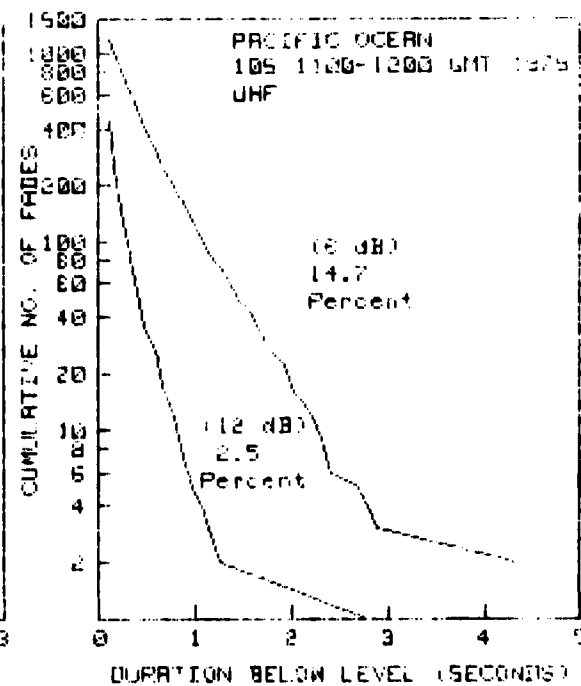
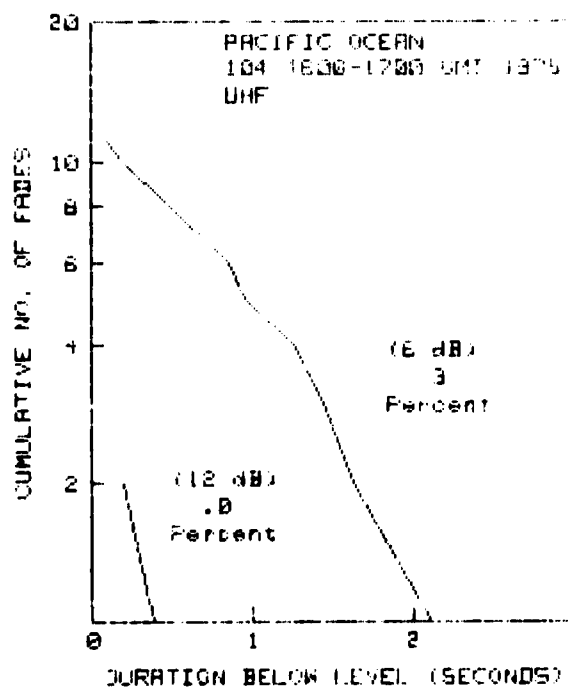
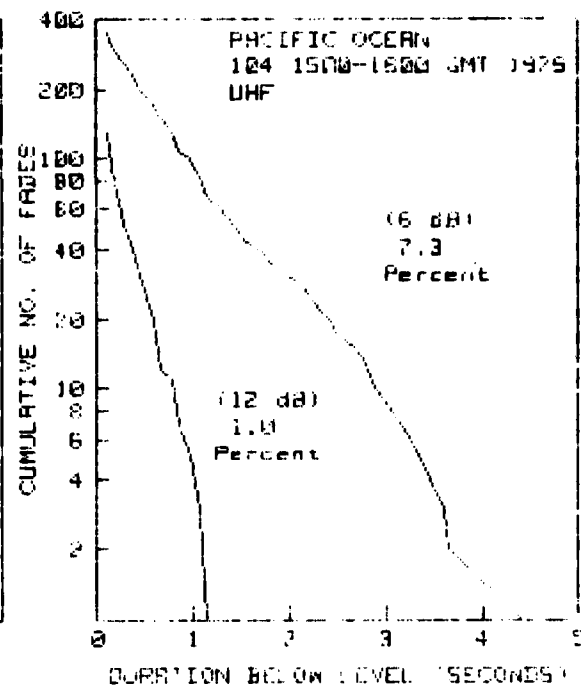
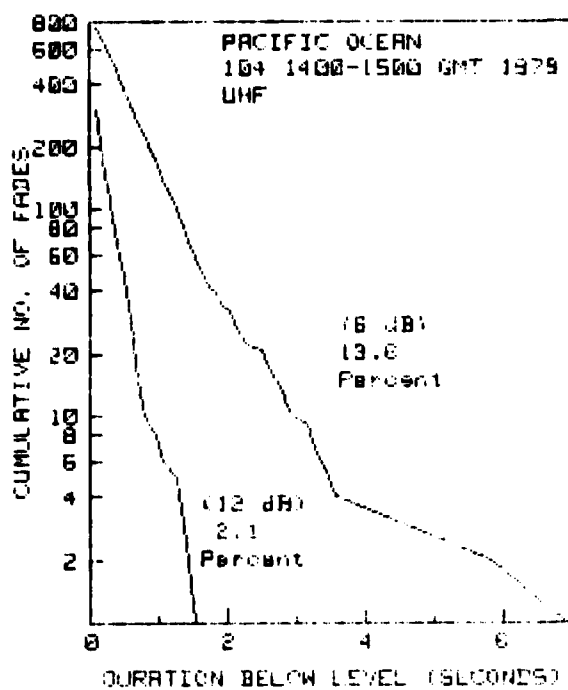


C1 (continued)

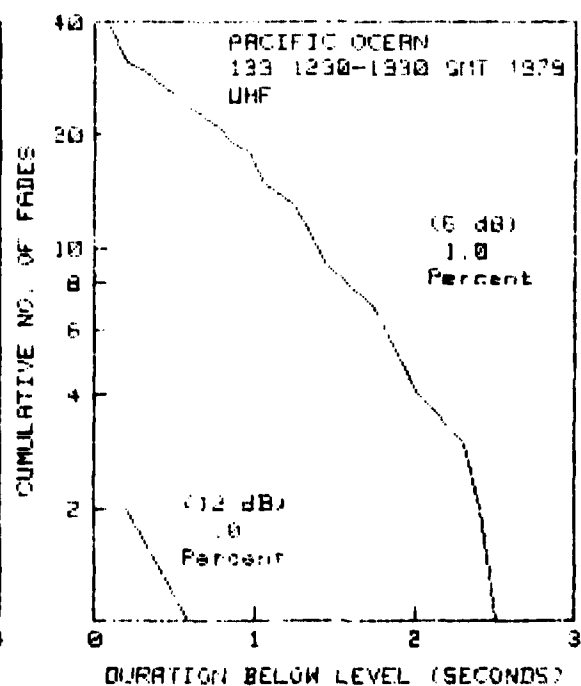
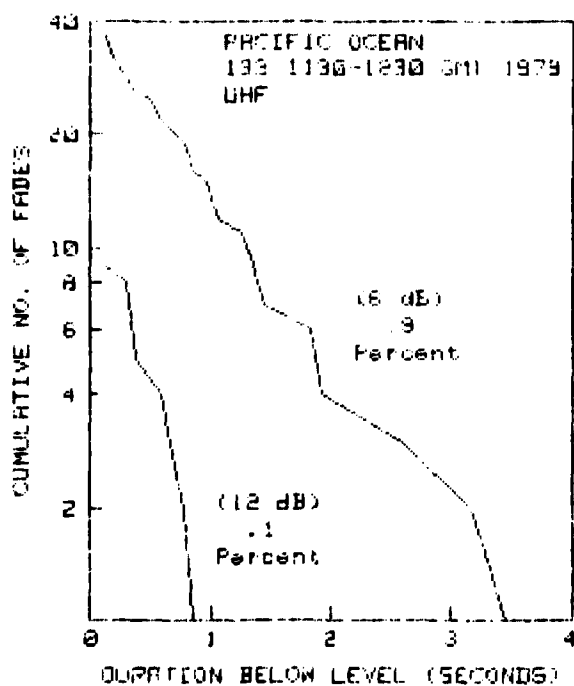
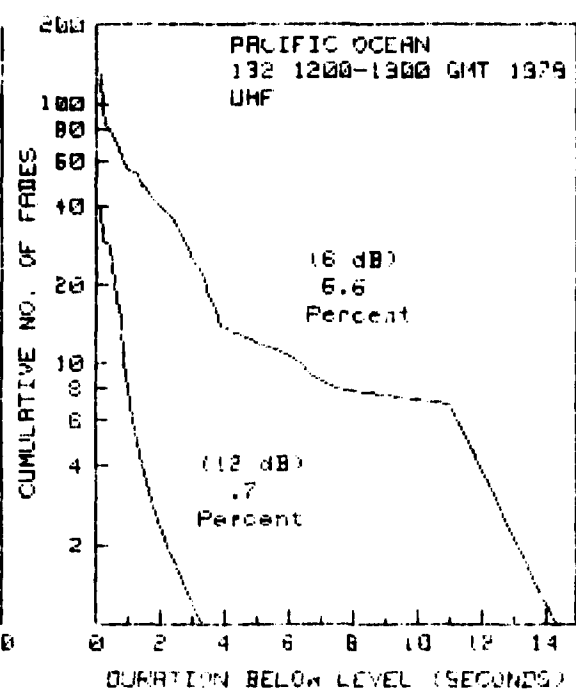
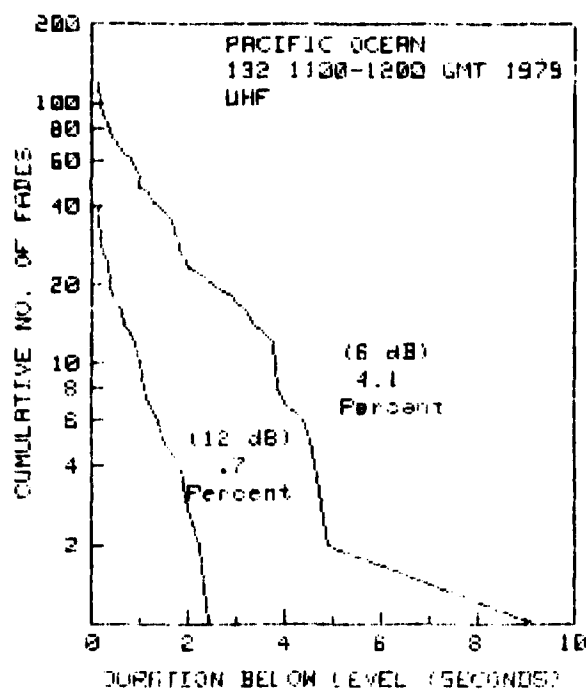




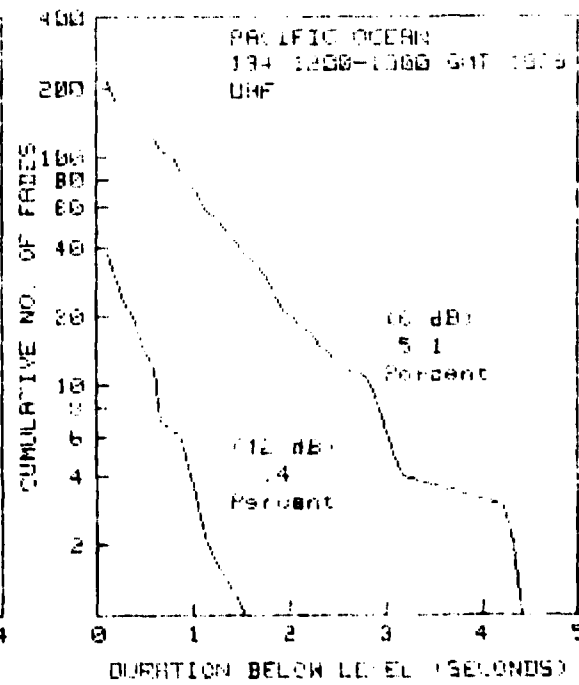
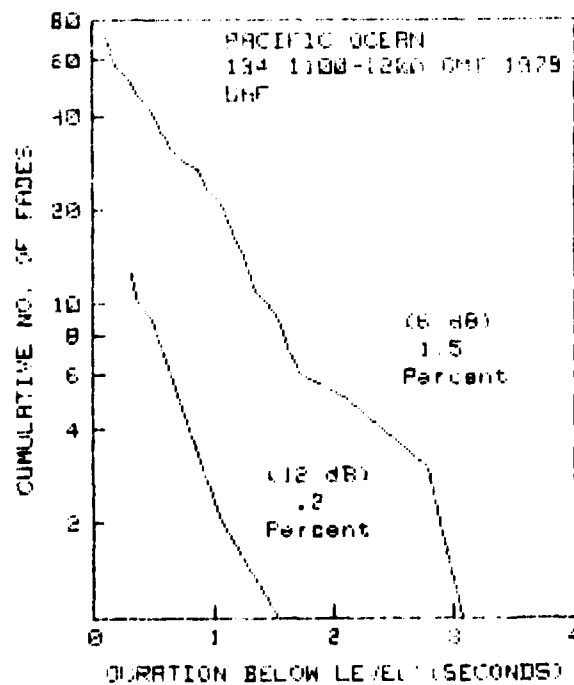
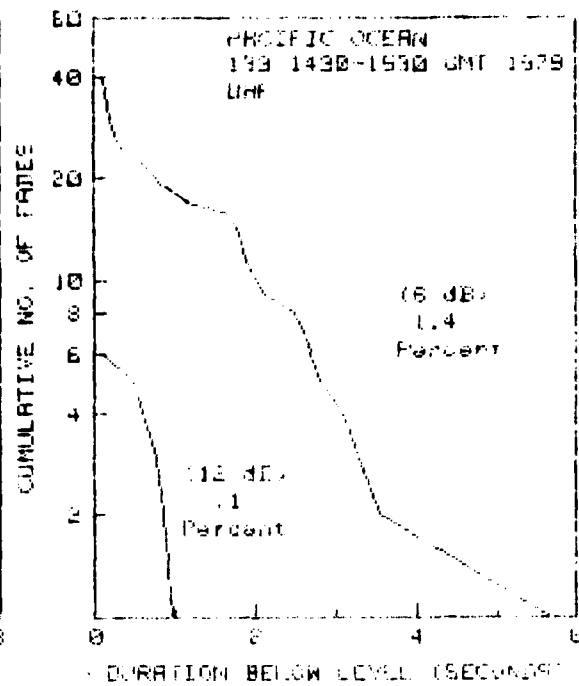
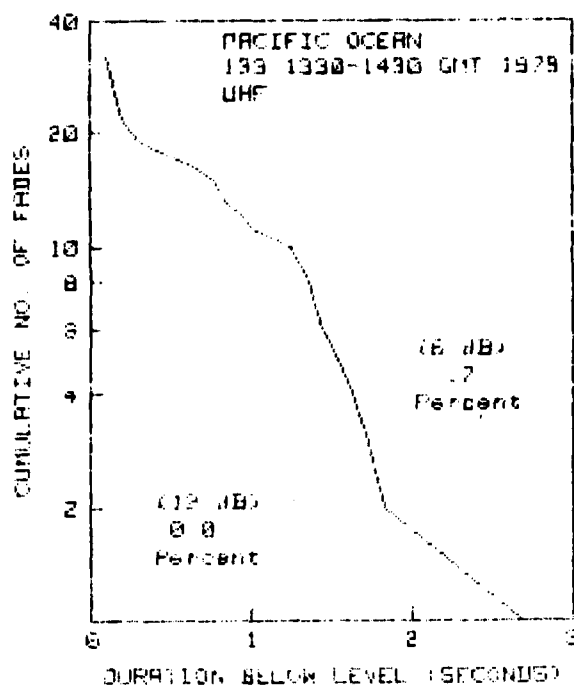
C1 (continued)



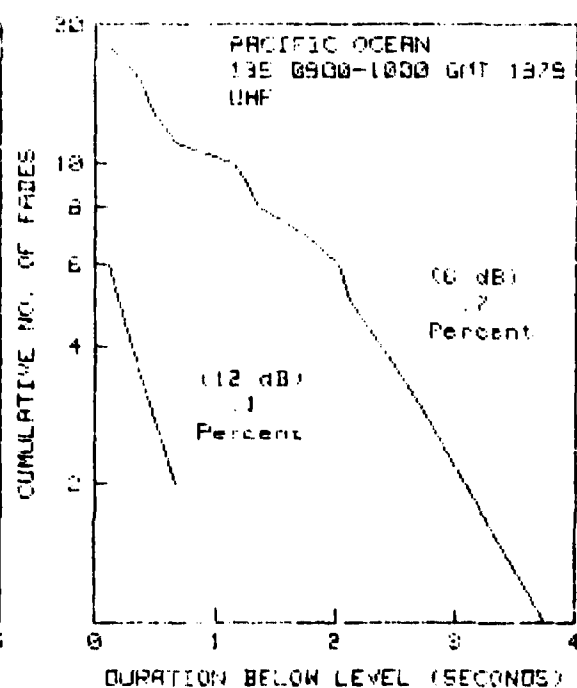
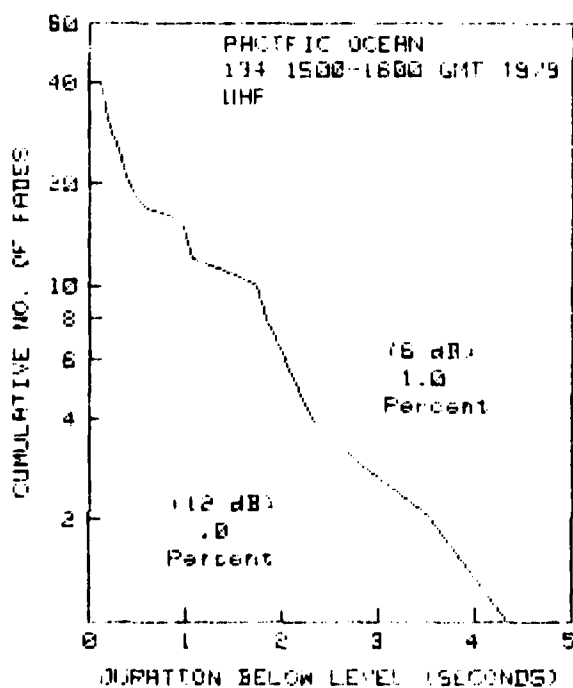
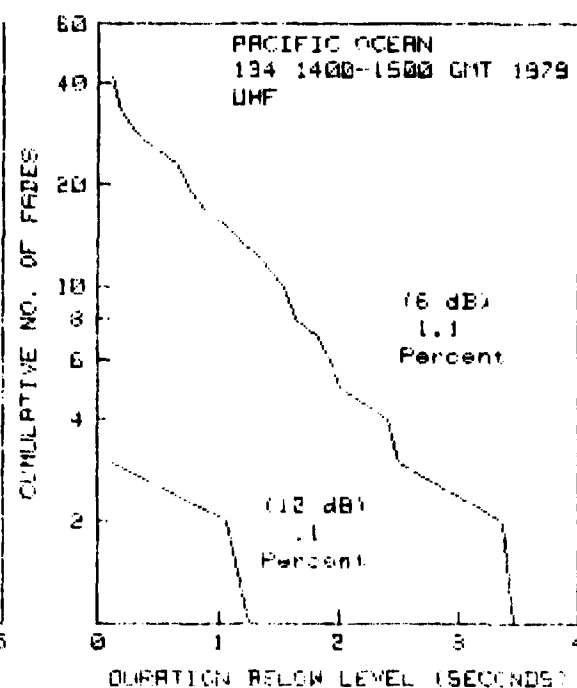
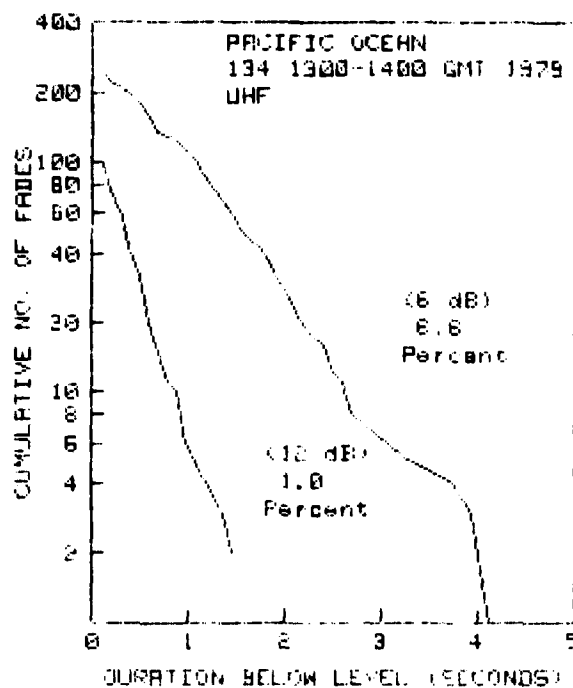
C1 (continued)



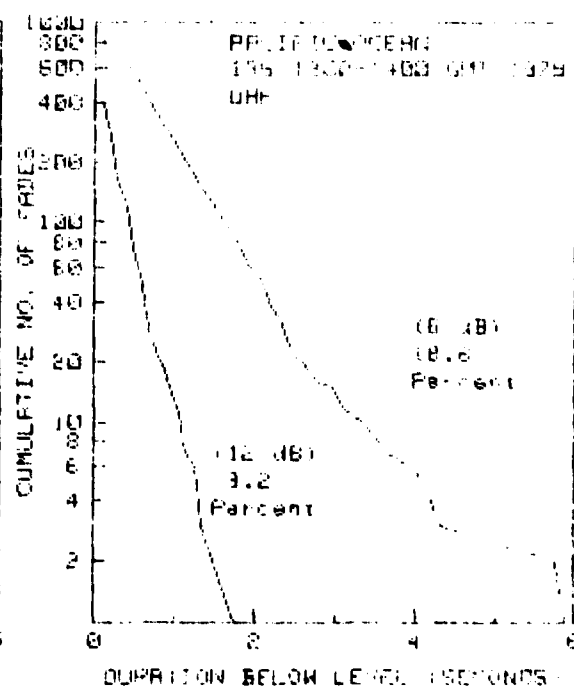
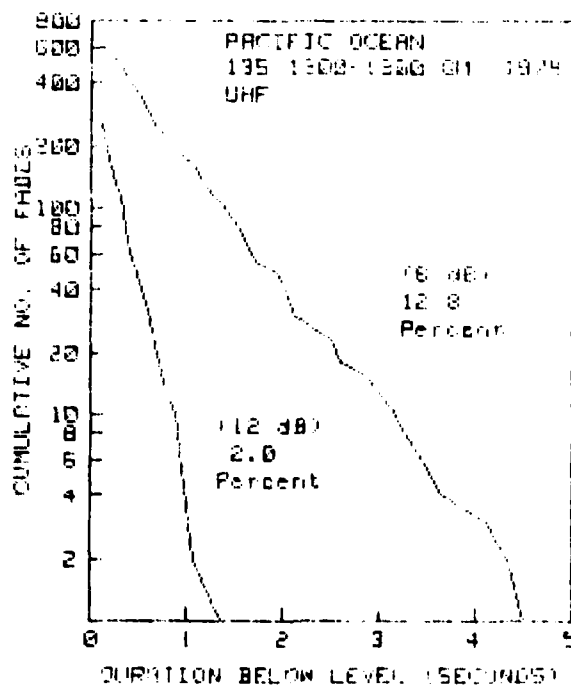
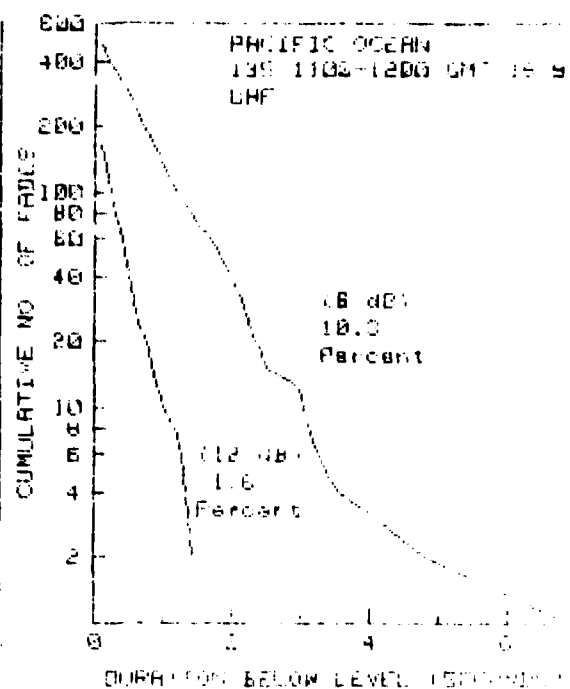
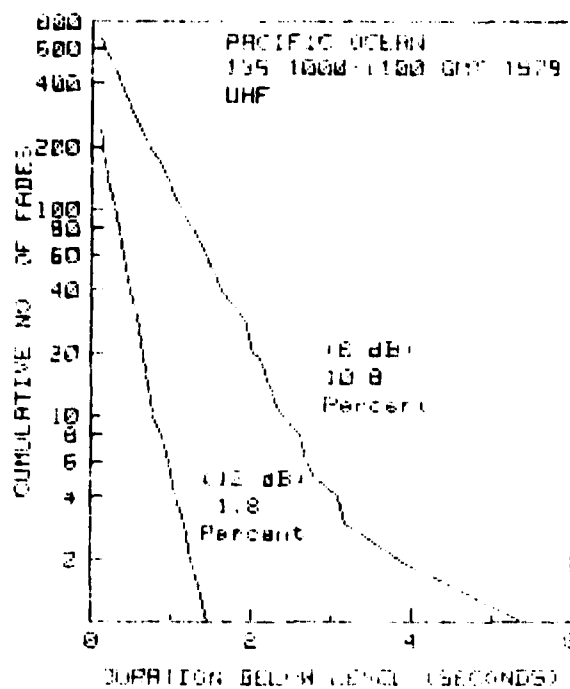
C1 (continued)



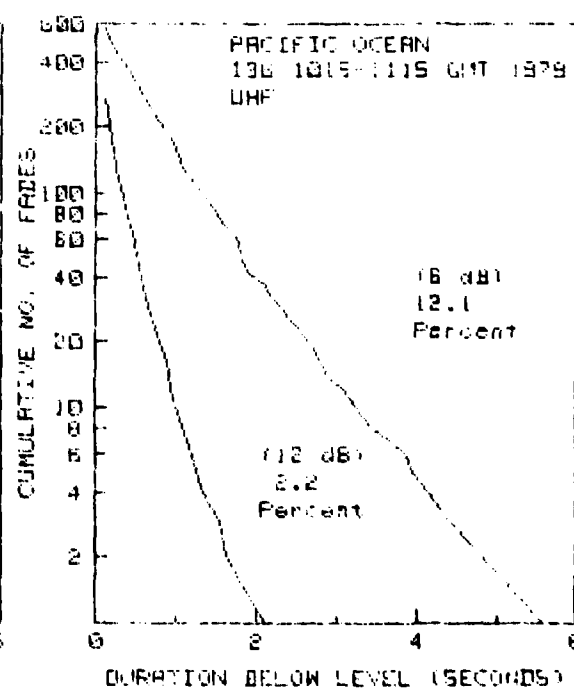
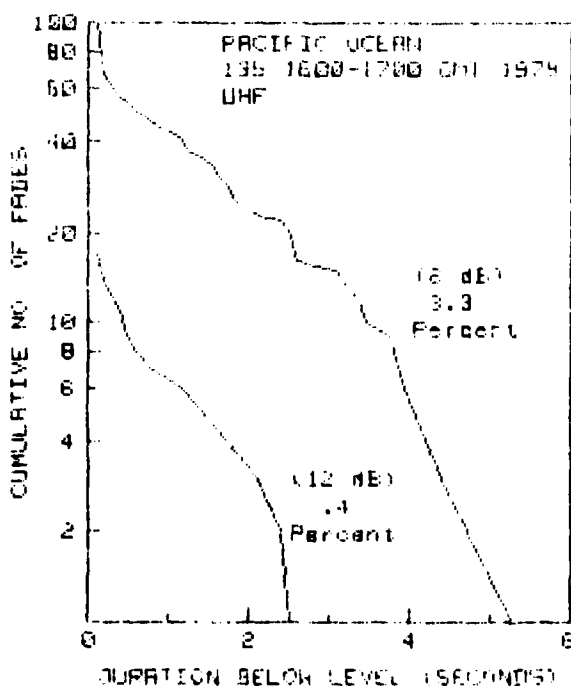
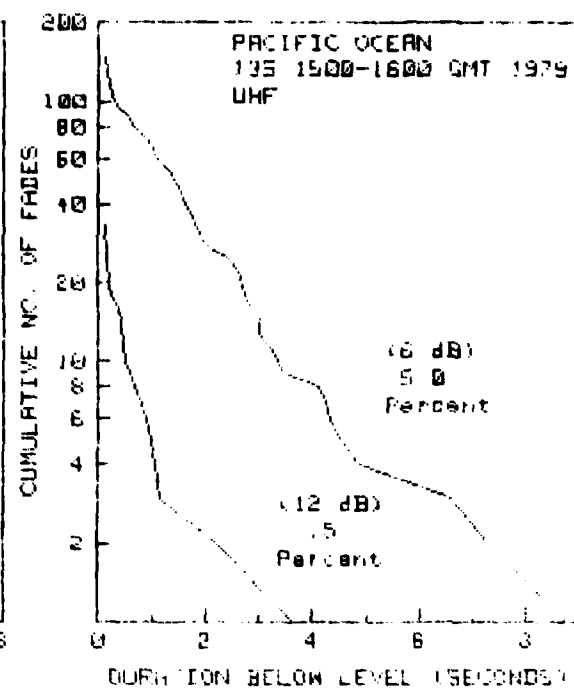
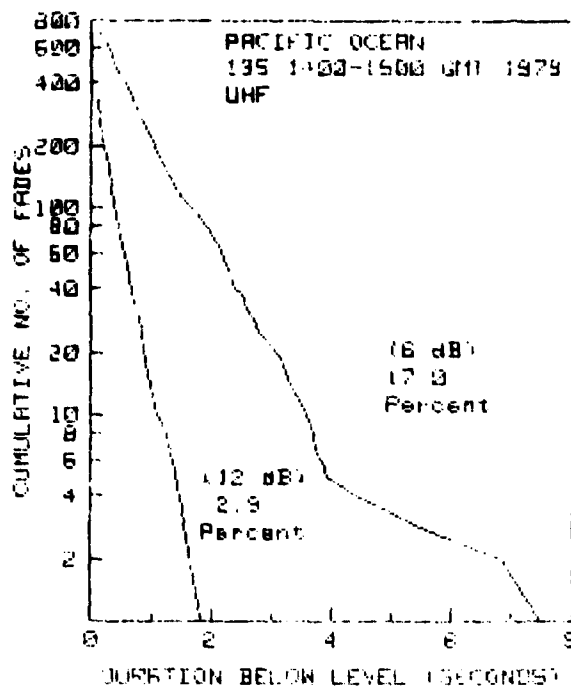
C1 (continued)



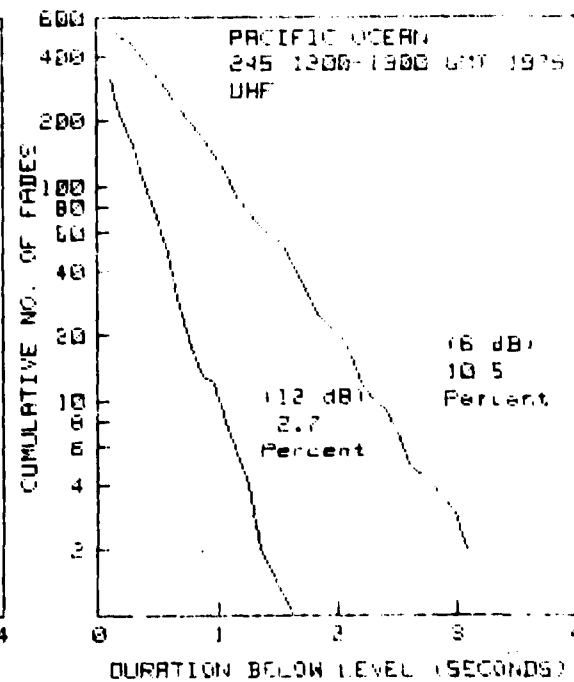
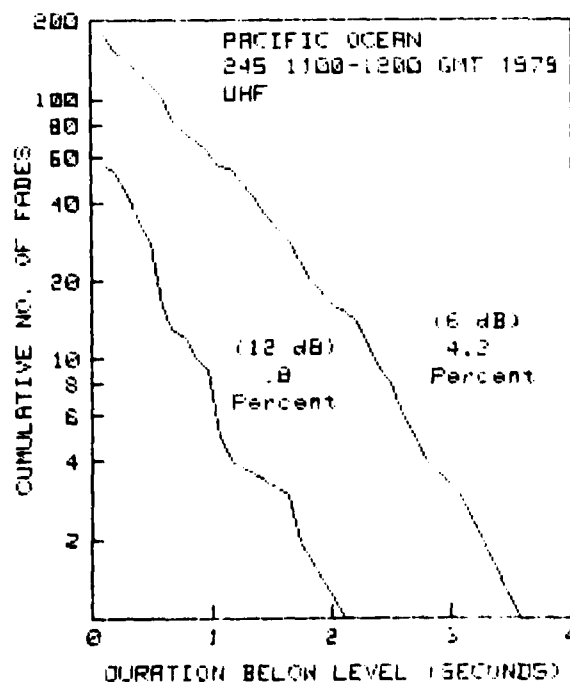
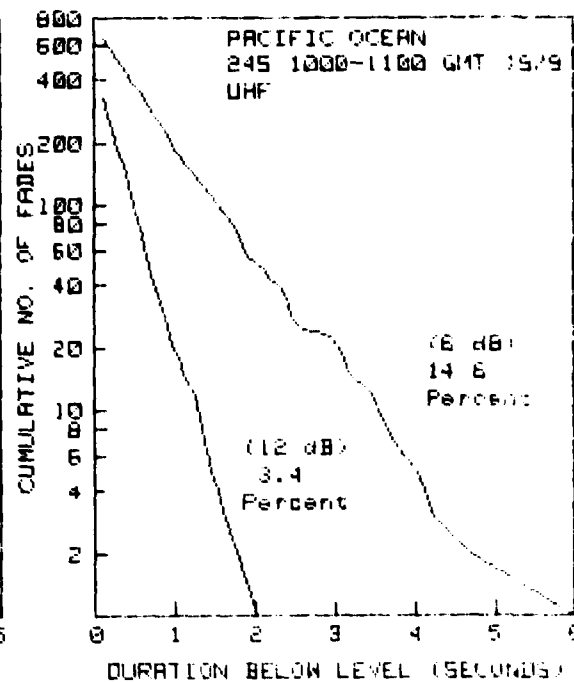
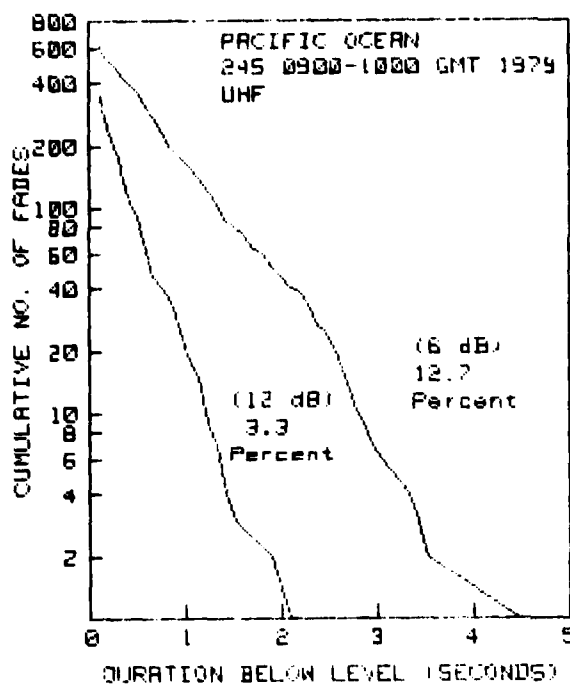
C1 (continued)



C1 (continued)

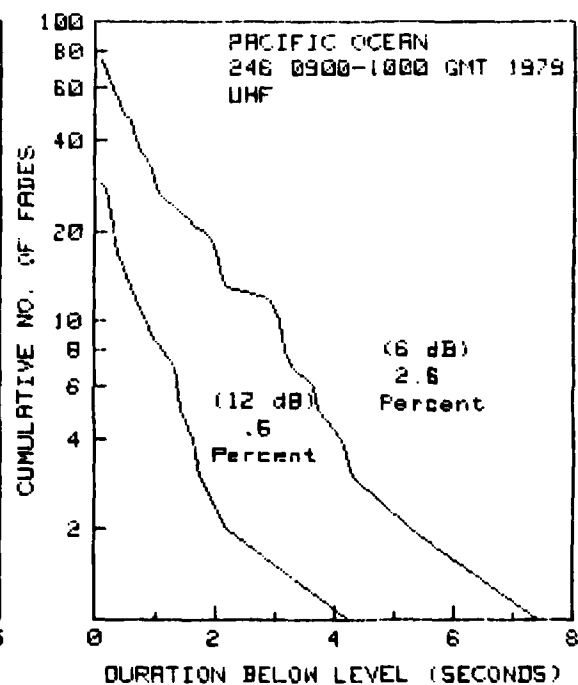
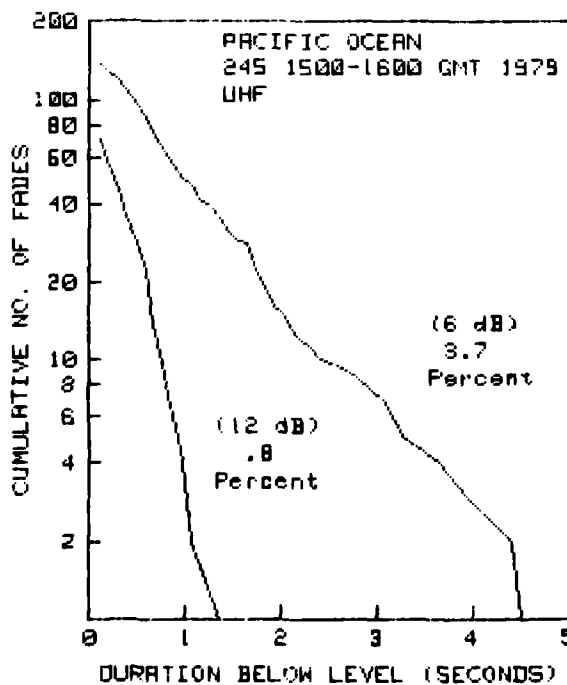
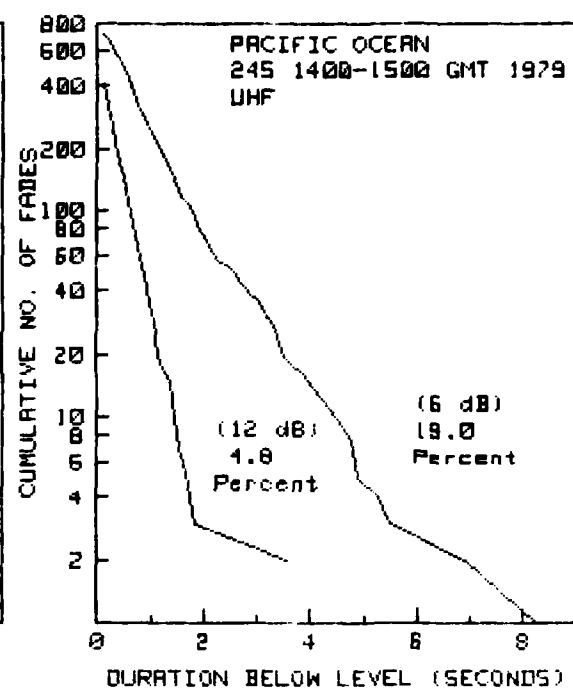
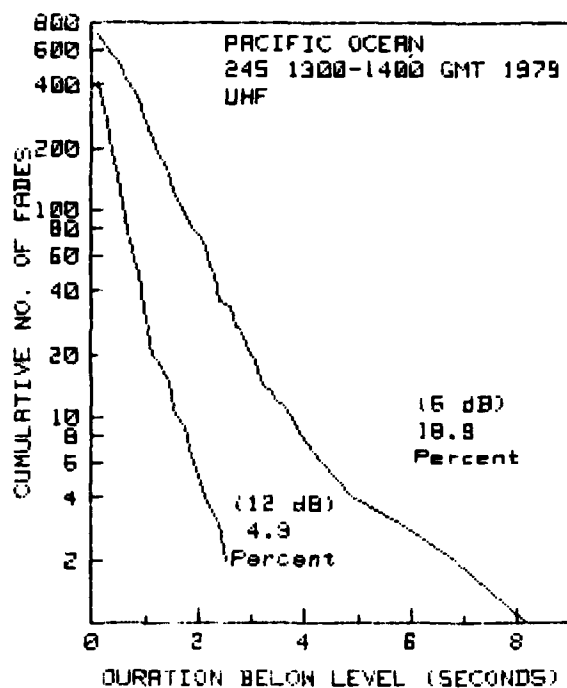


C1 (continued)

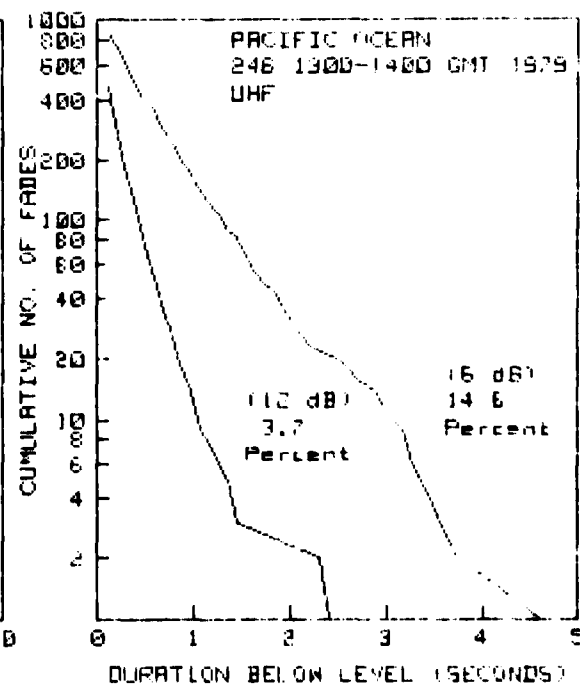
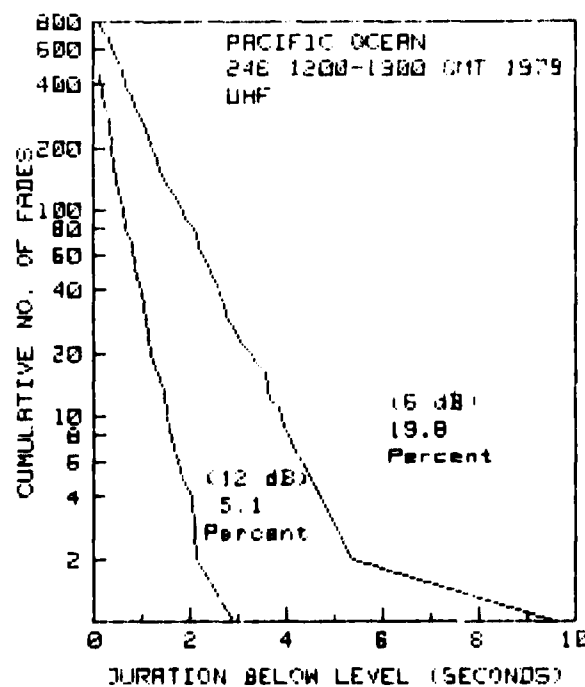
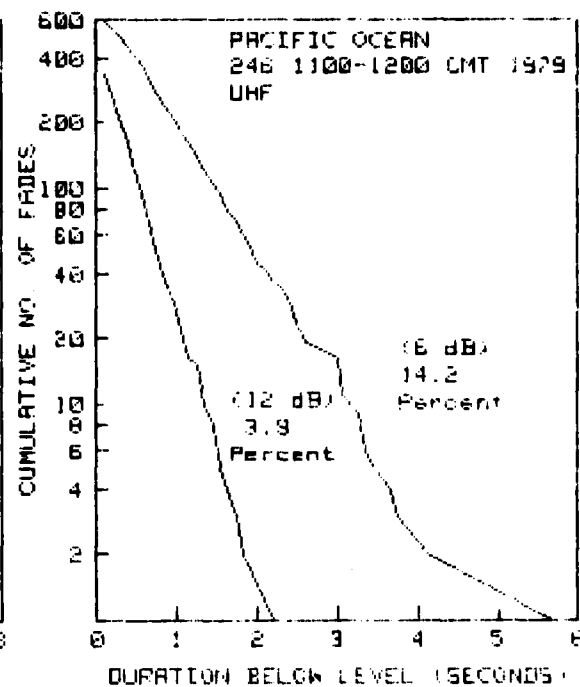
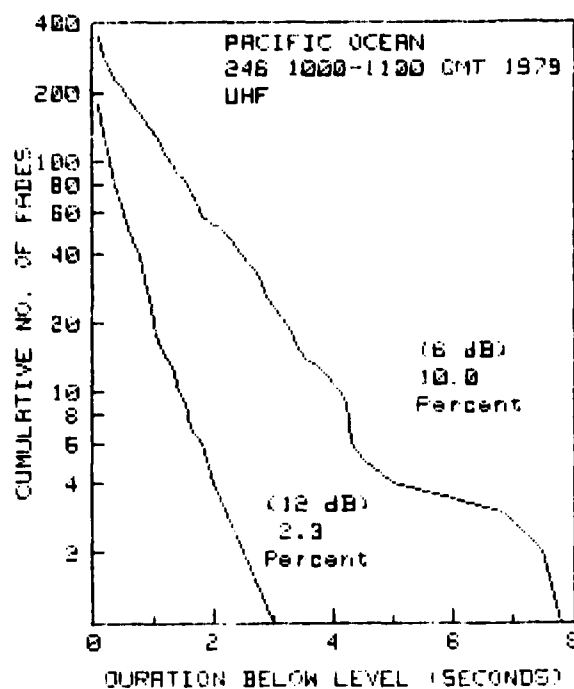


C1 (continued)

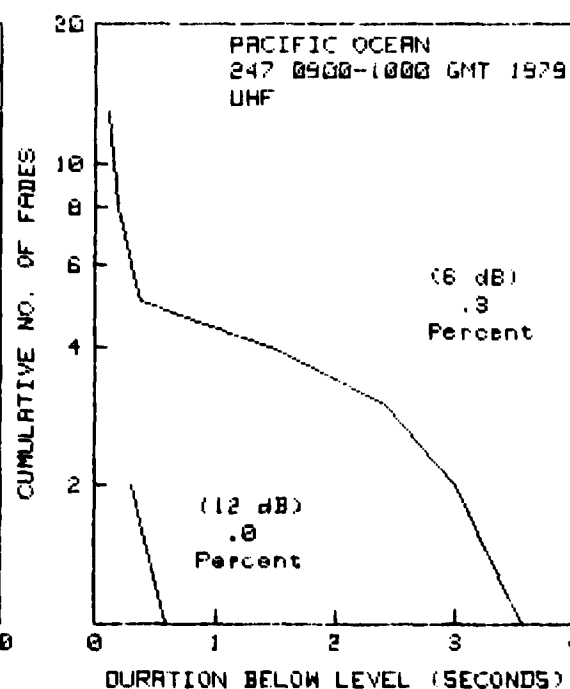
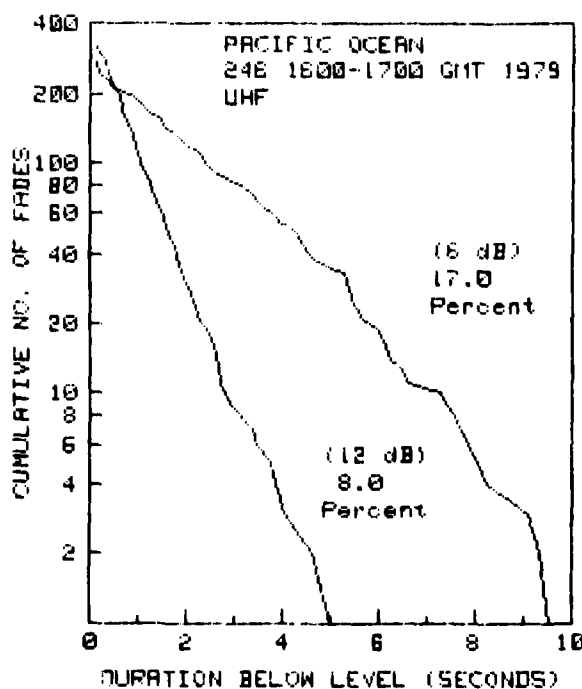
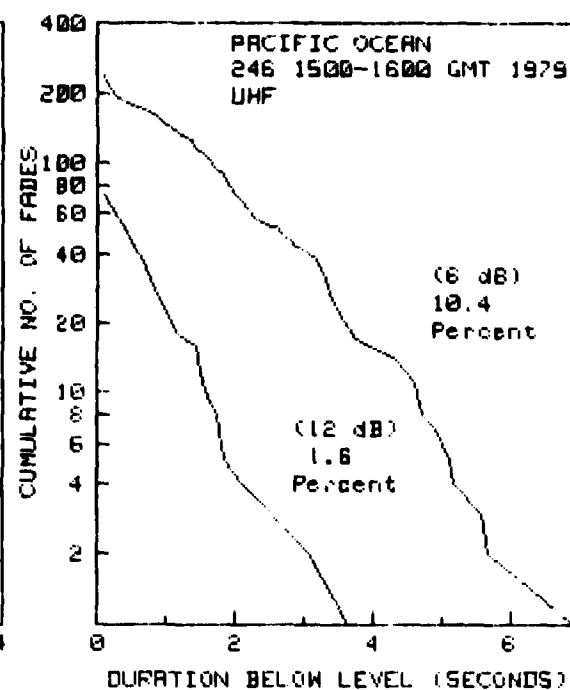
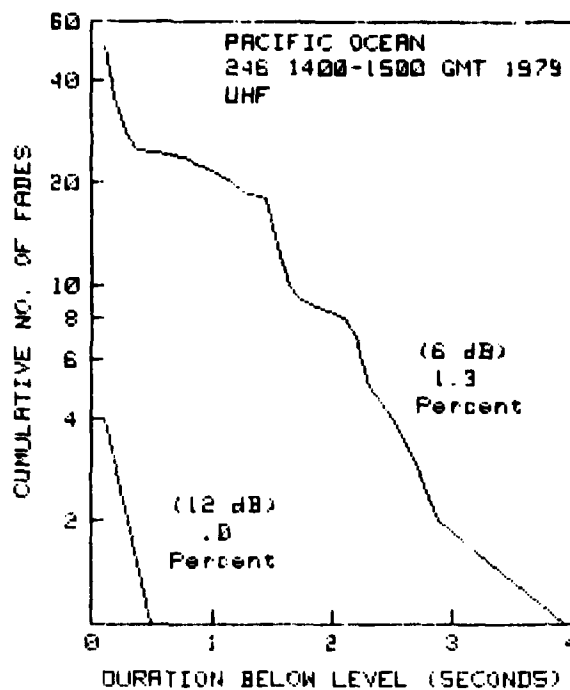




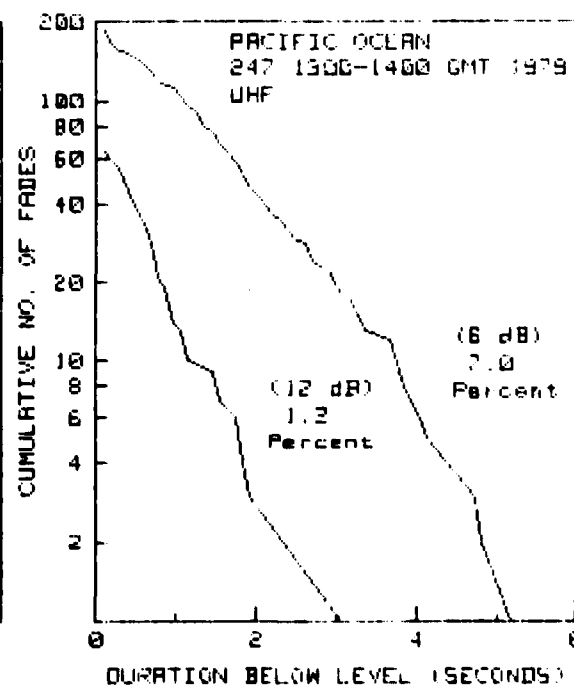
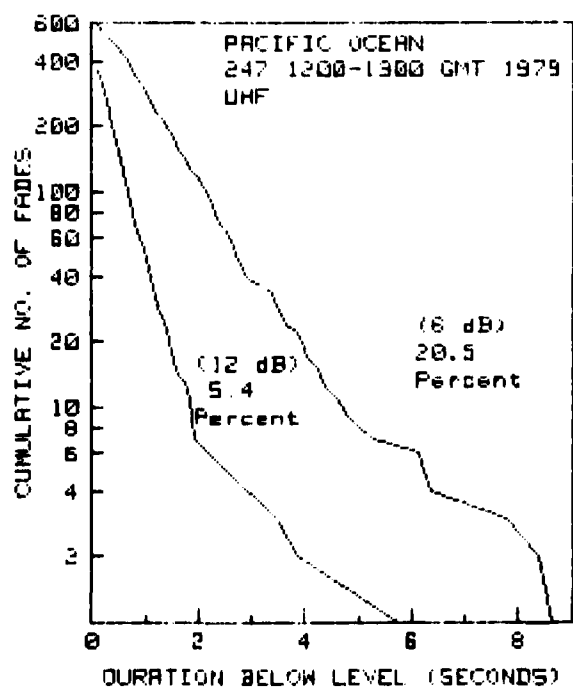
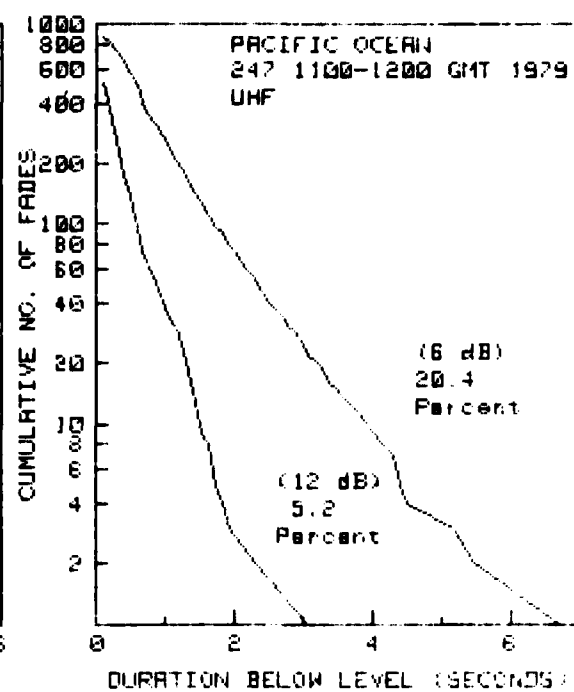
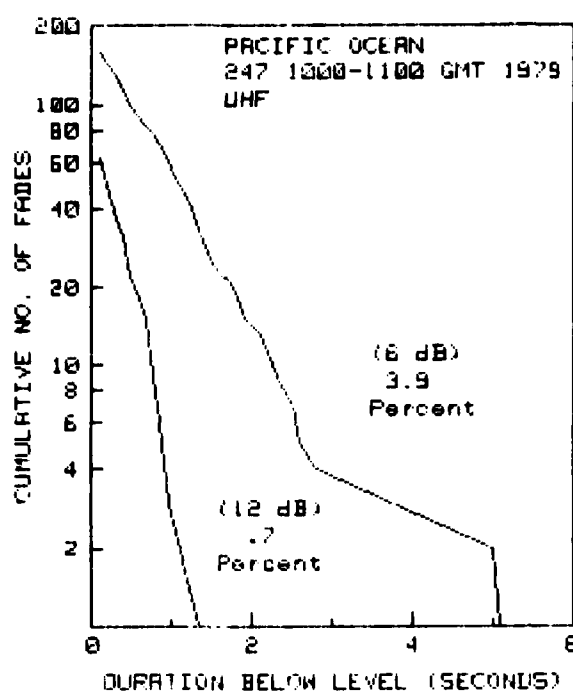
C1 (continued)



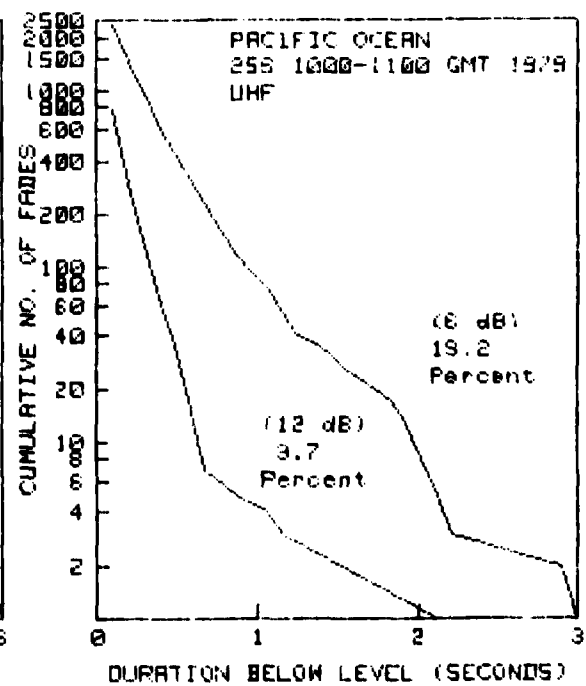
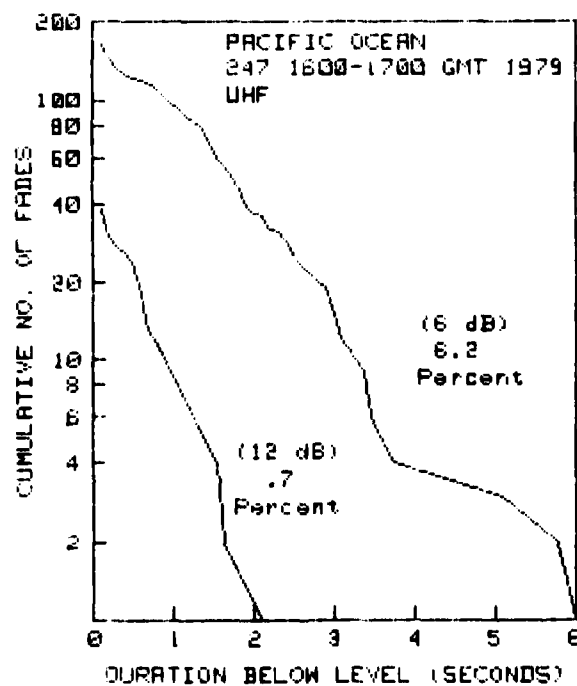
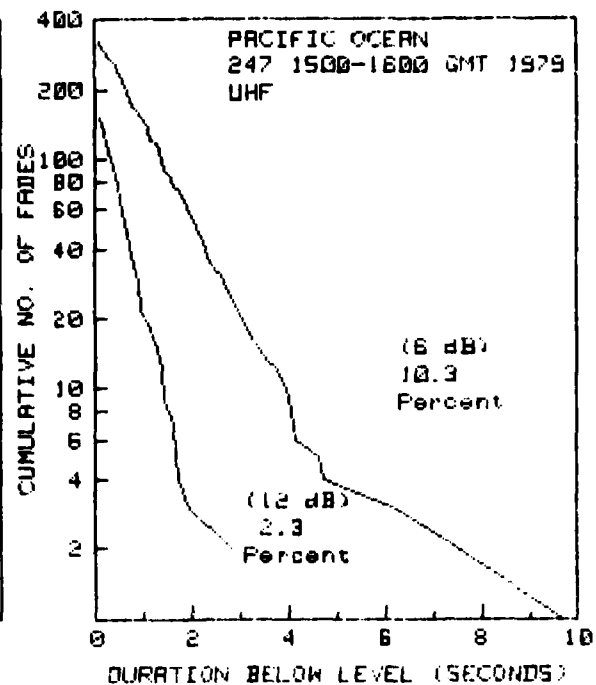
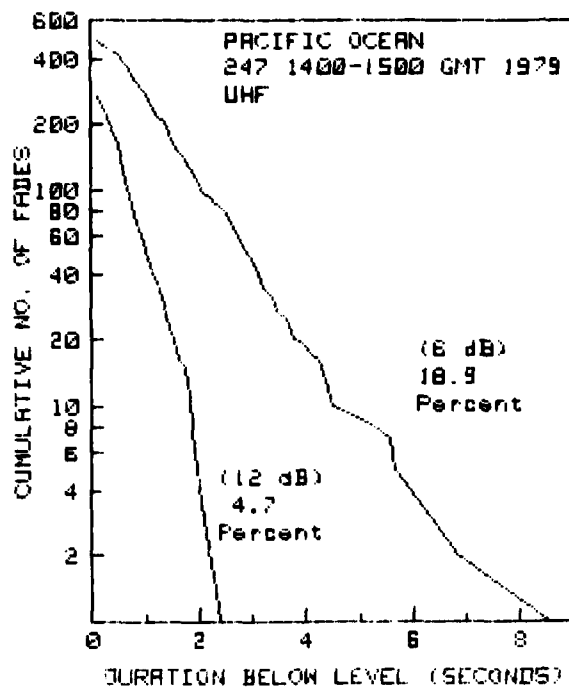
C1 (continued)



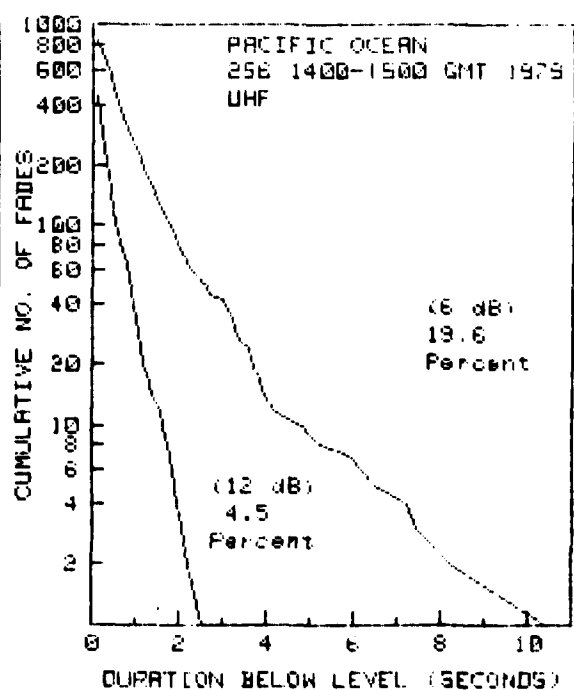
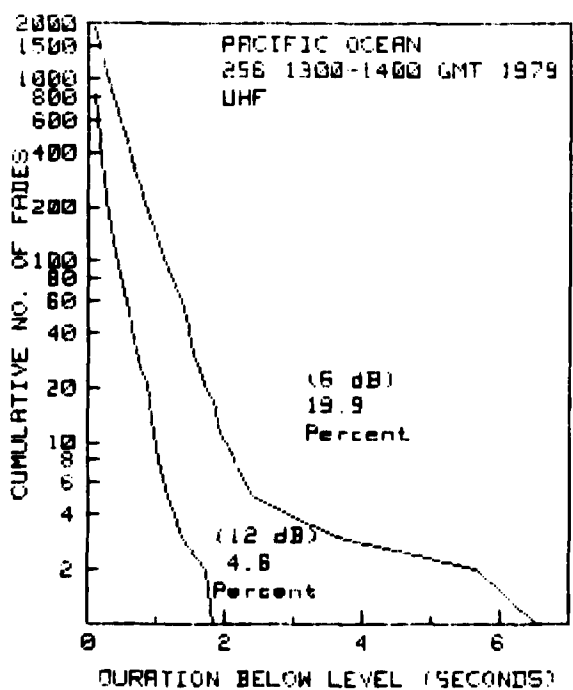
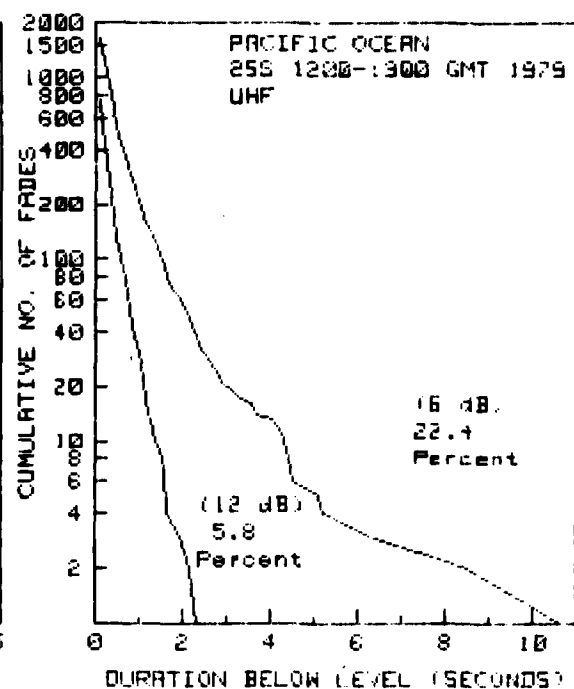
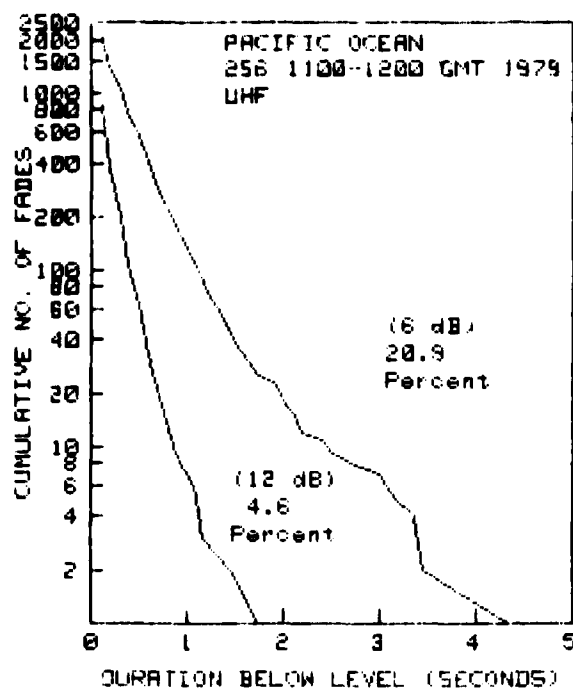
C1 (continued)



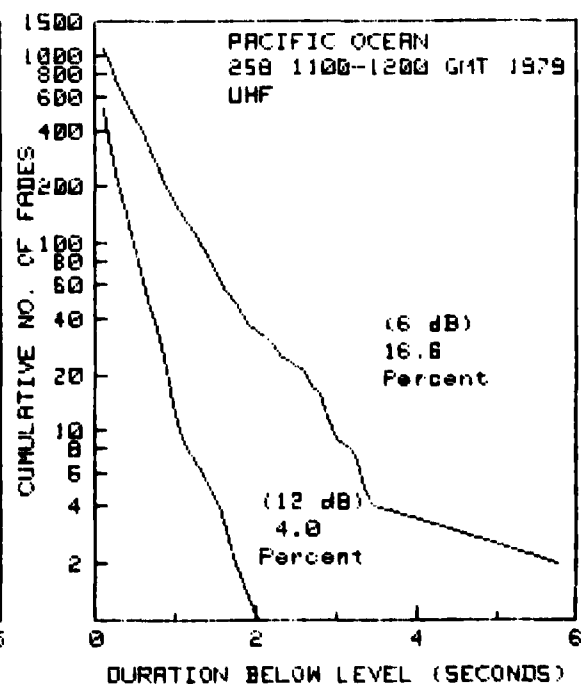
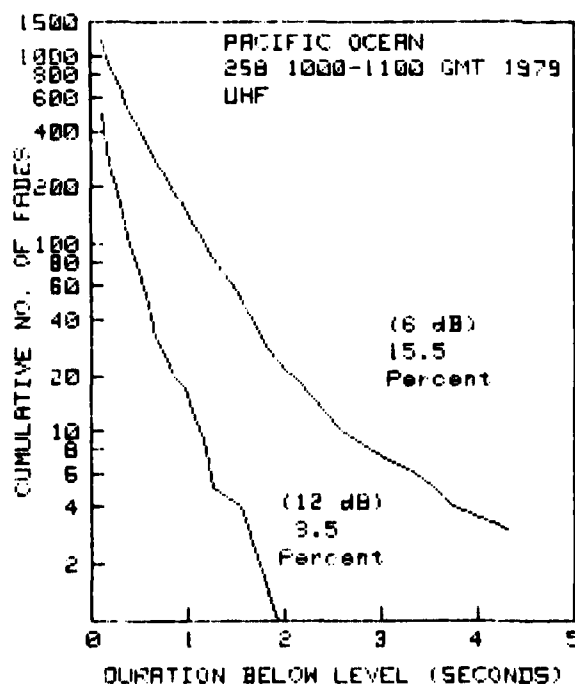
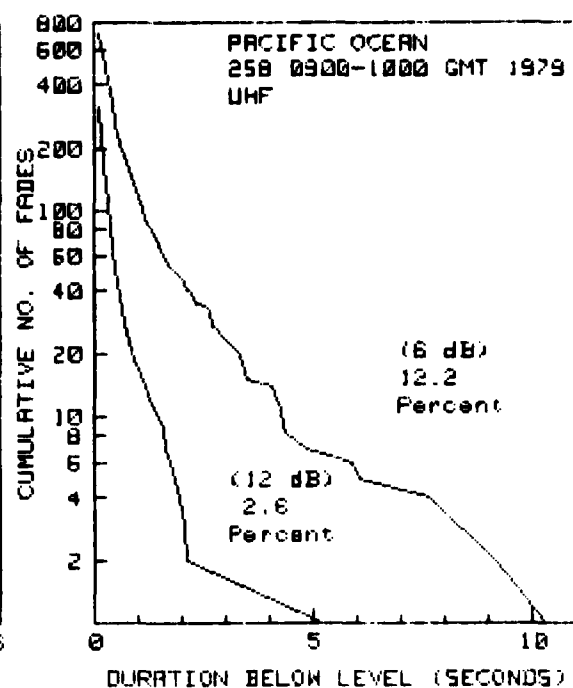
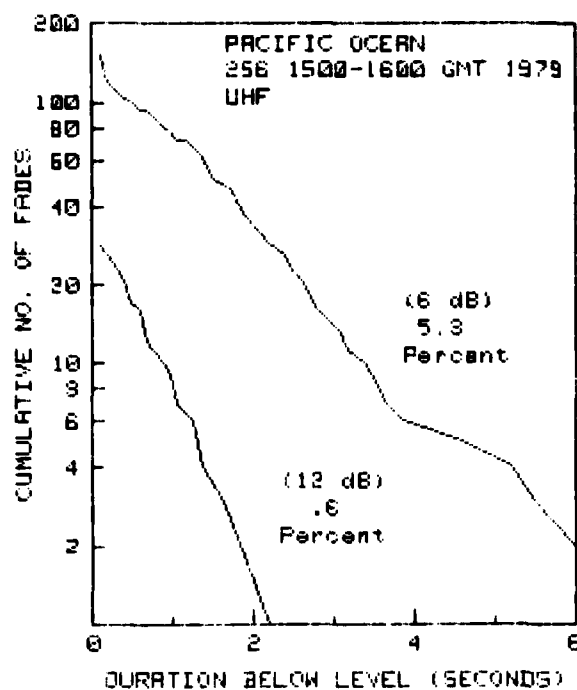
C1 (continued)



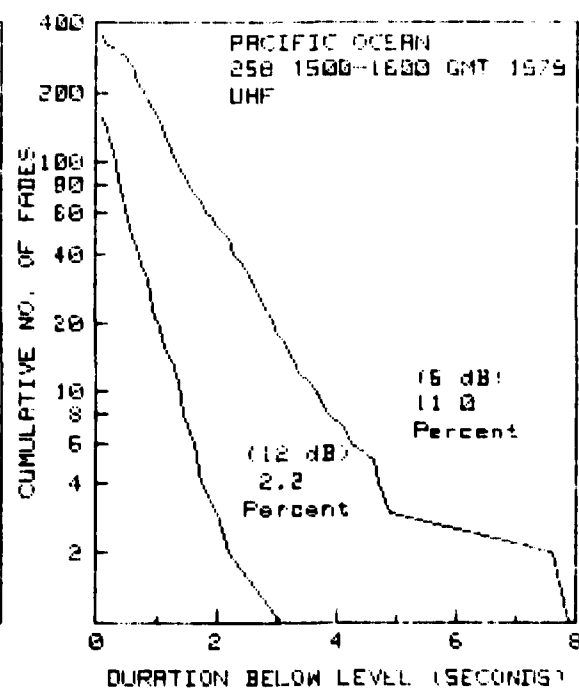
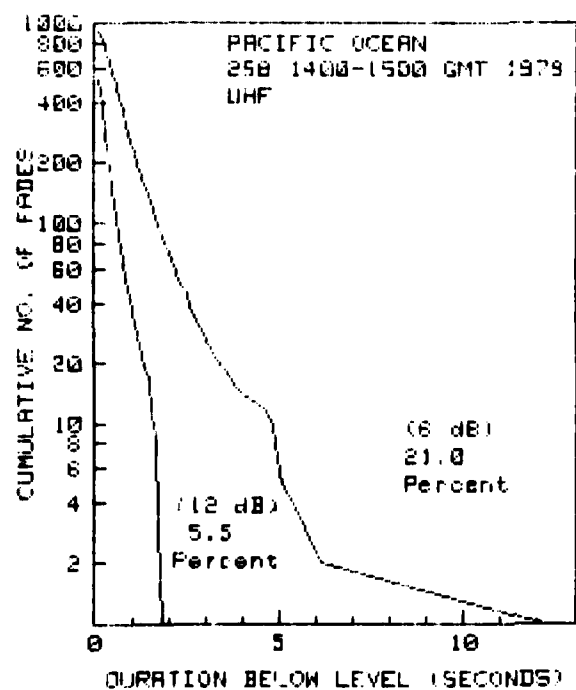
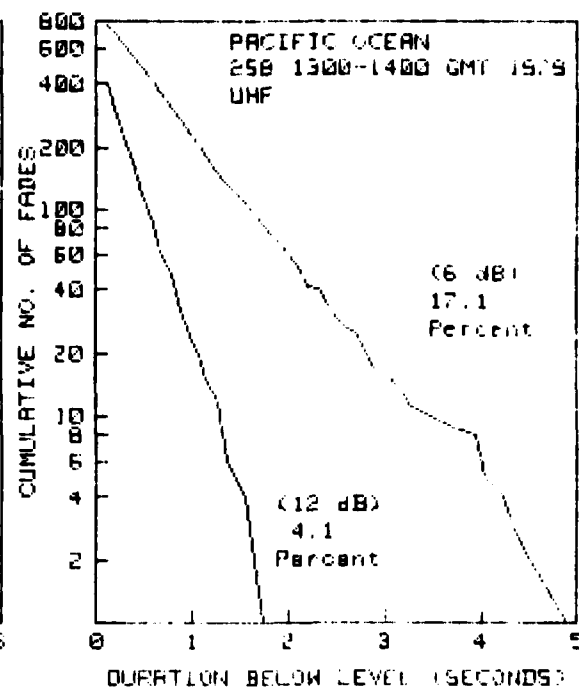
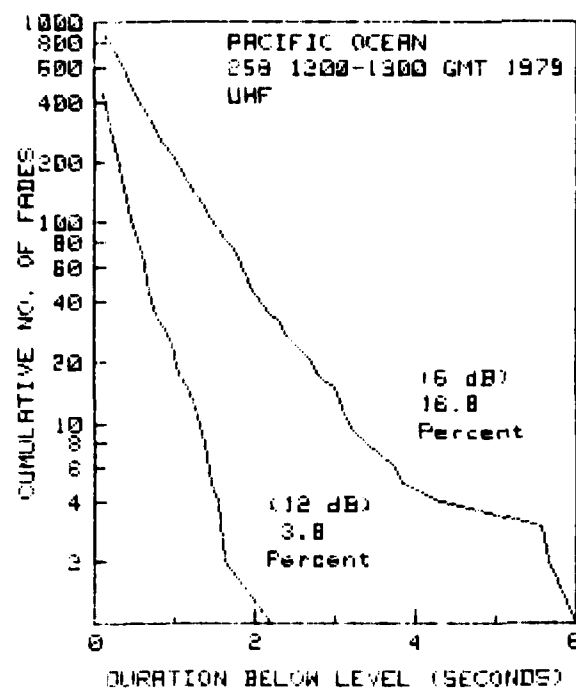
C1 (continued)



C1 (continued)

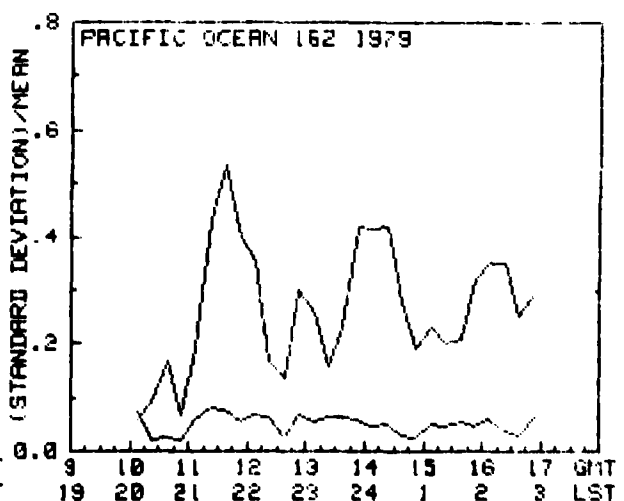
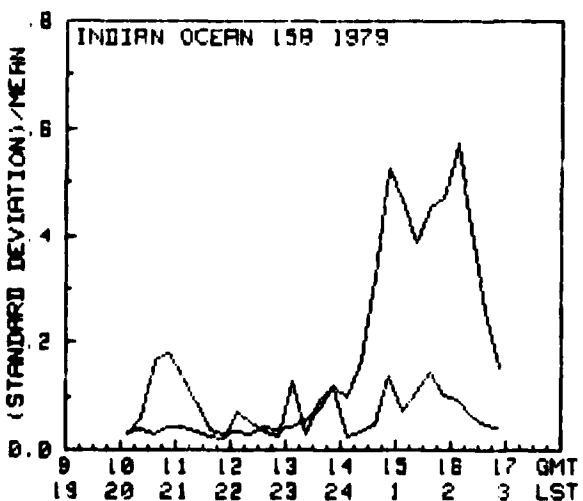
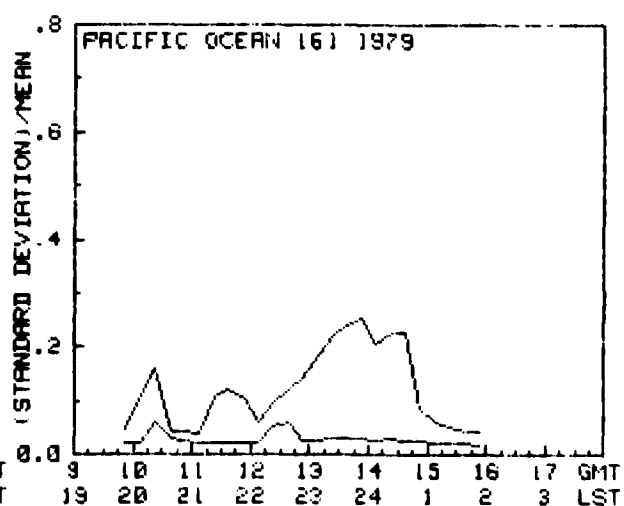
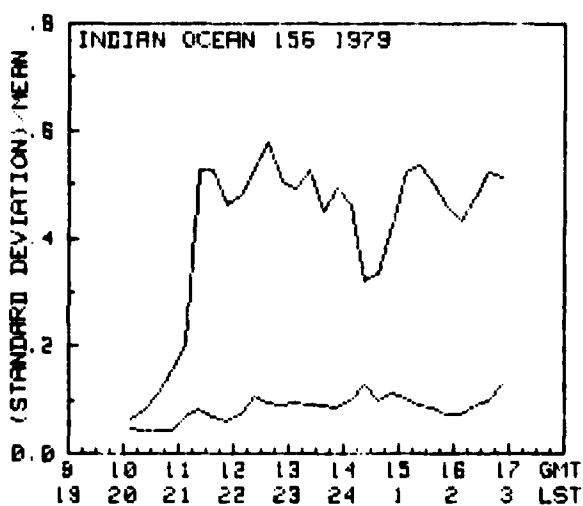
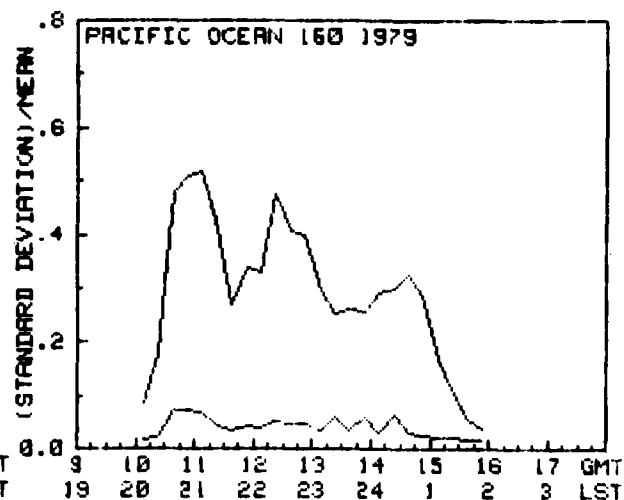
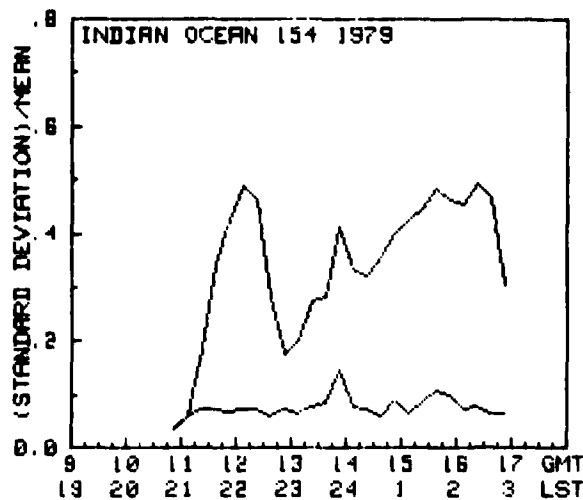


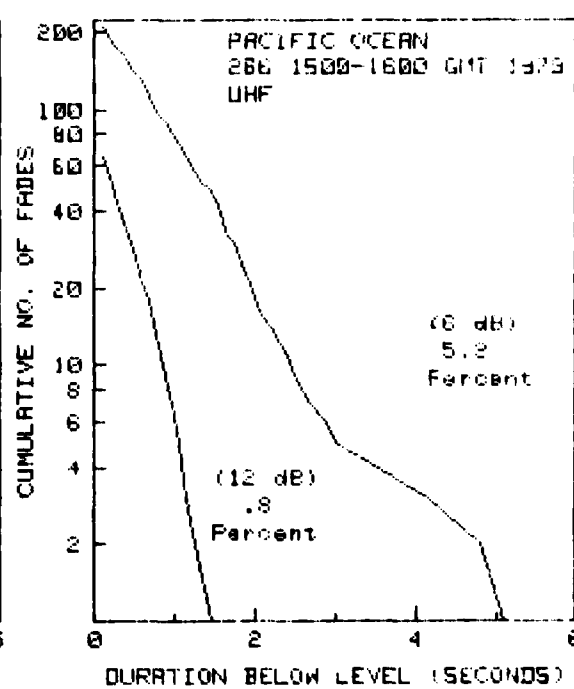
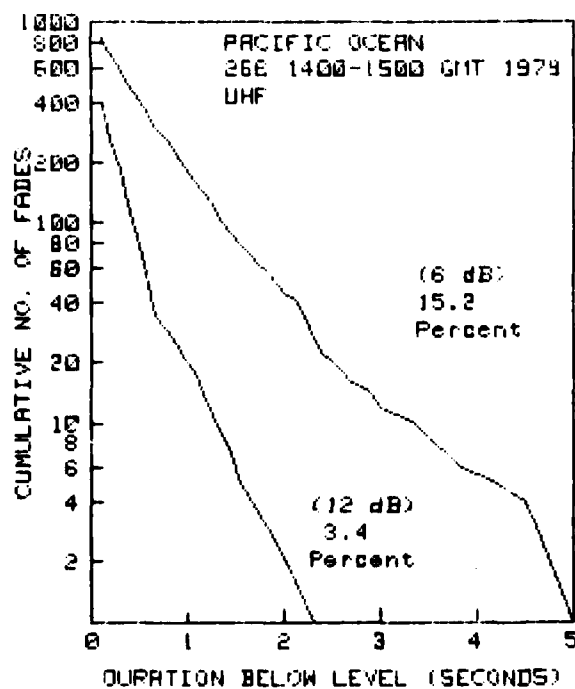
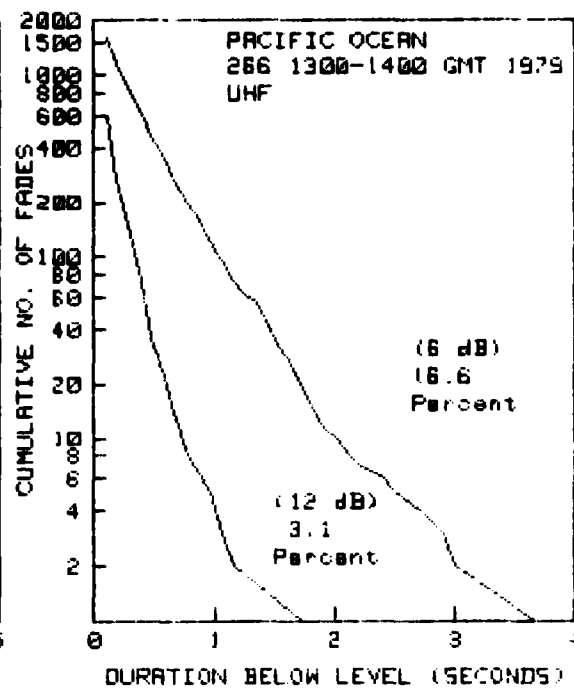
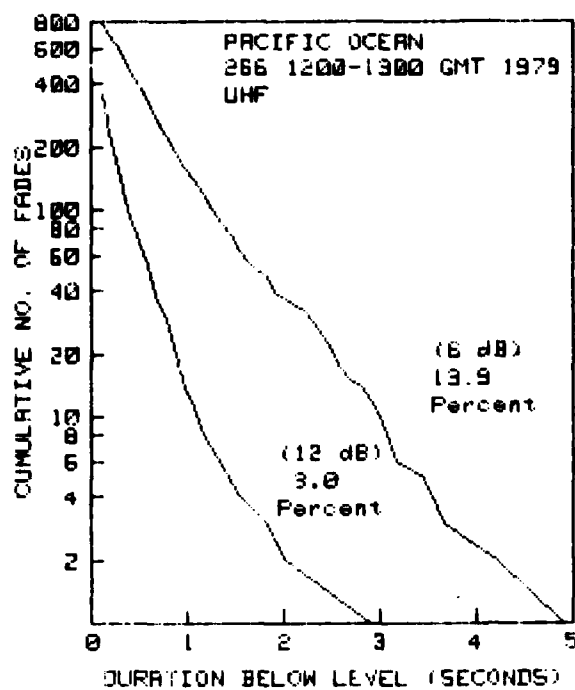
C1 (continued)



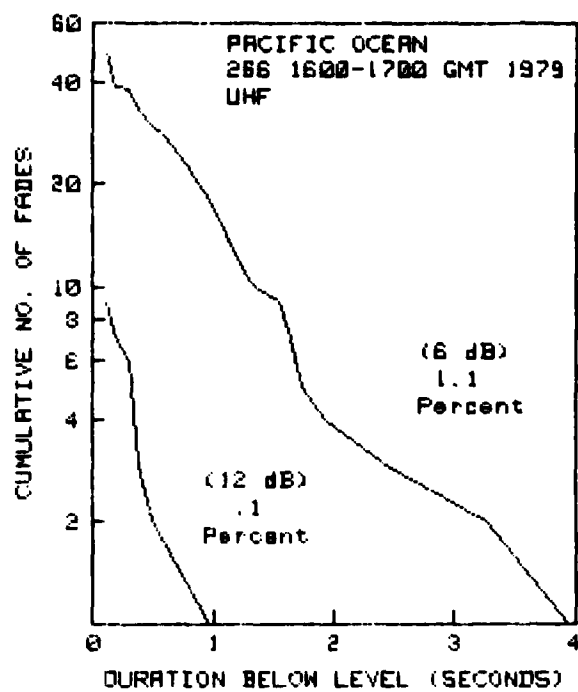
C1 (continued)







C1 (continued)



C1 (continued)

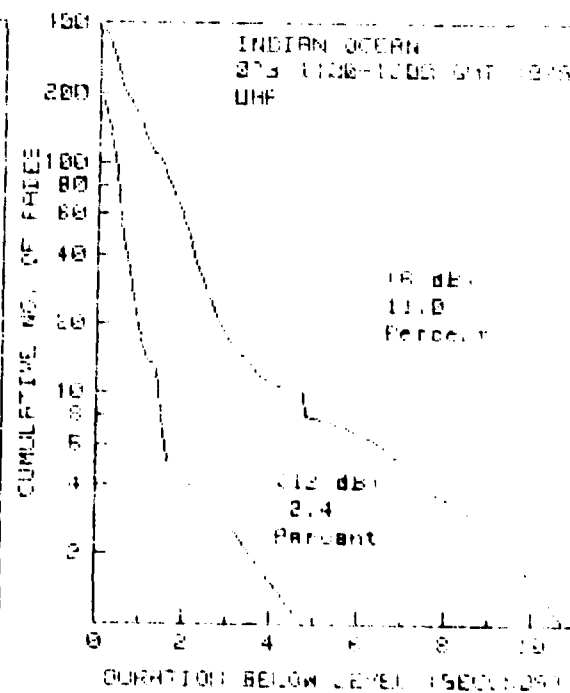
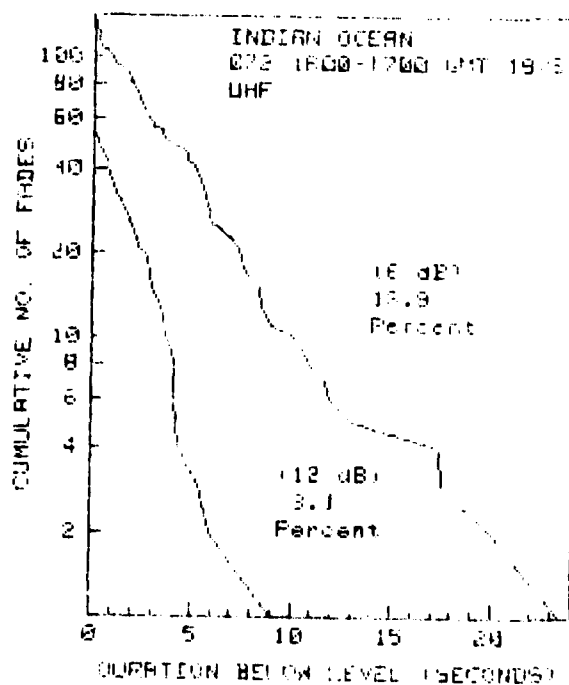
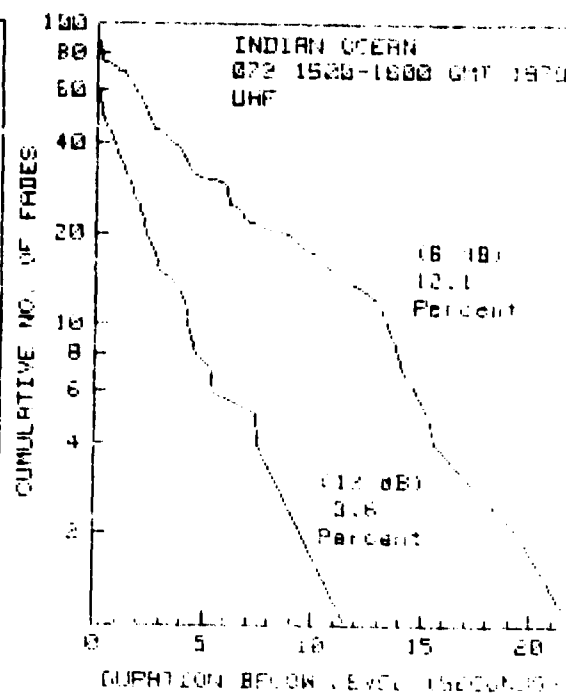
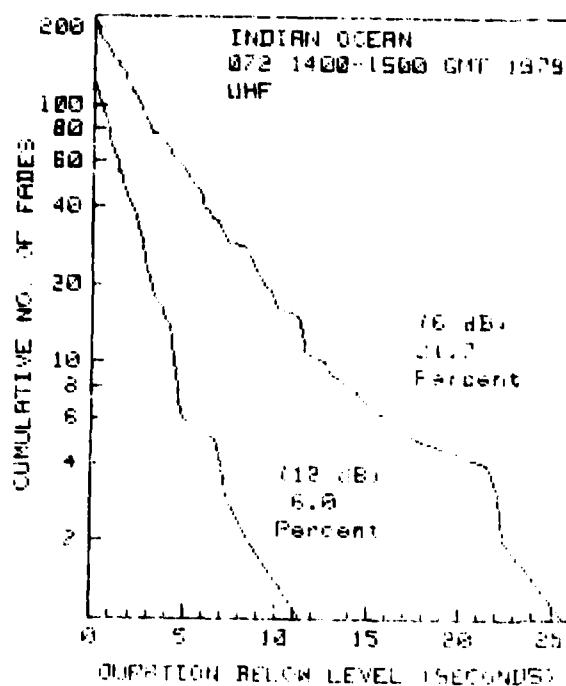
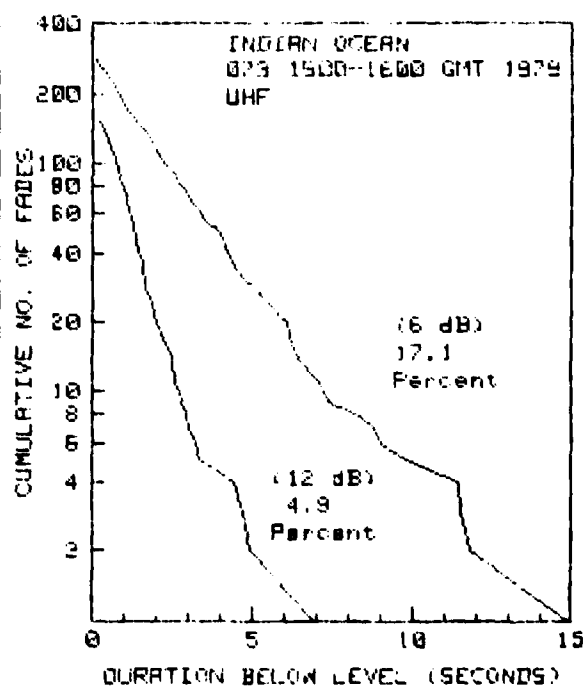
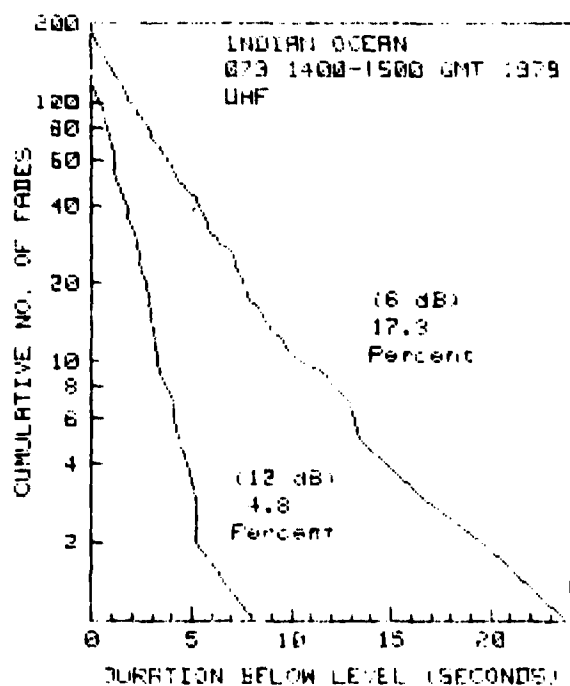
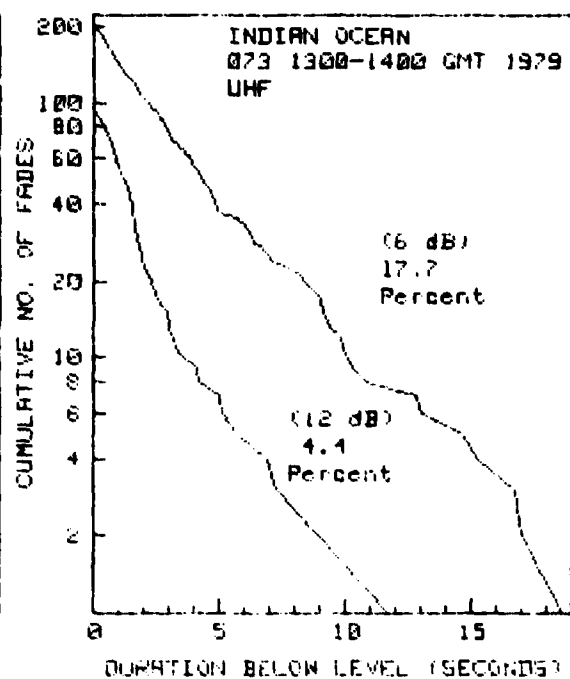
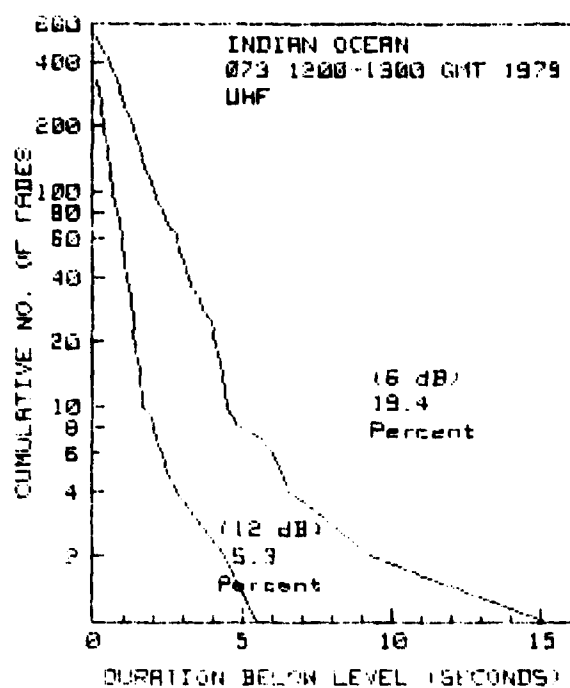
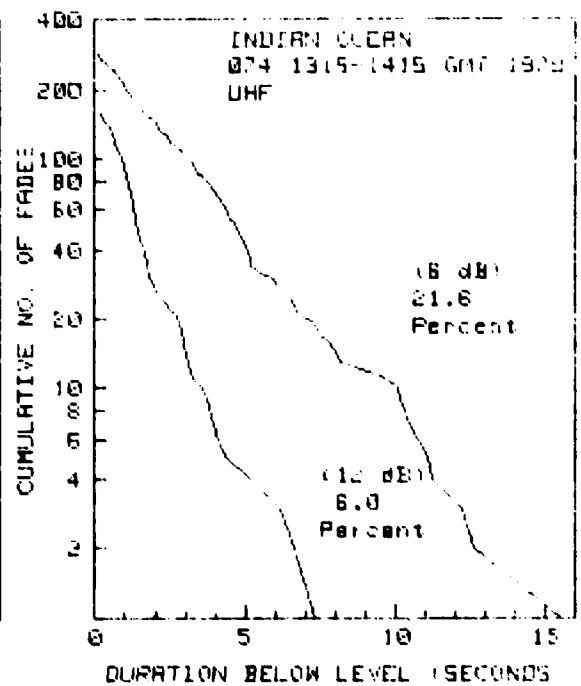
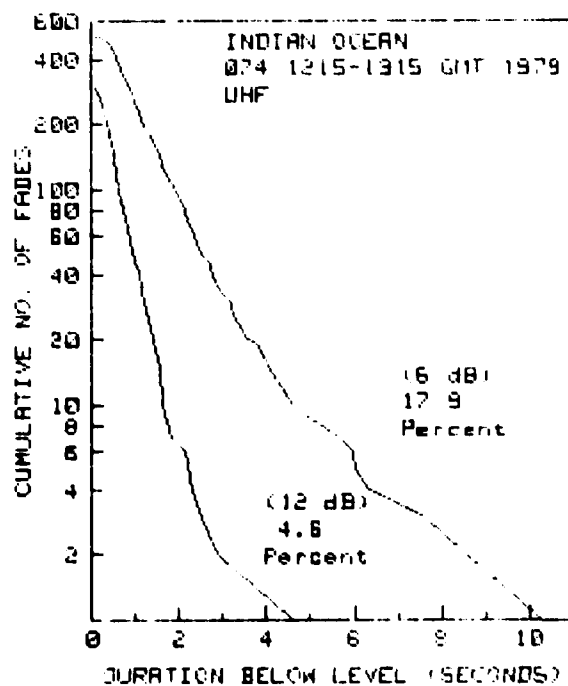
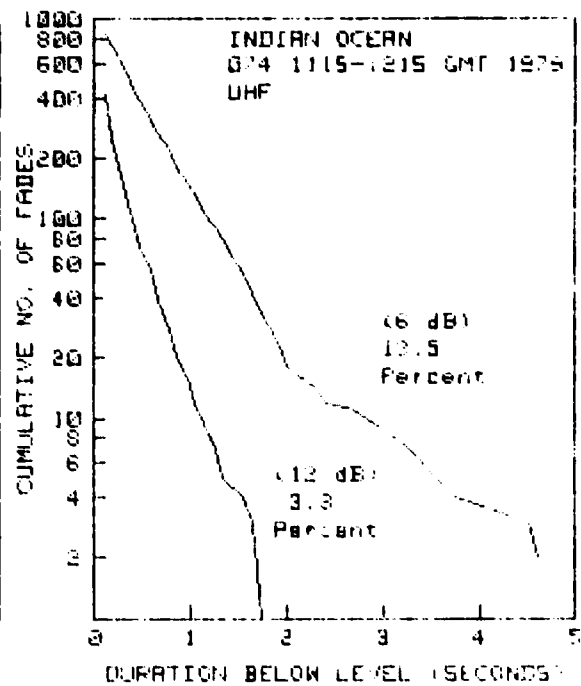
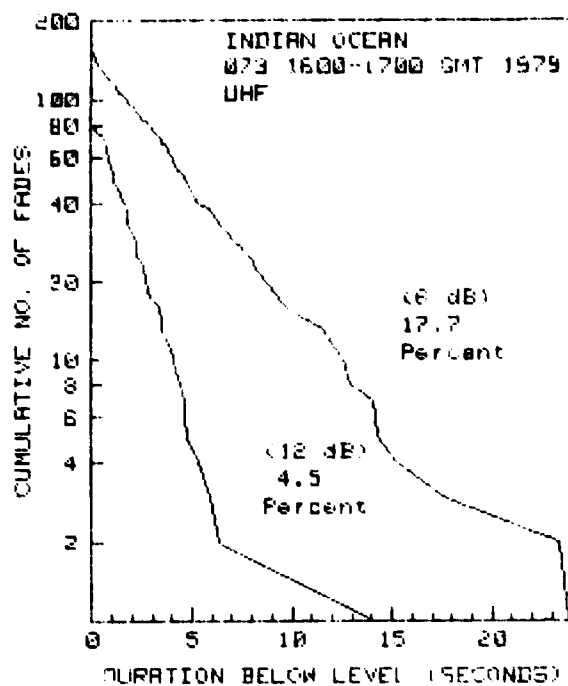


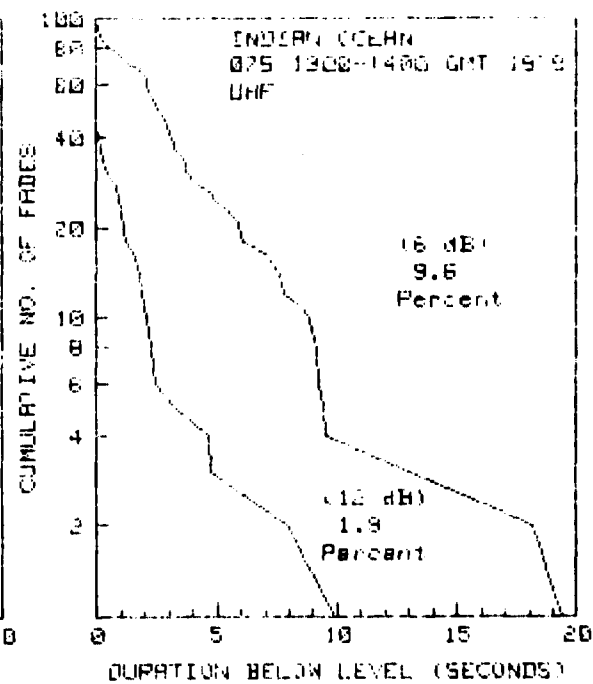
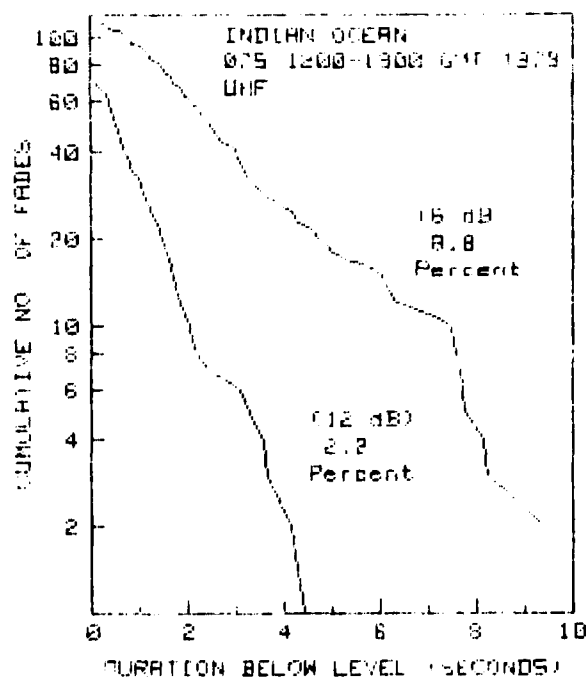
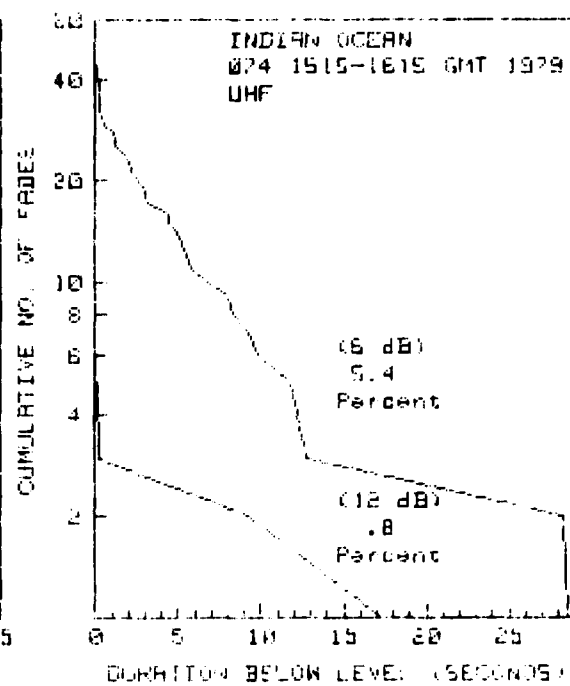
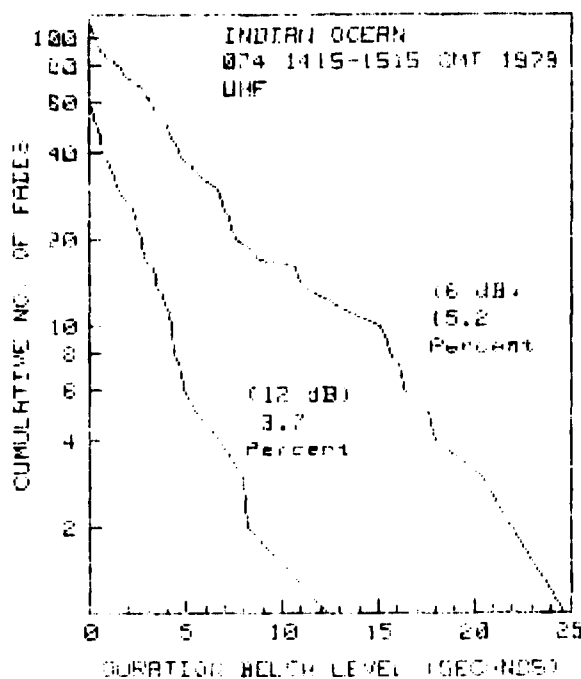
Figure C2. Cumulative uhf fade duration distribution for the Indian Ocean satellite (elevation angle about 10°).



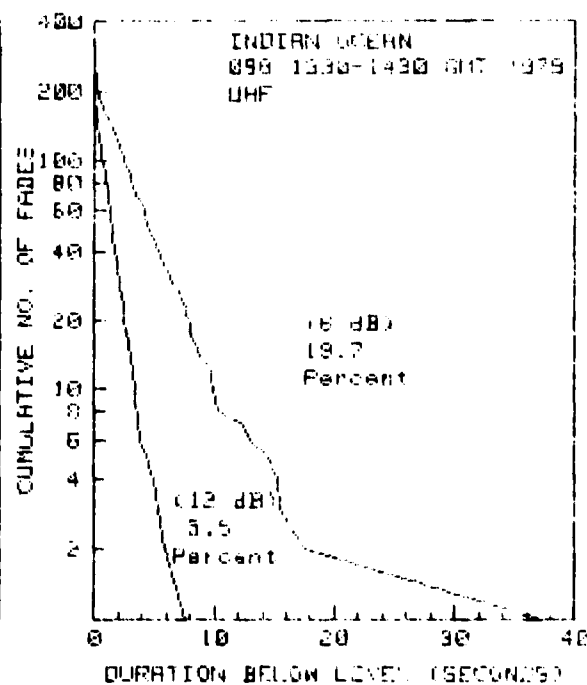
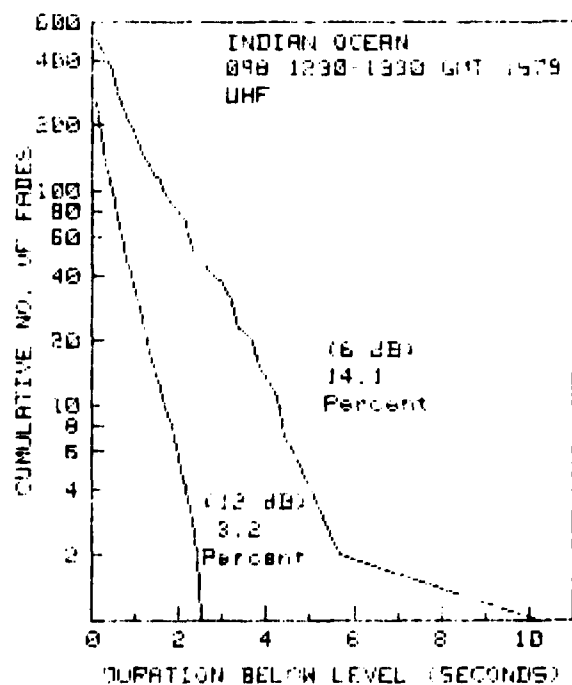
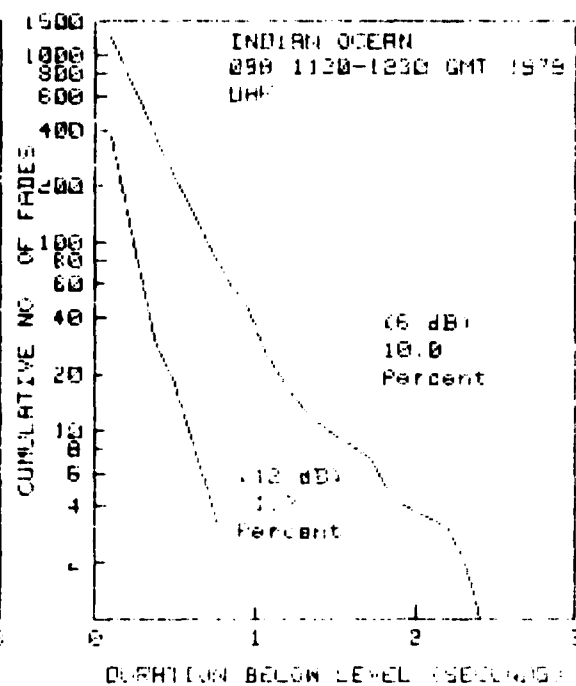
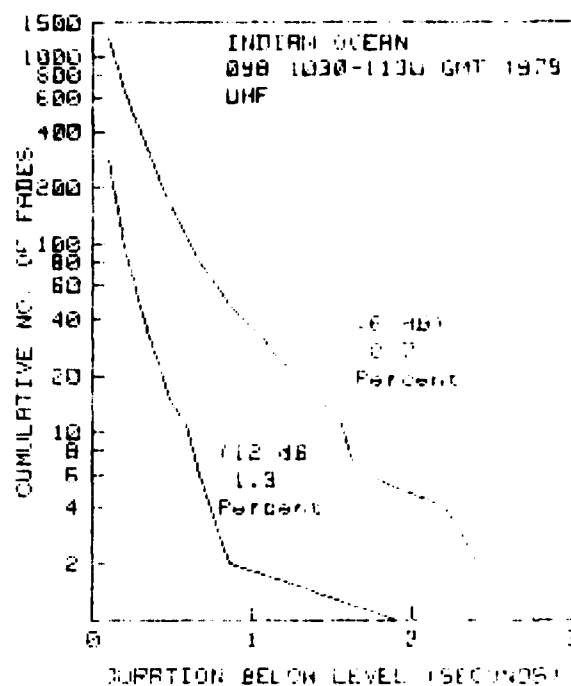
C2 (continued)



C2 (continued)

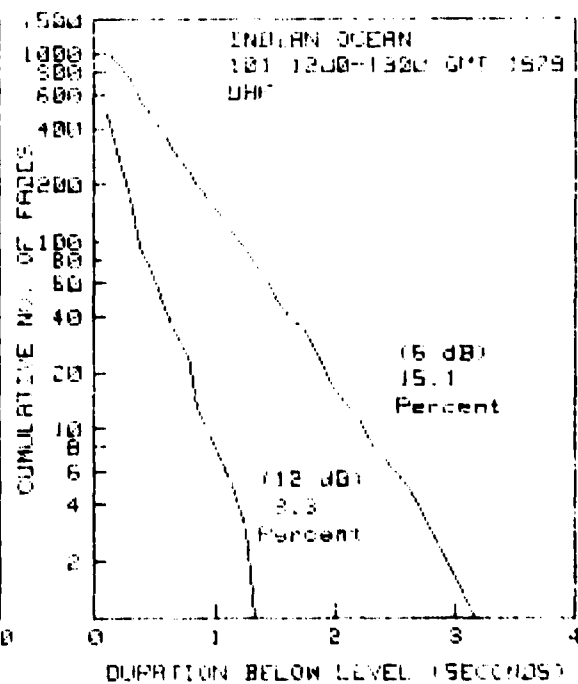
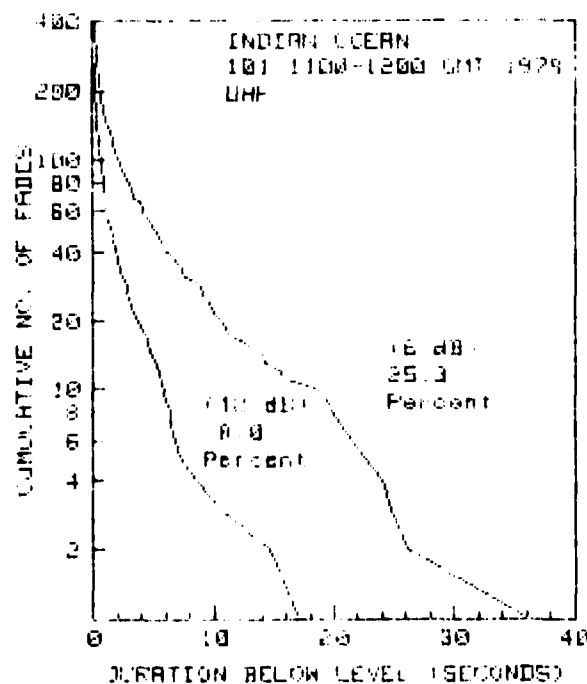
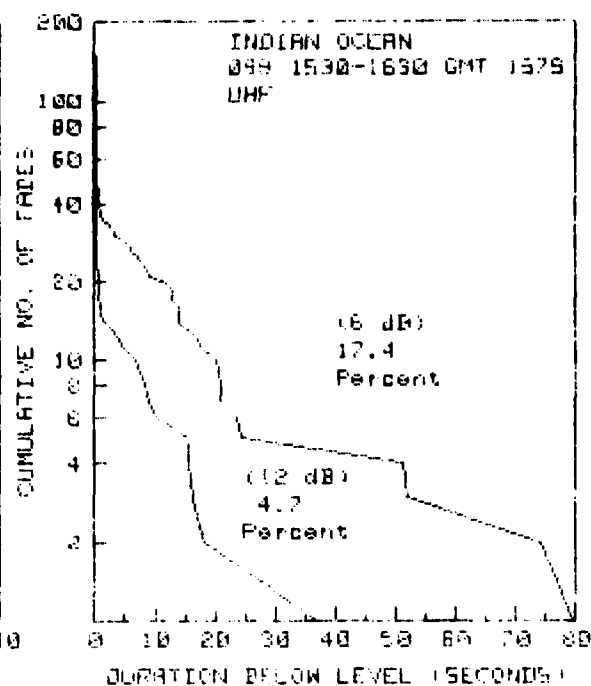
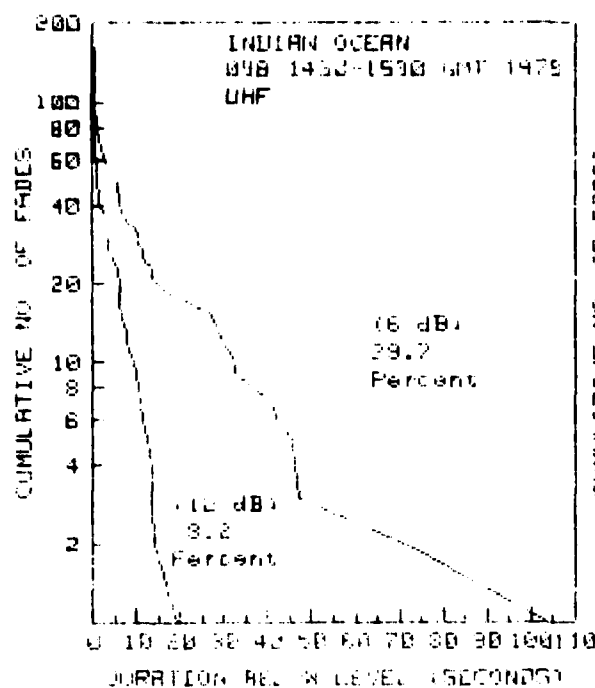


C2 (continued)

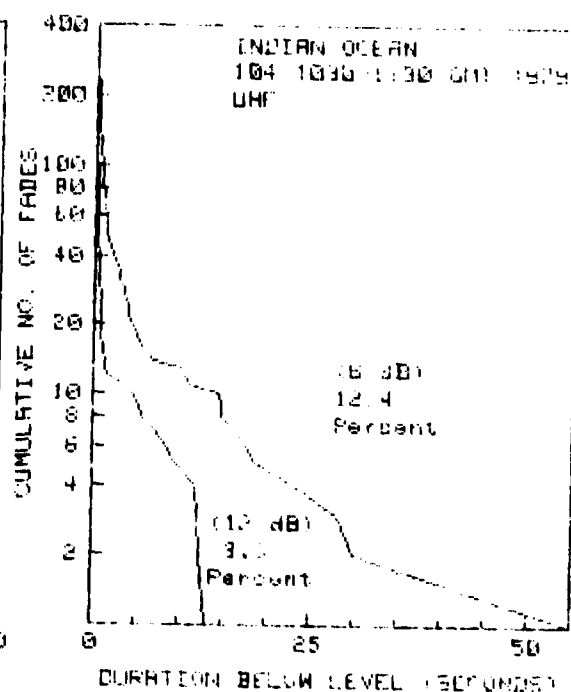
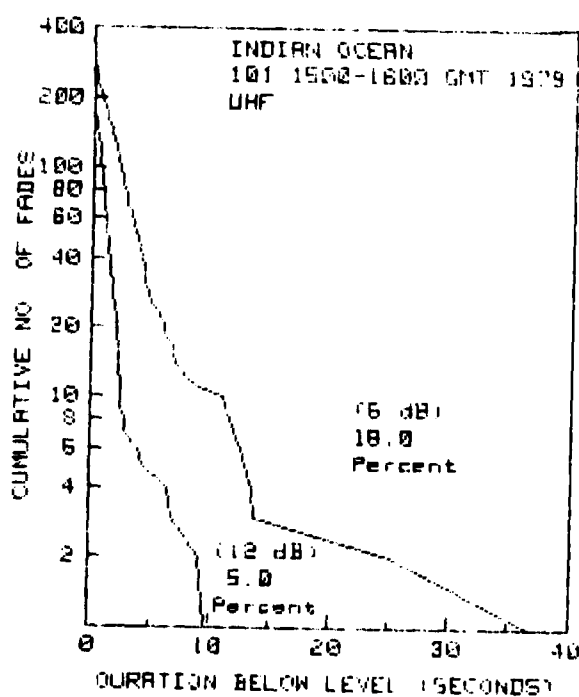
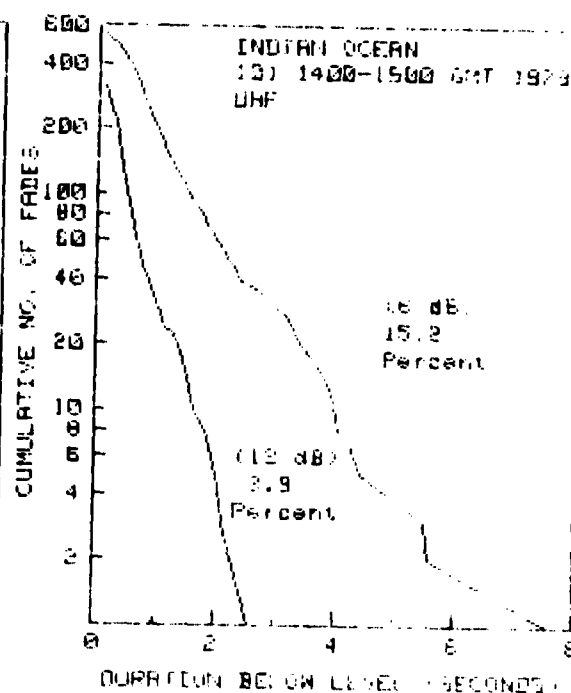
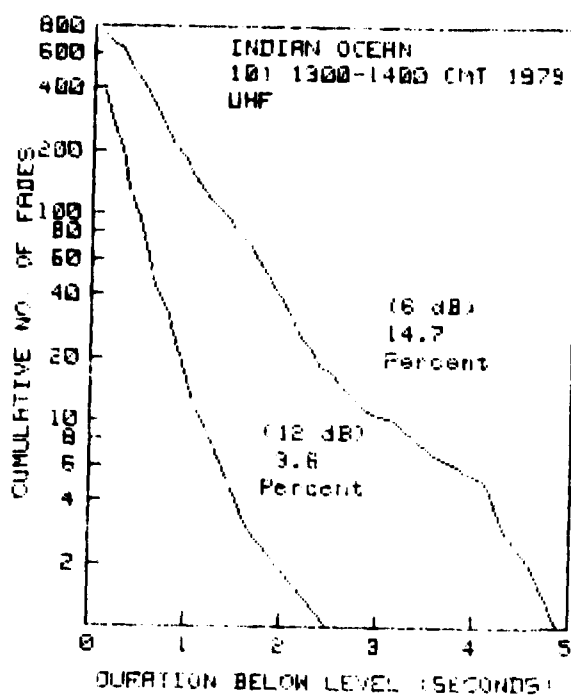


C2 (continued)

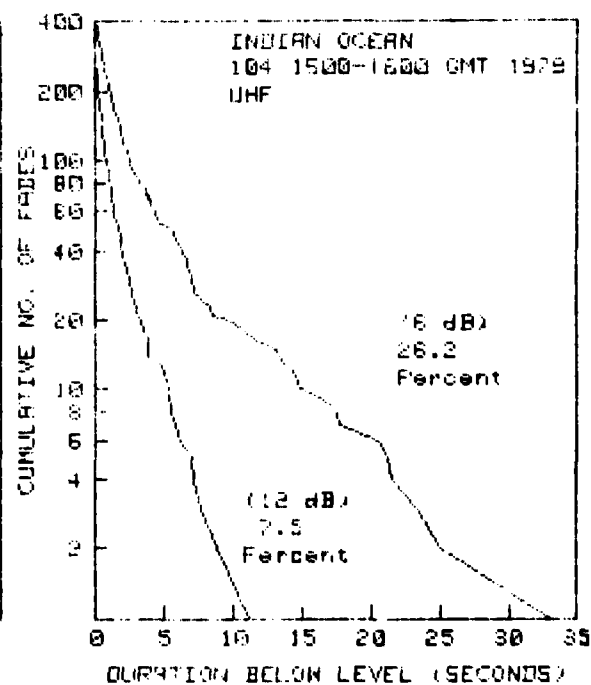
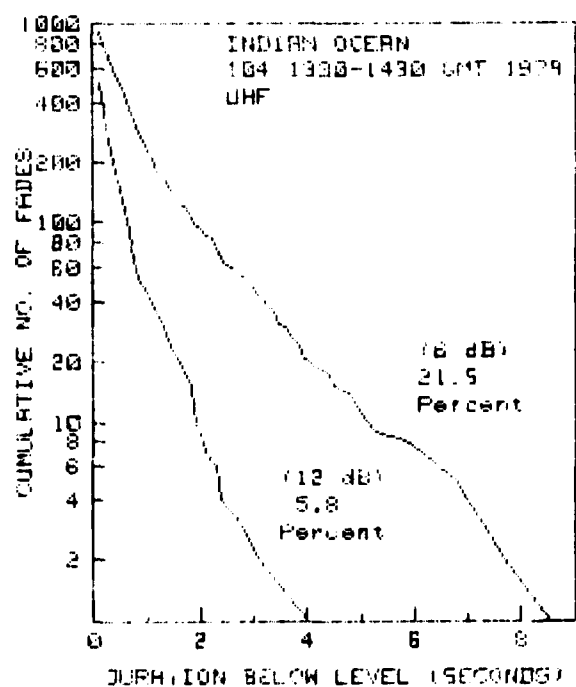
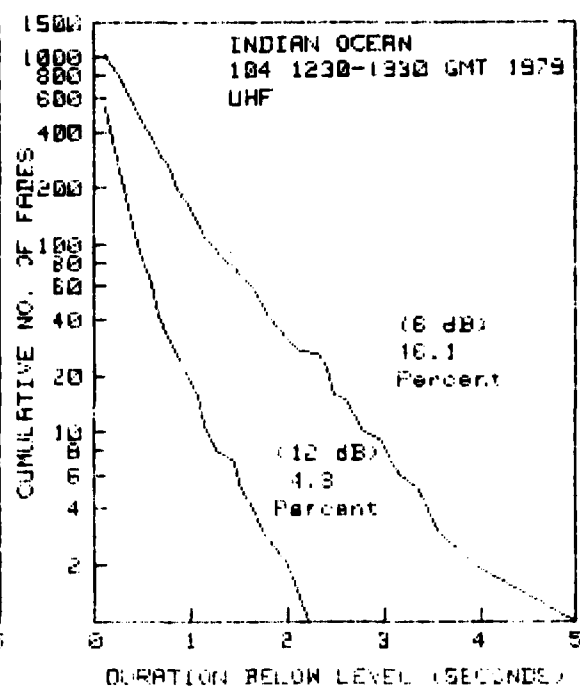
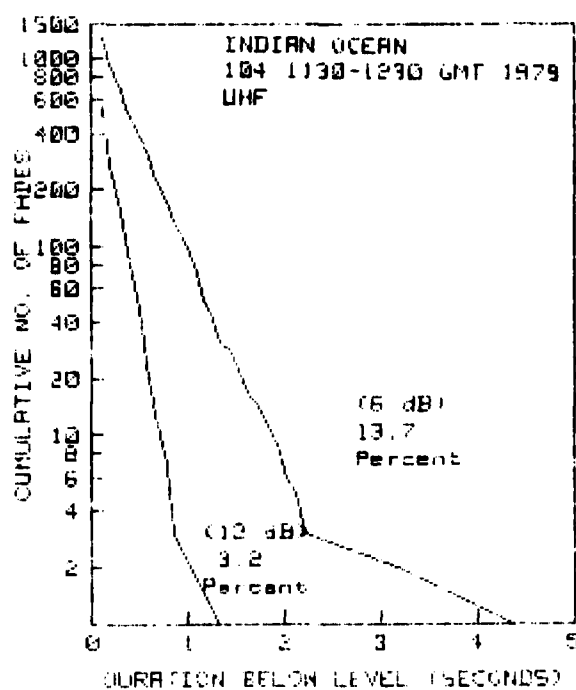




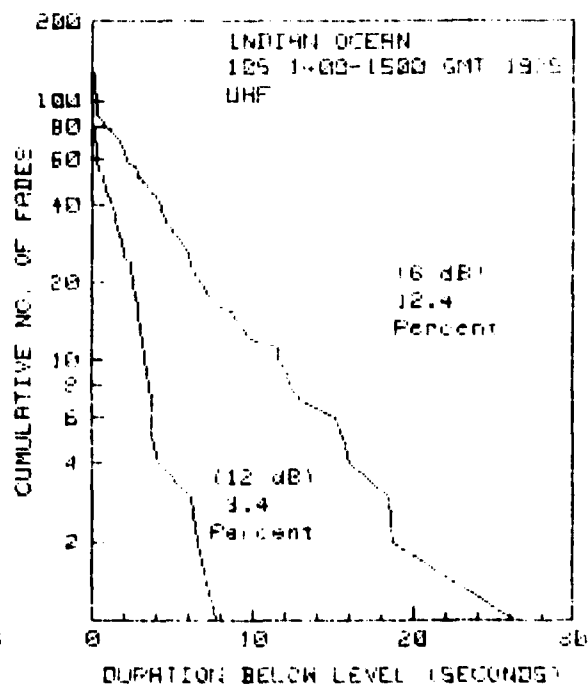
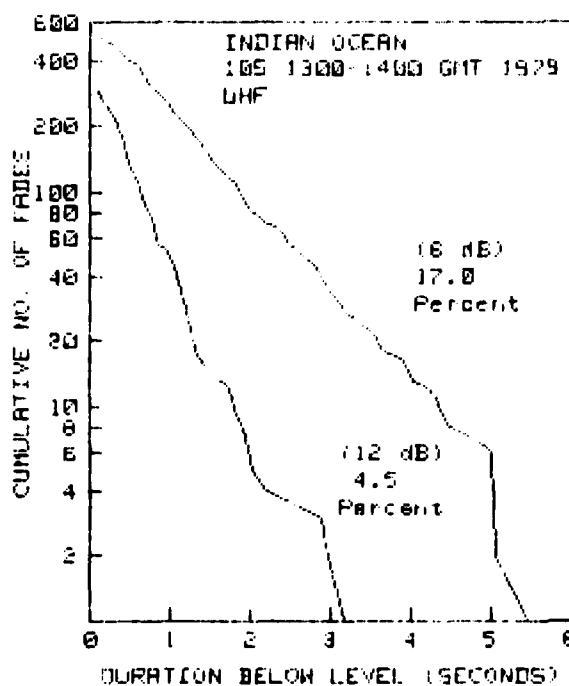
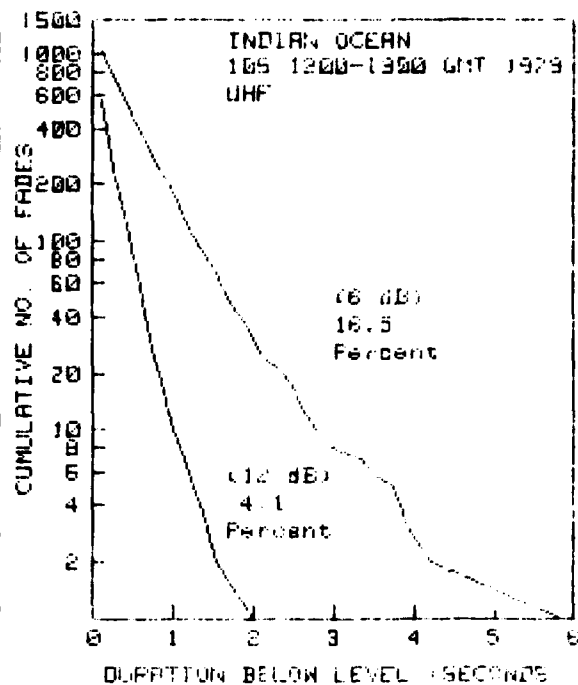
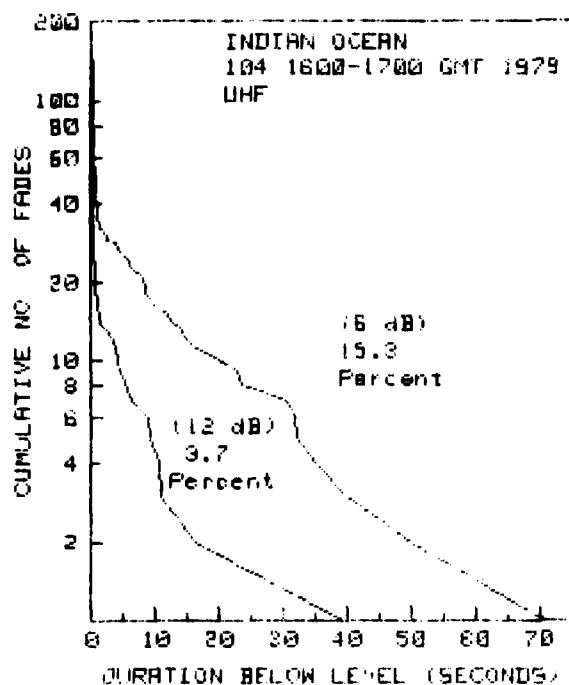
C2 (continued)



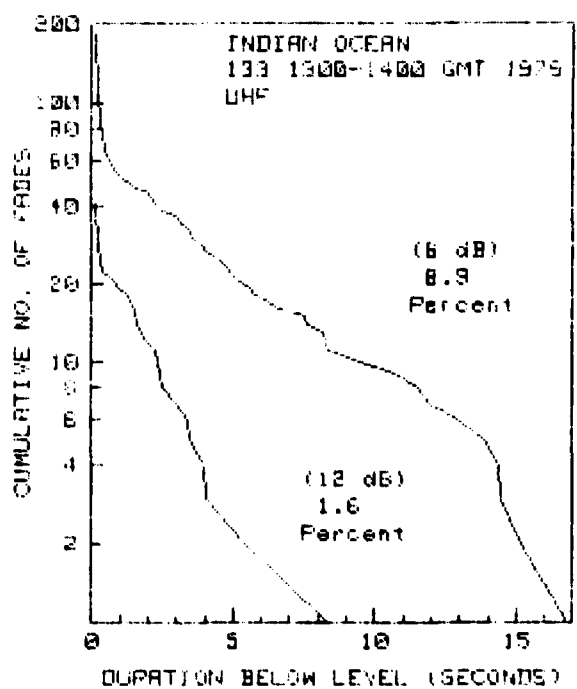
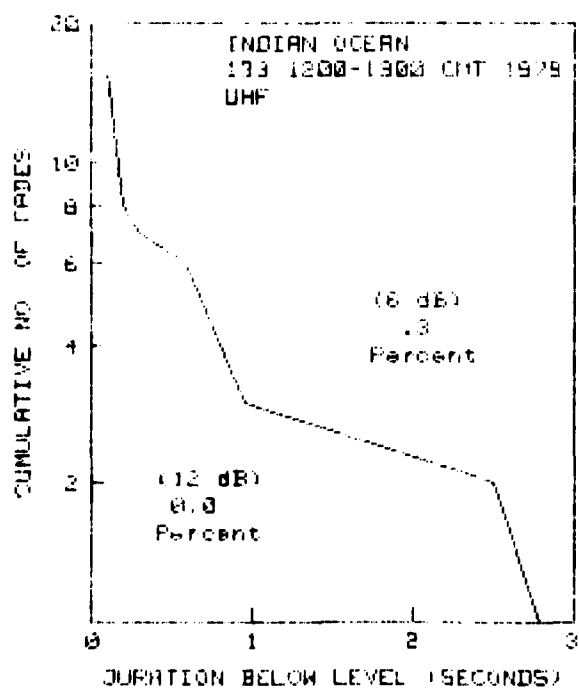
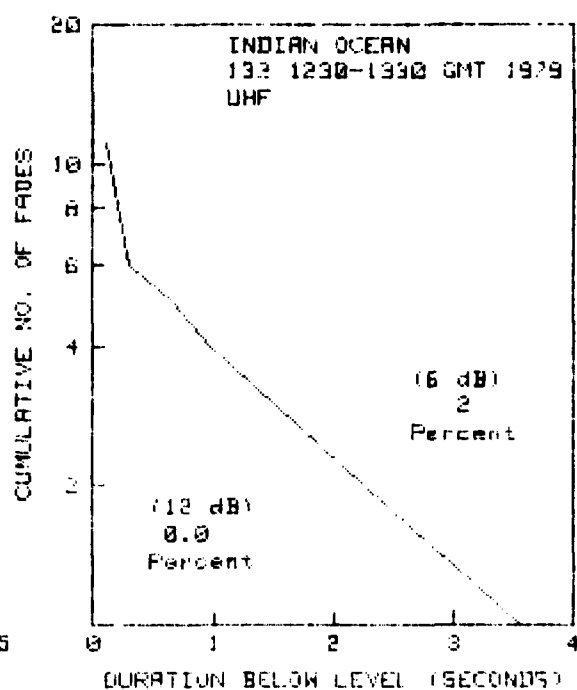
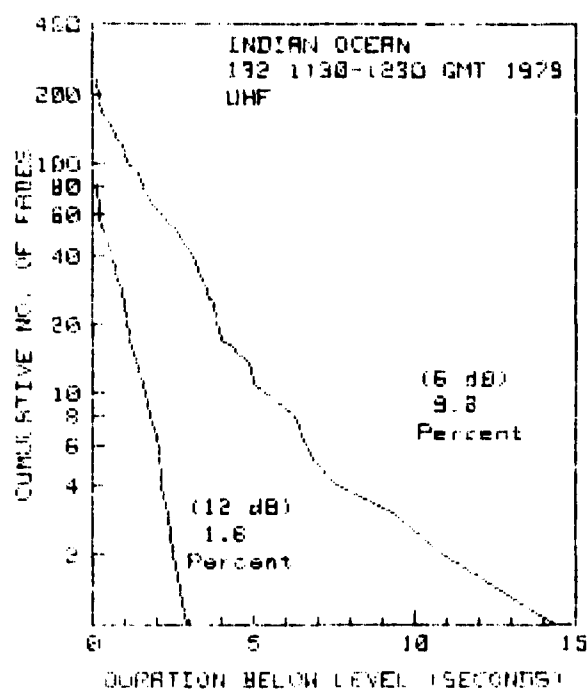
C2 (continued)



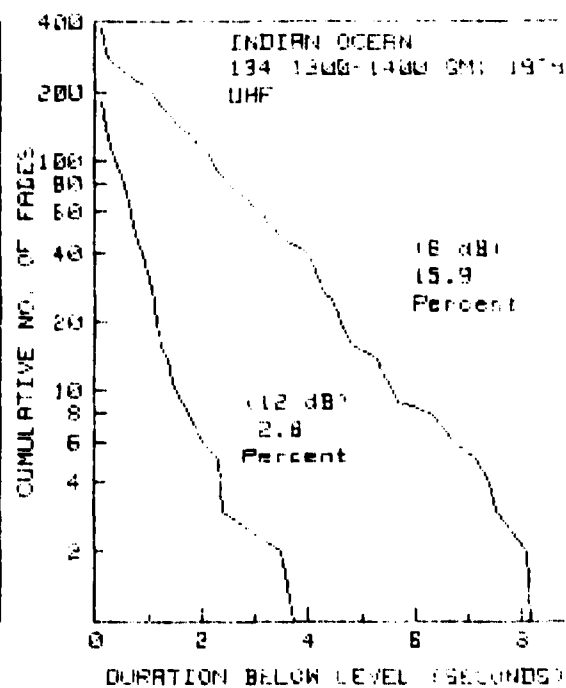
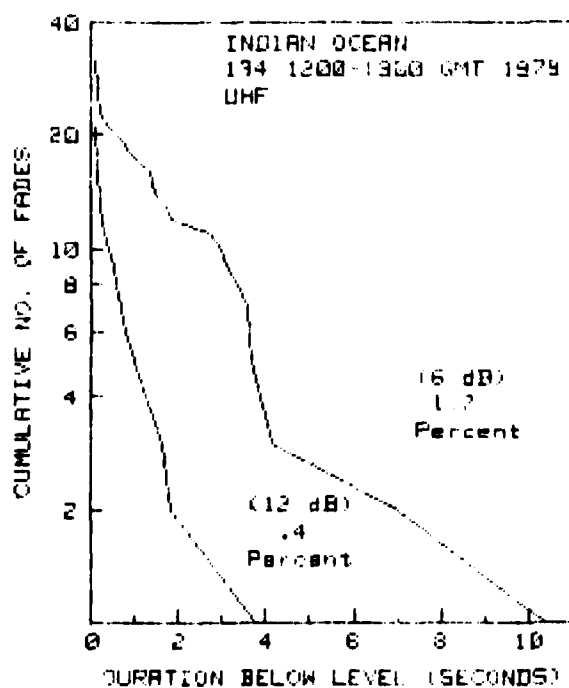
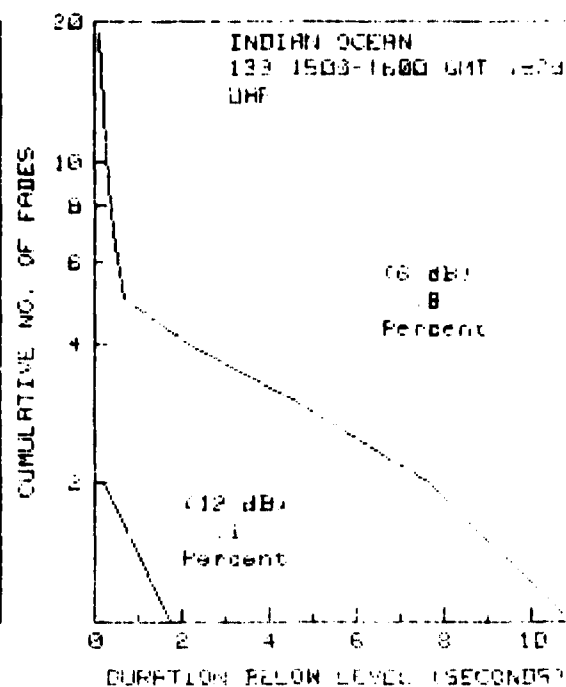
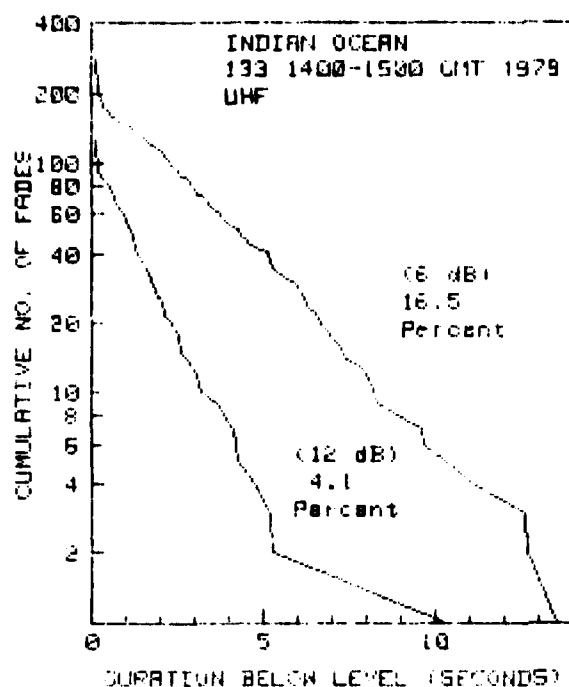
C2 (continued)



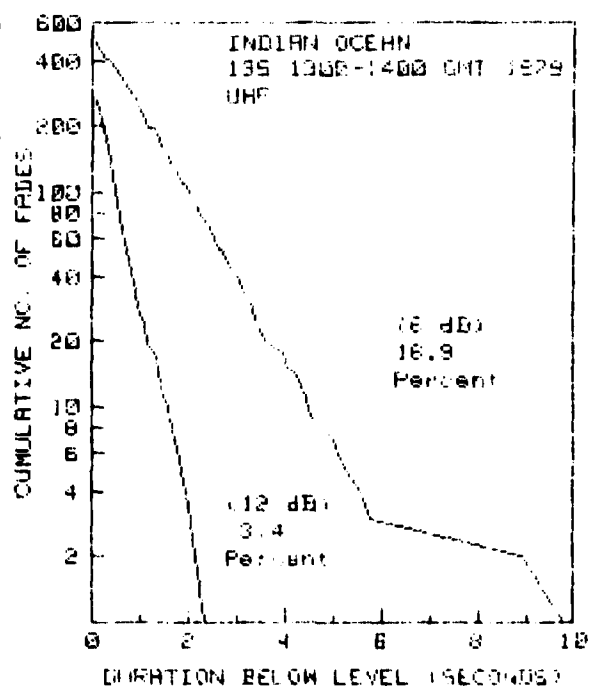
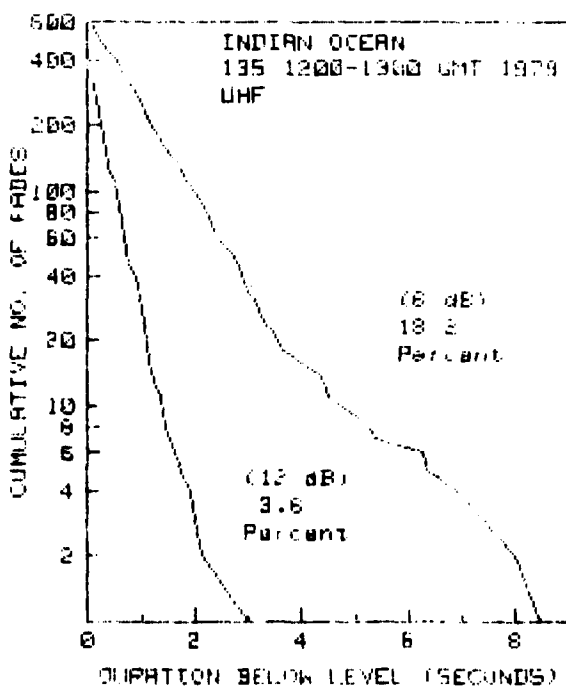
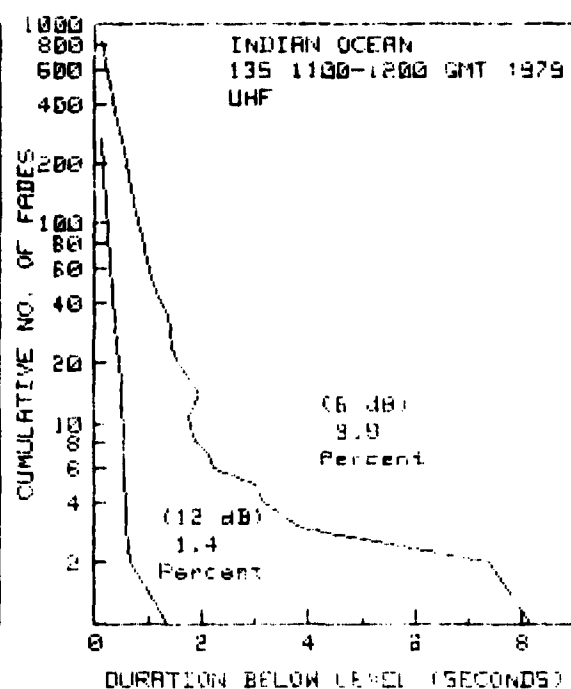
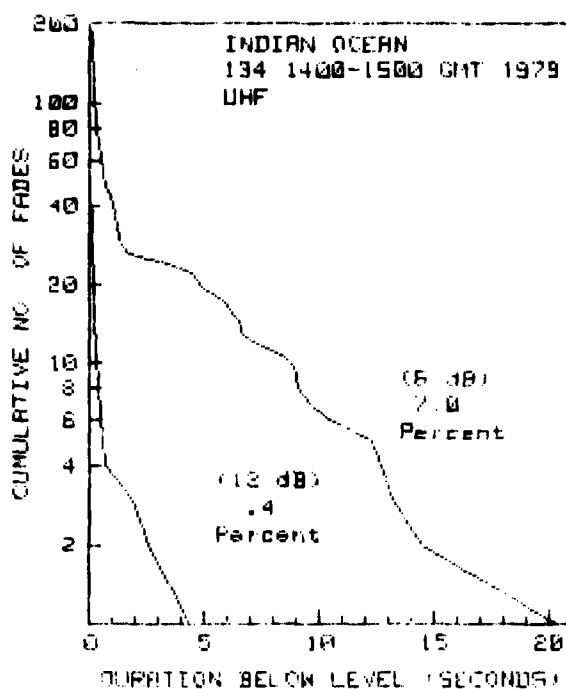
C2 (continued)



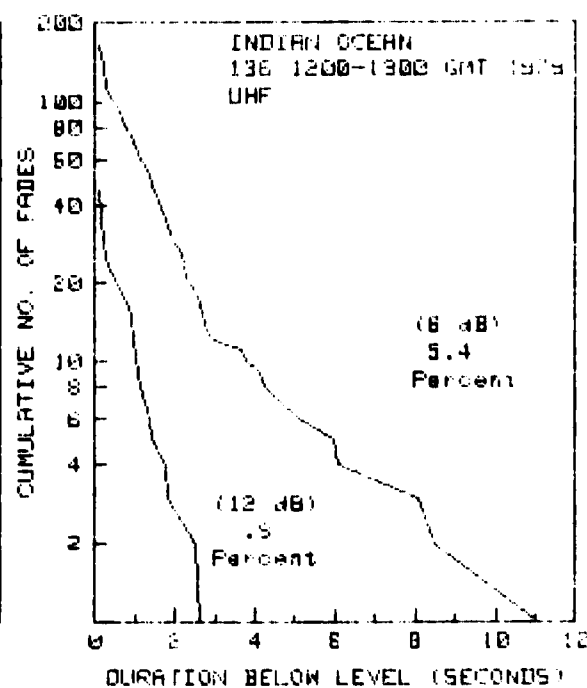
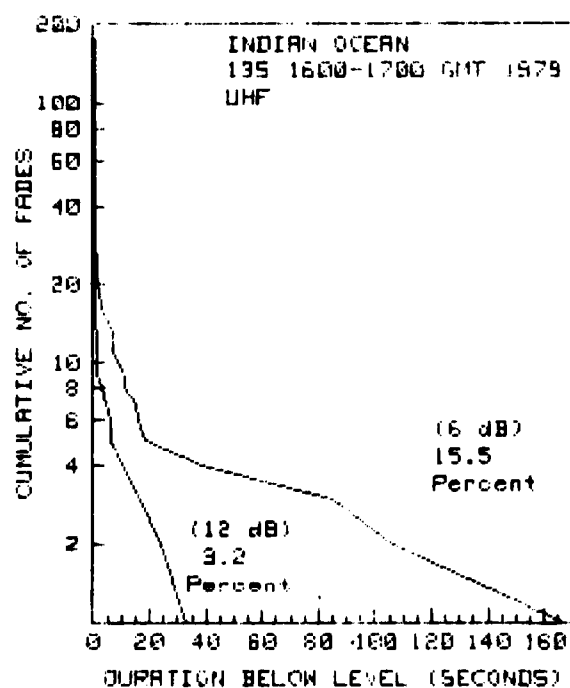
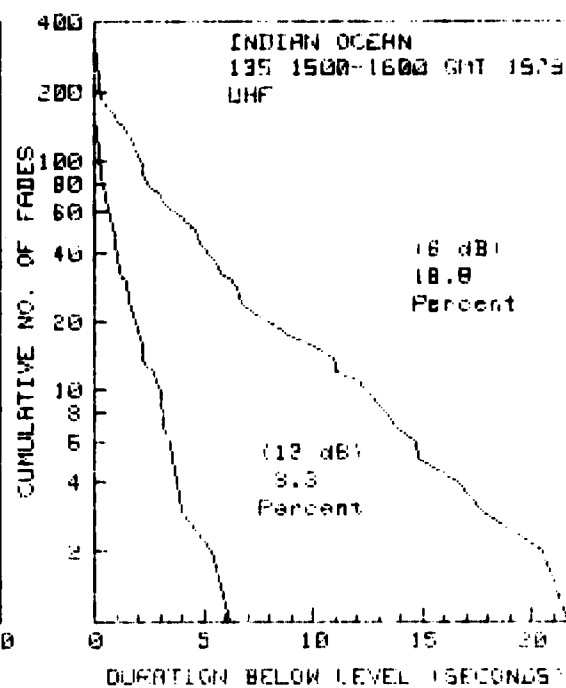
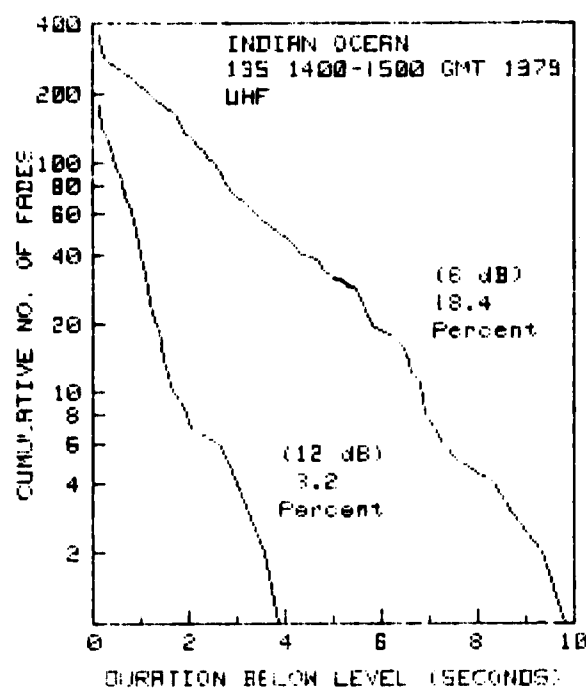
C2 (continued)



C2 (continued)

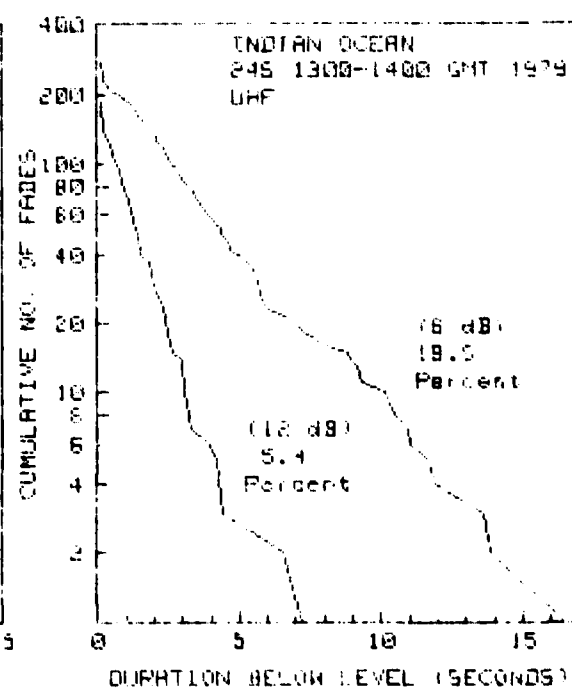
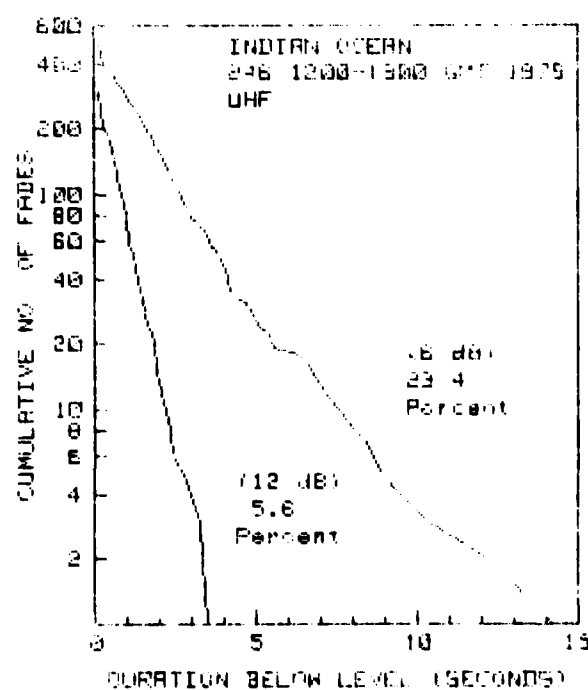
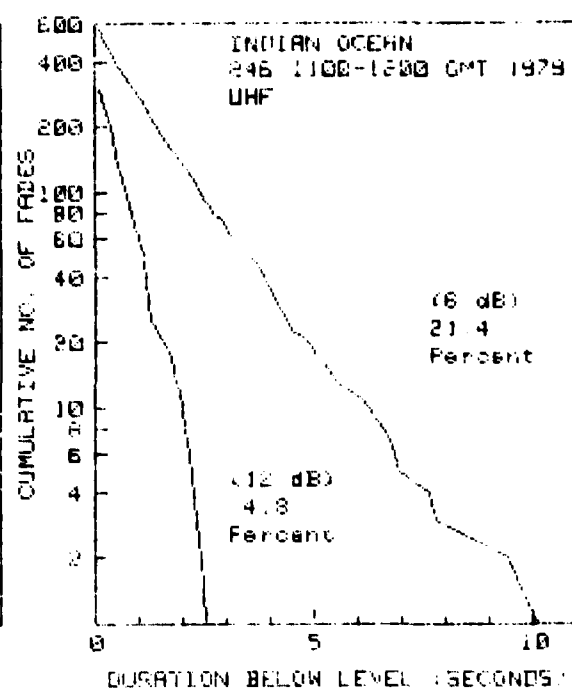
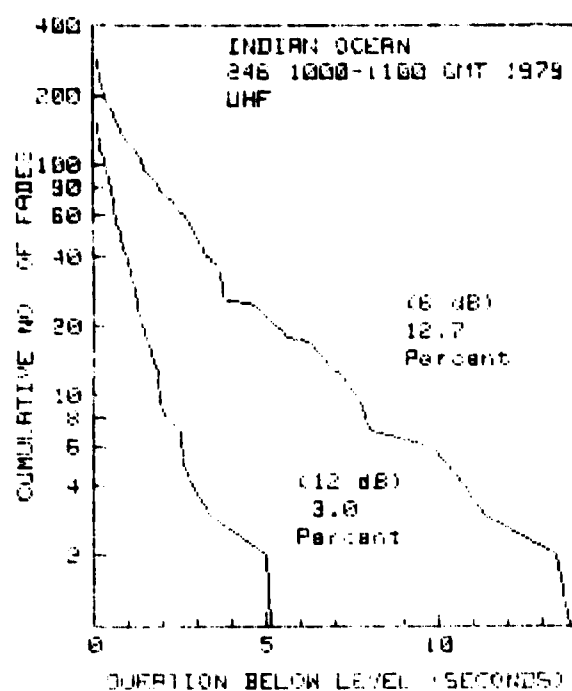


C2 (continued)

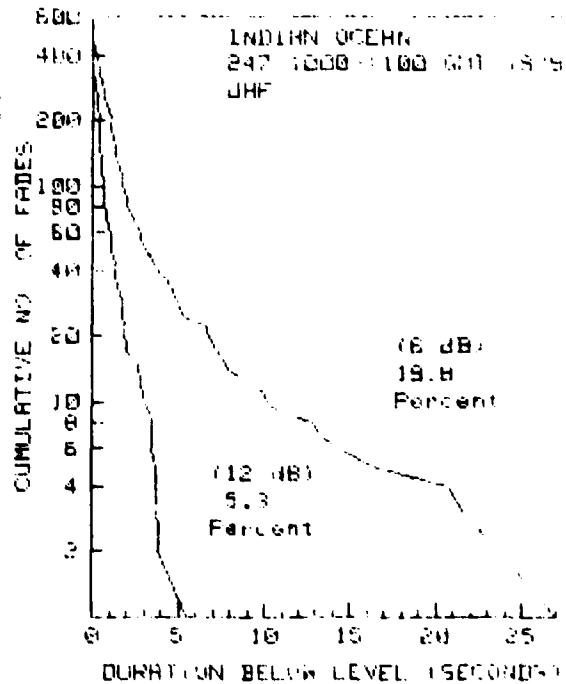
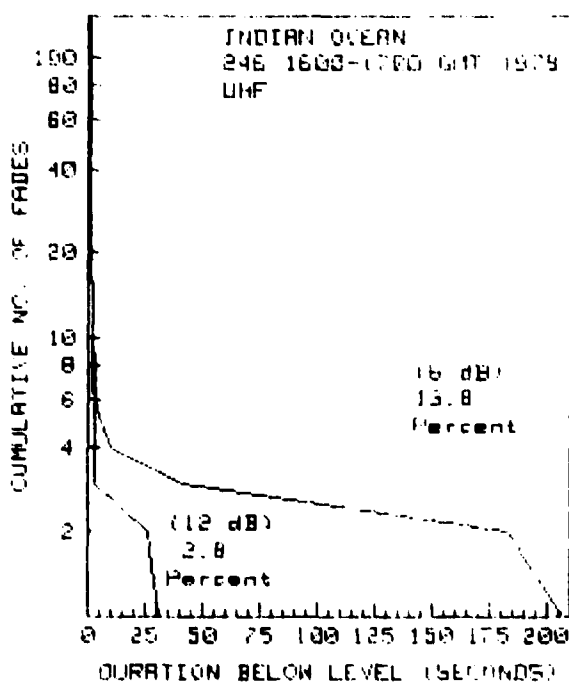
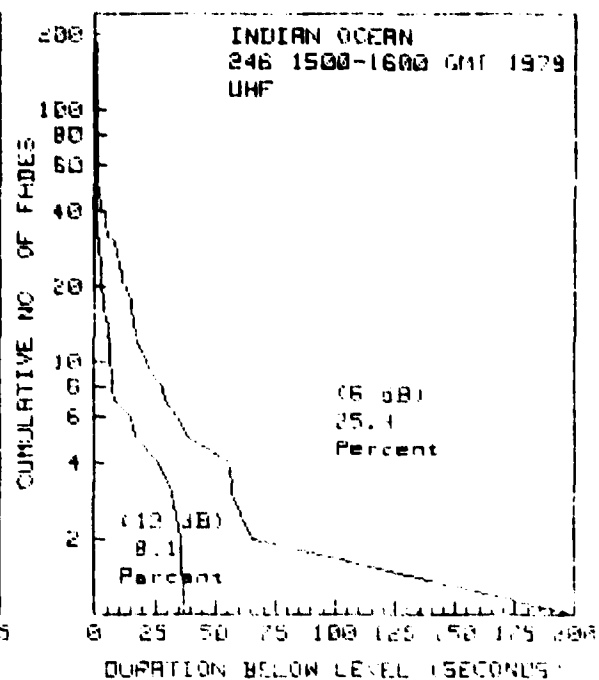
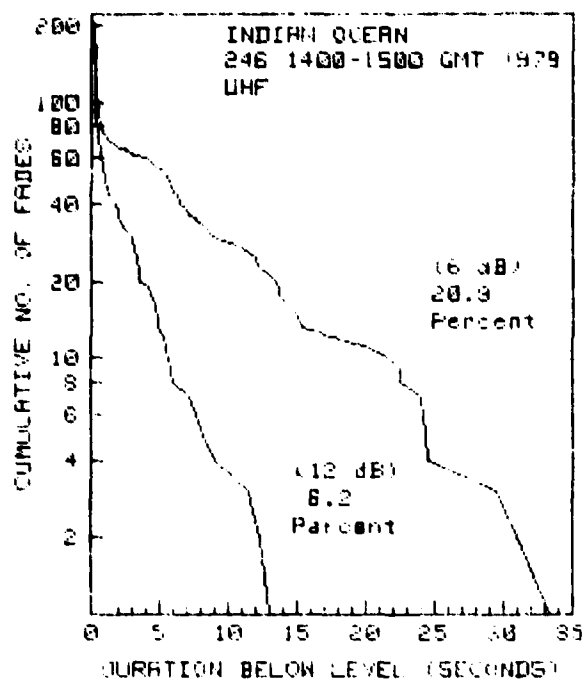


C2 (continued)

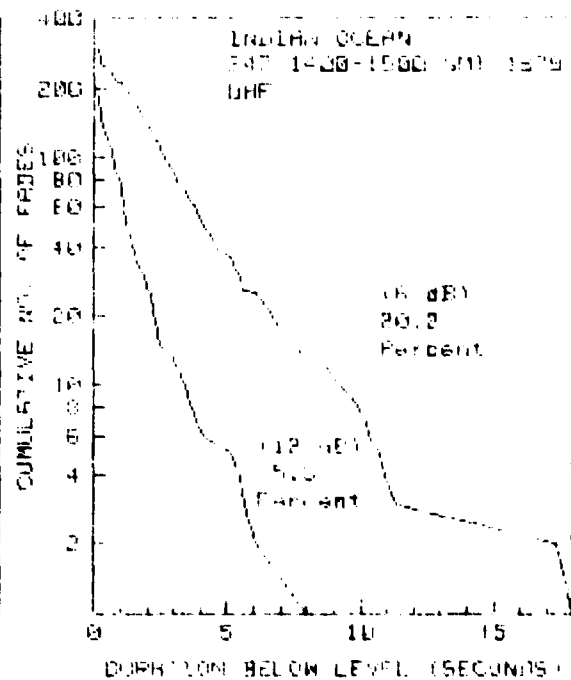
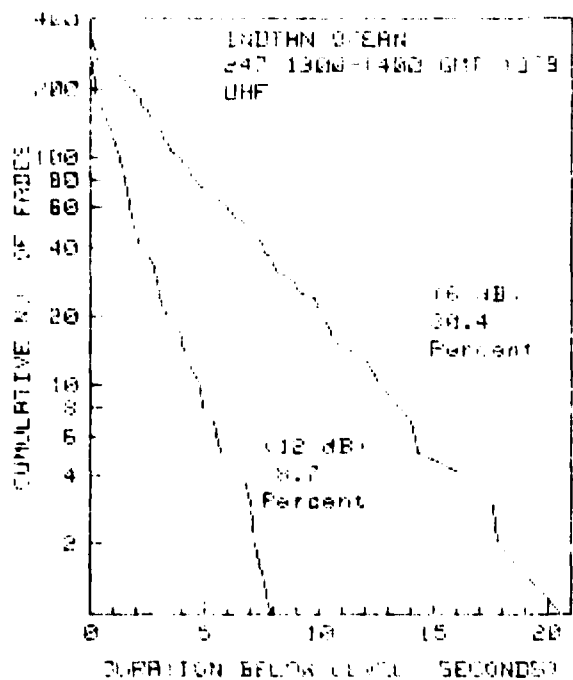
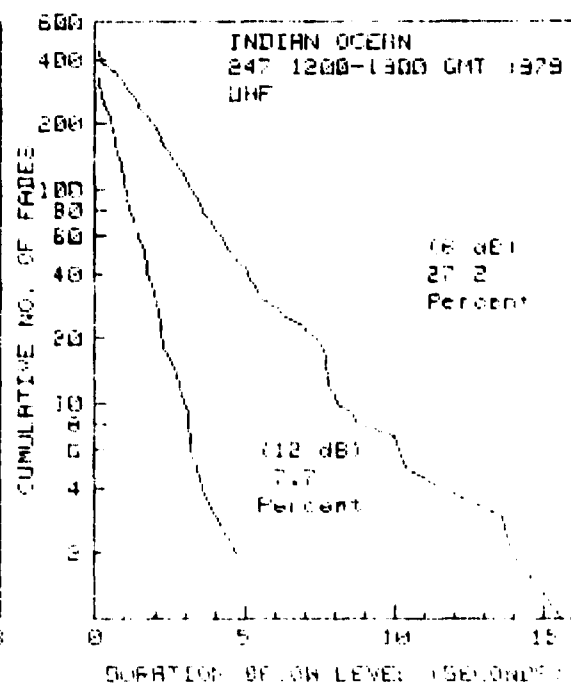
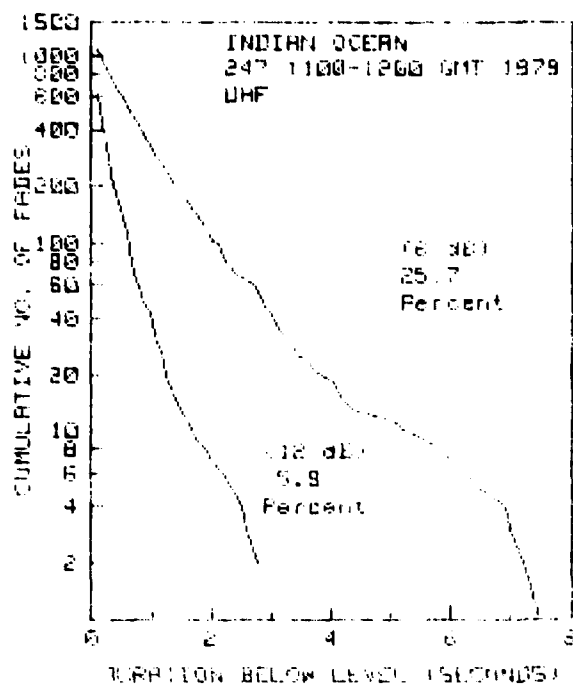




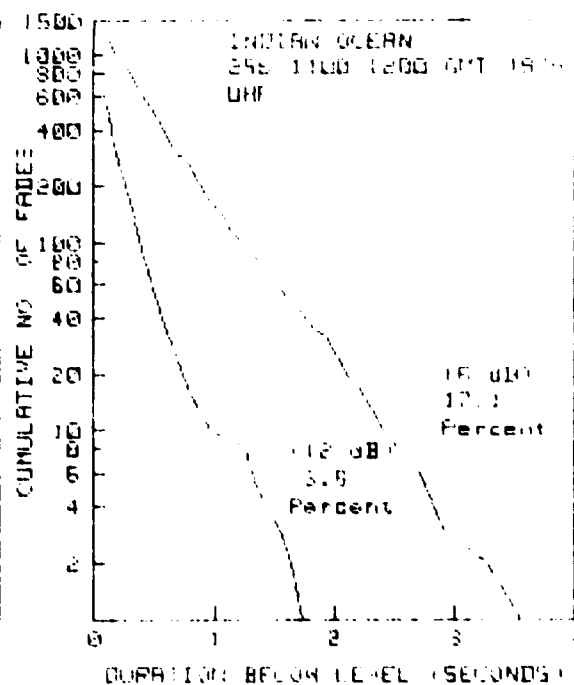
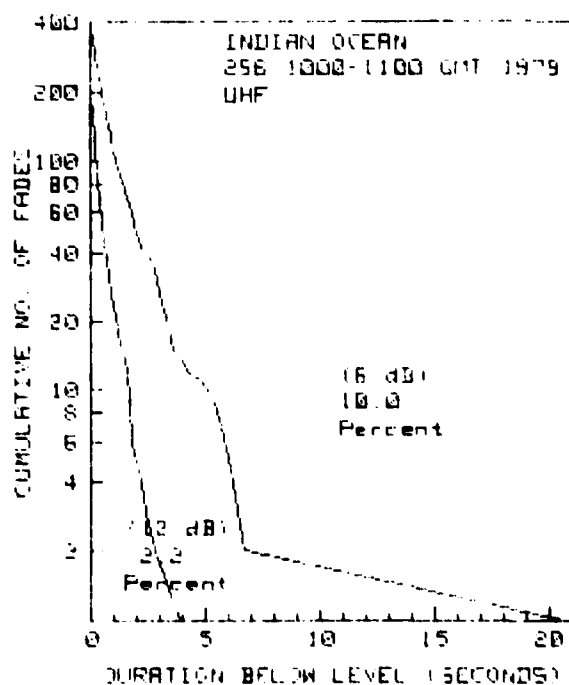
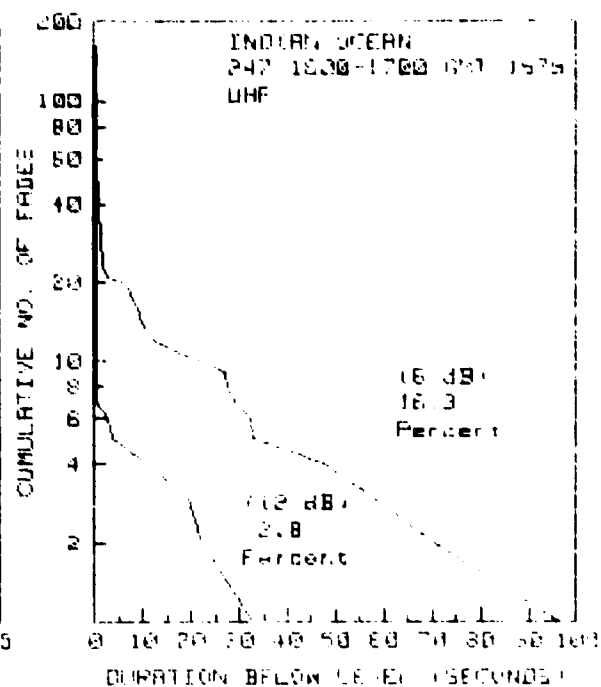
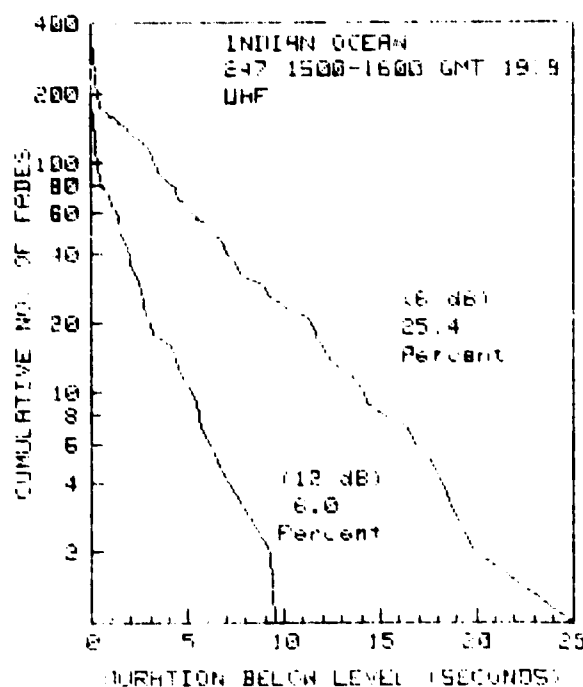
C2 (continued)



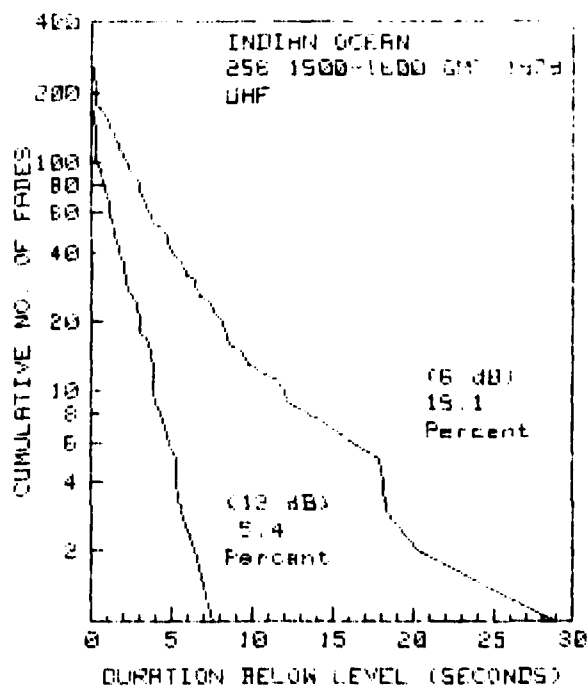
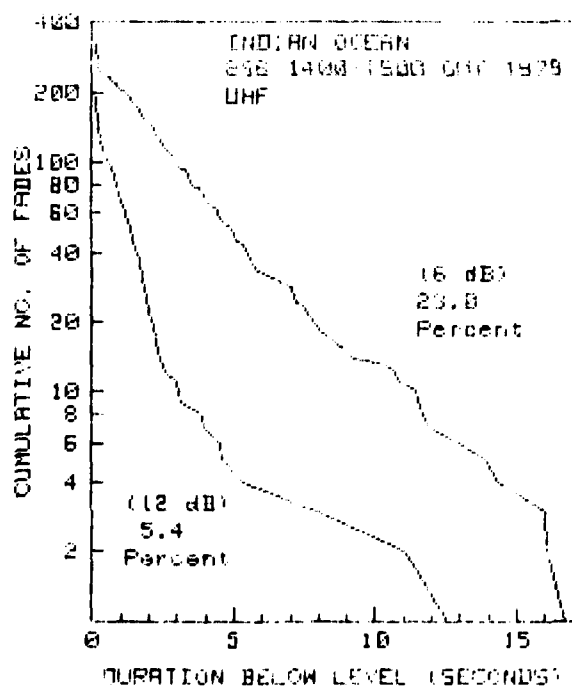
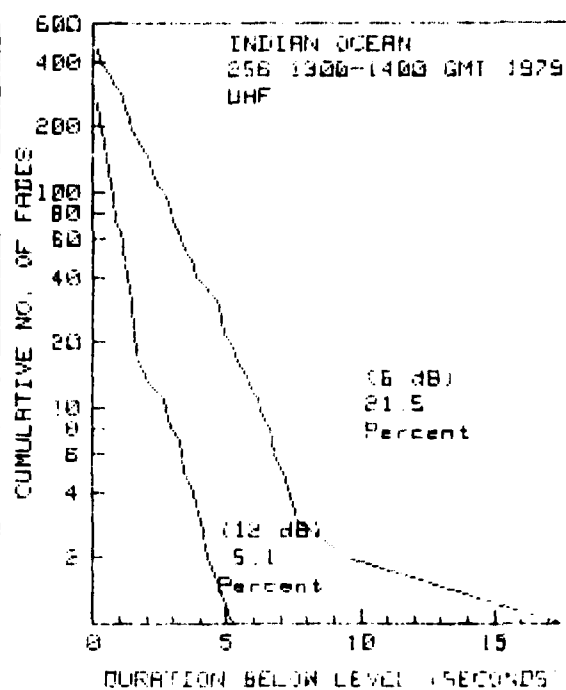
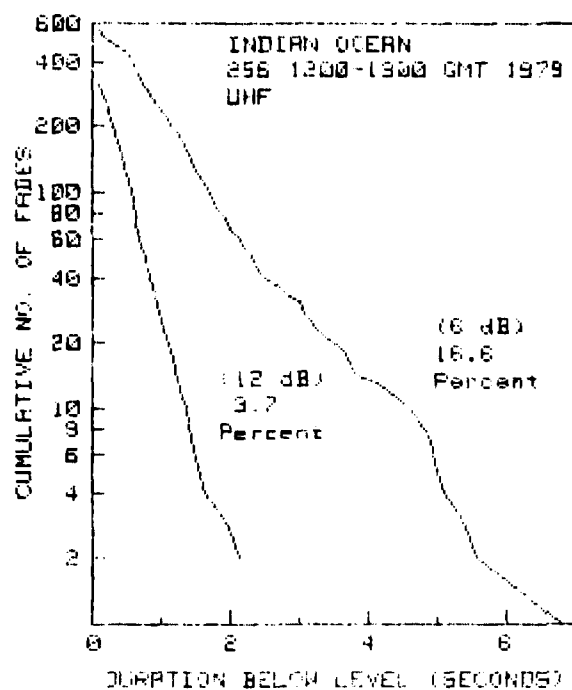
C2 (continued)



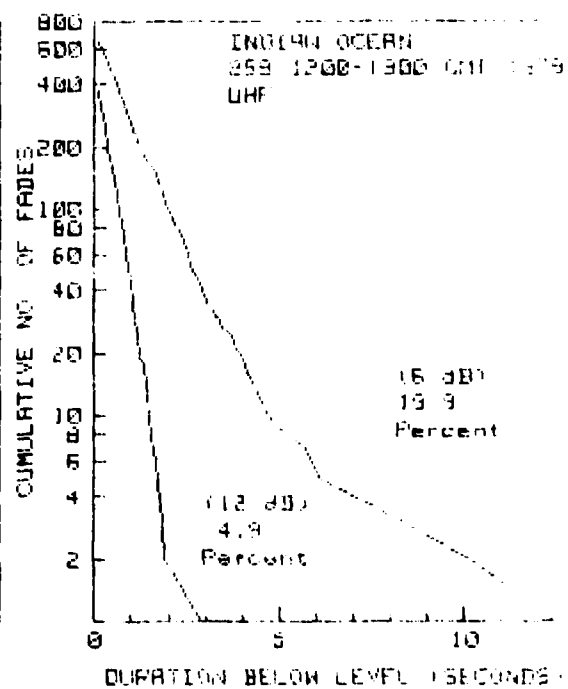
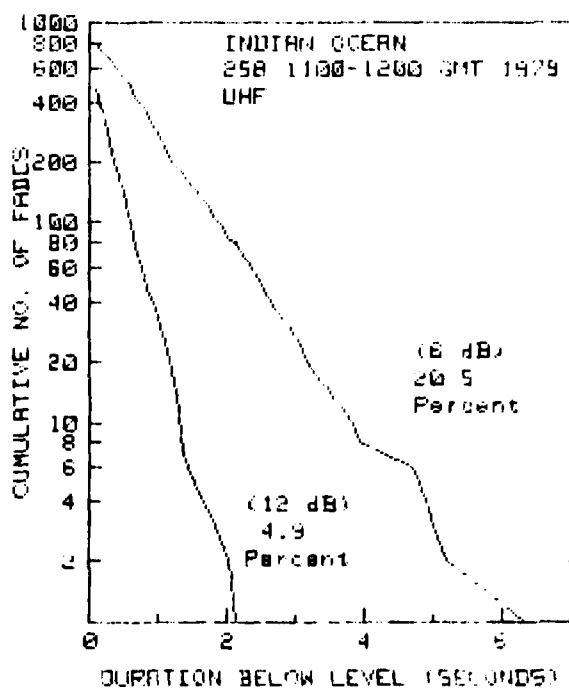
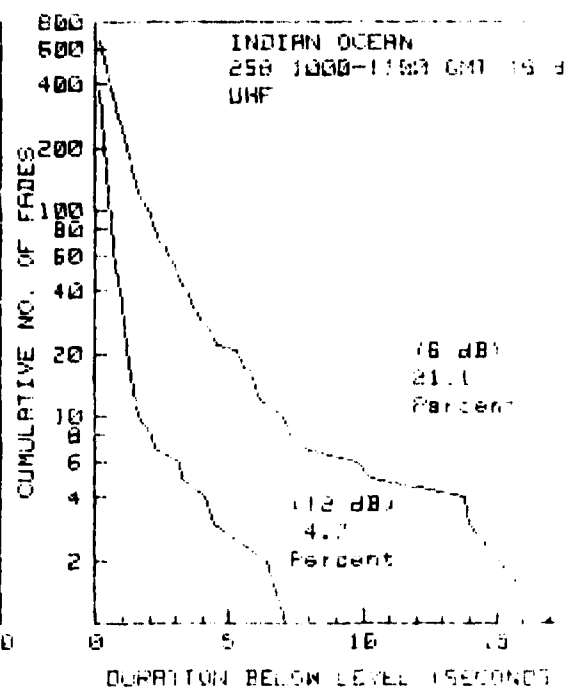
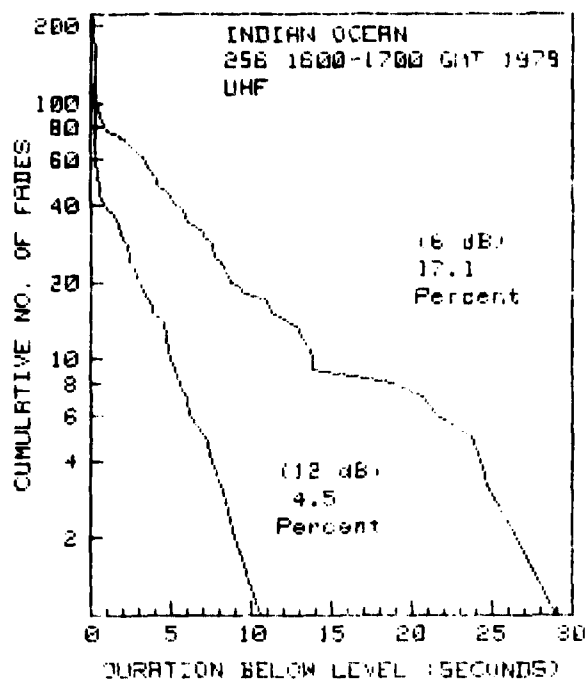
C2 (continued)



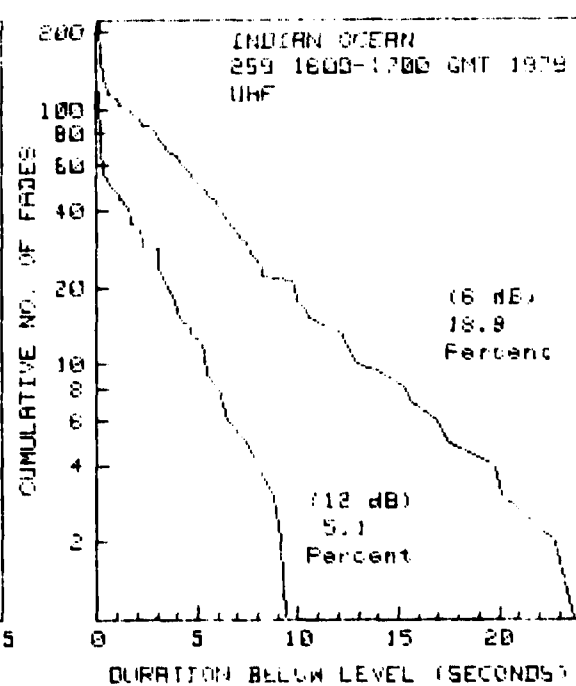
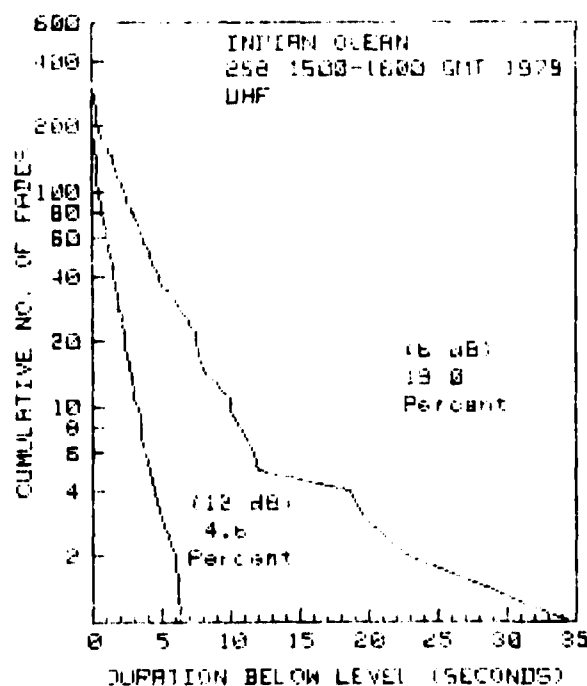
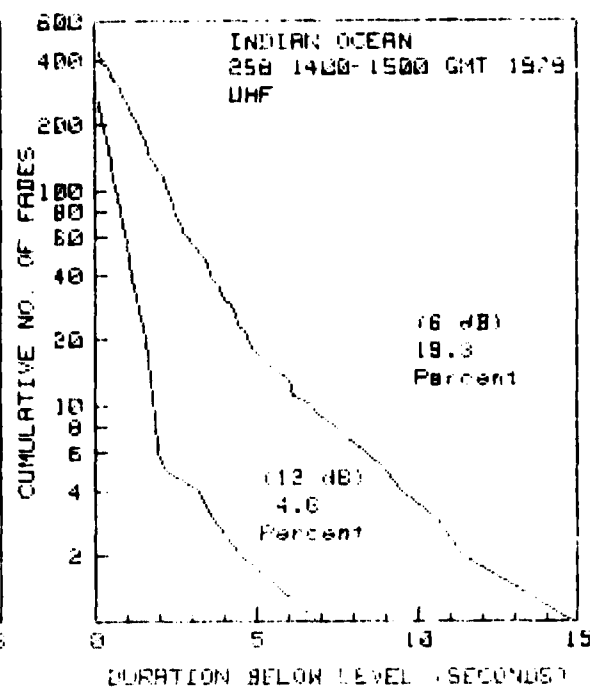
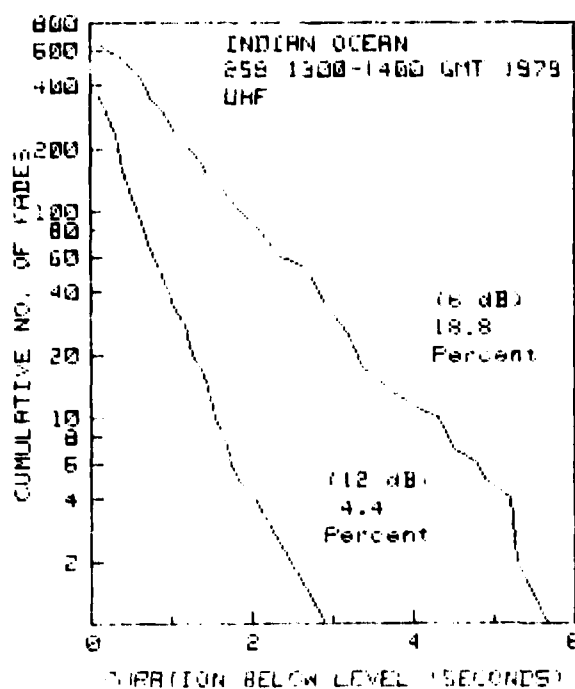
C2 (continued)



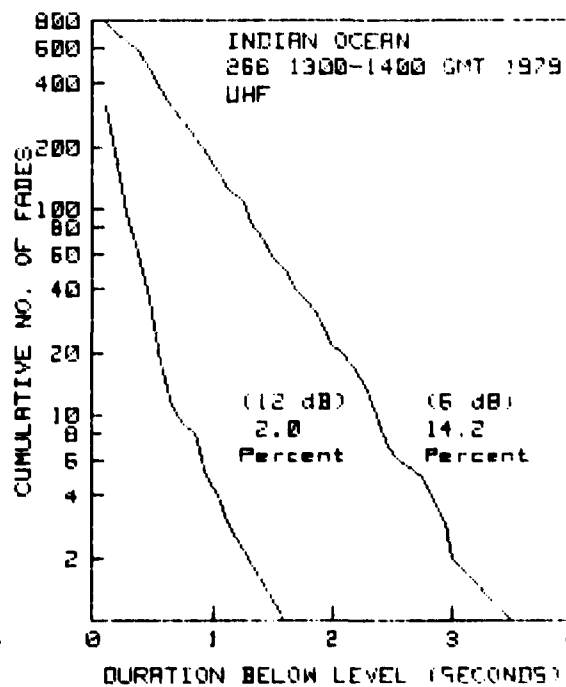
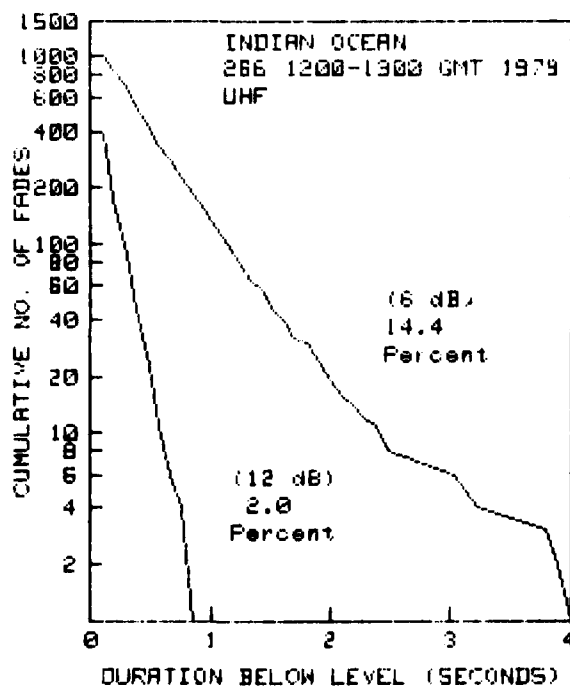
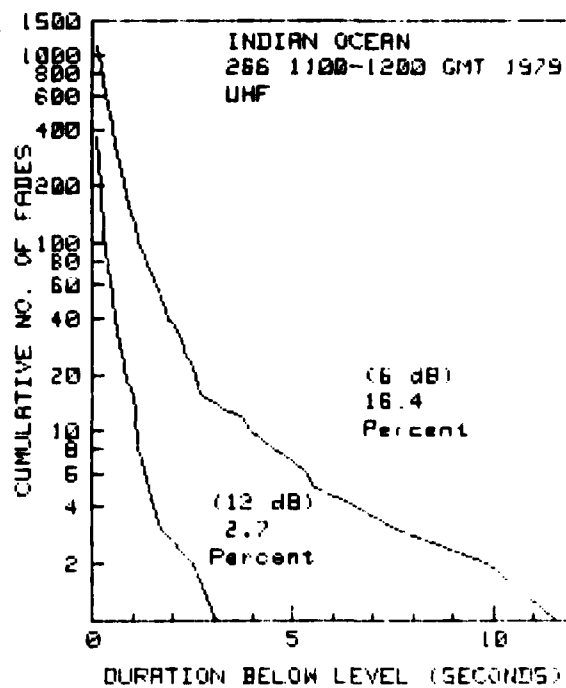
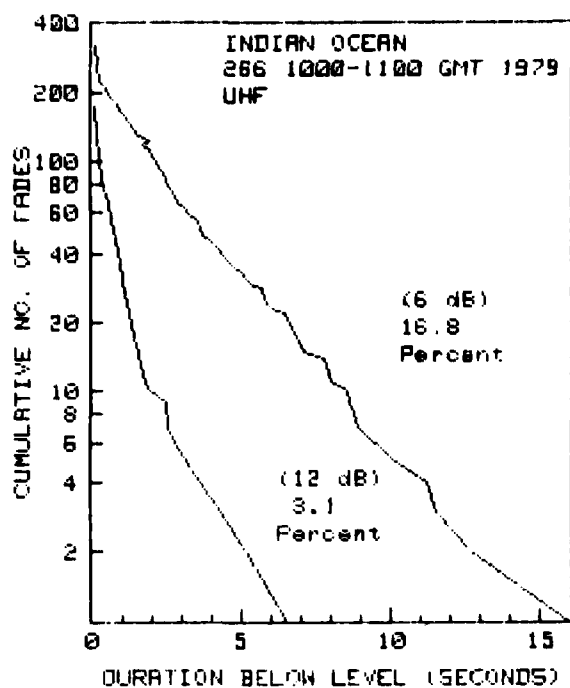
C2 (continued)



C2 (continued)

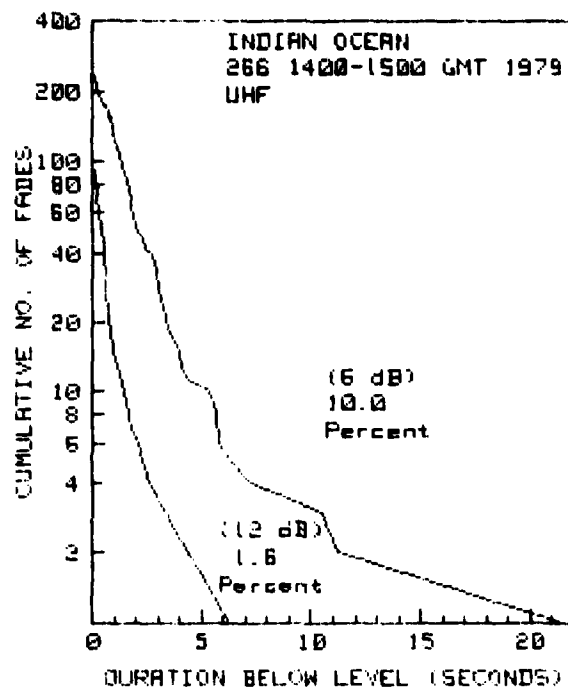


C2 (continued)



C2 (continued)





C2 (continued)

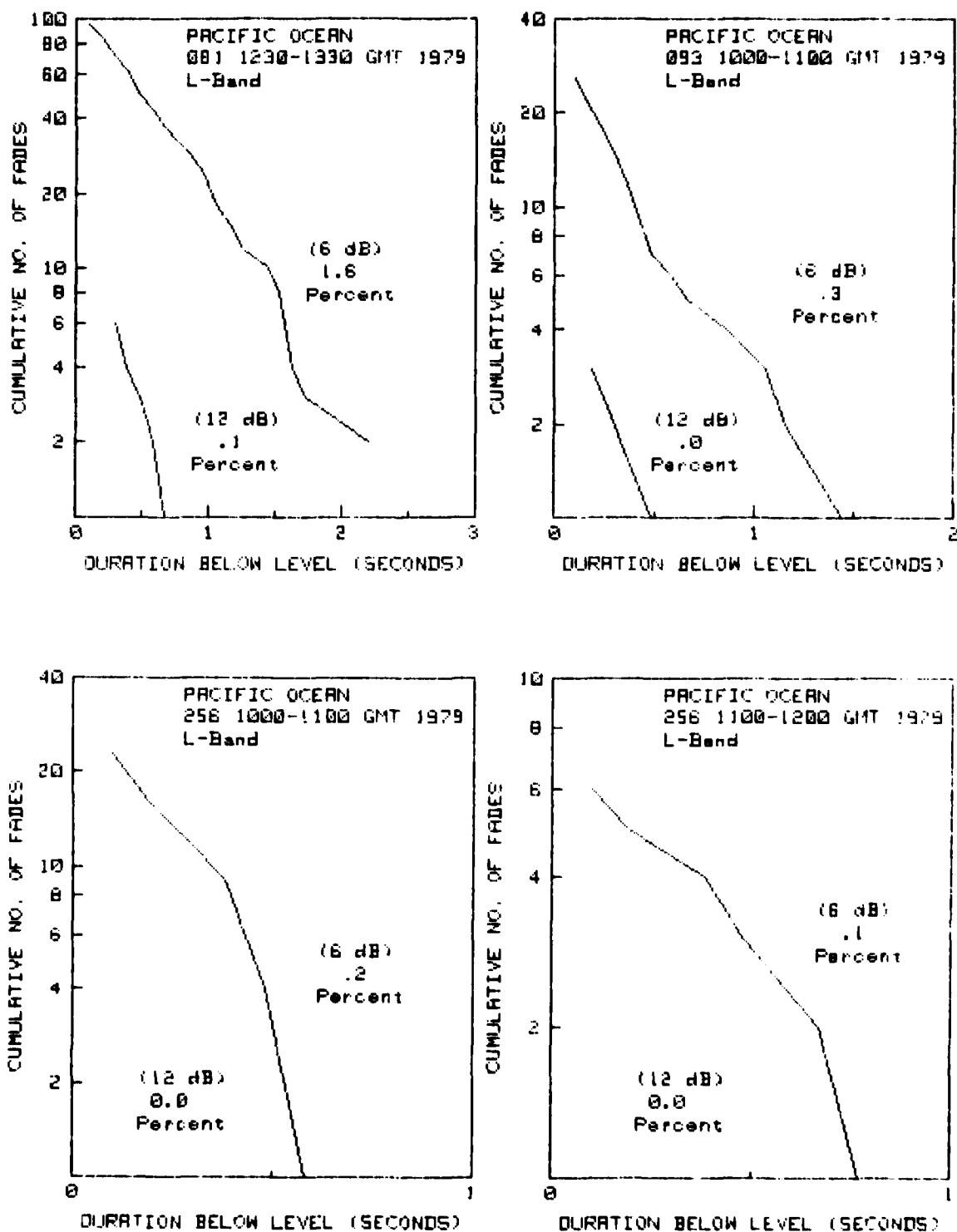
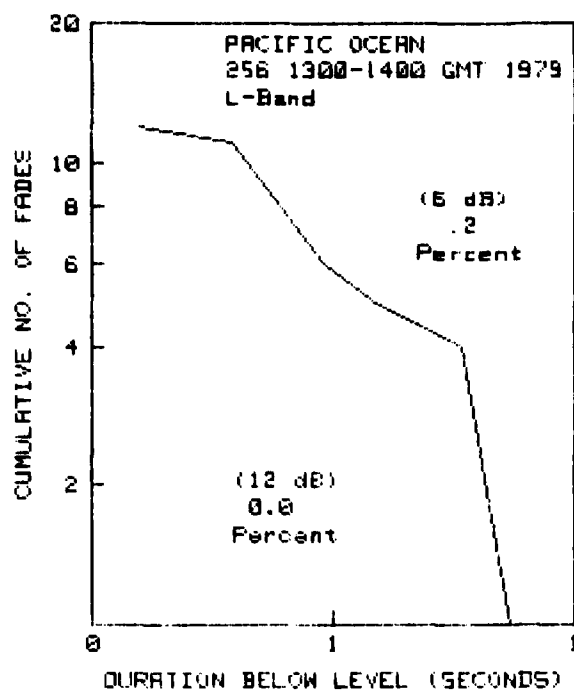


Figure C3. Cumulative L-band fade duration distribution for the Pacific Ocean satellite (elevation angle about 50°).



C 3 (continued)

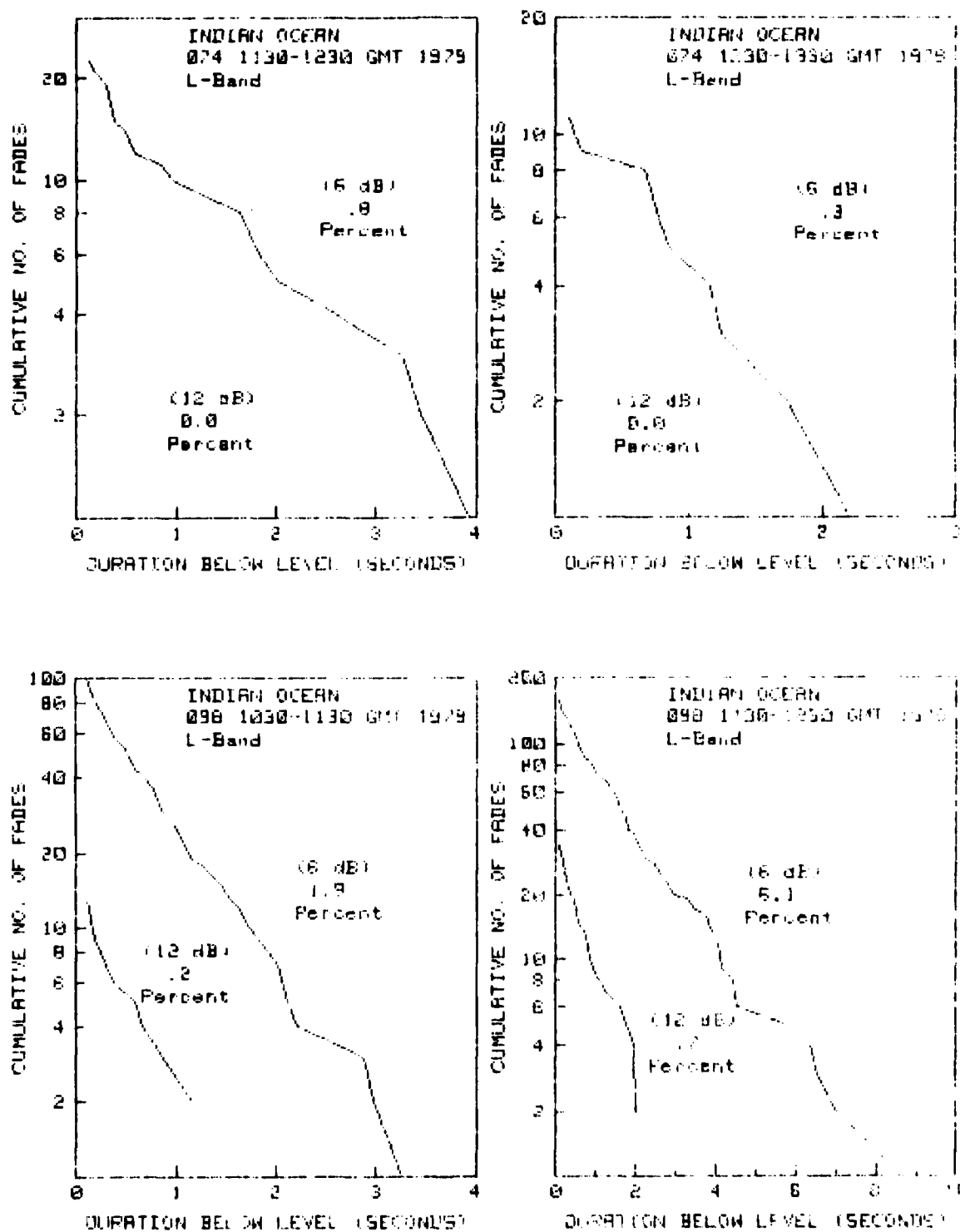
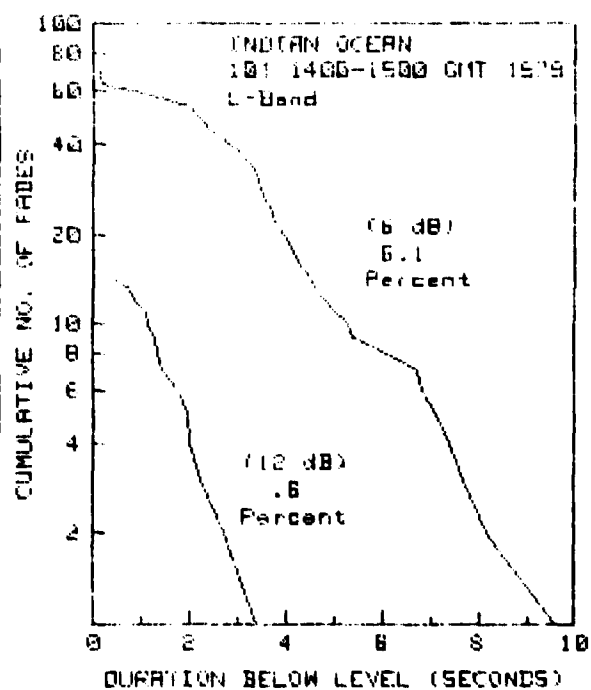
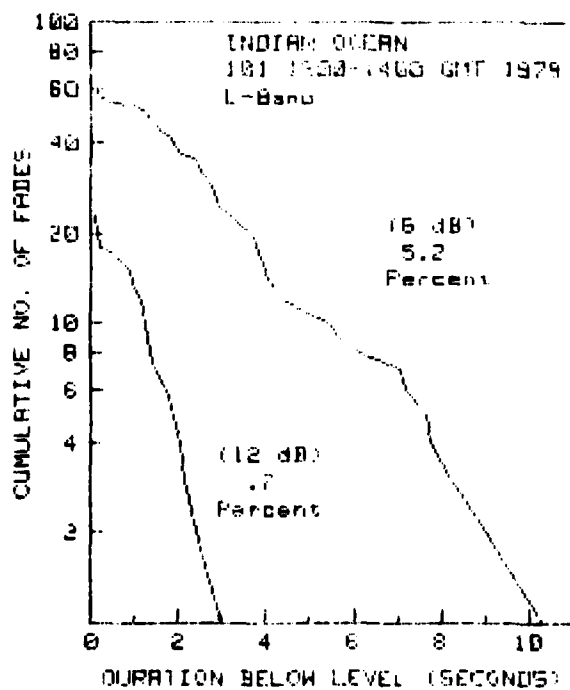
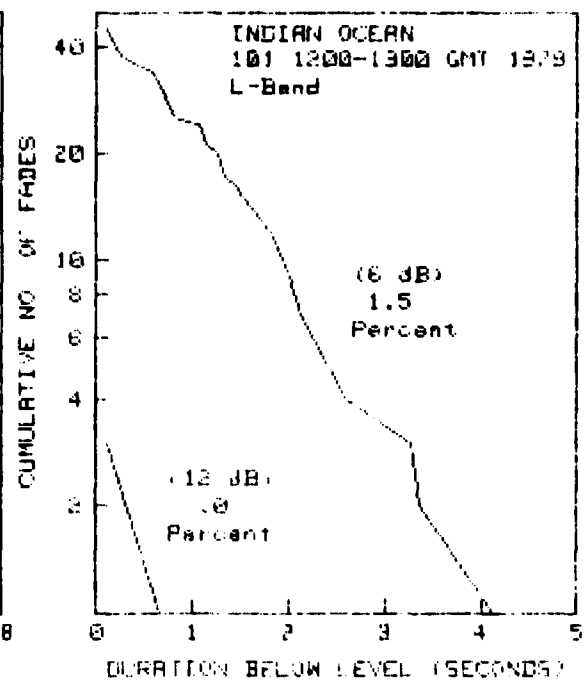
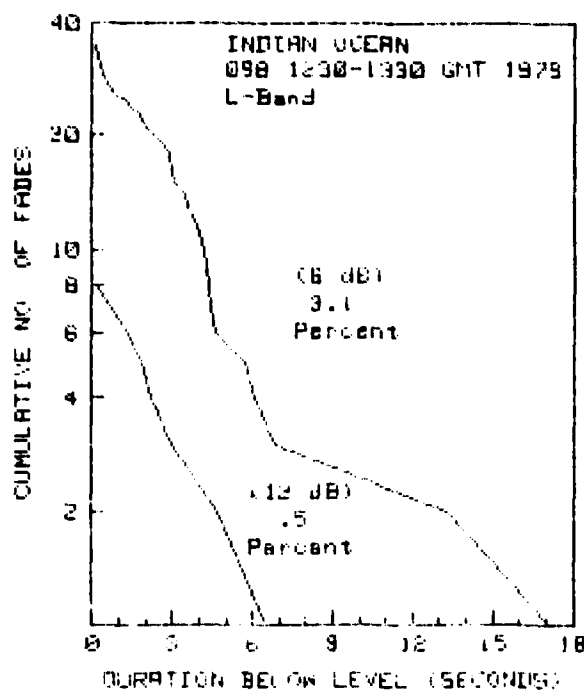
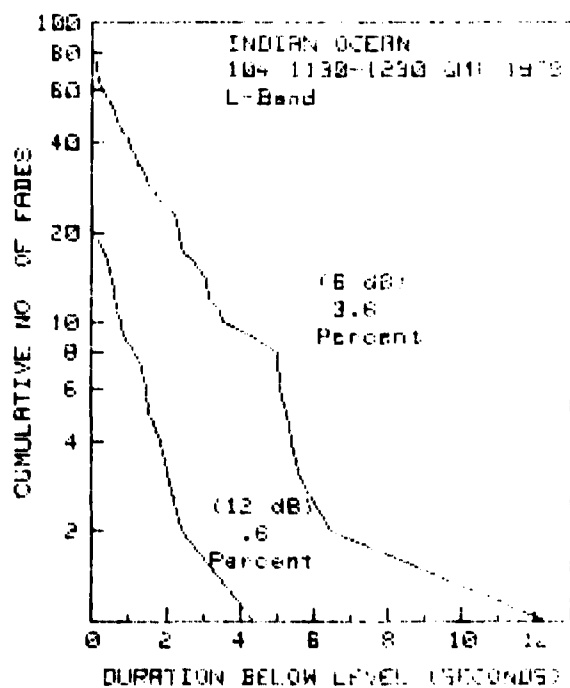
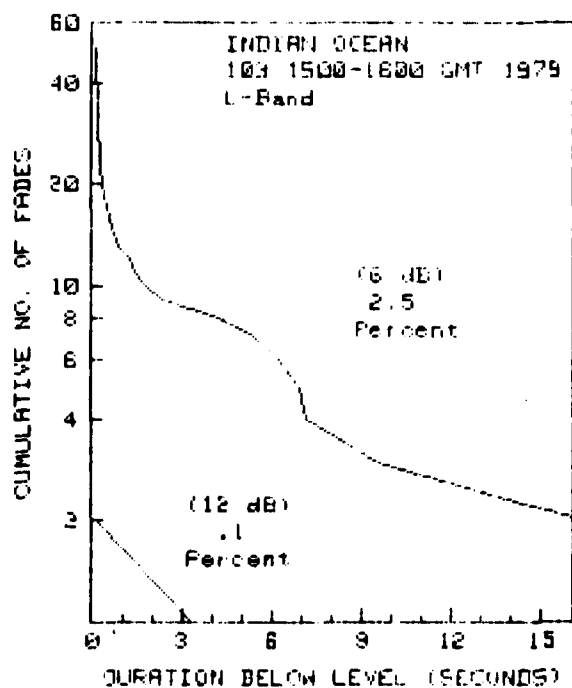
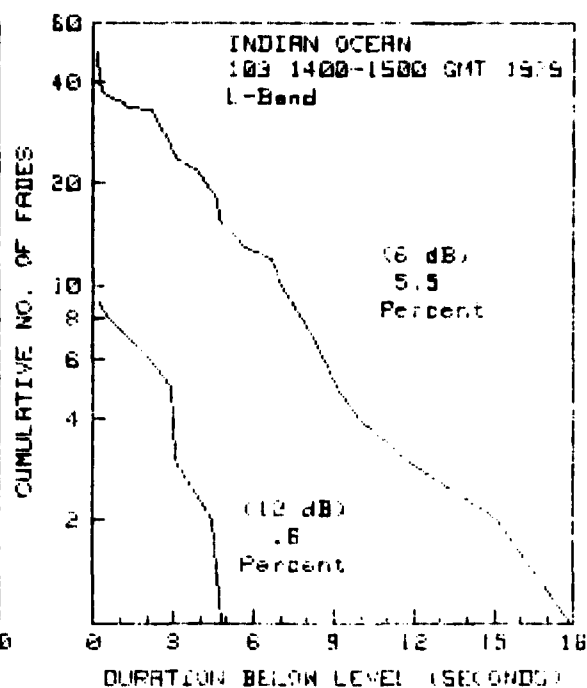
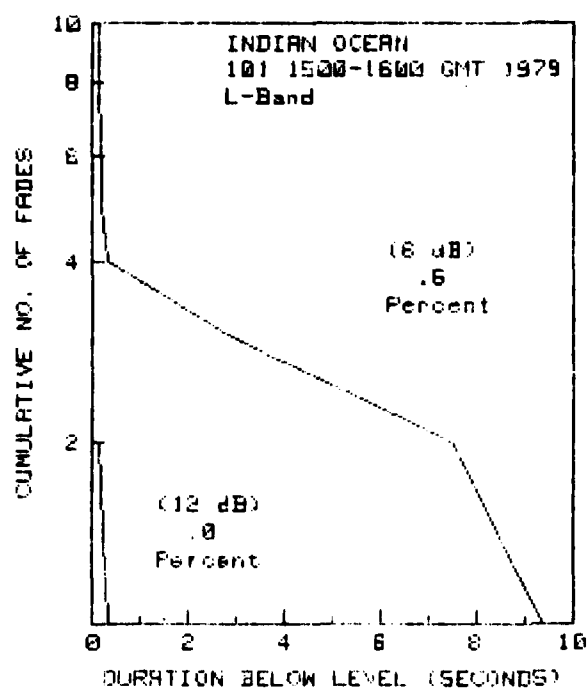


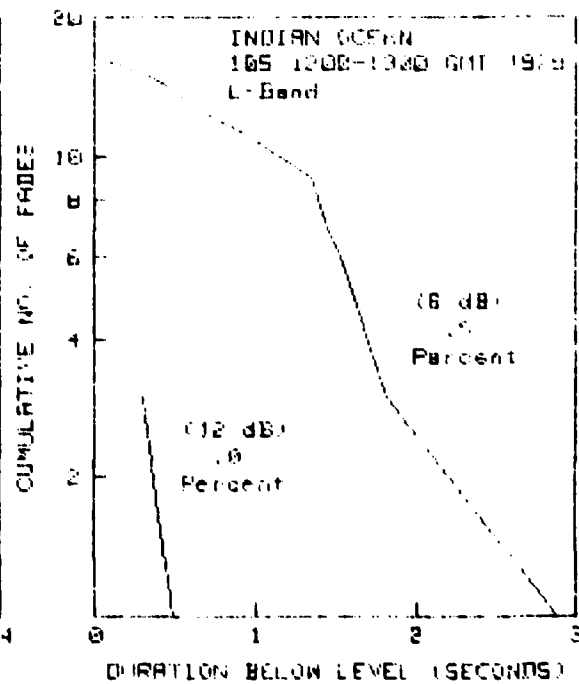
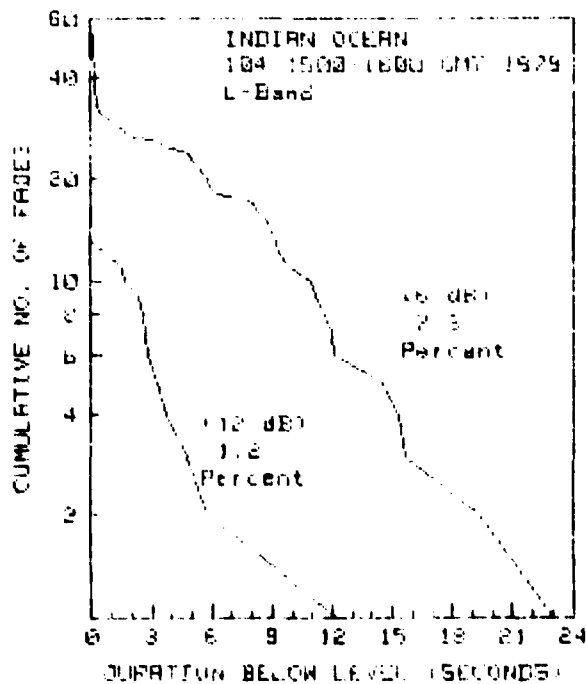
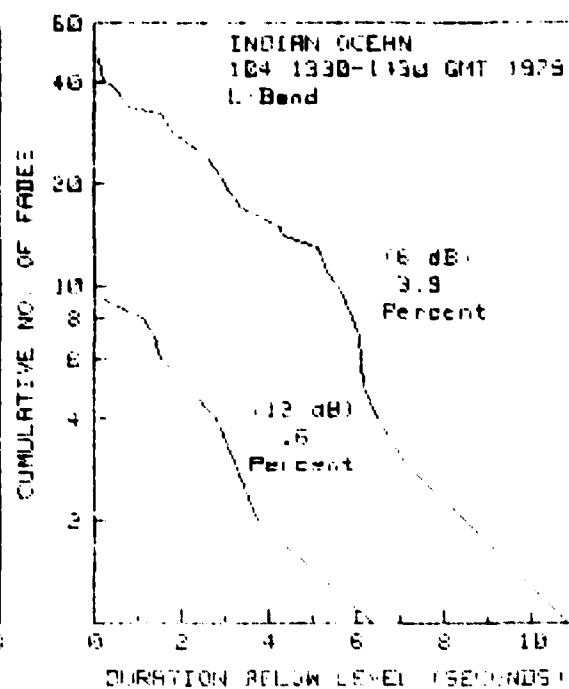
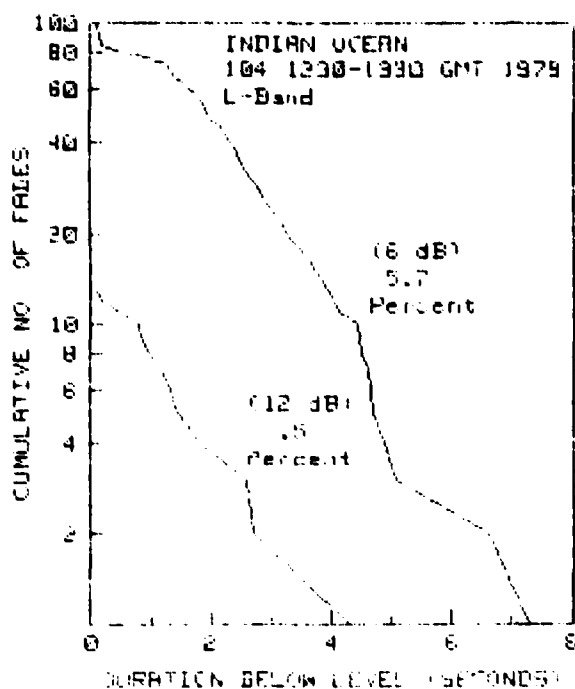
Figure C4. Cumulative L-band fade duration distribution for the Indian Ocean satellite (elevation angle about  $10^\circ$ ).



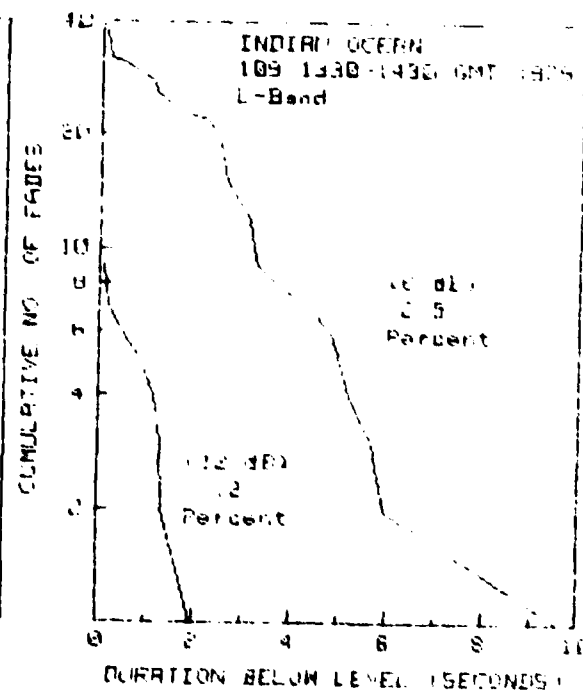
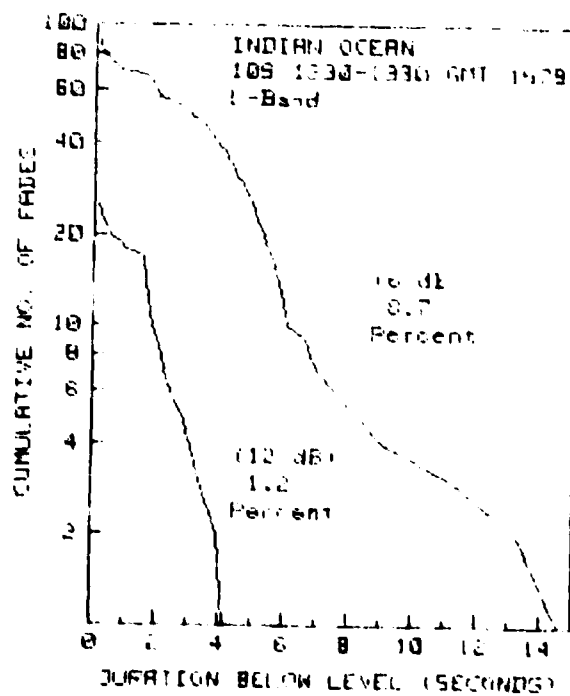
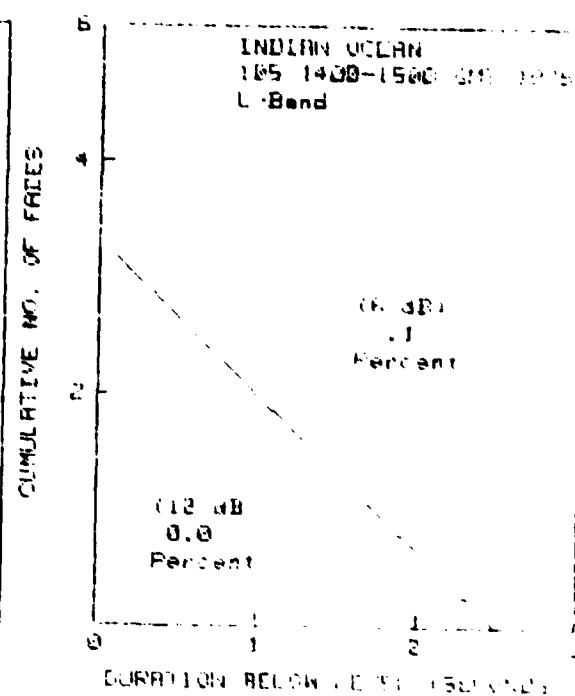
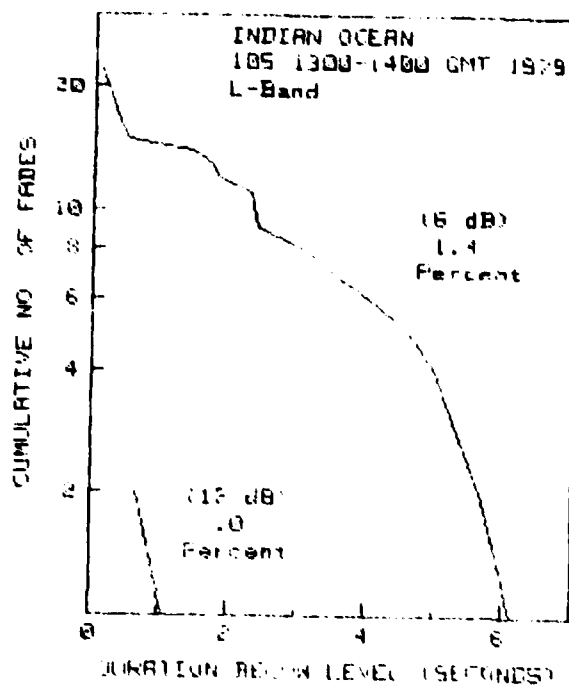
C4 (continued)



C4 (continued)

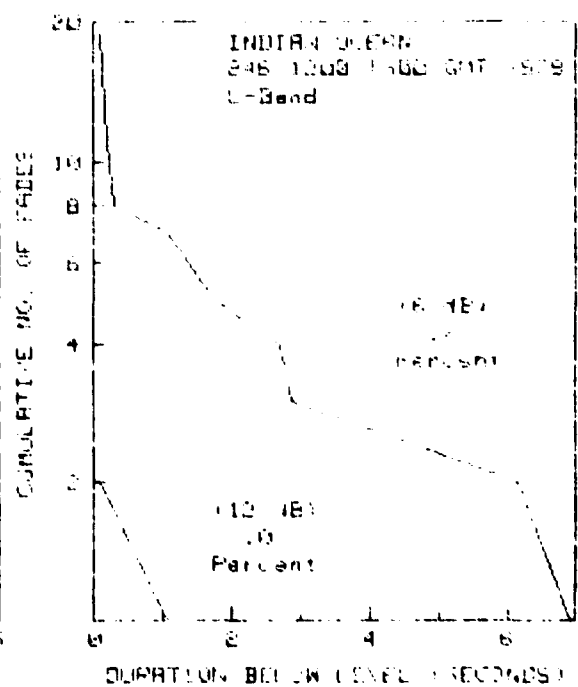
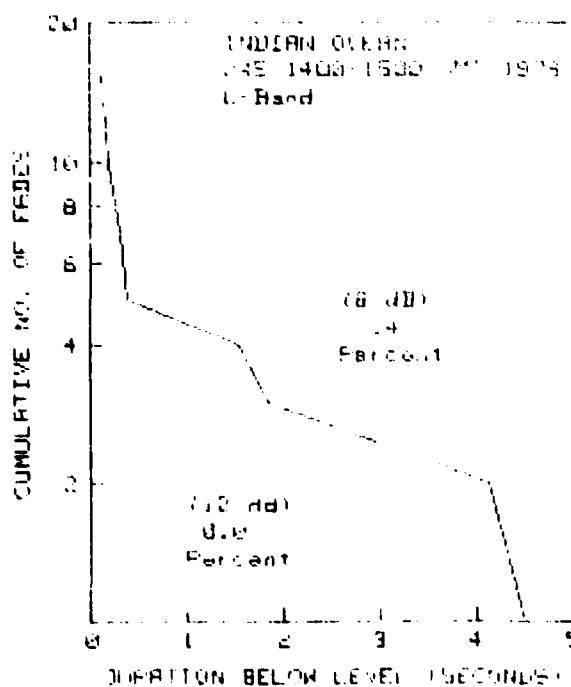
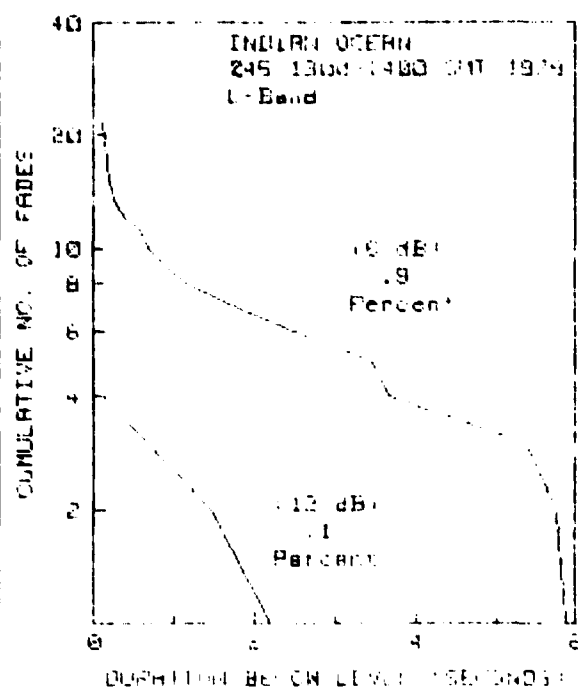
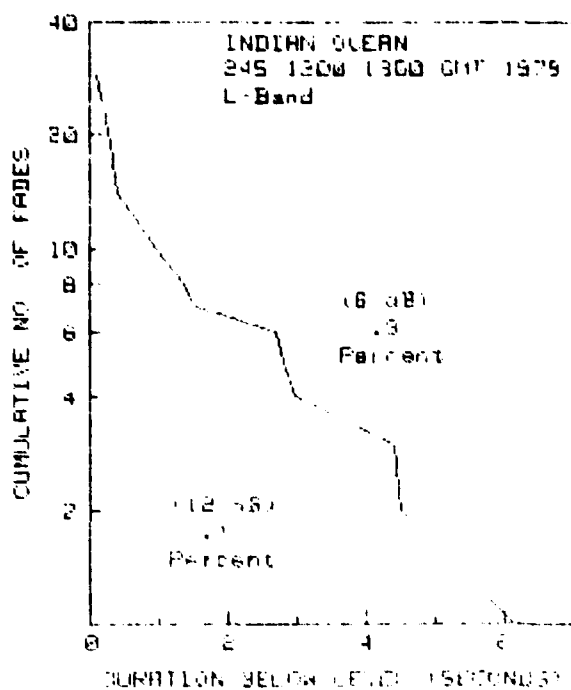


C4 (continued)

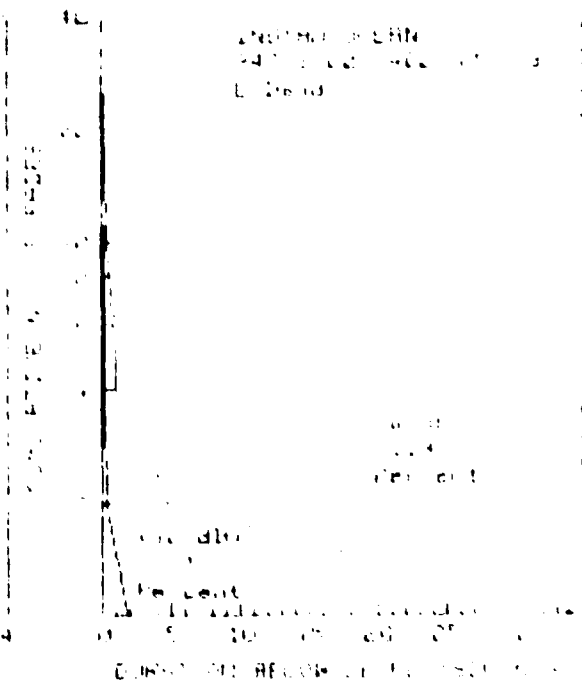
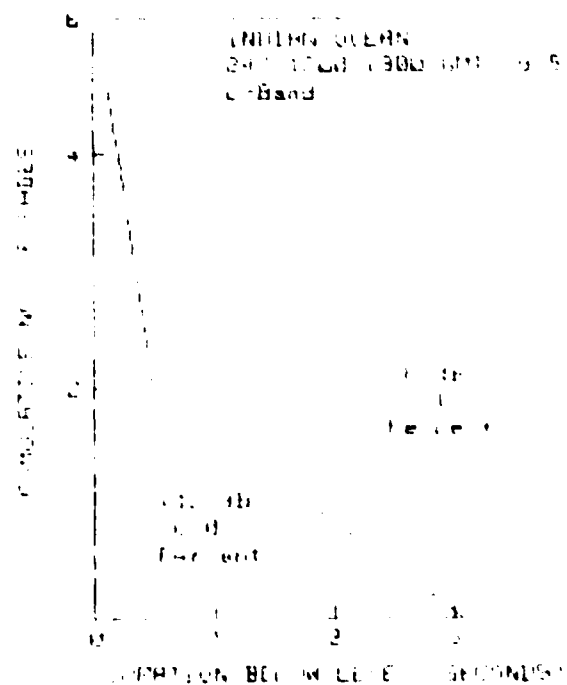
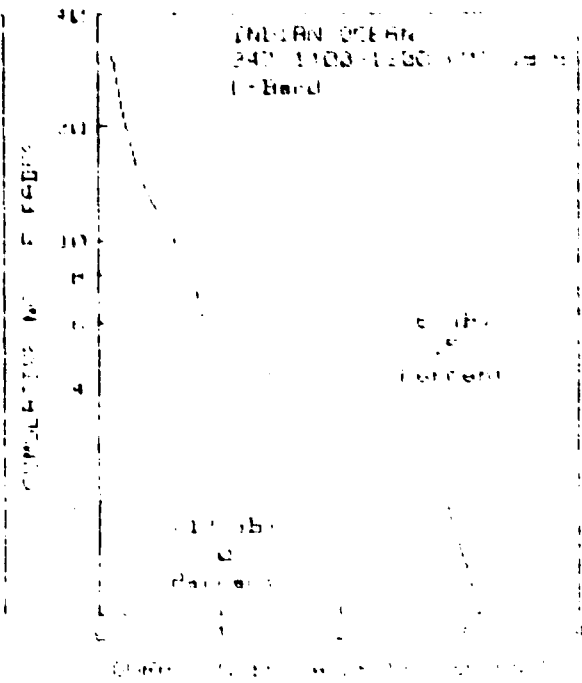
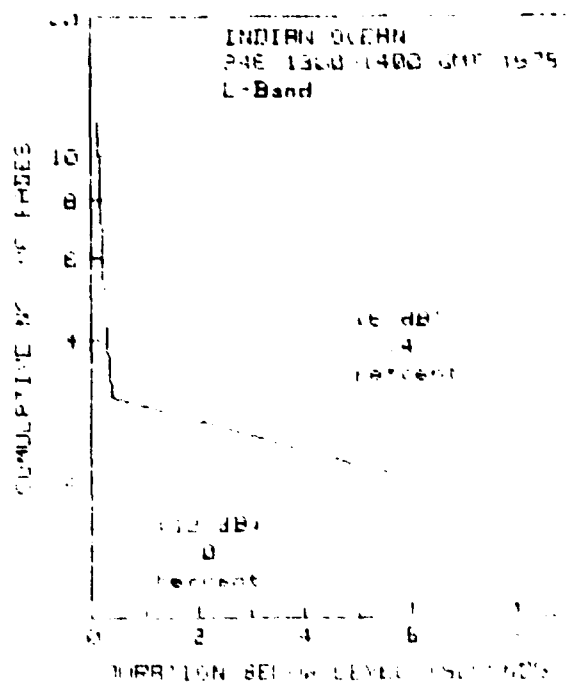


C4 (continued)

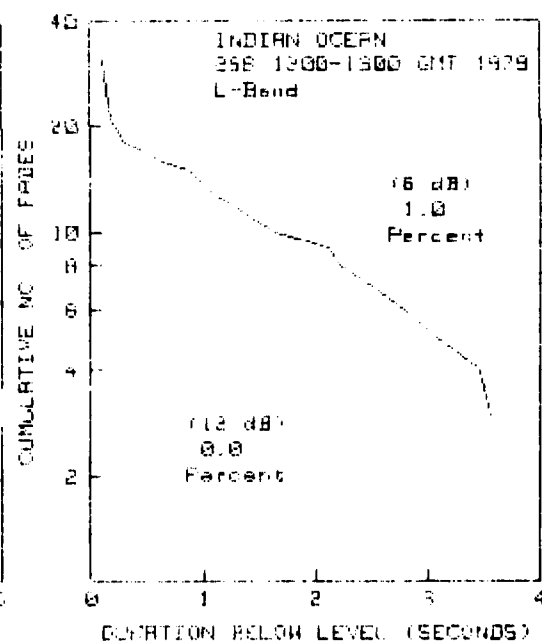
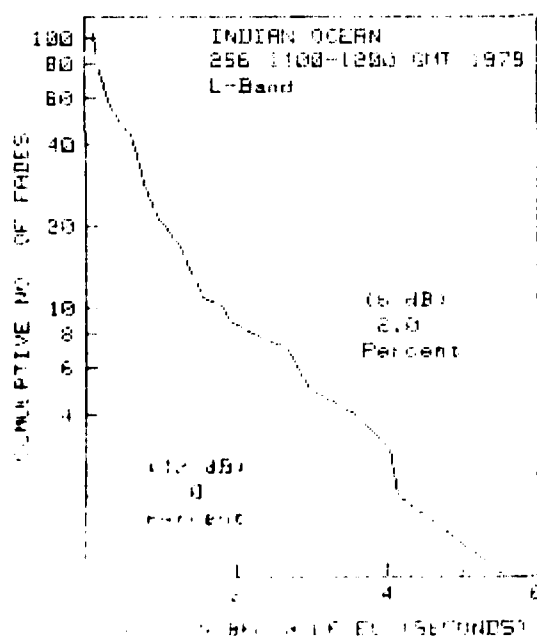
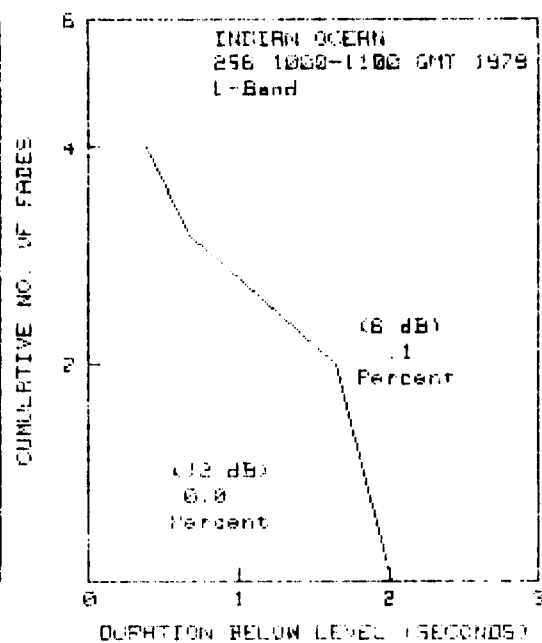
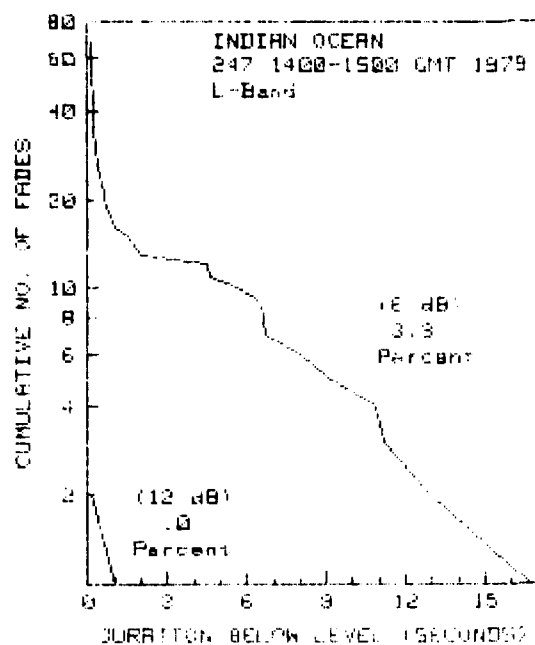




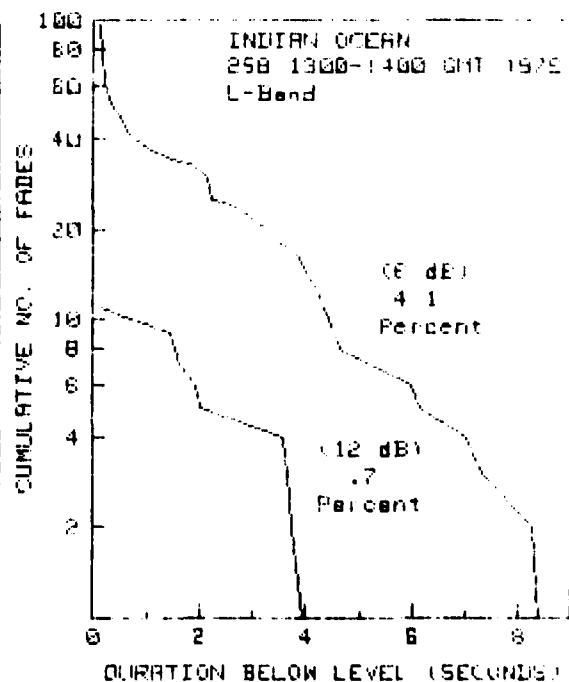
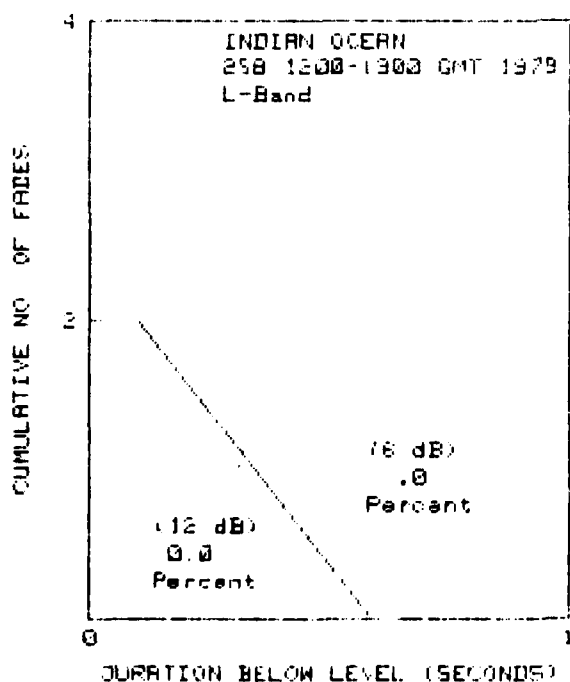
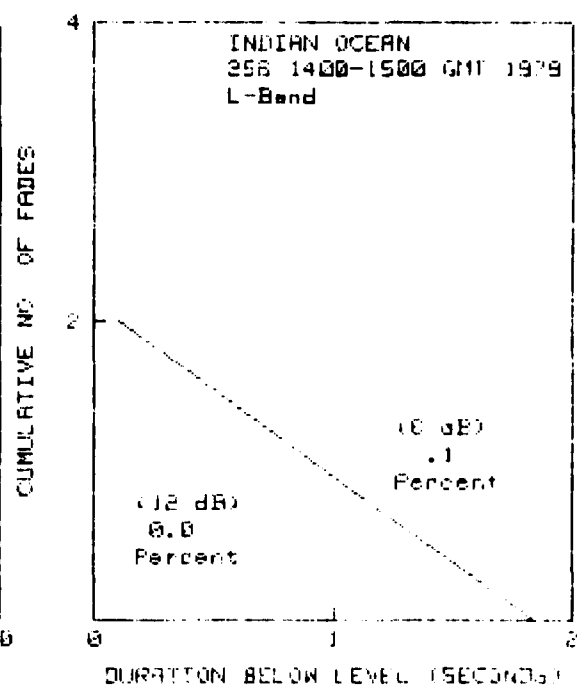
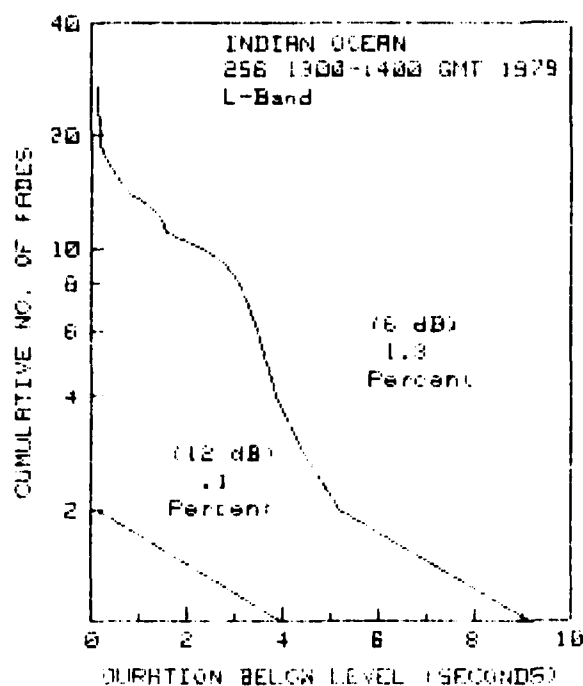
C4 (continued)



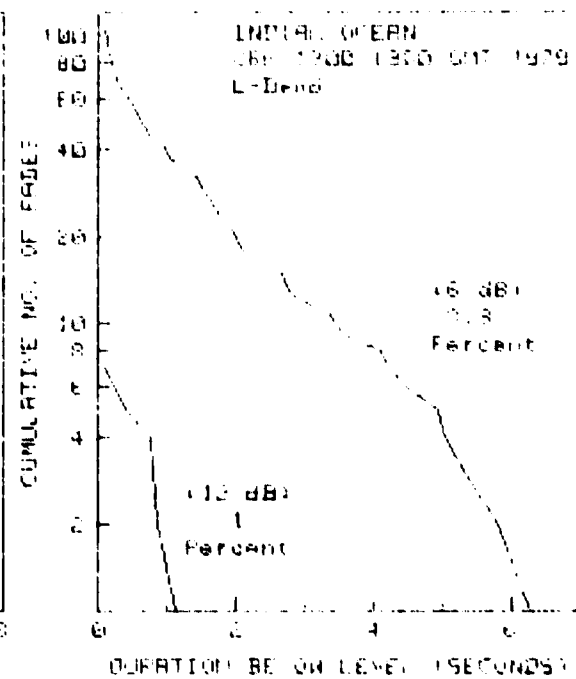
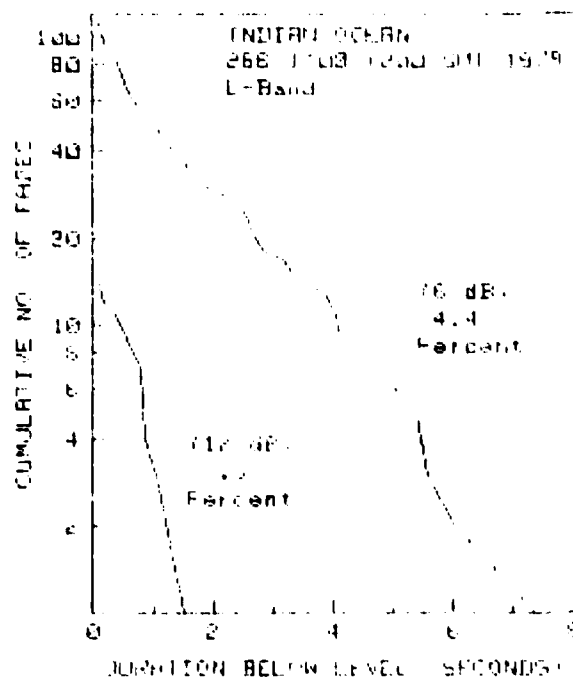
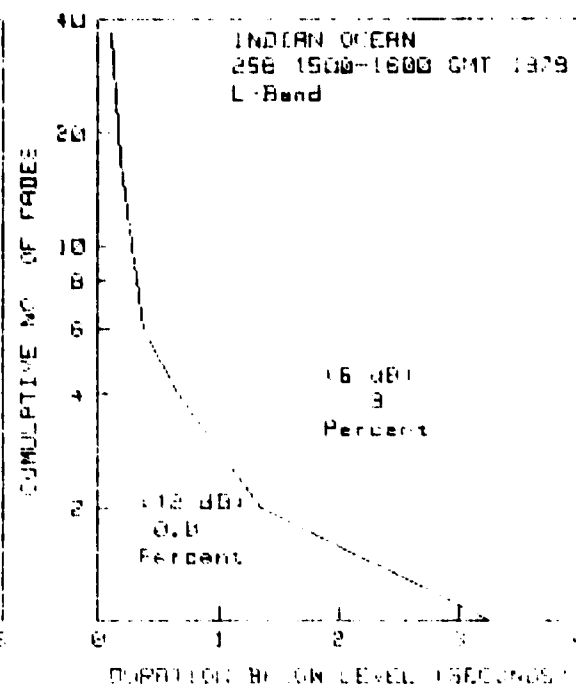
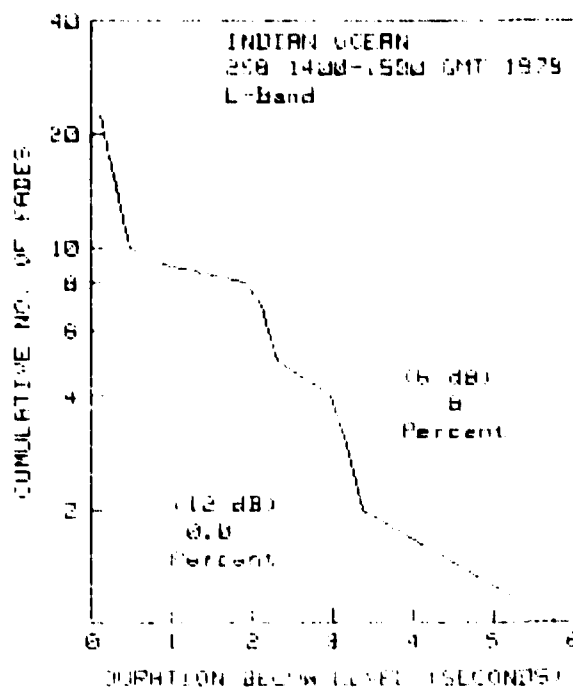
C4 (continued)



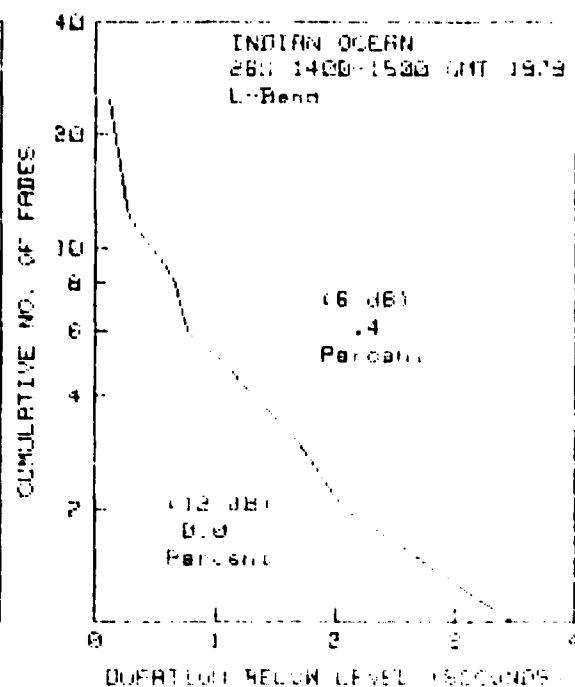
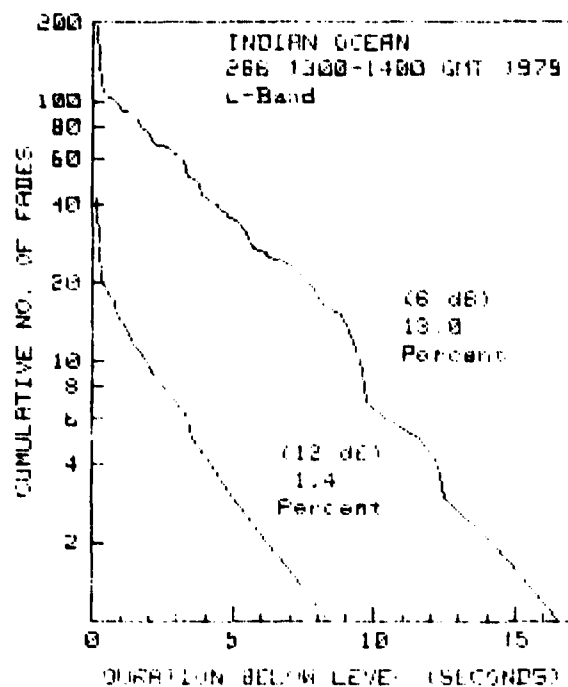
C4 (continued)



C4 (continued)



C4 (continued)



C4 (continued)

DEPARTMENT OF DEFENSE

DEPUTY UNDER SECRETARY OF DEFENSE R & E  
(COMMUNICATIONS, COMMAND CONTROL &  
INTEL)  
DIR., TELECOMM & CMD & CONTROL PROG.  
RESOURCES  
(ALDEN P. SULLIVAN)

DIRECTOR  
DEFENSE COMMUNICATIONS ENGINEERING CENTER  
TROY ELLINGTON

DEFENSE NUCLEAR AGENCY  
DOW EVELYN

DEFENSE ADVANCED RESEARCH PROJECTS  
AGENCY (2)

DEFENSE COMMUNICATIONS AGENCY  
CAPT D.W. FISCHER  
DR. F.E. BOND

DEFENSE TECHNICAL INFORMATION CENTER (12)

NAVAL ELECTRONIC SYSTEMS COMMAND  
PME-106-1 (6)

U.S. NAVAL COMMUNICATION AREA  
MASTER STATION WESTPAC  
COMMANDING OFFICER (2)

U.S. NAVAL COMMUNICATION AREA  
MASTER STATION WESTPAC  
FACILITIES CONTROL OFFICER/34 (4)

NAVAL COMMUNICATION AREA MASTER  
STATION EASTPAC  
FACILITIES CONTROL OFFICER (4)

COMMANDER OPERATIONAL TEST AND  
EVALUATION FORCE  
(CODE 645 (LT. STEINMAN)

U.S. NAVAL SHORE ELECTRONICS  
ENGINEERING ACTIVITY  
BOX 5  
FPO SEATTLE 98762

COMMANDER, NAVAL TELECOMMUNICATIONS  
COMMAND  
CAPT R.E. ENRIGHT

CHIEF OF NAVAL OPERATIONS  
NOP-941U TSAPG  
(CDR R.M. WELLS)

NAVAL AIR DEVELOPMENT CENTER  
CODE 8131 (OLIVER DELL)  
CODE 2033, AETC (DICK HOGG)

OFFICE OF NAVAL RESEARCH  
ONR-420 (DR. T.G. BERLINCOURT) (2)  
ONR-465 (R.G. JOINER) (6)

NAVAL RESEARCH LABORATORY  
CODE 4410 (J.M. GOODMAN)

AIR FORCE

AIR FORCE GEOPHYSICS LABORATORY  
HANSCOM AFB, MA 01731  
DR. JULES AARONS  
JOHN P. MULLEN

AIR FORCE AVIONICS LABORATORY  
AFSC  
WRIGHT-PATTERSON AFB, OH 45433  
A.L. JOHNSON  
WADE HUNT

GOVERNMENT (OTHER THAN DOD)

INSTITUTE FOR TELECOMMUNICATIONS  
SCIENCES/NTIA  
BOULDER, CO 80302  
R.W. HUBBARD  
MARTIN NESENBERGS

NATIONAL OCEANIC AND ATMOSPHERIC  
ADMINISTRATION  
325 BROADWAY  
BOULDER, CO 80302  
R. COHEN  
C.L. RUFENACH

DEPARTMENT OF TRANSPORTATION  
TRANSPORTATION SYSTEMS CENTER  
550 BROADWAY  
CAMBRIDGE, MA 92142  
PETER ENGLER  
LES KLEIN  
NORMAN KNABLE

NATIONAL BUREAU OF STANDARDS  
BOULDER, CO 80302  
DR. R.H. OTT

NATIONAL AERONAUTICS & SPACE  
ADMINISTRATION  
DANDAN, GUAM 96916  
JOHN CORNWELL (2)

UNIVERSITIES/INSTITUTES

INSTITUTE FOR DEFENSE ANALYSIS  
400 ARMY-NAVY DRIVE  
ARLINGTON, VA 22022  
DR. JOSEPH M. AEIN

MASSACHUSETTS INSTITUTE OF TECHNOLOGY  
LINCOLN LABORATORY  
P.O. BOX 73  
LEXINGTON, MA 02173  
B.E. NICHOLS  
J.V. EVANS  
E.A. BUCHER

AMERICAN INSTITUTE OF MERCHANT SHIPPING  
1625 K STREET, N.W.  
SUITE 1000  
WASHINGTON, DC 20006

PRIVATE COMPANIES

AEROSPACE CORP.  
P.O. BOX 95085  
LOS ANGELES, CA 90045  
VIRGIL WALL  
F.L. STRUBEL

ENVIRONMENTAL RESEARCH & TECHNOLOGY, INC.  
CONCORD, MA 01742  
R.K. CRANE

PHYSICAL DYNAMICS, INC.  
P.O. BOX 3027  
BELLEVUE, WA 98009  
DR. E.J. FREMOUW

MARTELLO COMMUNICATIONS, INC.  
277 78th STREET  
BROOKLYN, NY 11209  
H.F. MULLEN

MISCELLANEOUS

CAMP PARKS TEST STATION  
P.O. BOX 550  
PLEASANTON, CA 94566  
JOHN MEYER